

The Cretaceous world: plate tectonics, palaeogeography and palaeoclimate



Christopher R. Scotese^{1*}, Christian Vérard², Landon Burgener³,
Reece P. Elling⁴ and Adam T. Kocsis⁵

¹Department of Earth and Planetary Sciences, Northwestern University, 2145 Sheridan Road, Evanston, IL 60208, USA

²Department of Earth Sciences, University of Geneva, Rue des Maraîchers 13, CH-1205 Geneva, Switzerland

³Department of Geological Sciences, Brigham Young University, S389 Eyring Science Center, Provo, UT 84602, USA

⁴Department of Geology, Grand Valley State University, Padnos Hall of Science, 1 Campus Drive, Allendale, MI 49401, USA

⁵GeoZentrum Nordbayern, Friedrich-Alexander University Erlangen-Nürnberg, Schlossgarten 5, 91054 Erlangen, Germany

CRS, 0000-0002-9742-3581

*Correspondence: cscotese@gmail.com

Abstract: The tectonics, geography and climate of the Cretaceous world were very different from the modern world. At the start of the Cretaceous, the supercontinent of Pangaea had just begun to break apart and only a few small ocean basins separated Laurasia, West Gondwana and East Gondwana. Unlike the modern world, there were no significant continent–continent collisions during the Cretaceous, and the continents were low-lying and easily flooded. The transition from a Pangaea-like configuration to a more dispersed continental arrangement had important effects on the global sea level and climate. During the Early Cretaceous, as the continents rifted apart, the new continental rifts were transformed into young ocean basins. The oceanic lithosphere in these young ocean basins was thermally elevated, which boosted sea level. Sea level, on average, was c. 70 m higher than that of the present day. Sea level was highest during the mid-Cretaceous (90–80 Ma), with a subsidiary peak occurring c. 120 Myr ago (early Aptian). Overall, the Cretaceous was much warmer than the present-day climate (>10°C warmer). These very warm times produced oceanic anoxic events (OAEs), and the high temperatures in equatorial regions sometimes made terrestrial and shallow-marine ecosystems uninhabitable (temperatures >40°C). This is unlike anything we have seen in the last 35 Myr and may presage the eventual results of man-made global warming. This mostly stable, hot climate regime endured for nearly 80 Myr before dramatically terminating with the Chicxulub bolide impact 66 Myr ago. Temperatures plummeted to icehouse levels in the ‘impact winter’ as a result of sunlight-absorbing dust and aerosols being thrown into the atmosphere. As a consequence of the collapse of the food chain, c. 75% of all species were wiped out. The effect of this extinction event on global ecosystems was second only to the great Permo-Triassic Extinction.

Supplementary material: Complete sets of all kinds of maps discussed in the body of text, computer animations of: plate motions, palaeogeography, oceanic circulation and Köppen belt evolution, as well as supporting documentation in the form of tables, data files and spreadsheets, are available at <https://doi.org/10.5281/zenodo.10659104> [last accessed 8 August 2024], dealing exclusively with Cretaceous material, and <https://doi.org/10.5281/zenodo.10659112> [last accessed 16 August 2024], containing material that is Phanerozoic in scope.

The Cretaceous Period was defined by d’Halloy in 1822. It was divided into two epochs (Lower Cretaceous and Upper Cretaceous) by Conybeare and Phillips (1822), with each epoch having six stages (Fig. 1) (D’Orbigny 1840; Cohen *et al.* 2013). The Cretaceous is the longest period of the Phanerozoic Era (79 Myr), and is 33% longer than the other periods of long duration such as the Cambrian, Devonian and Carboniferous (each c. 60 Myr in length). In this

paper we present 17 plate tectonic and palaeogeographical reconstructions and nine palaeoclimatic reconstructions for the Cretaceous (Table 1).

A lot happened during the Cretaceous. It was the acme of the age of reptiles (dinosaurs and pterosaurs), and the great extinction event at the end of the period set the stage for the rise of mammals. Swimming reptiles (ichthyosaurs, plesiosaurs and mosasaurs), hard-shelled cephalopods (ammonites)

From: Hart, M. B., Batenburg, S. J., Huber, B. T., Price, G. D., Thibault, N., Wagreich, M. and Walaszczyk, I. (eds) *Cretaceous Project 200 Volume 1: the Cretaceous World*. Geological Society, London, Special Publications, **544**, <https://doi.org/10.1144/SP544-2024-28>

© 2024 The Author(s). This is an Open Access article distributed under the terms of the Creative Commons Attribution License (<http://creativecommons.org/licenses/by/4.0/>). Published by The Geological Society of London.

Publishing disclaimer: www.geolsoc.org.uk/pub_ethics

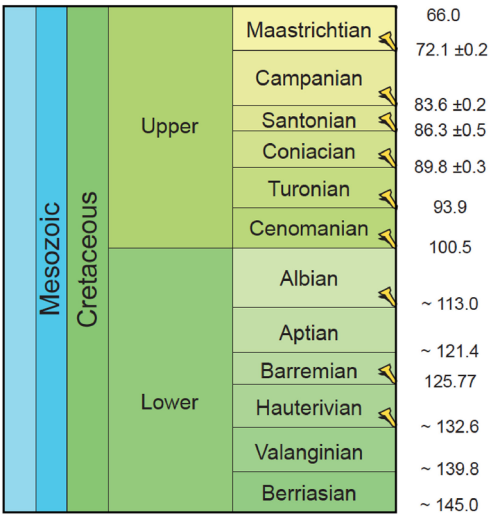


Fig. 1. Cretaceous timescale. Source: [Cohen *et al.* \(2013\)](#), version 2023/06).

and planktonic micro-organisms (foraminifera and coccoliths) filled the seas. Excellent summaries of the ecology and evolution of life during the Cretaceous can be found in [Bakker \(1986, 1995\)](#), [Weishampel *et al.* \(1990\)](#), [Wellnhofer \(1991\)](#), [Fastovsky and Weishampel \(1996\)](#), [Chatterjee \(1997\)](#); [Dingus and Rowe \(1998\)](#), [Morley \(2000\)](#), [Willis and](#)

Table 1. Cretaceous time intervals

| Map number | Stratigraphic Stage (plate tectonic reconstruction age) |
|------------|---|
| 1 | Cretaceous–Paleogene Boundary (65 Ma) |
| 2 | Late Cretaceous (Maastrichtian, 70 Ma) |
| 3 | Late Cretaceous (late Campanian, 75 Ma) |
| 4 | Late Cretaceous (early Campanian, 80 Ma) |
| 5 | Late Cretaceous (Coniacian–Santonian, 85 Ma) |
| 6 | Mid-Cretaceous (latest Turonian, 90 Ma) |
| 7 | Mid-Cretaceous (Cenomanian, 95 Ma) |
| 8 | Early Cretaceous (latest Albion, 100 Ma) |
| 9 | Early Cretaceous (middle Albion, 105 Ma) |
| 10 | Early Cretaceous (early Albion, 110 Ma) |
| 11 | Early Cretaceous (late Aptian, 115 Ma) |
| 12 | Early Cretaceous (early Aptian, 120 Ma) |
| 13 | Early Cretaceous (earliest Barremian, 125 Ma) |
| 14 | Early Cretaceous (Hauterivian, 130 Ma) |
| 15 | Early Cretaceous (Valanginian, 135 Ma) |
| 16 | Early Cretaceous (latest Berriasian, 140 Ma) |
| 17 | Jurassic–Cretaceous boundary (145 Ma) |

[McElwain \(2002\)](#), [Ellis \(2003\)](#), [Skelton \(2003\)](#), [Everhart \(2005\)](#), [Paul \(2016, 2022a, b\)](#), [Witton \(2013\)](#) and [Brusatte \(2018\)](#). In this paper we attempt to paint a comprehensive picture of what the Cretaceous world was like – the tectonic activity, the geographical distribution of the continents and ocean basins, the relative amounts of land and sea, the climatic zones, the river systems, and the ocean currents.

The plate tectonic reconstructions (e.g. [Fig. 2a](#)) are based on marine magnetic anomalies, the trends of oceanic fracture zones, hotspot tracks, mantle tomography and a new synthesis of palaeomagnetic data ([Elling 2022](#)). This Global Plate Model is used to predict the changing age of the ocean floor and, hence, the changing volume of the ocean basins and the resulting eustatic sea-level change and continental flooding. An additional 17 maps (e.g. [Fig. 2b](#)) illustrate the changing palaeogeography of the Cretaceous.

Palaeogeographical maps illustrate the changing distribution of mountains, uplands, lowlands, shallow seas and deep ocean basins. No major continent–continent collisional mountain ranges formed during the Cretaceous. Nearly all mountain building occurred along the subducting margins of the Panthalassic and Tethys oceans. Andean-type subduction and the collision of exotic terranes formed long, linear mountain belts. The interiors of the continents were largely flat, with the exception of Central Asia where late Paleozoic mountain ranges still towered over the landscape. The high sea level (+150 m: this study) during the mid-Cretaceous (Cenomanian–Turonian–Coniacian) flooded the continents. Sea level at the beginning and end of the Cretaceous was only slightly higher than the present-day sea level (0–+40 m).

Special attention is given in this paper to the changing climate of the Cretaceous. Palaeoclimate maps illustrate ancient temperatures ([Fig. 3a](#)), rainfall ([Fig. 3b](#)), ocean circulation ([Fig. 3c](#)) and, most importantly, the changing extent of the Köppen climatic belts (e.g. [Fig. 2c](#)) ([Burgener *et al.* 2023](#)). The Köppen climatic belts are defined by seasonal variations in temperature and precipitation ([Köppen 1918](#)), and are the best way to characterize and visualize past climates. Variations in regional climates create a mosaic of environments and ecological habitats. The extent of the principal Köppen zones – (A) tropical ever-wet, (B) subtropical arid, (C) warm temperate, (D) cool temperate and (E) polar – determines the distribution of the environments and habitats. There were no large permanent ice caps during the Cretaceous, although small ice caps (c. 4×10^6 km²) may have existed at the South Pole during the earliest and latest Cretaceous ([Scotese *et al.* 2021](#)). The palaeo-Köppen maps also show the likely drainage patterns and the course of Cretaceous rivers (e.g. [Fig. 2c](#)).

The Cretaceous world

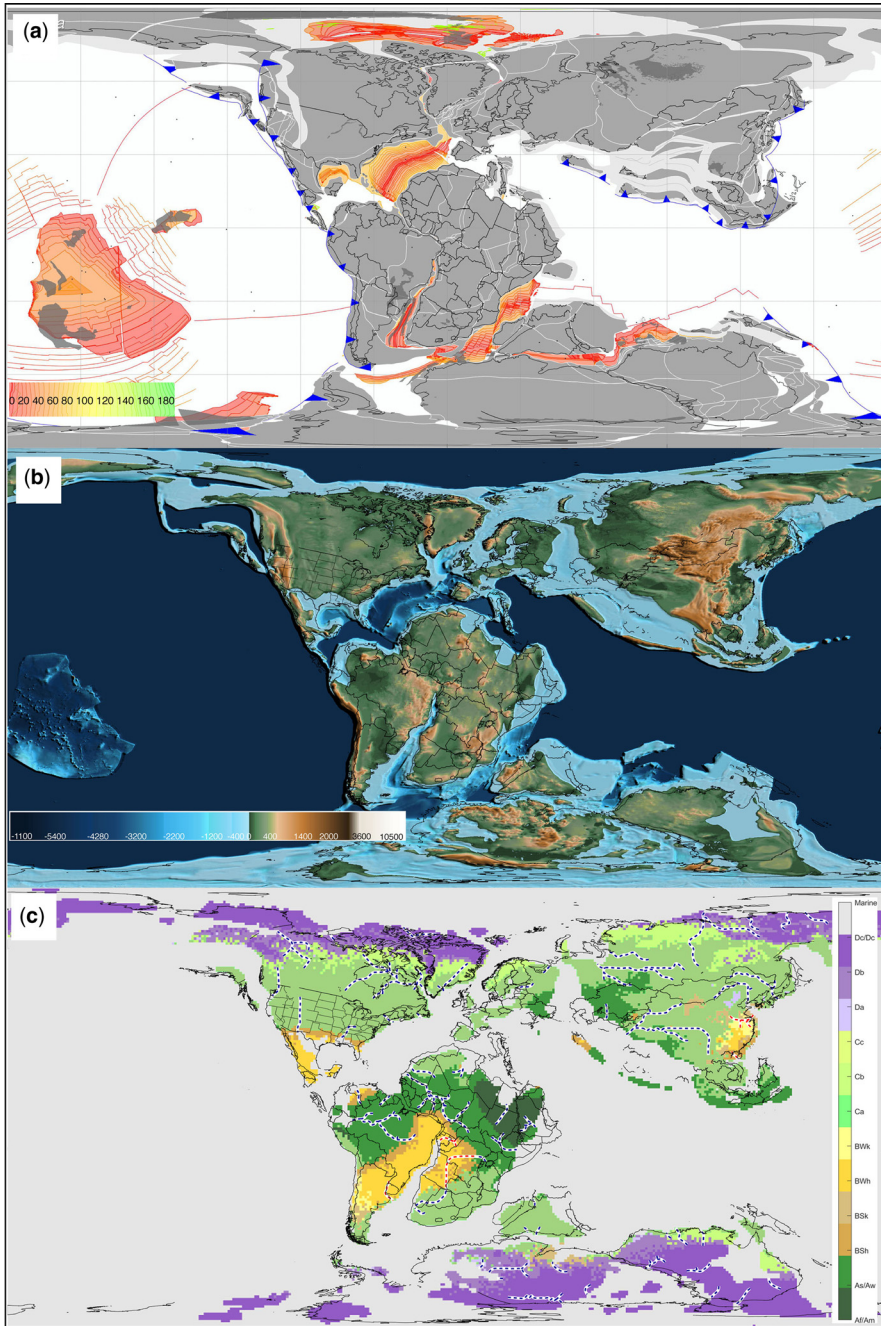


Fig. 2. Example Cretaceous plate tectonics, palaeogeographical and palaeoclimatic maps. **(a)** Plate tectonic reconstruction for the early Aptian (120 Ma). Black dots, hotspots; dark grey, hotspot tracks and LIPs; medium grey, continental lithosphere; light grey, areas of continental convergence; red lines, mid-ocean ridges; blue lines, subduction zones; colour shading, age of ocean floor; colour legend units are millions of years. **(b)** Palaeogeographical reconstruction. Dark blue, deep oceans; light blue, flooded continental lithosphere and ocean islands; green, lowlands; tan, uplands; brown, mountains; colour legend units are metres. **(c)** Palaeoclimatic reconstruction. Köppen belts: dark green, Tropical Ever-wet; yellow and tan, Subtropical Arid; light green, Warm Temperate; purple, Cold Temperate. Paleorivers: blue dashed lines, rivers; red dashed lines, dry rivers.

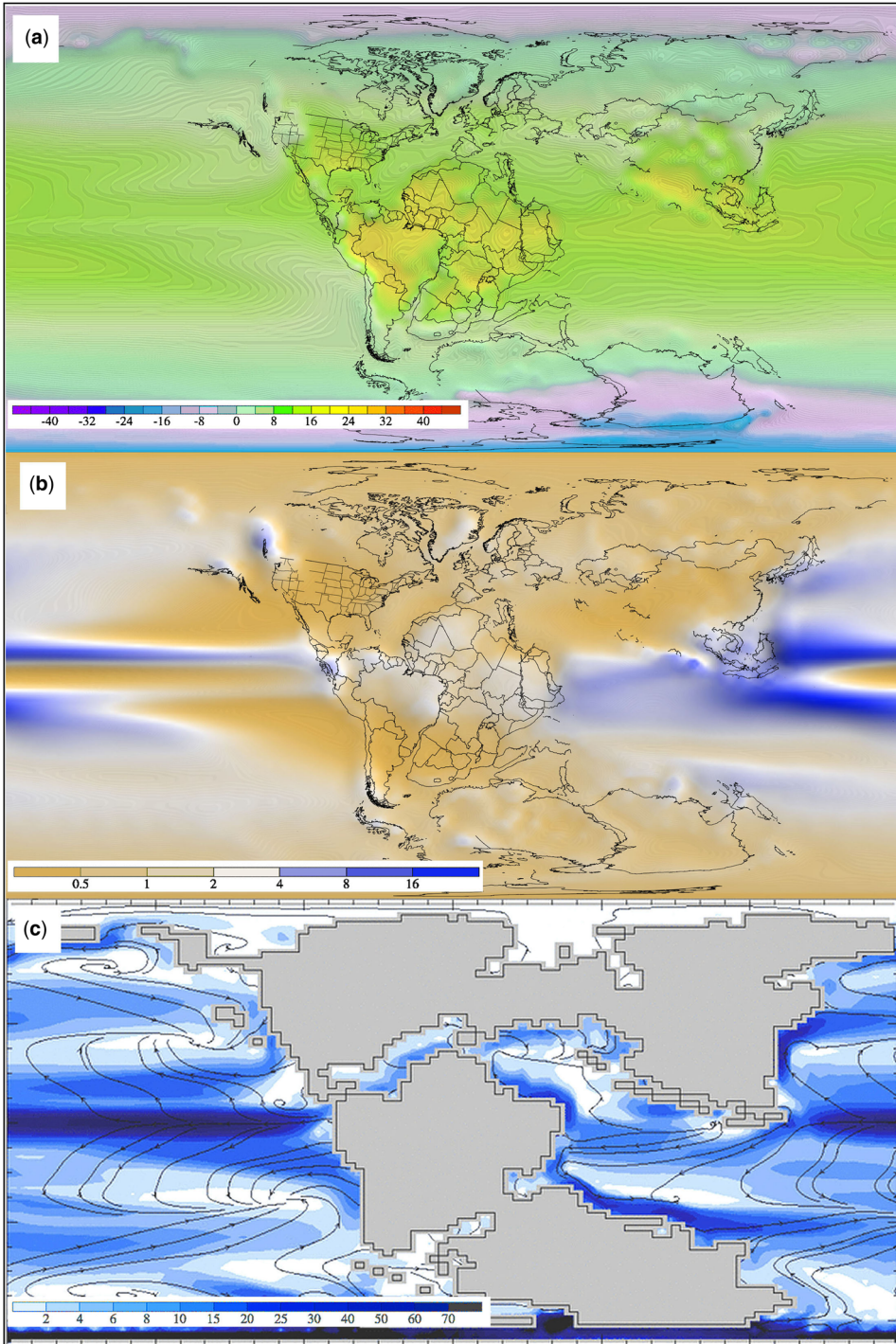


Fig. 3. Example Cretaceous palaeoclimatic maps. (a) Global average temperature for the early Aptian (120 Ma): red–yellow–green, warm; pale green, cool; purple, cool; blue, ice; The faint contours are isotherms; colour legend units are $^{\circ}\text{C}$. (b) Annual precipitation: blue, wet; orange, arid; colour legend units are mm/day. (c) Oceanic circulation: arrows indicate current flow; dark blue, high velocity; white, low velocity; colour legend units are cm s^{-1} .

The Cretaceous world

Table 2. PALEOMAP tectonic elements

| Plate_ID | | Plate_ID | |
|----------|---|----------|---|
| | North American tectonic elements | | Chinese and SE Asian tectonic elements |
| 101 | North American Craton | 601 | Tarim |
| 102 | Greenland | 602 | Qidam Block |
| 103 | North Slope–South Annui Block | 603 | Okinawa Trough |
| 104 | Mexico | 604 | N. China Craton |
| 105 | Baja California | 605 | Taiwan |
| 106 | Arctic Islands | 606 | Bai Shan Block |
| 107 | Grand Banks | 607 | N. South China Sea |
| 108 | West Avalonia | 610 | Japan |
| 109 | Florida–Piedmont | 611 | Yangtze |
| 110 | Alpha Ridge | 612 | Qiang Tang Block |
| 111 | Mendeleyev Ridge | 613 | Lhasa Block |
| 112 | Chukchi Cap | 614 | Song Pan Ganzi |
| 113 | Northwind Escarpment | 615 | Indochina |
| 114 | Lomonosov Ridge | 616 | Sibumasu |
| 121 | Angayucham | 618 | E. Andaman Sea |
| 123 | E. Yukon Tanana | 619 | Gulf of Thailand/E. Malaysia/E. Sumatra |
| 124 | North American Cordillera | 620 | Borneo and Java |
| 125 | N. Wrangellia | 621 | S. South China Sea |
| 126 | S. Wrangellia | 622 | Palawan and Sulu Sea |
| 127 | Stikine | 623 | Celebes Sea |
| 129 | Columbia Embayment | 624 | C. Burma Accretion |
| 130 | Sierra Nevada | 625 | W. Andaman Sea |
| 131 | Western Basin and Range | 626 | Sumatra–Java Trench and Banda Arc |
| 132 | Eastern Basin and Range | 628 | Amuria |
| 133 | Colorado Plateau | 631 | SE Japan |
| 134 | Southern Basin and Range | 632 | Kurile Island |
| 135 | Gulf Coast | 650 | N. Parece Vela Basin |
| 137 | ‘Northernmost Gulf of Mexico’ | 651 | Bonin Arc, N. Mariana Basin |
| 140 | NE Canada Basin | 652 | S. Mariana Basin |
| 141 | Makarov Basin | 653 | S. Parece Vela Basin |
| | | 654 | W. Parece Vela Basin |
| | South American tectonic elements | 655 | N. Philippine |
| 201 | South America Craton | 656 | S. Philippine |
| 202 | Rio de la Plata | 659 | Philippines |
| 203 | NW South America | 664 | N. Sulawesi |
| 204 | Chortis | 670 | N. Caroline |
| 205 | Yucatan | 671 | Molucca Sea |
| 206 | Cuba | 672 | Halmahera |
| 216 | Cayman Ridge | 673 | S. Caroline |
| 217 | West Cayman Trough | 675 | N. Bismarck Sea |
| 218 | East Cayman Trough | 676 | Bismarck Sea |
| 221 | Rosalind Bank | 679 | S. Sulawesi and Banda Sea |
| 222 | Jamaica | 680 | Timor |
| 223 | Quinto Sueno | 682 | Buru & Seram |
| 224 | Caribbean Plate | 684 | E. Sulawesi and Molucca Sea |
| 230 | Panama Arc | | |
| 237 | Puerto Rico | | African tectonic elements |
| 239 | Lesser Antilles | 701 | SC Africa |
| 251 | ‘Southern GOM oceanic crust’ | 702 | Madagascar |
| 252 | Hispaniola | 704 | Seychelles |
| 257 | Yucatan Basin | 705 | Mascarene Bank |
| 290 | Salado subplate | 706 | Nazareth Bank |
| 291 | Patagonia | 707 | Morocco, Atlas Mountains |
| | | 708 | Danakil |
| | European tectonic elements | 709 | Somalia Block |
| 301 | Russian Platform | 712 | Lake Victoria Block |
| 303 | Northern Highlands | 714 | NW Africa |

(Continued)

Table 2. *Continued.*

| Plate_ID | | Plate_ID | |
|----------|---------------------------------------|----------|---|
| 304 | Iberia | 715 | NE Africa |
| 305 | Variscan Europe | 716 | Sudan Block |
| 306 | Corsica and Sardinia | | |
| 307 | Apulia | | Australian–Antarctic tectonic elements |
| 308 | Balkans | 800 | New Guinea |
| 309 | W. Svalbard | 801 | Australian Craton |
| 310 | Barents Sea | 802 | East Antarctic Craton |
| 313 | Midland Valley | 803 | Palmer Peninsula |
| 315 | East Avalonia | 804 | Marie Byrdland |
| 317 | E. Rockall Bank | 805 | Ellsworth Mt. |
| 318 | W. Rockall Bank | 806 | North Island, New Zealand |
| 319 | Moesia | 807 | South Island, New Zealand |
| 320 | Balearic Island Menorca | 808 | Gulf of Papua |
| 321 | Alboran Sea | 809 | Rennell Ridge |
| 322 | Gulf of Gascogne transitional crust | 810 | N. Coral Sea |
| 323 | Malta–Gulf of Gabes | 811 | S. Shetland Island |
| 324 | Faroes | 812 | S. Orkney Island Block |
| 325 | West Rockall Gap | 813 | Chatham Rise |
| 326 | East Rockall Gap | 814 | Campbell Plateau (New Zealand Plateau) |
| 327 | Voring Plateau | 815 | South Fiji Basin |
| 328 | Cantabrian transitional crust | 816 | Balleny Island |
| 330 | Crete | 817 | South Solomon Sea |
| 331 | Cyprus | 818 | North Solomon Sea |
| 332 | Porcupine Bank | 819 | Melanesian Border Plateau |
| 350 | Yermak Plateau | 820 | Wharton Basin |
| | | 821 | Lord Howe Rise Stretched Crust |
| | Siberian tectonic elements | 822 | S. Coral Sea |
| 401 | Siberian Craton | 823 | East Tasman Sea |
| 402 | Kazakhstan | 824 | New Hebrides Basin and E. Coral Sea Basin |
| 403 | Omolon | 825 | W. Fiji Basin |
| 405 | Verkhoyansk Mt–Kolyma | 826 | Coral Sea Plateau |
| 406 | Kamchatka/Koni-Murgal Arc | 829 | Solomon Arc |
| 407 | Tien Shan–Junghar | 830 | Vanuatu Arc |
| 408 | North Sea of Okhotsk | 833 | Lord Howe Rise |
| 409 | C. Sea of Okhotsk | 834 | Norfolk Ridge |
| 410 | Sea of Okhotsk | 840 | Marion Reef |
| 413 | Kamchatka Trench | 846 | E. Fiji Basin |
| 414 | Kronotsky Terrane | 847 | W. Havre Trough, Colville Ridge |
| 415 | Shirshov Ridge | 848 | E. Havre Trough, Kermadec Trench |
| 416 | Alaskan Aleutians | 870 | Great Australian Bight |
| 417 | Bowers Ridge | 871 | Tasman Rise |
| 418 | Komandorsky– West Aleutian island arc | 872 | Naturaliste Plateau |
| 419 | Koryak | 873 | NW Australian Basin and Exmouth Plateau |
| 420 | Bering Sea | 875 | Timor Sea |
| | | 876 | Cuvier – Perth Abyssal Plains |
| | Indian tectonic elements | 877 | NE Indian Ocean – Argo Abyssal Plain |
| 501 | India | 888 | Broken Ridge |
| 502 | Sri Lanka | 895 | Berkner Island and Ronne Ice Shelf |
| 503 | Arabia | 896 | Sentinel Range |
| 504 | Turkey | 897 | Trans-Antarctic Range |
| 505 | Lut Block | | |
| 506 | Sistan Block | | Oceanic tectonic elements |
| 507 | Farah Block | 901 | Pacific Plate |
| 508 | Isreal | 902 | Nazca Plate |
| 510 | Pontides | 904 | ‘Aluk’ |
| 511 | Black Sea | 905 | Cape Basin |
| 512 | Sanandaj–Sirjan Zone | 906 | Henry Hudson plate |
| 513 | South Caspian | 907 | E. Jan Meyen |

(Continued)

Table 2. *Continued.*

| Plate_ID | | Plate_ID | |
|----------|------------------|----------|-----------------------------------|
| 514 | North Caspian | 908 | W. Jan Mayen |
| 515 | Makran Accretion | 909 | Cocos Plate |
| 516 | Laxmi Ridge | 910 | Juan de Fuca |
| 550 | Erzurum | 911 | Bauer |
| | | 912 | N. Scotia Sea |
| | | 913 | S. Scotia Sea |
| | | 916 | Kula |
| | | 930 | South Georgia Island |
| | | 931 | W. Scotia Sea |
| | | 932 | E. Scotia Sea |
| | | 940 | Easter Island microplate |
| | | 944 | 'A little bit of Aluk or Phoenix' |
| | | 985 | N. Kerguelen Plateau |
| | | 992 | S. Kerguelen Plateau |
| | | 995 | Kula |
| | | 996 | Izanagi |
| | | 997 | Phoenix |
| | | 998 | Farallon |

How to read this chapter

This paper is organized into two principal sections: (1) a detailed discussion of the data and methods used to produce the plate tectonic, palaeogeographical and palaeoclimatic maps of the Cretaceous; and (2) a description of the chronology of Cretaceous plate tectonic, palaeogeographical and palaeoclimatic events. Although it was written to be read through from beginning to end, each of these sections stands alone and can be read in any order. An alternate approach would be to start with the concise outline in the Summary section and then read the more detailed descriptions in each of the sections on plate tectonics, palaeogeography and palaeoclimate. For those who want to quickly get to the gist of this essay, the Conclusions contain a condensed overview of the important ideas presented in this work.

Data and methods

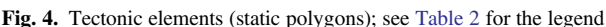
Global Plate Model: philosophy and model construction

The first step in producing a plate tectonic reconstruction is to build a global plate tectonic model that describes the evolution of the continents and ocean basins. The Cretaceous plate tectonic and palaeogeographical maps do not stand alone but, rather, are part of a global plate tectonic and palaeogeographical model that describes the evolution of the continents and ocean basins during the last 1.5 Gyr (Scotese and Elling 2017; Scotese 2018).

This dynamic Earth model has been assembled through the research efforts of the PALEOMAP Project over the last 40 years (Scotese and Sager 1988; Scotese *et al.* 1988; Scotese 1990, 2001a, b, 2014b, 2016b, 2018, 2021; Scotese and McKerrow 1990; Scotese and Dammrose 2008; Scotese and Elling 2017).

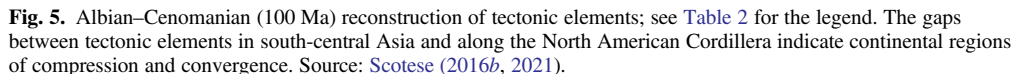
This description of global plate motions has two important components: (1) a global set of tectonic elements defined by ancient plate boundaries (rifts, subduction zones and sutures that mark zones of collision); and (2) a description of how these tectonic elements move through time. The first component, the tectonic element map, defines the crustal fragments that have had a history of independent motion. A description of the tectonic elements used to produce the Cretaceous plate tectonic reconstructions is given in Table 2. Figure 4 shows the present-day location of these tectonic elements. Figure 5 illustrates the palaeoposition of these tectonic elements during the Cenomanian (100 Ma).

The second component of the PALEOMAP Global Plate Model is a set of hierarchical finite rotations that precisely describes how these tectonic elements have moved through time. This plate modelling technique was first described by Ross and Scotese (1988), and is based on the concept of a plate tectonic circuit (Cox and Hart 1986). As an example, Table 3 lists the finite rotations that describe the movement of the continents that comprised Gondwana during the Cretaceous. Figure 6 illustrates the hierarchical relationship of these relative rotations: in other words, 'India moves relative to Madagascar', 'Madagascar moves relative to Somalia' and 'Somalia moves relative to Arabia'



Through the years, the software used to produce plate tectonic and palaeogeographical reconstructions has evolved. The software started out as simple FORTRAN programs (Scotese and Baker 1975; Scotese 1976, 1983; Scotese *et al.* 1980) and were subsequently translated into a succession of programming languages (e.g. Pascal, C, C++, Visual

Basic and Python: Scotese *et al.* 1985; Scotese and Denham 1988; Walsh and Scotese 1993). Plate-modelling software has evolved to the point where we can produce plate tectonic reconstructions for any instant in time as far back as the early Proterozoic (Eglington *et al.* 2017; Evans and Eglington 2022; Scotese and Elling 2017). The current version of this plate-modelling software, GPlates (Müller *et al.* 2018), is widely used and can be freely download from the EarthByte website (<https://www.earthbyte.org/>).



The Cretaceous world

Table 3. Finite rotations for Gondwana

| Moving plate | Age (my) | Latitude | Longitude | Angle | Fixed plate |
|--------------|----------|----------|-----------|-------|-------------|
| 201 | 0.0 | 90.0 | 0.0 | 0.0 | 701 |
| 201 | 1.0 | 60.0 | −39.0 | 0.3 | 701 |
| 201 | 2.0 | 60.0 | −39.0 | 0.5 | 701 |
| 201 | 3.6 | 60.0 | −39.0 | 0.8 | 701 |
| 201 | 5.2 | 60.0 | −39.0 | 1.2 | 701 |
| 201 | 6.6 | 60.0 | −39.0 | 1.8 | 701 |
| 201 | 8.2 | 60.0 | −39.0 | 2.3 | 701 |
| 201 | 9.0 | 60.0 | −39.0 | 2.8 | 701 |
| 201 | 9.7 | 60.0 | −38.9 | 3.1 | 701 |
| 201 | 20.1 | 58.1 | −37.4 | 7.0 | 701 |
| 201 | 26.6 | 57.2 | −35.3 | 10.0 | 701 |
| 201 | 33.5 | 56.6 | −33.9 | 13.4 | 701 |
| 201 | 43.8 | 57.6 | −32.1 | 17.6 | 701 |
| 201 | 49.7 | 59.3 | −31.6 | 20.1 | 701 |
| 201 | 56.4 | 61.1 | −31.5 | 22.3 | 701 |
| 201 | 65.0 | 63.2 | −33.2 | 24.4 | 701 |
| 201 | 70.0 | 63.7 | −33.7 | 26.4 | 701 |
| 201 | 75.0 | 63.6 | −33.3 | 29.4 | 701 |
| 201 | 80.0 | 62.5 | −34.0 | 31.5 | 701 |
| 201 | 85.0 | 60.5 | −33.3 | 34.3 | 701 |
| 201 | 118.7 | 51.7 | −33.1 | 52.7 | 701 |
| 201 | 121.0 | 50.1 | −31.9 | 53.4 | 701 |
| 201 | 143.8 | 46.9 | −30.5 | 57.5 | 701 |
| 201 | 206.0 | 46.9 | −30.5 | 57.5 | 701 |
| 202 | 0.0 | 90.0 | 0.0 | 0.0 | 201 |
| 202 | 83.0 | 90.0 | 0.0 | 0.0 | 201 |
| 202 | 105.0 | 90.0 | 0.0 | 0.0 | 201 |
| 202 | 143.8 | −21.7 | −63.9 | 1.9 | 201 |
| 202 | 206.0 | −21.7 | −63.9 | 1.9 | 201 |
| 203 | 0.0 | 90.0 | 0.0 | 0.0 | 201 |
| 203 | 56.4 | 90.0 | 0.0 | 0.0 | 201 |
| 203 | 94.0 | −25.6 | 79.8 | 2.6 | 201 |
| 203 | 206.0 | −25.6 | 79.8 | 2.6 | 201 |
| 290 | 0.0 | 90.0 | 0.0 | 0.0 | 202 |
| 290 | 105.0 | 90.0 | 0.0 | 0.0 | 202 |
| 290 | 143.8 | −34.5 | −103.1 | 1.4 | 202 |
| 290 | 206.0 | −34.5 | −103.1 | 1.4 | 202 |
| 291 | 0.0 | 90.0 | 0.0 | 0.0 | 290 |
| 291 | 105.0 | 90.0 | 0.0 | 0.0 | 290 |
| 291 | 143.8 | 43.8 | 162.7 | 1.1 | 290 |
| 291 | 206.0 | 43.8 | 162.7 | 1.1 | 290 |
| 307 | 0.0 | 90.0 | 0.0 | 0.0 | 714 |
| 307 | 50.0 | 90.0 | 0.0 | 0.0 | 714 |
| 307 | 65.0 | 90.0 | 0.0 | 0.0 | 714 |
| 307 | 70.0 | 53.9 | 126.9 | −0.8 | 714 |
| 307 | 75.0 | 17.9 | 17.3 | 5.0 | 714 |
| 307 | 80.0 | 32.1 | 11.6 | 10.1 | 714 |
| 307 | 90.0 | 43.1 | 17.7 | 6.4 | 714 |
| 307 | 100.0 | 42.3 | −3.4 | 3.8 | 714 |
| 307 | 120.0 | 56.8 | 80.2 | −1.5 | 714 |
| 307 | 130.0 | 45.0 | 7.6 | −5.5 | 714 |
| 307 | 140.0 | 35.9 | 0.5 | −7.3 | 714 |
| 307 | 150.0 | −26.0 | 176.4 | 8.1 | 714 |
| 307 | 160.0 | 33.7 | 106.6 | 2.5 | 714 |
| 307 | 180.0 | −1.0 | 136.8 | 4.1 | 714 |
| 307 | 306.0 | −41.1 | −177.0 | 17.3 | 714 |
| 320 | 0.0 | 90.0 | 0.0 | 0.0 | 304 |
| 320 | 6.0 | 90.0 | 0.0 | 0.0 | 304 |

(Continued)

Table 3. *Continued.*

| Moving plate | Age (my) | Latitude | Longitude | Angle | Fixed plate |
|--------------|----------|----------|-----------|-------|-------------|
| 320 | 16.0 | 38.2 | −0.8 | 23.3 | 304 |
| 320 | 206.0 | 38.2 | −0.8 | 23.3 | 304 |
| 501 | 0.0 | 90.0 | 0.0 | 0.0 | 802 |
| 501 | 9.7 | 13.1 | 36.1 | −6.6 | 802 |
| 501 | 20.0 | 17.1 | 28.6 | −11.8 | 802 |
| 501 | 30.0 | 14.9 | 33.1 | −19.5 | 802 |
| 501 | 40.0 | 17.3 | 27.2 | −24.4 | 802 |
| 501 | 50.0 | 14.0 | 21.8 | −32.1 | 802 |
| 501 | 60.0 | 11.7 | 16.5 | −43.7 | 802 |
| 501 | 65.0 | 10.0 | 15.0 | −49.0 | 802 |
| 501 | 70.0 | 9.9 | 12.5 | −53.3 | 802 |
| 501 | 83.0 | −9.2 | −168.0 | 64.0 | 802 |
| 501 | 83.0 | −17.8 | −154.7 | 55.3 | 702 |
| 501 | 85.0 | −18.6 | −155.0 | 56.2 | 702 |
| 501 | 90.0 | −18.0 | −156.1 | 58.2 | 702 |
| 501 | 100.0 | −19.3 | −156.3 | 58.8 | 702 |
| 501 | 166.0 | −20.2 | −156.8 | 58.1 | 702 |
| 501 | 206.0 | −22.3 | −159.2 | 56.8 | 702 |
| 502 | 0.0 | 90.0 | 0.0 | 0.0 | 501 |
| 502 | 112.0 | 90.0 | 0.0 | 0.0 | 501 |
| 502 | 120.0 | 9.8 | 80.3 | −29.8 | 501 |
| 502 | 130.2 | −10.2 | −98.6 | 18.4 | 501 |
| 502 | 206.0 | −10.2 | −98.6 | 18.4 | 501 |
| 503 | 0.0 | 90.0 | 0.0 | 0.0 | 715 |
| 503 | 9.7 | 36.5 | 18.0 | −3.3 | 715 |
| 503 | 24.0 | 36.5 | 18.0 | −5.2 | 715 |
| 503 | 33.0 | −35.3 | −158.4 | 8.5 | 715 |
| 503 | 206.0 | −35.3 | −158.4 | 8.5 | 715 |
| 504 | 0.0 | 90.0 | 0.0 | 0.0 | 510 |
| 504 | 13.5 | −29.4 | −156.7 | 5.2 | 510 |
| 504 | 33.5 | −20.5 | −148.2 | 10.8 | 510 |
| 504 | 33.5 | −13.4 | −118.5 | 8.0 | 715 |
| 504 | 47.9 | −28.2 | −124.8 | 9.9 | 715 |
| 504 | 143.9 | 42.6 | 17.4 | −21.5 | 715 |
| 504 | 206.0 | 42.6 | 17.4 | −21.5 | 715 |
| 508 | 0.0 | 90.0 | 0.0 | 0.0 | 715 |
| 508 | 9.7 | 36.8 | 31.3 | −2.6 | 715 |
| 508 | 24.0 | 36.8 | 31.3 | −2.6 | 715 |
| 508 | 33.0 | 36.8 | 31.3 | −3.6 | 715 |
| 508 | 206.0 | 36.8 | 31.3 | −3.6 | 715 |
| 702 | 0.0 | 90.0 | 0.0 | 0.0 | 709 |
| 702 | 112.0 | 90.0 | 0.0 | 0.0 | 709 |
| 702 | 125.1 | 10.0 | −113.1 | 8.0 | 709 |
| 702 | 136.0 | 10.0 | −113.1 | 18.1 | 709 |
| 702 | 166.0 | −0.8 | −88.1 | 20.3 | 709 |
| 702 | 206.0 | −0.9 | −92.0 | 24.4 | 709 |
| 704 | 0.0 | 90.0 | 0.0 | 0.0 | 702 |
| 704 | 30.0 | 44.1 | −23.1 | −0.8 | 702 |
| 704 | 40.0 | 11.3 | −29.7 | −0.6 | 702 |
| 704 | 60.0 | 38.1 | −22.1 | −3.3 | 702 |
| 704 | 70.0 | 24.9 | 7.8 | −7.1 | 702 |
| 704 | 80.0 | 25.8 | −3.9 | −9.8 | 702 |
| 704 | 206.0 | 25.8 | −3.9 | −9.8 | 702 |
| 709 | 0.0 | 90.0 | 0.0 | 0.0 | 503 |
| 709 | 2.0 | 26.5 | 21.5 | 0.6 | 503 |
| 709 | 5.2 | 26.5 | 21.5 | 1.6 | 503 |
| 709 | 8.2 | 26.5 | 21.5 | 2.8 | 503 |
| 709 | 24.0 | 24.6 | 17.0 | 6.2 | 503 |

(Continued)

The Cretaceous world

Table 3. *Continued.*

| Moving plate | Age (my) | Latitude | Longitude | Angle | Fixed plate |
|--------------|----------|----------|-----------|-------|-------------|
| 709 | 33.0 | −23.4 | −154.1 | −10.2 | 503 |
| 709 | 206.0 | −23.4 | −154.1 | −10.2 | 503 |
| 712 | 0.0 | 90.0 | 0.0 | 0.0 | 701 |
| 712 | 30.0 | −17.8 | 37.1 | 2.5 | 701 |
| 712 | 206.0 | −17.8 | 37.1 | 2.5 | 701 |
| 714 | 0.0 | 90.0 | 0.0 | 0.0 | 701 |
| 714 | 60.0 | 33.2 | −114.8 | 0.4 | 701 |
| 714 | 84.0 | 90.0 | 0.0 | 0.0 | 701 |
| 714 | 110.0 | 90.0 | 0.0 | 0.0 | 701 |
| 714 | 118.7 | 22.0 | 11.6 | 2.2 | 701 |
| 714 | 130.2 | 17.9 | 11.0 | 5.0 | 701 |
| 714 | 143.8 | 22.0 | 11.6 | 6.0 | 701 |
| 714 | 206.0 | 22.0 | 11.6 | 6.0 | 701 |
| 715 | 0.0 | 90.0 | 0.0 | 0.0 | 701 |
| 715 | 110.0 | 90.0 | 0.0 | 0.0 | 701 |
| 715 | 118.7 | −18.0 | 38.4 | 1.9 | 701 |
| 715 | 206.0 | −18.0 | 38.4 | 1.9 | 701 |
| 716 | 0.0 | 90.0 | 0.0 | 0.0 | 701 |
| 716 | 110.0 | 90.0 | 0.0 | 0.0 | 701 |
| 716 | 118.7 | −17.8 | 37.1 | 1.9 | 701 |
| 716 | 143.8 | −17.8 | 37.1 | 2.4 | 701 |
| 716 | 206.0 | −17.8 | 37.1 | 2.4 | 701 |
| 800 | 0.0 | 90.0 | 0.0 | 0.0 | 801 |
| 800 | 20.0 | 24.1 | −44.1 | 17.6 | 801 |
| 800 | 206.0 | 24.1 | −44.1 | 17.6 | 801 |
| 801 | 0.0 | 90.0 | 0.0 | 0.0 | 501 |
| 801 | 34.9 | 90.0 | 0.0 | 0.0 | 501 |
| 801 | 41.5 | 90.0 | 0.0 | 0.0 | 501 |
| 801 | 41.5 | 16.6 | 29.9 | −23.6 | 802 |
| 801 | 43.8 | 15.1 | 31.3 | −24.5 | 802 |
| 801 | 53.3 | 12.5 | 31.7 | −25.2 | 802 |
| 801 | 68.7 | 8.7 | 33.2 | −25.8 | 802 |
| 801 | 75.0 | 7.7 | 34.3 | −25.4 | 802 |
| 801 | 79.1 | 6.2 | 35.1 | −26.4 | 802 |
| 801 | 83.0 | 4.9 | 35.8 | −26.8 | 802 |
| 801 | 85.0 | 2.5 | 37.9 | −28.4 | 802 |
| 801 | 96.0 | 9.2 | −135.9 | 33.8 | 802 |
| 801 | 206.0 | 9.2 | −135.9 | 33.8 | 802 |
| 802 | 0.0 | 90.0 | 0.0 | 0.0 | 701 |
| 802 | 9.7 | 6.4 | −54.1 | 1.5 | 701 |
| 802 | 20.1 | 7.4 | −44.9 | 2.6 | 701 |
| 802 | 33.5 | 9.1 | −36.4 | 5.5 | 701 |
| 802 | 40.1 | 10.9 | −41.9 | 7.0 | 701 |
| 802 | 43.8 | 11.4 | −43.7 | 7.8 | 701 |
| 802 | 47.9 | 10.3 | −42.9 | 8.8 | 701 |
| 802 | 53.3 | 6.7 | −40.6 | 10.0 | 701 |
| 802 | 57.9 | 3.8 | −39.7 | 10.6 | 701 |
| 802 | 63.6 | 0.6 | −39.2 | 11.3 | 701 |
| 802 | 64.7 | −0.4 | −39.4 | 11.6 | 701 |
| 802 | 68.7 | 1.1 | −41.6 | 11.8 | 701 |
| 802 | 71.3 | −1.8 | −41.4 | 13.5 | 701 |
| 802 | 79.1 | −4.7 | −39.7 | 16.0 | 701 |
| 802 | 83.0 | −2.0 | −39.2 | 17.9 | 701 |
| 802 | 83.0 | 9.2 | 12.0 | 64.0 | 501 |
| 802 | 84.0 | 8.8 | 11.3 | 63.9 | 501 |
| 802 | 90.0 | 5.9 | 10.0 | 70.6 | 501 |
| 802 | 96.0 | 5.9 | 7.1 | 77.7 | 501 |
| 802 | 118.7 | 0.2 | 8.8 | 86.4 | 501 |

(Continued)

Table 3. *Continued.*

| Moving plate | Age (my) | Latitude | Longitude | Angle | Fixed plate |
|--------------|----------|----------|-----------|-------|-------------|
| 802 | 136.0 | -2.7 | 13.7 | 90.4 | 501 |
| 802 | 166.0 | -5.2 | 17.4 | 94.2 | 501 |
| 802 | 1100.0 | -5.2 | 17.4 | 94.2 | 501 |
| 803 | 0.0 | 90.0 | 0.0 | 0.0 | 804 |
| 803 | 90.0 | 67.7 | 150.4 | 3.2 | 804 |
| 803 | 95.0 | 72.6 | 83.6 | -6.8 | 804 |
| 803 | 100.0 | 47.4 | -177.0 | 0.5 | 804 |
| 803 | 110.0 | 67.6 | 104.1 | -7.8 | 804 |
| 803 | 120.0 | 73.8 | 102.7 | -17.0 | 804 |
| 803 | 130.0 | 74.8 | 38.4 | -15.9 | 804 |
| 803 | 135.0 | 73.7 | 6.2 | -14.6 | 804 |
| 803 | 140.0 | 75.8 | 42.5 | -20.8 | 804 |
| 803 | 150.0 | 74.6 | 23.0 | -17.2 | 804 |
| 803 | 160.0 | 74.4 | 32.7 | -19.7 | 804 |
| 803 | 170.0 | 69.3 | 23.9 | -19.3 | 804 |
| 803 | 180.0 | 73.4 | 27.8 | -21.7 | 804 |
| 803 | 190.0 | 77.3 | 33.2 | -24.2 | 804 |
| 803 | 200.0 | 75.6 | 53.1 | -27.9 | 804 |
| 803 | 210.0 | 70.7 | 18.4 | -25.2 | 804 |
| 804 | 0.0 | 90.0 | 0.0 | 0.0 | 802 |
| 804 | 60.0 | 69.9 | 71.6 | -2.2 | 802 |
| 804 | 70.0 | 40.7 | -154.6 | 0.2 | 802 |
| 804 | 80.0 | 57.0 | 24.3 | 1.0 | 802 |
| 804 | 90.0 | 75.2 | 90.7 | 1.2 | 802 |
| 804 | 100.0 | 77.1 | -144.0 | -1.5 | 802 |
| 804 | 110.0 | 70.1 | 18.6 | 2.3 | 802 |
| 804 | 120.0 | 56.0 | 1.6 | 4.1 | 802 |
| 804 | 130.0 | 52.4 | 15.1 | 9.9 | 802 |
| 804 | 200.0 | 49.2 | 14.9 | 8.7 | 802 |
| 804 | 206.0 | 49.2 | 14.9 | 8.7 | 802 |
| 805 | 0.0 | 90.0 | 0.0 | 0.0 | 803 |
| 805 | 206.0 | 90.0 | 0.0 | 0.0 | 803 |
| 811 | 0.0 | 90.0 | 0.0 | 0.0 | 803 |
| 811 | 3.8 | -63.9 | -68.0 | -9.1 | 803 |
| 811 | 206.0 | -63.9 | -68.0 | -9.1 | 803 |
| 813 | 0.0 | 90.0 | 0.0 | 0.0 | 814 |
| 813 | 84.0 | 90.0 | 0.0 | 0.0 | 814 |
| 813 | 90.0 | 47.5 | -7.1 | 20.1 | 814 |
| 813 | 206.0 | 47.5 | -7.1 | 20.1 | 814 |
| 814 | 0.0 | 90.0 | 0.0 | 0.0 | 804 |
| 814 | 5.2 | 66.2 | -96.5 | 4.1 | 804 |
| 814 | 9.7 | 75.4 | -76.5 | 9.5 | 804 |
| 814 | 25.2 | 73.5 | -64.9 | 20.2 | 804 |
| 814 | 28.7 | 74.2 | -61.4 | 23.2 | 804 |
| 814 | 33.5 | 74.7 | -57.0 | 27.9 | 804 |
| 814 | 40.1 | 75.1 | -51.3 | 32.6 | 804 |
| 814 | 47.9 | 74.2 | -50.9 | 36.9 | 804 |
| 814 | 56.4 | 70.1 | -63.6 | 37.9 | 804 |
| 814 | 63.6 | 70.4 | -58.0 | 45.2 | 804 |
| 814 | 65.0 | 69.1 | -46.4 | 49.5 | 804 |
| 814 | 70.0 | 68.3 | -55.3 | 48.7 | 804 |
| 814 | 75.0 | 63.4 | -51.3 | 51.1 | 804 |
| 814 | 80.0 | 60.5 | -61.2 | 46.7 | 804 |
| 814 | 85.0 | 60.5 | -64.5 | 48.2 | 804 |
| 814 | 90.0 | 64.9 | -51.0 | 61.0 | 804 |
| 814 | 94.0 | 67.1 | -55.9 | 63.2 | 804 |
| 814 | 206.0 | 67.1 | -55.9 | 63.2 | 804 |
| 833 | 0.0 | 90.0 | 0.0 | 0.0 | 801 |

(Continued)

| Moving plate | Age (my) | Latitude | Longitude | Angle | Fixed plate |
|--------------|----------|----------|-----------|-------|-------------|
| 833 | 40.1 | 90.0 | 0.0 | 0.0 | 801 |
| 833 | 56.4 | 5.3 | -24.1 | 0.7 | 801 |
| 833 | 64.7 | 9.7 | -38.8 | 7.3 | 801 |
| 833 | 79.1 | 9.8 | -33.9 | 16.5 | 801 |
| 833 | 94.0 | 9.2 | -22.7 | 23.5 | 801 |
| 833 | 1100.0 | 9.2 | -22.7 | 23.5 | 801 |
| 834 | 0.0 | 90.0 | 0.0 | 0.0 | 833 |
| 834 | 94.0 | 90.0 | 0.0 | 0.0 | 833 |
| 834 | 130.0 | -46.8 | 168.1 | 8.1 | 833 |
| 834 | 1100.0 | -46.8 | 168.1 | 8.1 | 833 |

gplates.org). GPlates was the principal tool used to produce the plate tectonic reconstructions shown here. A complete set of digital files comprising the PALEOMAP Global Plate Tectonic Model is included with the [Supplementary material](#) and also can be found online at <https://doi.org/10.5281/zenodo.5460860>

The fundamental importance of the Global Plate Tectonic Model (GPTM) cannot be overemphasized. It is paramount. The GPTM provides the framework upon which everything else is built and evaluated. We do not make a map for the Early Cretaceous, a map for the mid-Cretaceous and another map for the Late Cretaceous; rather, we build a continuously evolving plate tectonic model that illustrates the dynamic evolution of the plate boundaries and

describes the ever-changing configuration of continents and ocean basins. There is a strong sense of contingency. In a very real sense, the Early Cretaceous plate reconstruction predicts and provides a context for the mid-Cretaceous plate reconstruction, and the mid-Cretaceous plate reconstruction provides the context for the Late Cretaceous plate reconstruction, and so on. Much like a trained neural network, the global plate tectonic model is a complex web of linked interdependencies. No one map or time interval can stand alone.

All palaeontological, palaeoclimatic, geological and geophysical data are evaluated in the context of the global plate tectonic model. If there is a mismatch between the data and the model, either the model is adjusted to better explain the data or the

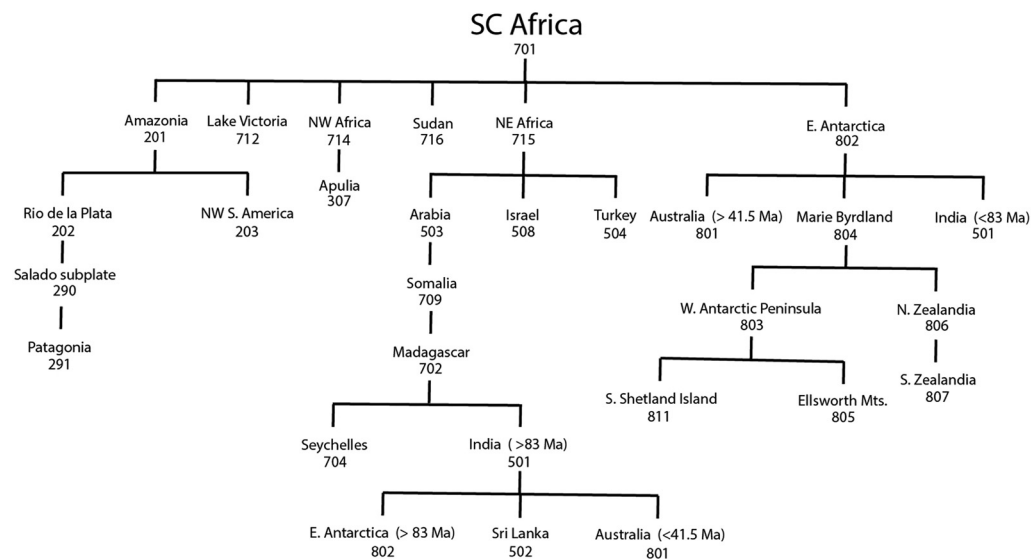


Fig. 6. Plate tectonic hierarchy describing the movement of the 30 tectonic elements that make up Gondwana. Note that some plates, such as India, move with respect to different fixed plates depending on the time. These transitional times are called cross-overs.

contrarian data are rejected. The goal is to eventually have a self-consistent, dynamic Earth system model that describes how the Earth has evolved through time.

In the [Supplementary material](#) there is a brief essay describing how global plate tectonic models developed from the mid-1970s to the present day. This chronology describes the plate-modelling software and research groups that produced them. Recently, [Buffan *et al.* \(2023\)](#) estimated the reliability and similarity of recent global plate tectonic models. Their conclusions were that the models are in very good agreement back to 100 Ma but they diverge significantly for times older than 300 Myr.

Geological and geophysical evidence used to build the Cretaceous plate tectonic model

[Figure 7](#) summarizes the various kinds of information used to build the PALEOMAP Global Plate Tectonic Model. The diagram shows how the number and the relative importance of various lines of evidence changes through time. For example, when making Precambrian plate tectonic reconstructions, only six of the 10 lines of evidence can be brought to bear. The other four lines of evidence are not available. For the Cretaceous, we are fortunate that all 12 lines of evidence can be used to find a solution. In

order of importance, these lines of evidence are: (1) age of the ocean basins; (2) oceanic fracture zones; (3) hotspots and hotspot tracks; (4) palaeopoles and apparent polar wander (APW) paths; (5) continental tectonics; (6) the Rules of Plate Tectonics; (7) synthetic seafloor spreading isochrons; (8) Large Igneous Provinces; (9) subduction zone graveyards; (10) palaeobiogeography; (11) palaeoclimate; and (12) true polar wander. In the following sections, we describe the role that each line of evidence plays when making Cretaceous plate tectonic reconstructions.

Many of these lines of evidence are plotted in [Figure 8](#) (with the legend shown in [Fig. 9](#)). The *Tectonic Map of the World* is an update of the map originally published by [Larson *et al.* \(1985\)](#) and is similar to other recent efforts ([Francois *et al.* 2021](#)). It illustrates a variety of continental tectonic features such as: the trends of mountain ranges, ophiolites, Large Igneous Provinces (LIPs) and continental volcanic arcs, as well as important oceanic tectonic features such as the age of the ocean floor, trends of fracture zones, hotspot tracks, oceanic volcanic island arcs, and subduction-related features such as trenches, accretionary prisms and forearc basins ([Fig. 8](#)). Large-format versions of the *Tectonic Map of the World* are available in the [Supplementary material](#); one version identifies more than 300 oceanic and continental features.

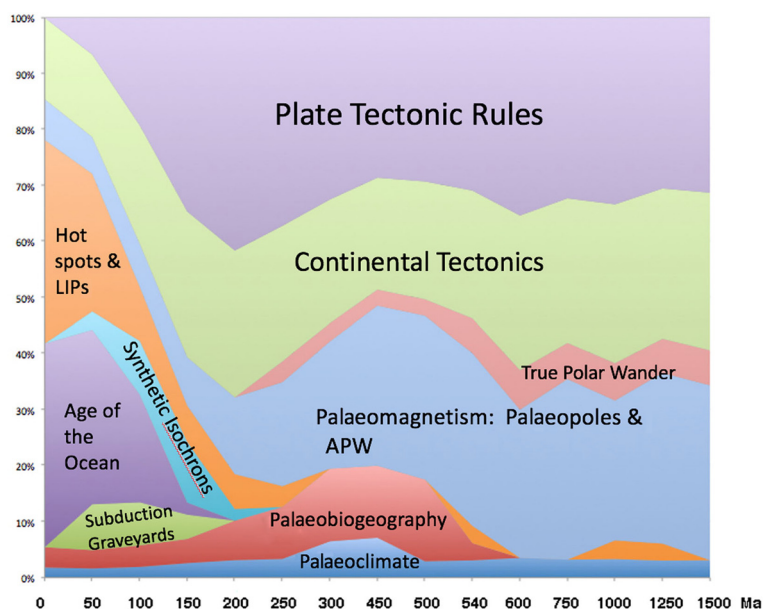


Fig. 7. Lines of evidence used to produce a plate tectonic reconstruction. The width of the coloured bands indicates the relative importance of each kind of evidence. Note that the width of the bands changes back through time and that fewer lines of evidence are available for ages greater than 600 Myr.

The Cretaceous world

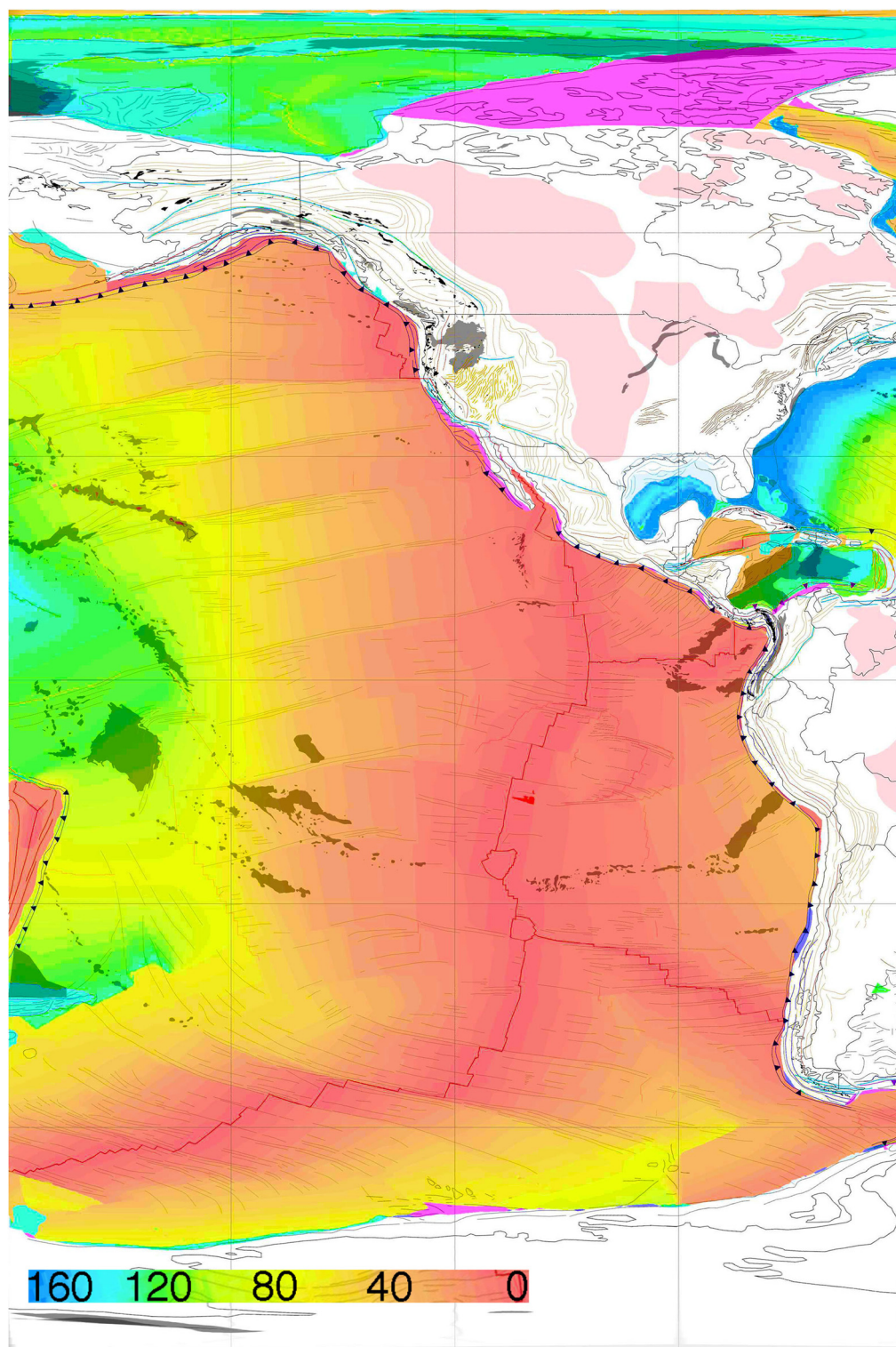


Fig. 8. (a) Tectonic Map of the World (part 1).

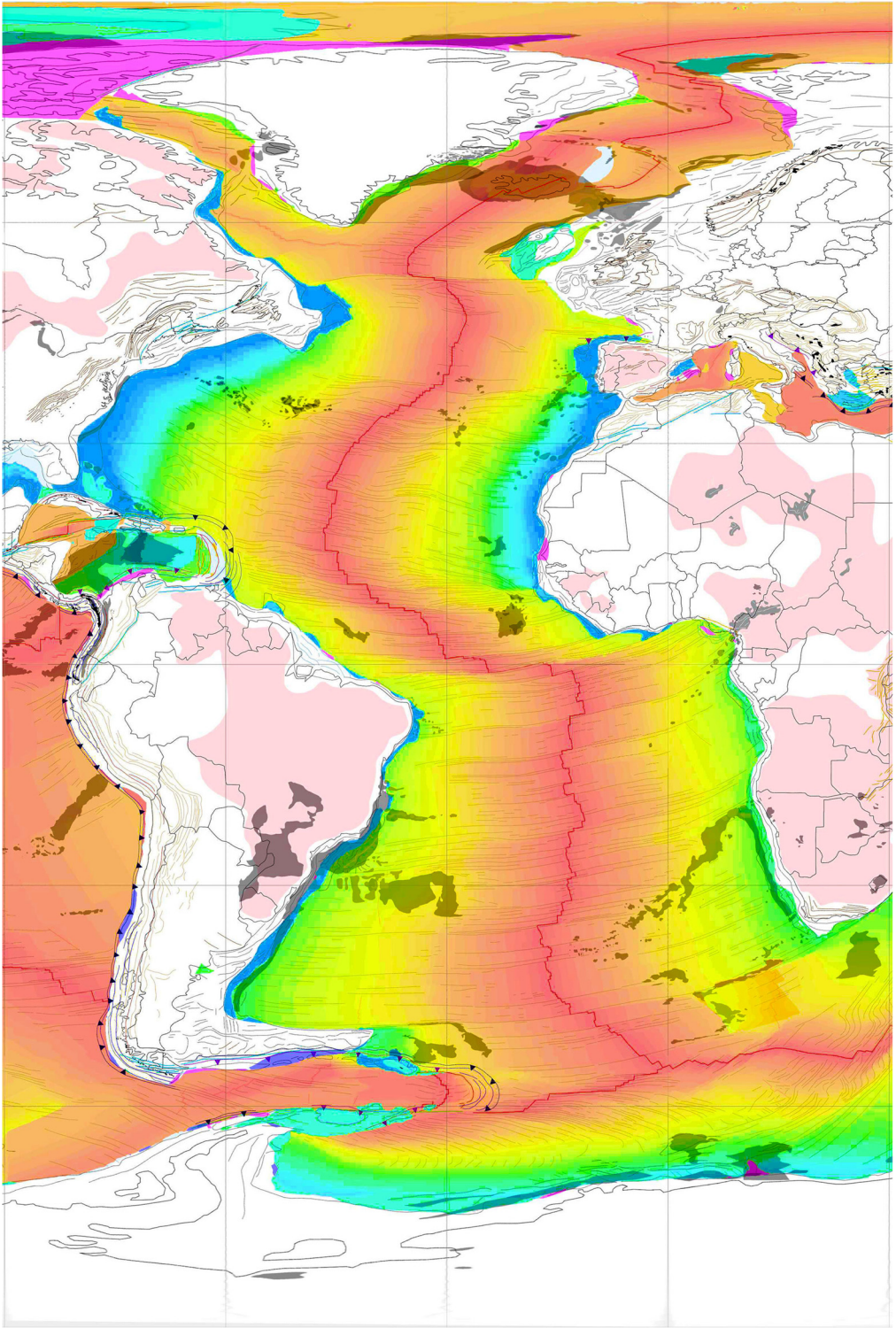


Fig. 8. *Continued.* (b) Tectonic Map of the World (part 2).

The Cretaceous world

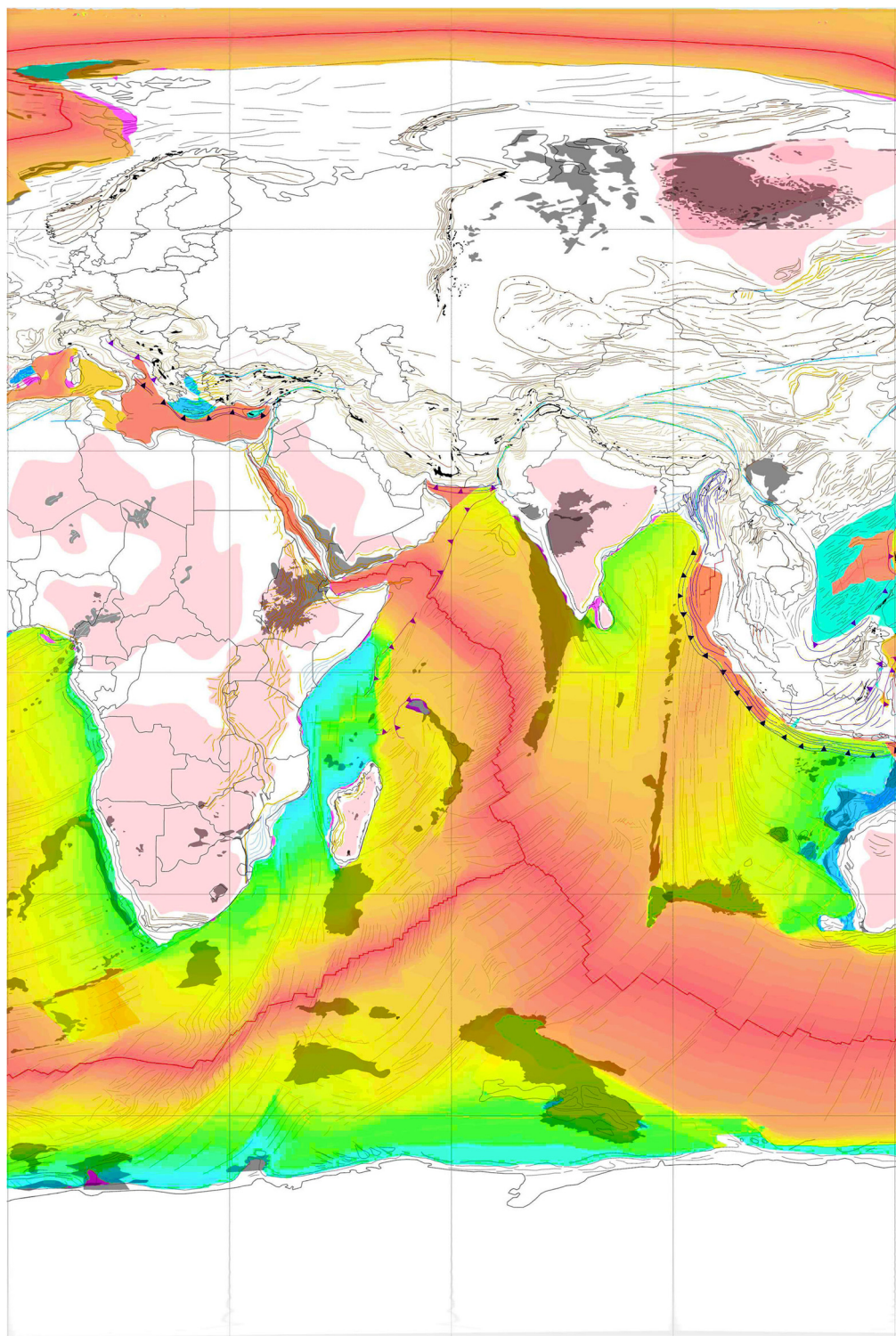


Fig. 8. *Continued.* (c) Tectonic Map of the World (part 3).

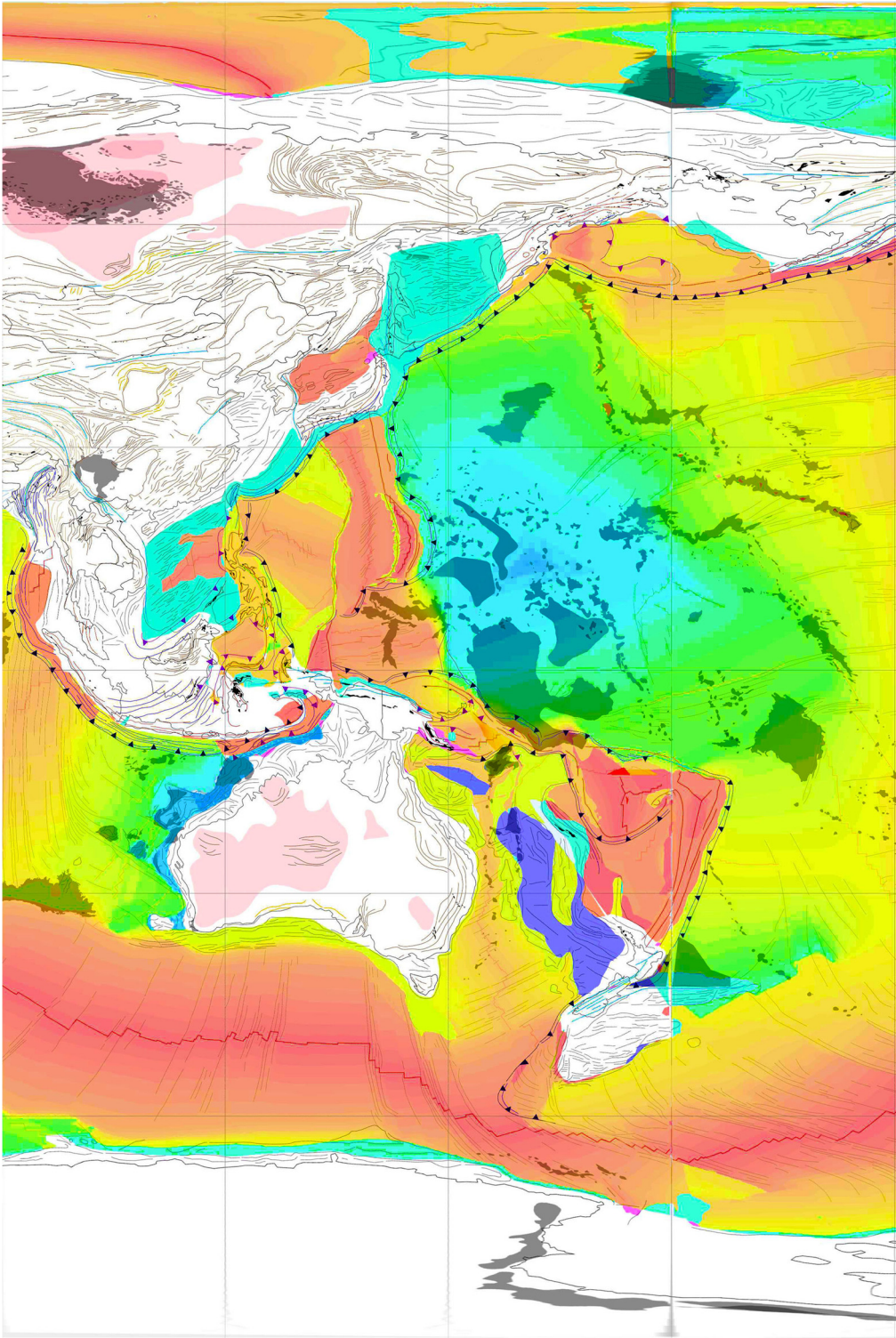


Fig. 8. *Continued.* (d) Tectonic Map of the World (part 4). See [Figure 9](#) for the legends of (a)–(d).

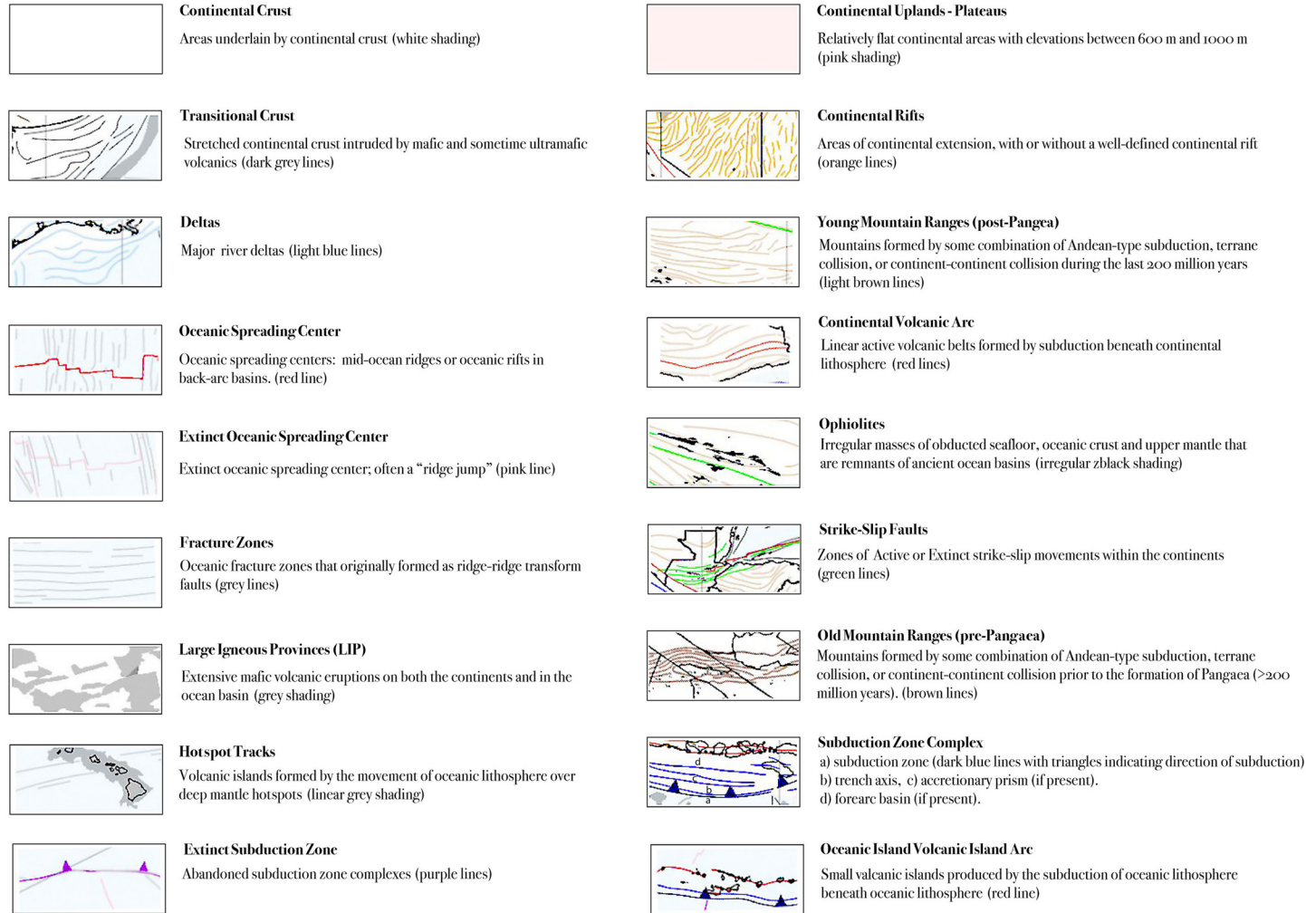


Fig. 9. Legend for the tectonic maps of the world shown in Figure 8.

Age of the ocean basins

As described in most introductory Earth Science textbooks, the polarity of Earth's magnetic field frequently reverses, causing the rocks that form at mid-ocean ridges to be magnetized in opposite directions. These linear magnetic anomalies were first dated and mapped on a global scale by [Larson *et al.* \(1985\)](#) and [Cande *et al.* \(1989\)](#). The first global digital compilation of oceanic magnetic anomalies was made by the research team at the Institute for Geophysics at the University of Texas in the mid-1980s and was published in the 1990s ([Royer *et al.* 1992a, b](#); [Müller *et al.* 1993a, b, 1997](#)) and updated by [Müller *et al.* \(2008a, b\)](#) and [Seton *et al.* \(2020, 2023\)](#).

Oceanic fracture zones

Major oceanic fracture zones generally form at right angles to the mid-ocean ridges. In many cases, the zigzag pattern of major fracture zones represents the offset patterns of the continental rifts that formed when the continents began to separate. Often oceanic fracture zones can be traced from one side of the ocean to the other side (e.g. Romanche, St Paul and Falkland–Aghulas fracture zones: [Granot and Dymant 2015](#)) and therefore provide important constraints on the pre-break-up configuration of the continents. Also shown in [Figure 8](#) is the 'tectonic fabric' of the ocean basins ([Gahagan *et al.* 1988](#); [Smith and Sandwell 1997](#); [Sandwell *et al.* 2013](#)) that has been generated by seafloor spreading, hotspot and subduction-related processes.

Hotspots and hotspot tracks

There are approximately 60 important mantle plumes or hotspots ([Richards *et al.* 1989](#); [Ernst 2014](#); [Koppers *et al.* 2021](#)), and approximately 30 of these hotspots were active during the Cretaceous. Volcanic islands and plateaus form where these hotspots penetrate the oceanic lithosphere. The motion of the plates over the relatively fixed hotspots generates hotspot tracks, the most well-known being the Hawaiian–Emperor hotspot track ([Fig. 8](#)). Hotspots generally do not produce hotspot tracks on continents because the thicker continental crust and lithosphere is more difficult to penetrate and often deflects the mantle plume. The heating and melting of the deep regions of the continental crust often produces kimberlites ([Crough *et al.* 1980](#)).

Ten well-dated hotspot tracks in the Atlantic and Indian oceans were used to constrain the motion of the plates relative to the mantle during the Cretaceous ([Müller *et al.* 1993a, b](#)). Several hotspot tracks in the Pacific, including the Hawaiian–Emperor hotspot track, were also used to constrain relative plate motions. Palaeomagnetic information, however,

indicates that these hotspots may have moved by about 20° relative to the Atlantic Ocean and Indian Ocean hotspots ([Antretter 2001](#); [Sager 2007](#); [Koppers *et al.* 2021](#)).

Palaeopoles and apparent polar wander (APW) paths

All plate tectonic reconstructions rely on palaeomagnetic measurements to estimate the latitudinal position of the continents. The inclination (I) of the remanent magnetization of an orientated rock sample provides a direct estimate of the ancient latitudinal position of a continent ([McElhinny 1973](#)). Although palaeobiogeographical, palaeoclimatic and tectonic information can provide additional constraints ([Fig. 7](#)), palaeopoles are the single most important quantitative line of evidence. For an excellent summary of palaeomagnetic methods see [McElhinny \(1973\)](#), [van der Voo \(1993\)](#), [Butler \(1998\)](#), [McElhinny and McFadden \(2000\)](#), [Tauxe \(2002\)](#) and [Lowrie \(2007\)](#). [Van Hinsbergen *et al.* \(2015\)](#) constructed a website (<https://palaeolatitude.org/>) that estimates the palaeolatitude of ancient geographical terranes based on palaeomagnetic information.

Although palaeomagnetic data are extremely useful, there are large uncertainties in the location of a palaeopole due to confounding diagenetic, tectonic and sedimentological effects. The greatest uncertainty is the age of magnetization. Often the age of the magnetization of a palaeomagnetic sample is reset by younger thermal and chemical events. For these reasons, individual palaeomagnetic determinations are often unreliable. It is not wise to rely on a single palaeopole to orientate a palaeocontinent or terrane, no matter how well determined the pole appears to be. Palaeomagnetic analysis is a statistical endeavour (see the grey dots and circle in [Fig. 10](#)). When building a plate tectonic model, it is necessary to use as many palaeomagnetic measurements as possible and not to reduce the available dataset by preselecting preferred palaeopoles prior to testing their validity. If possible, palaeopole compilations should be based on site-level statistics rather than aggregated palaeopole positions ([Vaes 2023](#); [Vaes *et al.* 2023](#)).

In order to provide a consistent and comprehensive palaeomagnetic framework, more than 15 000 palaeopoles covering the last 1.5 Gyr were compiled by [Elling \(2022\)](#) from four primary sources: [van der Voo \(1993\)](#) and [Scotese and van der Voo \(2017\)](#), with 1636 palaeopoles; [Torsvik *et al.* \(2008, 2012\)](#), with 941 palaeopoles; [Veikkolainen *et al.* \(2017\)](#), with 3798 palaeopoles; and [Pisarevsky \(2005\)](#), with 9514 palaeopoles. These palaeopoles were combined with additional sources: [Evans *et al.* \(2021\)](#), with 298 palaeopoles; [Merdith *et al.* \(2021\)](#), with 153 palaeopoles; [Tetley \(2018\)](#), [Tetley *et al.* \(2019\)](#), with 345 palaeopoles; [Pisarevsky *et al.* \(2022\)](#), with 10 023

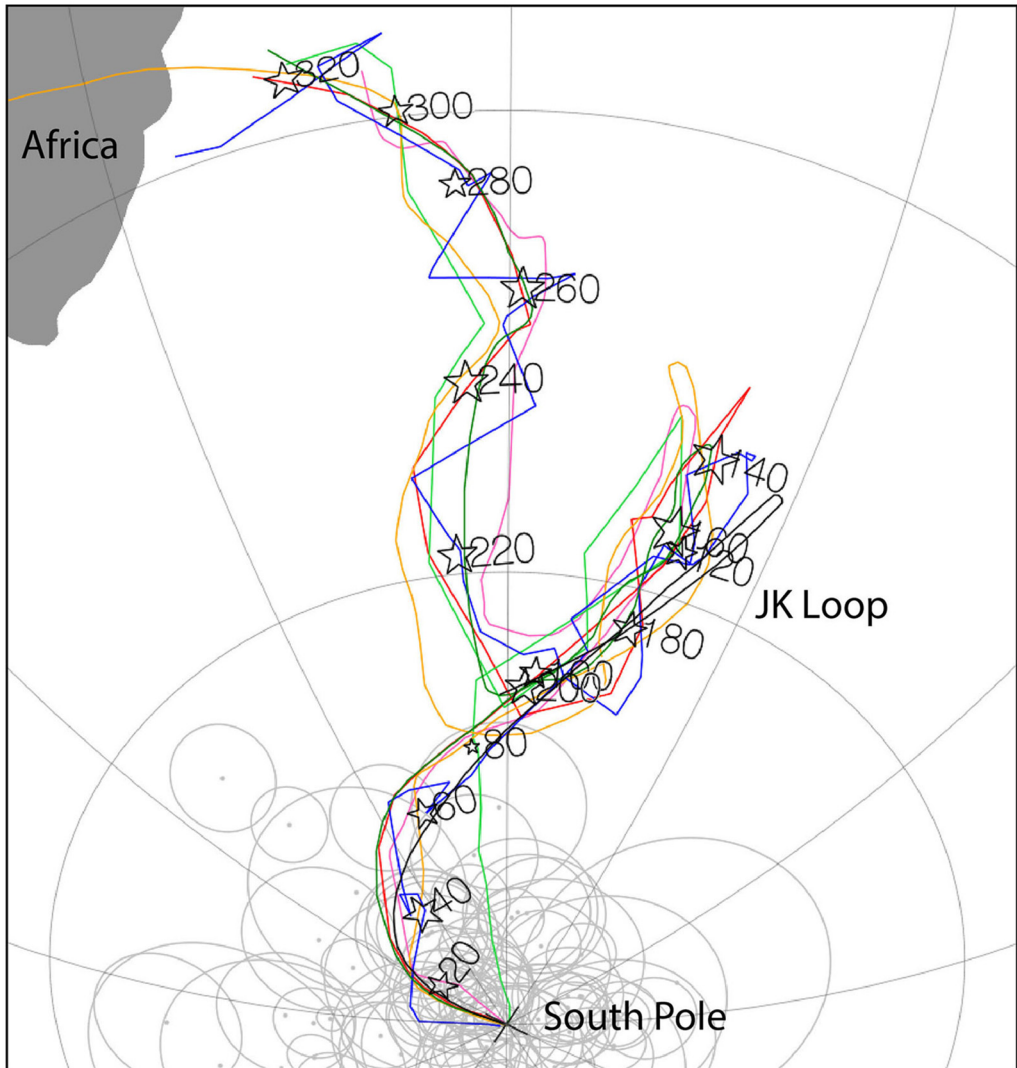


Fig. 10. Apparent polar wander path (APW) of the South Pole in African coordinates during the last 320 Myr (Carboniferous): stars, age in millions of years of mean path, the diameter of the star is proportional to the uncertainty (A95); black path, Schettino and Scotese (2005); red path, Torsvik *et al.* (2008, 2012); light green path, Scotese (2016*b*); orange path, Scotese and Elling (2017) and Elling (2022); dark green path, V  rard (2019); pink path, Meredith *et al.* (2021); blue path, Vaes *et al.* (2023). Note that the locations of the South Pole at 200 and 100 Ma are nearly coincident; the locations of the South Pole are also nearly coincident at 160 and 120 Ma. The blue path (Vaes *et al.* 2023) is more erratic because no smoothing factor has been applied. These zigs and zags are a good representation of the fundamental uncertainty of the palaeomagnetic data. The Cenozoic portion of the APW path of Scotese (2016*a, b*: in green) diverges from the other paths. This is due to the fact that it is based on a combined hotspot (mantle)–palaeomagnetic reference frame. This divergence implies that either the Earth’s magnetic field was not a perfect axial geocentric dipole during the Cenozoic, or that a rapid episode of true polar wander has occurred during the last 10 Myr. The dispersion of the palaeomagnetic data during the Cenozoic does not permit resolution of this dilemma. The grey dots and circles illustrate typical dispersion of individual palaeopoles (0–5 Myr) and precision estimates (A95) of each palaeopole.

palaeopoles; and Vaes (2023) and Vaes *et al.* (2023), with 705 palaeopoles. The palaeopoles from these compilations were standardized in a format that

included 18 principal fields (Table 4). A complete listing of all of the palaeopoles in the PALEOMAP Paleomagnetic Database is provided in the

Table 4. Palaeopole data fields

| | Field name | Abbreviation | Description |
|----|------------------------|--------------|---|
| a. | Unique Record Number | URN | Each pole in the database must have a unique identification number |
| b. | Description | Name | A descriptive name for the palaeopole, usually the name of the rock formation |
| c. | Plate Identification | PlateID | The identification number of the tectonic element where the sample site resides |
| d. | Site Latitude | SLat | The present-day latitude of the sample site |
| e. | Site Longitude | SLong | The present-day longitude of the sample site |
| f. | Palaeopole Latitude | PLat | The latitude of the palaeopole calculated from the inclination (I) and declination (D) of the remanent magnetization |
| g. | Palaeopole Longitude | PLong | The longitude of the palaeopole calculated from the inclination (I) and declination (D) of the remanent magnetization |
| h. | Palaeolatitude | PaleoLat | The ancient latitude of the sample site calculated from the inclination (I) of the remanent magnetization |
| i. | Declination | D | The declination of the remanent magnetization, i.e. the direction of the magnetic vector in the horizontal plane |
| j. | Inclination | I | The inclination of the remanent magnetization, i.e. the dip of the magnetic vector in the vertical plane |
| k. | Quality Score | QSum | An estimate of the quality of the palaeopole based on the reliability criteria of Van der Voo (1993) . The maximum value is 7 |
| l. | Maximum Age | OldAge | The oldest possible age of the remanent magnetization |
| m. | Minimum Age | YoungAge | The youngest possible age of the remanent magnetization |
| n. | Mean Age | Mean Age | The average of the oldest and youngest ages of magnetization |
| o. | alpha-95 | A95 | Fisherian statistic that estimates the precision of the geographical location of the palaeopole. An A95 value <5° is a good result |
| p. | Author(Year) | Ref | The name of the primary author and the year of publication |
| q. | Database | DB | The name of the palaeomagnetic database that was the source of the palaeopole |
| r. | Database Record Number | DBNo | The reference number assigned to the palaeopole in the original database |

Supplementary material. The PALEOMAP Global Plate Tectonic Model was then used to reconstruct the palaeocoordinates of these palaeopoles.

Global mean poles (GMPs) describing the location of the Earth's spin axis through time were determined at intervals of 10, 20 and 50 Myr, depending on the age of the plate tectonic reconstruction. Fisherian statistics ([Fisher 1953](#); [Fisher *et al.* 1987](#)) were calculated using the online tools at the <https://palaeolatitude.org/> website ([van Hinsbergen *et al.* 2015](#)). Each palaeopole was only used once when calculating the GMPs in order to minimize the bias of poorly dated, long-lived palaeopoles. [Table 5](#) lists the Mesozoic and Cenozoic global mean palaeopoles in the reference frames of Africa, North America, South America, Europe, India, China, Australia and Antarctica. A complete list of the palaeopoles used to calculate these GMPs is given in the [Supplementary material](#).

[Figure 10](#) plots the apparent polar wander path of the South Pole in African coordinates over the last 320 Myr. The locations of the palaeopoles that comprise the consensus APW path (stars in [Fig. 10](#)) are given in [Table 5](#). These independently determined

apparent polar wander paths are in good agreement. The southward motion of Africa during the Jurassic was reversed in the Early Cretaceous (Jurassic–Cretaceous (JK) Loop) and Africa moved steadily northwards during the Cretaceous and Cenozoic.

Continental tectonics

While most of the direct evidence for plate motions comes from the ocean basins, the continents also provide important clues regarding the history of plate tectonic interactions. Five important continental lines of evidence are: (1) the timing of continental rifting; (2) subduction-related volcanic activity along Andean-type mountain ranges, continental island arcs and oceanic island arcs; (3) the obduction of ophiolites onto continents due to the closure both of back-arc basins and a major ocean; (4) the complex tectonic histories associated with convergent plate boundaries; and (5) the collision of exotic terranes along ocean-facing active continental. Some of the key sources that were used to construct the history of continental tectonics are given in [Table 6](#). These references are listed in chronological order,

Table 5. Apparent polar wander paths for major continents according to the PALEOMAP Global Plate Model (north poles)

| Age | Africa (701) | | North America (101) | | South America (201) | | Eurasia (301) | | India (501) | | Australia (801) | | Antarctica (802) | | Consensus APW Africa (701) | | A95 |
|-----|--------------|----------|---------------------|----------|---------------------|----------|---------------|----------|-------------|----------|-----------------|----------|------------------|----------|----------------------------|----------|-----|
| | Longitude | Latitude | Longitude | Latitude | Longitude | Latitude | Longitude | Latitude | Longitude | Latitude | Longitude | Latitude | Longitude | Latitude | Longitude | Latitude | |
| 0 | 0 | 90.0 | 0 | 90.0 | 0 | 90.0 | 0 | 90.0 | 0 | 90.0 | 0 | 90.0 | 0 | 90.0 | 0 | −90.0 | |
| 10 | −105.9 | 89.4 | −151.4 | 89.4 | −44.5 | 83.0 | −44.5 | 83.0 | −44.5 | 83.0 | −44.5 | 83.0 | 16.8 | 88.9 | −4.5 | −86.7 | 1.6 |
| 20 | −113.4 | 88.5 | −156.9 | 88.6 | −49.5 | 78.2 | −49.5 | 78.2 | −49.5 | 78.2 | −49.5 | 78.2 | 19.9 | 88.7 | 3.7 | −85.0 | 2.0 |
| 30 | −126.0 | 86.6 | −171.9 | 87.6 | −50.5 | 72.7 | −50.5 | 72.7 | −50.5 | 72.7 | −50.5 | 72.7 | 48.6 | 88.7 | 17.2 | −83.2 | 2.2 |
| 40 | −128.0 | 83.8 | −168.3 | 85.6 | −54.1 | 67.3 | −54.1 | 67.3 | −54.1 | 67.3 | −54.1 | 67.3 | 17.8 | 89.3 | 25.6 | −80.5 | 2.5 |
| 50 | −127.5 | 79.9 | −161.6 | 82.3 | −64.3 | 59.1 | −57.1 | 64.8 | −64.3 | 59.1 | −57.1 | 64.8 | −97.9 | 88.9 | 34.1 | −77.3 | 2.2 |
| 60 | −128.5 | 77.7 | −159.5 | 79.5 | −70.1 | 48.4 | −58.1 | 64.3 | −70.1 | 48.4 | −58.1 | 64.3 | −122.8 | 88.6 | 39.9 | −74.5 | 2.0 |
| 70 | −126.6 | 74.9 | −157.6 | 77.0 | −73.5 | 35.7 | −58.7 | 62.4 | −73.5 | 35.7 | −58.7 | 62.4 | −102.9 | 87.3 | 48.3 | −72.8 | 1.4 |
| 80 | −125.7 | 71.1 | −164.1 | 75.8 | −73.2 | 26.8 | −57.4 | 61.5 | −73.2 | 26.8 | −57.4 | 61.5 | −98.7 | 87.1 | 53.2 | −70.9 | 1.0 |
| 90 | −126.5 | 70.3 | −179.4 | 77.3 | −72.8 | 24.2 | −39.4 | 60.9 | −72.8 | 24.2 | −39.4 | 60.9 | 65.8 | 84.5 | 59.2 | −69.3 | 1.4 |
| 100 | −124.9 | 66.7 | 164.9 | 76.9 | −74.7 | 20.3 | −30.6 | 59.5 | −74.7 | 20.3 | −30.6 | 59.5 | 71.4 | 80.0 | 64.3 | −66.2 | 2.0 |
| 120 | −100.0 | 56.9 | 177.0 | 78.0 | −65.7 | 5.7 | −28.5 | 47.5 | −65.7 | 5.7 | −28.5 | 47.5 | 18.9 | 74.7 | 80.3 | −57.0 | 2.1 |
| 140 | −103.4 | 48.7 | 172.8 | 70.2 | −62.8 | −6.3 | −34.2 | 42.2 | −62.8 | −6.3 | −34.2 | 42.2 | −4.0 | 72.9 | 80.9 | −50.7 | 3.1 |
| 160 | −110.7 | 58.4 | 125.5 | 71.4 | −56.6 | 8.1 | −12.2 | 47.4 | −56.6 | 8.1 | −12.2 | 47.4 | 39.9 | 66.1 | 78.9 | −55.8 | 3.1 |
| 180 | −108.4 | 64.2 | 96.6 | 69.8 | −49.8 | 12.9 | −0.5 | 44.6 | −49.8 | 12.9 | −0.5 | 44.6 | 45.7 | 57.9 | 76.7 | −62.5 | 2.2 |
| 200 | −120.5 | 68.5 | 81.6 | 64.6 | −49.1 | 18.5 | 8.2 | 46.9 | −49.1 | 18.5 | 8.2 | 46.9 | 55.8 | 54.5 | 62.7 | −67.1 | 2.4 |
| 220 | −129.6 | 59.1 | 96.3 | 58.4 | −58.7 | 15.1 | −2.5 | 54.0 | −58.7 | 15.1 | −2.5 | 54.0 | 60.7 | 64.0 | 53.9 | −58.7 | 2.5 |
| 240 | −127.1 | 48.8 | 111.4 | 54.9 | −65.7 | 7.3 | −20.2 | 55.5 | −65.7 | 7.3 | −20.2 | 55.5 | 54.8 | 74.2 | 56.0 | −47.9 | 2.8 |

The Consensus APW is the mean apparent polar wander path based on multiple estimates (South Pole, see Fig. 10).

Table 6. Continental tectonics

| Date | Author | Title |
|--|--|---|
| A. Continental rifting and the formation of passive margins | | |
| 1965 | E. Bullard, J.E. Everett and A.G. Smith | The fit of the continents around the Atlantic |
| 1970 | A.G. Smith and A. Hallam | The fit of the southern continents |
| 1974 | C.A. Burk and C.L. Drake | The Geology of Continental Margins |
| 1974 | J.F. Dewey and K.C.A. Burke | Hot spots and continental break-up: Implications for collisional orogeny |
| 1981 | P.F. Barker and I.A. Hill | Back-arc extension in the Scotia Sea |
| 1983 | P. Morgan and B.H. Baker | Processes of Continental Rifting |
| 1985 | S.P. Srivastava | Evolution of the Eurasian Basin and its implications to the motion of Greenland along the Nares Strait |
| 1986 | S.P. Srivastava and C. Tapscott | Plate kinematics of the North Atlantic |
| 1987 | L.A. Lawver and C.R. Scotese | A revised reconstruction of Gondwanaland |
| 1988 | J.D. Fairhead | Mesozoic plate tectonic reconstructions of the South Atlantic Ocean: the role of the West and Central African Rift System |
| 1988 | C. Mc. Powell, S.R. Roots, and J.J. Veevers | Pre-breakup continental extension in East Gondwanaland and the early opening of the eastern Indian Ocean |
| 1988 | P. Unternehr, P. Curie, J.L. Olivet, J. Goslin, and P. Beuzart | South Atlantic fits and intraplate boundaries in Africa and South America |
| 1989 | J.D. Edwards and P.A. Santogrossi | Divergent/Passive Margin Basins |
| 1989 | S.P. Srivastava and W.R. Roest | Sea-floor spreading in the Labrador Sea; a new reconstruction |
| 1991 | A. Salvador | The Gulf of Mexico |
| 1992 | P.A. Ziegler | Geodynamics of Rifting, Volume I. Case History Studies of Rifts: Europe and Asia |
| 1992 | J.S. Watkins, Feng, Z.Q., and K.J. McMillen | Geology and Geophysics of Continental Margins |
| 1998a | C. Gaina, R.D. Müller, J.Y. Royer, J. Stock, J. Hardebeck, and P.A. Symonds | The tectonics history of the Tasman Sea: a puzzle with 13 pieces |
| 2000 | J. Skogseid, S. Planke, J.I. Faleide, T. Pedersen, O. Eldholm, and F. Neverdal | NE Atlantic continental rifting and volcanic margin formation |
| 2001 | A.M.C. Sengor and B.A. Natal'in | Rifts of the world. Mantle plumes: Their identification through time |
| 2001 | G.M. Stampfli, J. Mosar, P. Favre, A. Pillevuit, and J.C. Vanay | Permo-Mesozoic evolution of the western Tethys realm: the Neo-Tethys East Mediterranean Basin connection |
| 2001 | R.C.L. Wilson, R.B. Whitmarsh, B. Taylor, and N. Froitzheim | Non-volcanic Rifting of Continental Margins: A Comparison of Evidence from Land and Sea |
| 2002 | M.A. Menzies, S.L. Klemperer, C.J. Ebinger, and J. Baker | Volcanic Rifted Margins |
| 2002 | R.W. Renault and G.M. Ashley | Sedimentation in Continental Rifts |
| 2008 | D.C. Bradley | Passive margins through Earth history |
| 2008 | H. Johnson, T. Dore, R.W. Gatliff, R. W. Holdsworth, E.R. Lundin. and J.D. Ritchie | The Nature and Origin of Compression in Passive Margins |
| 2011 | L. Beccaluva, G. Bianchini, and M. Wilson | Volcanism and Evolution of the African Lithosphere |
| 2012a | D.G. Roberts and A.W. Bally | Regional Geology and Tectonics :Phanerozoic Rift systems and Sedimentary Basins |
| 2012b | D.G. Roberts and A.W. Bally | Regional Geology and Tectonics: Phanerozoic Passive Margins, Cratonic Basins, and Global Tectonic Maps |
| B. Subduction along Andean-type margins and continental volcanic arcs | | |
| 1970 | J.M. Bird and J.F. Dewey | Lithosphere plate-continental margin tectonics and the evolution of the Appalachian orogen |
| 1975 | W.G. Ernst | Subduction Zone Metamorphism |

(Continued)

The Cretaceous world

Table 6. *Continued.*

| Date | Author | Title |
|-------|---|--|
| 1977 | M. Talwani and W.C. Pitman III | Island Arcs, Deep Sea Trenches, and Back-Arc Basins |
| 1981 | F.J. Vine and A.G. Smith | Extensional Tectonics Associated with Convergent Boundaries |
| 1982 | J.K. Leggett | Trench–Forearc Geology: Sedimentation and Tectonics on Modern and Ancient Active Plate Margins |
| 1988 | J. Pindell, S.C. Cande, W.C. Pitman III, D. B. Rowley, J.F. Dewey, J.F. LaBrecque, and W. Haxby | A plate kinematic framework for models of Caribbean evolution |
| 1988 | M.I. Ross and C.R. Scotese | A hierarchical tectonic model of the Gulf of Mexico and Caribbean Region |
| 1989 | C.S. Hutchison | Geological Evolution of Southeast Asia |
| 1990 | G. Dengo and J.E. Case | The Caribbean Region |
| 1990 | R.S. D’Lemos, R.S. Strachan, and C.G. Topley | The Cadomian Orogeny |
| 1990 | J. Pindell and S.F. Barrett | Geological evolution of the Caribbean region: a plate tectonic perspective |
| 1991 | K.T. Biddle | Active Margin Basins |
| 1992a | B.C. Burchfiel, P.W. Lipman, and G.A. Davis | Tectonic overview of the Cordilleran orogen in the western United States |
| 1992b | B.C. Burchfiel, D.S. Cowan, and G.A. Davis | The Cordilleran Orogen: Conterminous U.S. |
| 1995 | P. Mann | Geologic and Tectonic Development of the Caribbean Plate Boundary in Southern Central America |
| 1996 | G.E. Bebout, D.W. Scholl, S.H. Kirby, and J.P. Platt | Subduction: Top to Bottom |
| 1998 | R.J. Pankhurst and C.W. Rapela | The Proto-Andean Margin of Gondwana |
| 2000 | U.G. Cordani, E.J. Milani, A. Thomaz-Filho, and D.A. Campos | Tectonic Evolution of South America |
| 2004 | S. Lamb | Devil in the Mountain: A Search for the Origin of the Andes |
| 2006 | S.M. Kay and V.A. Ramos | Evolution of an Andean margin: A tectonic and magmatic view from the Andes to the Neuquen Basin (35°–39° S lat) |
| 2006 | O. Oncken, G. Chong, G. Fraunz, P. Giese, H.J. Götze, V.A. Ramos, M.R. Strecker, and P. Wigger | The Andes: Active Subduction Orogeny |
| 2009 | J. Pindell and L. Kennan | Tectonic evolution of the Gulf of Mexico, Caribbean, and northern South America in the mantle reference frame: an update |
| 2014 | A. Gómez-Tuena, S.M. Straub, and G.F. Zellmer | Orogenic Andesites and Crustal Growth |
| 2015 | P.G. DeCelles, M.N. Ducea, B. Carrapa, and P.A. Kapp | Geodynamics of the Cordilleran Orogenic System: The Central Andes of Argentina and Northern Chile |
| 2016 | N.R. McKenzie, B.K. Horton, S.E. Loomis, D.F. Stockli, N.J. Planavsky, and C.T.A. Lee | Continental arc volcanism as the principal driver of icehouse–greenhouse variability |
| 2016 | T. Moreno, S. Wallis, T. Kojima, and W. Gibbons | The Geology of Japan |
| 2017 | W. Cao, C.T.A. Lee, and J.S. Lackey | Episodic nature of continental arc activity since 750 Ma: A global compilation |
| 2019 | B. Vaes, D.J.J. van Hinsbergen, L.M. Boschman | Reconstruction of subduction and back-arc spreading in the NW Pacific and Aleutian Basin: Clues to the causes of Cretaceous and Eocene plate reorganizations |
| 2022 | L.M. Boschman | Andean mountain building since the Late Cretaceous: A paleoelevation reconstruction |

(Continued)

Table 6. *Continued.*

| Date | Author | Title |
|--|--|--|
| C. Obduction of ophiolites onto continents due to the closure of back-arc basins and large ocean basins | | |
| 1977 | R.G. Coleman | Ophiolites: Ancient Oceanic Lithosphere? |
| 1980 | A. Panayiotou | Ophiolites: Proceedings of the International Ophiolite Symposium |
| 1983 | G.J.H. McCall | Ophiolitic and Related Melanges |
| 1984 | I.G. Gass, S.J. Lippard, and A.W. Shelton | Ophiolites and Oceanic Lithosphere |
| 2000 | Y. Dilek, Moores, E.M., D. Elthon, and A. Nicolas | Ophiolites and Oceanic Crust: New Insights from Field Studies and the Ocean Drilling Program |
| 2002 | E.M. Moores | Pre–1 Ga (pre-Rodinian) ophiolites: Their tectonic and environmental implications |
| 2003 | Y. Dilek and P.T. Robinson | Ophiolites in Earth History |
| 2004 | W.G. Ernst | Serpentine and Serpentinites: Mineralogy, Petrology, Geochemistry, Ecology, Geophysics, and Tectonics |
| 2006 | M. Metzler | The Formation and Obduction of Ophiolites Since the Late Precambrian |
| 2008 | J.E. Wright and J.W. Shervais | Ophiolites, Arcs, Batholiths: A Tribute to Cliff Hopson |
| 2009 | Y. Dilek and P.T. Robinson | Special Issue on Mantle Dynamics and Crust–Mantle Interactions in Collisional Orogens |
| 2014 | Y. Dilek and H. Furnes | Ophiolites |
| 2021 | Wakabayashi and Dilek | |
| D. Continent–continent collisions | | |
| 1964 | A. Gansser | Geology of the Himalayas |
| 1966 | J.T. Wilson | Did the Atlantic Close and then Re-open? |
| 1968 | E.E. Oxburgh | The Geology of the Eastern Alps |
| 1970 | W. Hamilton | The Uralides and the Motion of the Russian and Siberian Platforms |
| 1970 | J. Rodgers | The Tectonics of the Appalachians |
| 1972 | T. Strand and O. Kulling | Scandinavian Caledonides |
| 1973 | J.F. Dewey and K.C.A. Burke | Tibetan, Variscan, and Precambrian basement reactivation: products of continental collision |
| 1973 | J.F. Dewey, W.C. Pitman III, W.B.F. Ryan, and J. Bonin | Plate Tectonics and the Evolution of the Alpine System |
| 1974 | A.M. Spencer | Mesozoic–Cenozoic Orogenic Belts: Data for Orogenic Studies |
| 1975 | P. Molnar and P. Tapponnier | Cenozoic tectonics of Asia: Effects of a continental collision |
| 1975 | J.H. Ostrom and P.M. Orville | Tectonics and Mountain Ranges, A special volume of the American Journal of Science Dedicated to John Rodgers |
| 1979 | A.L. Harris, C.H. Holland, and B.E. Leake | The Caledonides of the British Isles – reviewed |
| 1981 | K.R. McClay and N.J. Price | Thrust and Nappe Tectonics |
| 1982 | K.J. Hsü | Mountain Building Processes |
| 1983 | R.D. Hatcher, H. William, and I. Zietz | Contributions to the Tectonics and Geophysics of Mountain Chains |
| 1985 | D.G. Gee and B.A. Strutt | The Caledonide Orogen – Scandinavia and Related Areas, Parts 1 and 2 |
| 1987 | J.P. Schaer and J. Rodgers | The Anatomy of Mountain Ranges |
| 1988 | A. L. Harris and D.J. Fettes | The Caledonian-Appalachian Orogen |
| 1988 | P.F. Hoffman | Birth of a Craton: Early Proterozoic Assembly and Growth of Laurentia |
| 1988 | R.D. Nance, T.R. Worsley, and J.B. Moody | The Supercontinent Cycle |
| 1989 | M.P. Coward, Dietrich, D., and R.G. Park | Alpine Tectonics |
| 1989 | R.A. Gayer | The Caledonide Geology of Scandinavia |
| 1991 | R. Meissner, T. Wever, and P. Sadowiak | Continental collisions and seismic signature |

(Continued)

The Cretaceous world

Table 6. *Continued.*

| Date | Author | Title |
|--|---|---|
| 1995 | H. Williams | Geology of the Appalachian-Caledonian Orogen in Canada and Greenland |
| 1996 | A. Yin and T.M. Harrison | The Tectonic Evolution of Asia |
| 1996 | O. Yilmaz, I.O. Norton, D. Leary, and R.J. Chuchla | Tectonic evolution and paleogeography of Europe |
| 1997 | J.P. Burg and M. Ford | Orogeny Through Time |
| 1999 | A. Macfarlane, R.B. Sorkhabi, and J. Quade | Himalaya and Tibet: Mountain Roots to Mountain Tops |
| 2000 | W. Franke, V. Haal, O. Oncken, and D. Tanner | Orogenic Processes: Quantification and Modelling in the Variscan Belt |
| 2001 | M.S. Hendrix and G.A. Davis | Paleozoic and Mesozoic tectonic evolution of central Asia: From continental assembly to intracontinental deformation |
| 2002 | J.R.M. Catalan, R.D. Hatcher, R. Arenas, and F.D. Garcia | Variscan–Appalachian dynamics: The building of the late Paleozoic basement |
| 2002 | J.A. Winchester, T.C. Pharoah, and J. Verniers | Palaeozoic Amalgamation of Central Europe |
| 2004 | G.M. Stampfli and G.D. Borel | The TRANSMED transects in space and time: Constraints on the paleotectonic evolution of the Mediterranean domain |
| 2006 | G.M. Stampfli and H.W. Kozur | Europe from the Variscan to the Alpine cycles |
| 2007 | R.D. Hatcher, Carlson, M.P., and J.H. McBride | 4-D Framework of Continental Crust |
| 2007 | U. Linnemann, R.D. Nance, P. Kraft, and G. Zulauf | The Evolution of the Rheic Ocean: From Avalonian–Cadomian Active Margin to Alleghenian–Variscan Collision |
| 2008 | S. Siegesmund, B. Fügenschuh, and N. Froitzheim | Tectonic Aspects of the Alpine–Dinaride–Carpathian System |
| 2009 | D.J.J. van Hinsbergen, M.A. Edwards, and R. Govers | Collision and Collapse at the Africa–Arabia–Eurasia Subduction Zone |
| 2011 | D.C. Bradley | Secular trends in the geologic record and the supercontinent cycle |
| 2011 | R. Gloaguen and L. Ratschbacher | Growth and Collapse of the Tibetan Plateau |
| 2011 | A. Schettino and E. Turco | Tectonic history of the western Tethys since the late Triassic |
| 2013 | R.D. Nance and J.B. Murphy | Origins of the supercontinent cycle |
| 2014 | F. Corfu, D. Gasser, and D.M. Chew | New Perspectives on the Caledonides of Scandinavia and Related Areas |
| 2014 | R.D. Nance, J.B. Murphy, and M. Santosh | The supercontinent cycle: A retrospective essay |
| 2014 | O.A. Pfiffner | Geology of the Alps |
| 2015 | J.P. Hibbard, J.C. Pollock, J.B. Murphy, C.R. van Staal, and J.D. Greenough | Reeltime Geological Syntheses: Remembering Harold ‘Hank’ Williams |
| 2017 | C.J. Hawkesworth, P.A. Cawood, B. Dhuime, and K.I.S. Kemp | Earth’s continental lithosphere through time |
| 2019 | A.S. Merdith, S.E. Williams, S. Brune, A.S. Collins, and R.D. Müller | Rift and plate boundary evolution across two supercontinent cycles |
| 2020 | D.J.J. van Hinsbergen, T.H. Torsvik, S.M. Schmid, L.C. Matenco, M. Maffione, R.L.M. Vissers, D. Gürer, and W. Spakman | Orogenic architecture of the Mediterranean region and kinematic reconstruction of its tectonic evolution since the Triassic |
| 2021 | A.S. Collins, M.L. Blades, A.S. Merdith, and J.D. Foden | Closure of the Proterozoic Mozambique Ocean was instigated by a late Tonian plate reorganization event |
| 2023 | Z.X. Li, Y. Liu, and R. Ernst | A dynamic 2000–540 Ma earth history: from cratonic amalgamation to the age of supercontinent cycle |
| E. Exotic terranes and accretion along active continental margins | | |
| 1974 | C. Burrett | Plate tectonics and the fusion of Asia |
| 1983 | M. Audley-Charles | Reconstruction of eastern Gondwanaland |

(Continued)

Table 6. *Continued.*

| Date | Author | Title |
|------|---|---|
| 1983 | R.M. Friedman | Accretionary History of Western North America during the Mesozoic and Cenozoic Eras |
| 1984 | M. Audley-Charles | Cold Gondwana, warm Tethys, and Tibetan Lhasa Block |
| 1984 | I. Metcalfe | Stratigraphy, palaeontology and palaeogeography of the Carboniferous of Southeast Asia |
| 1985 | D.C. Engebretson, A. Cox, and R.G. Gordon | Relative Motions between Oceanic and Continental Plates in the Pacific Basin |
| 1988 | M. Audley-Charles | Evolution of the southern margin of Tethys (North Australian region) from early Permian to late Cretaceous |
| 1988 | A.M.C. Şengör, D. Altiner, A. Cin, T. Ustaomer, and K. Hsü | Origin and assembly of the Tethyside orogenic collage at the expense of Gondwana Land |
| 1989 | J.W. Hillhouse | Deep Structure and the Past Kinematics of Accreted Terranes |
| 1989 | D.G. Howell | Tectonics of Suspect Terranes: Mountain Building and Continental Growth |
| 1990 | Y. Isozaki, S. Maruyama, and F. Furuoka | Accreted oceanic materials in Japan |
| 1991 | J.F. Dewey, I.G. Gass, G.B. Curry, N.B.W. Harris, and A.M.C. Sengor | Allochthonous Terranes |
| 1992 | B.C. Burchfiel, P.W. Lipman, and G.A. Davis | Tectonic overview of the Cordilleran orogen in the western United States |
| 1992 | H. Gabrielse and C.J. Yorath | Geology of the Cordilleran Orogen in Canada |
| 1993 | I. Metcalfe | Southeast Asian terranes: Gondwanaland origins and evolution |
| 1994 | M.G. Mihalynuk, J. Nelson, and L.J. Diakow | Cache Creek terrane entrapment: Oroclinal paradox with the Canadian Cordillera |
| 1996 | J.W.H. Monger and W.J. Nokleberg | Evolution of the northern North American Cordillera: generation, fragmentation, displacement and accretion of successive North American plate margin arcs |
| 1996 | R.D. Nance and M.D. Thompson | Avalonian and Related Peri-Gondwanan Terranes of the Circum-North Atlantic |
| 1996 | A.M.C. Şengör and B.A. Nata'lin | Paleotectonics of Asia: fragments of a synthesis |
| 1999 | I. Metcalfe | Gondwana dispersion and Asian accretion: An overview |
| 2000 | R.A. Price and J.W.H. Monger | A transect of the southern Canadian Cordillera from Calgary to Vancouver |
| 2005 | A.P.M. Vaughan, P.T. Leat, and R.J. Pankhurst | Terrane Processes at the Margins of Gondwana |
| 2006 | J.W. Haggart, R.J. Enkin, and J.W.H. Monger | Paleogeography of the North American Cordillera: Evidence for and Against Large-Scale Displacements |
| 2007 | J.W. Sears, T.A. Harms, and C.A. Evenchick | Whence the Mountains? Inquiries into the Evolution of Orogenic Systems: A Volume in Honor of Raymond A. Price |
| 2007 | B.F. Windley, D. Alexeiev, W.J. Xiao, A. Kroner, and G. Bardach | Tectonic models for the accretion of the Central Asian Orogenic Belt |
| 2008 | J.W. H. Monger | The Evolution of Canada's Western Mountains |
| 2008 | I.Y. Safonova, V. Simonov, M. Buslov, T. Ota, and S. Maruyama | Neoproterozoic basalts of the Paleo-Asian Ocean (Kurai accretionary zone, Gorny Altai, Russia): geochemistry, petrogenesis, and geodynamics |
| 2010 | Y. Isozaki, K. Aoki, T. Nakam, and S. Yanai | New insight into a subduction-related orogen: a reappraisal of the geotectonic framework and evolution of the Japanese Islands |
| 2010 | L.M. Parfenov, N.A. Berzin, G. Bardach, V.G. Belichenko, A.N. Bulgatov, A.N. Dril, and others | Metallogenesis and Tectonics of Northeast Asia |

(Continued)

Table 6. *Continued.*

| Date | Author | Title |
|-------|--|---|
| 2011 | I. Metcalfe | Southeast Asian terranes: Gondwanaland origins and evolution |
| 2011 | L.M. Parfenov, W.J. Nokleberg, N.A. Berzin, G. Bardach, and others | Tectonic and metallogenic model for Northeast Asia |
| 2011 | J.P. Burg | The Asia–Kohistan–India Collision: Review and Discussion |
| 2013 | T. Kusky, B. Windley, I. Safonova, K. Wakita, J. Wakabayashi, A. Polat, and M. Santosh | Recognition of ocean plate stratigraphy in accretionary orogens through Earth history: A record of 3.8 billion years of sea floor spreading, subduction, and accretion. |
| 2014 | C. Burrett, K. Zaw, S. Meffre, C.K. Lai, K. Somboon, and C. Pol | The configuration of Greater Gondwana – Evidence from LA ICPMS, U–Pb geochronology of detrital zircons from the Palaeozoic and Mesozoic of Southeast Asia and China |
| 2014 | Y. Isozaki | Memories of pre-Jurassic lost oceans: How to retrieve them from extant lands. |
| 2014b | A.M.C. Şengör, B.A. Nata’lin, R. van der Voo, and G. Sunal | A new look at the Altaids: A superorogenic complex in Northern and Central Asia as a factory of continental crust, Part II |
| 2014a | A.M.C. Şengör, B.A. Nata’lin, G. Sunal, and R. van der Voo | A new look at the Altaids: A superorogenic complex in Northern and Central Asia as a factory of continental crust, Part I |
| 2014 | S. Zahirovic, M. Seton, and R.D. Müller | The Cretaceous and Cenozoic tectonic evolution of Southeast Asia |
| 2024 | E.L. Advokaat and D.J.J. van Hinsbergen | Finding Argoland: Reconstructing a microcontinental archipelago from the SE Asian accretionary orogen |
| 2023 | A.M.C. Sengor, D. Altiner, C. Zabcı, G. Sunal, N. Lom, E. Aylan, and T. Öner | On the nature of the Cimmerian Continent |

providing a concise history of the development of our ideas on these topics. The lineations on the continents (Fig. 8) map the trends of ancient and modern mountain ranges.

The Rules of Plate Tectonics

Unfortunately, one cannot produce plate tectonic reconstructions with a high level of confidence that are based solely on available geological and geophysical evidence. This is especially true for the distant past. Too much of the geological record is missing and the available geophysical data (e.g. palaeopoles) are often in conflict or can be interpreted in a variety of ways. To resolve this dilemma, we must rely on the insights we have gained over the last 50 years regarding the dynamics of the plate tectonic process (e.g. Scotese and Rowley 1985; Scotese *et al.* 1988; Scotese 1991, 2014a, b, c). The key insights are summarized in Table 7 as the ‘Rules of Plate Tectonics’. A more complete description of the Rules of Plate Tectonics is provided in the [Supplementary material](#).

One of the most important insights we have learned regarding the evolution of plates and plate boundaries is the nature of the driving forces that

motivates the plates. Plates are driven primarily by two endogenic forces (i.e. forces that arise from within the oceanic lithosphere): slab pull and ridge push. Only at a secondary level are plates affected by the movement of the underlying asthenosphere. It is true that hotspots and Large Igneous Provinces (LIPs) can profoundly weaken the continental lithosphere and help to focus the forces that tear continents apart but hotspots do not drive plate motions. Approximately 70–80% of the driving force of plate tectonics comes from the sinking of the cooler, denser oceanic lithosphere (slab pull and slab rollback).

‘Ridge push’, on the other hand, is a bit of a misnomer. As a plate moves away from the mid-ocean ridge it cools and becomes denser and heavier, creating lateral gradients in the gravitational potential energy (GPE). A plate tends to gain weight as it approaches the trench; this added weight helps it to subduct faster. In a very real sense, the plates drive themselves (For-syth and Uyeda 1975; Clennett *et al.* 2023).

Understanding the nature of plate tectonic driving forces allows us to properly motivate plate movements (Clennett *et al.* 2023). Oceanic plates will tend to move towards subduction zones – pulled along by slab pull. The plates attached to the greatest

Table 7. Rules of Plate Tectonics**Rule 1. Plates move only if they are pushed or pulled, not dragged (mostly)**

The pattern of flow in the mantle is largely driven by lithospheric motions. Although intuitively attractive, the idea of organized convection cells upon which the plates ride is incorrect and misleading. Oceanic plates move faster than continental plates. Plates carrying large continents move slowly (e.g. Eurasia and Pangaea). Plates that are not driven by ridge push or slab pull do not move (Caribbean Plate and Scotia Plate). Plate motion can be modelled by ‘balancing the forces’ that drive and resist plate motion

Rule 2. Subduction rules

Slab pull is more important than ridge push (80% v. 20% of the driving force). The Phanerozoic speed limit is $c. 20 \text{ cm a}^{-1}$ (India, 65 Ma)

Rule 3. Mid-ocean ridges are passive features

Mid-ocean ridges are there because the crust, which is weak in tension, breaks when it is pulled. Continental crust breaks first, because at the same depth it is closer to its melting temperature. Mid-ocean ridges tend to align parallel to trenches

Rule 4. Subduction is forever

Collision is the only way to stop subduction. Subduction is hard to start. Subduction graveyards exist in the mantle

Rule 5. Pacific v. Tethyan subduction systems

Pacific-style subduction systems are characterized by a ring of subduction with a spreading ridge in the middle that can exist for tens of millions of years. Tethyan-style subduction systems that are asymmetrical or ‘one-sided’ are unstable.

Rule 6. Plates subduct normally

Orthogonal convergence (perpendicular to the active margin) is least work

Rule 7. The style of convergent margin depends of the absolute motions of the plates

Andean margins – net convergence ($c. 10 \text{ cm a}^{-1}$); western Pacific margins – net divergence (rollback $1\text{--}2 \text{ cm a}^{-1}$)

Rule 8. Island arcs don’t ride their trenches across oceans

Back-arc basins never evolve into wide ($>30\,000 \text{ km}$) ocean basins. 90% of all ophiolites form due to the collapse of back-arc basins.

Rule 9. Slab rollback can create odd intracontinental ocean basins

Oceanic lithosphere can become trapped (encircled) by continents (e.g. Mediterranean, Arctic and the Tethys north of the Alps). Small, short-lived subduction zones can consume this ocean floor creating intracontinental extension

Rule 10. Mantle plumes (i.e. hotspots) are important (sort of)

Many hotspots are derived from the core–mantle boundary. They provide a ‘good enough’ reference frame for absolute plate motions. Hotspots ‘help’ to break apart continents.

Rule 11. Continental collisions are important (really important)

Collisions destroy subduction zones and cause the global balance of plate-driving forces to change. A continent with many sutures will be weak and easily deformed (e.g. Asia following collision with India)

Rule 12. Plate tectonics is a catastrophic system (but not chaotic)

Plate motions are generally gradual but every once and a while ‘WHAM!’ Two important instabilities: (1) continent–continent collision and (2) ridge subduction. Ridge subduction both breaks supercontinents apart and brings them back together (Wegener and Wilson cycles). Supercontinents form and break apart because of the metastable nature of plate evolution

volume of subducting oceanic lithosphere will move fastest (Forsyth and Uyeda 1975). Subduction is inexorable and subduction zones will continue to draw the plates together until the oceanic lithosphere between them is entirely consumed. This eventually results in a continent–continent collision (i.e. Wilson cycle: Wilson 1966, 1968; Burke and Dewey 1975; Wilson *et al.* 2019; or Wegener cycle: Nance *et al.*

1988; Nance and Murphy 2013), or the obduction of an island arc. Subduction is a reliable driving force, pulling the plates ever onwards and downwards. Although the notion that plates are passively carried along by well-organized mantle convection cells continues to be taught in schools and in the popular media, this explanation of plate motions is incorrect and misleading.

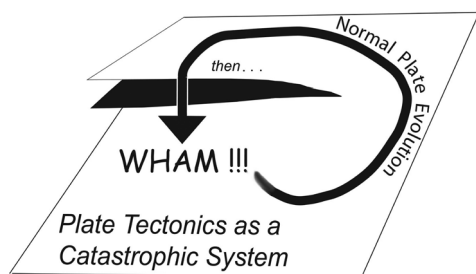


Fig. 11. Plate tectonics as a catastrophic system (Scotese 2014a, b, c).

Another important insight gained from our modelling of plate motions is that plate tectonics is a catastrophic system (Rule 12: Fig. 11). Most of the time plate geometries evolve in a slow and steady manner but every once and a while, seemingly out of nowhere, interplate stresses change rapidly and dramatically produce an entirely different plate tectonic regime. The two most important plate tectonic events that can trigger global plate reorganizations are: (1) continent–continent collision; and (2) the complete subduction of a mid-ocean ridge.

These catastrophic plate tectonic events often trigger coincident Earth system-wide events such as rapid changes in global sea level or abrupt shifts in climate, which in turn may cause global mass extinctions. Our modern understanding of Earth system processes combines the uniformitarian model, which emphasizes that the present is the key to the past (Lyell 1830, 1832, 1833), with the catastrophic model, which characterizes Earth history as long periods of stasis interrupted by short periods of catastrophic change (i.e. mass extinctions: Cuvier 1831).

Synthetic seafloor spreading isochrons

Plate tectonics is a grand recycling system. On average, it takes about 100 Myr for the ocean floor created at a mid-ocean ridge to return to the mantle. Since all ocean floor is created in a nearly symmetrical fashion at a mid-ocean ridge, if half of the ocean floor is missing, we can reconstitute the missing portion by creating a mirror-image of the remaining half. For example, the conjugate partners of the old ocean floor in the central and western Pacific Ocean have been subducted. Synthetic isochrons representing the missing ocean floor are shown as unshaded isochrons in Figure 2a.

The recreation of synthetic ocean floor is at best an educated guess. It is unlikely that the missing ocean floor was originally created in a perfectly symmetrical fashion. Also, this subducted ocean floor may have been broken into smaller plates before it

was subducted. This is what happened when the Farallon Plate was subdivided into the Cocos, Nazca (Wortel and Cloetingh 1981; Lonsdale 2005) and Kula plates (Engelbreton *et al.* 1985) as it approached the western American subduction zone. We must remember that we will never know the exact extent of these vast, long-gone regions of subducted oceanic lithosphere.

The problem of reconstructing subducted oceanic plates is much more severe when conjugate, synthetic isochrons are lacking (i.e. for times >180 Myr). In these cases, our reconstructions of long-subducted oceanic plates is little more than guesswork.

Subduction graveyards

Seismologists use shear and compressional waves to map the interior of the Earth (e.g. Spakman and Nolet 1988; van der Meer *et al.* 2018). The depths of important boundaries such as the inner core–outer core boundary (5154 km), the core–mantle boundary (2889 km), the lower mantle–upper mantle boundary (660 km), the 410 km discontinuity (Kennett and Engdahl 1991) and the base of the continental lithosphere (up to 400 km: Artemieva 2006; Conrad and Lithgow-Bertelloni 2006), as well as the base of the oceanic lithosphere (low velocity zone, c. 150 km: Conrad and Lithgow-Bertelloni 2006), are well determined. In recent years, mantle tomographic maps have been produced that identify regions of slow and fast velocities in the mantle that are thought to represent less dense (warmer) and more dense (cooler) regions. It has been hypothesized that the cooler and denser material of the mantle corresponds with the location of subducted oceanic lithosphere, or subduction graveyards (van der Meer *et al.* 2018).

Figure 12 is a ‘time-lapse’ image that illustrates the changing location of Cretaceous subduction zones. The location of ocean trenches changes relatively slowly through time (c. 2 km Ma^{−1}). This is due to the inherent inertia of the large, entrained volume of subducting oceanic lithosphere. Young subduction zones can move more quickly. A phenomenon called slab rollback (Stern 2002; Royden and Husson 2006; Boutelier and Cruden 2013) results when oceanic lithosphere can freely move in a retrograde fashion in a direction opposite to convergent plate motion. Slab rollback produces back-arc basins (Uyeda and Kanamori 1979; Barker and Hill 1981), whereas trenches that are actively overridden by the adjacent continental plate produce Andean-style margins (Lamb 2004).

Superimposed on the locations of Cretaceous trenches (blue lines) in Figure 12 are the corresponding, deeply buried subduction zone graveyards (coloured zones). These subduction graveyards encircle

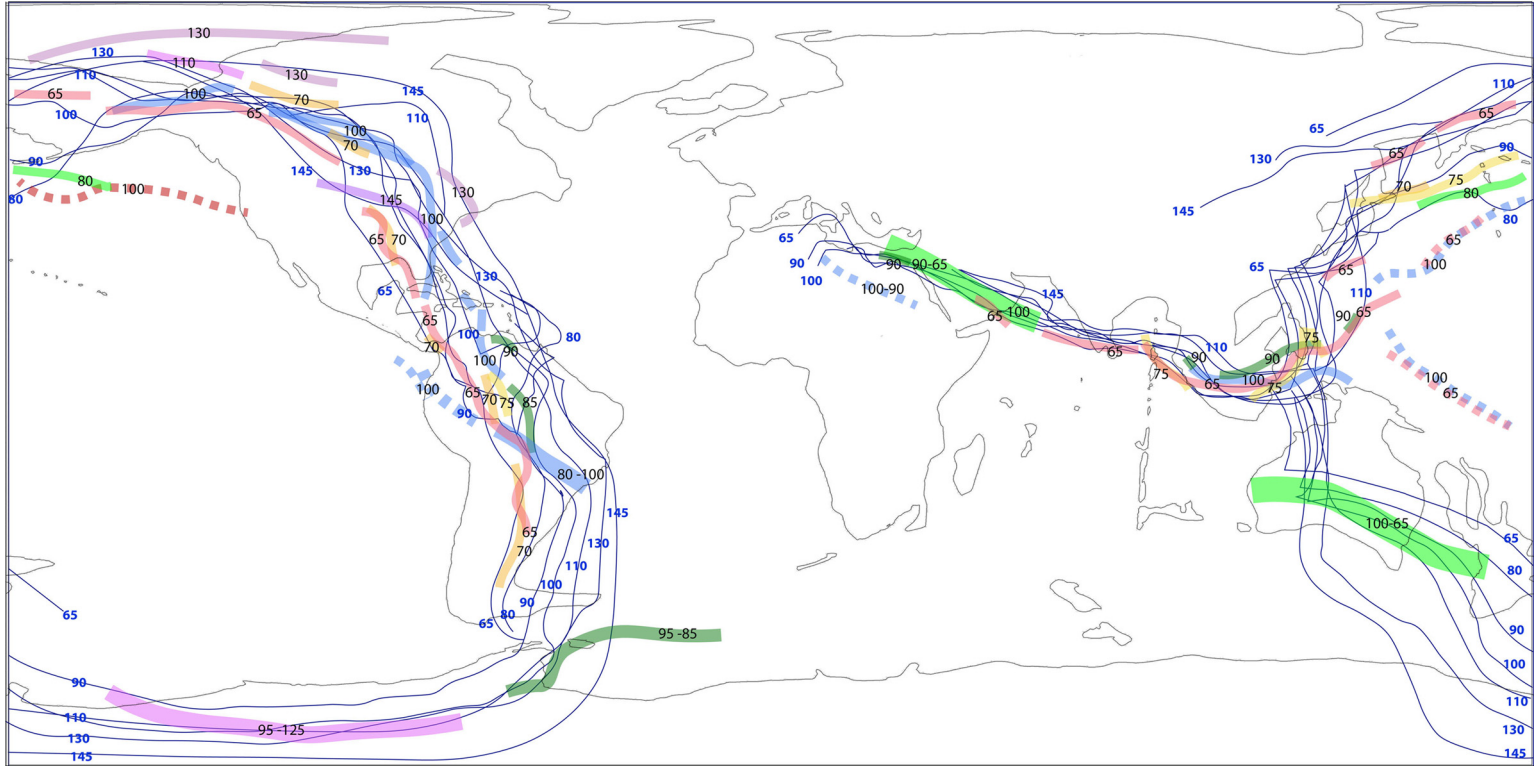


Fig. 12. Location of Cretaceous trenches and subduction zone graveyards. The thin, dark blue lines mark the successive locations of subduction zone trenches of the Cretaceous (145–65 Ma). Note how the locations of the trenches along western North and South America move progressively westwards from 145 to 65 Ma. The trenches in the SW Pacific, NE of Australia, moved northwards, whereas the locations of the trenches bordering the southern margin of Eurasia remained stationary throughout the Cretaceous. The coloured bands indicate the locations of corresponding subduction zone graveyards of Cretaceous age. The labelled age indicates when the lithosphere in that graveyard was subducted (i.e. the location of the trench at that time) (van der Meer *et al.* 2018). The trends and age progression of the subduction zone graveyards, for the most part, match the ages of the predicted trench locations.

the Panthalassic Ocean and also form a broad NW–SE-trending belt that marks the former northern border of the Tethys Ocean. Other subduction graveyards indicate that there may have been Cretaceous subduction beneath northern Africa and along the rim of the western Pacific Ocean basin (dashed lines in Fig. 12) (van der Meer *et al.* 2017).

The fact that most of these subduction graveyards closely match the predicted locations of Cretaceous trenches strongly suggests that there has been little or no true polar wander since the Early Cretaceous, otherwise there would be a demonstrable mismatch between our palaeomagnetically derived reference frame and the mantle reference frame. The lack of significant true polar wander during the last 150 Myr, and possibly the last 300 Myr, is discussed more fully later in this paper.

Large Igneous Provinces (LIPs)

Large Igneous Provinces, or LIPs, are the extrusive component of voluminous mantle plumes or hotspots. Mahoney and Coffin (1997), Foulger and Jurdy (2007), Ernst (2014), Neal *et al.* (2015), Ernst and Youbi (2017), Srivastava *et al.* (2022) and Percival *et al.* (2024, this volume) have documented over 200 LIPs that occur as far back as the Archean. The statistics of more than 30 LIPs and hotspot tracks that erupted during the Cretaceous are listed in Table 8. Roughly half of these LIPs were erupted on the continents, forming extensive volcanic edifices (e.g. Deccan Traps); other LIPs, erupted on the ocean floor, formed large submarine plateaus (e.g. Ontong Java Plateau: Erba *et al.* 2015; Taylor 2006). As one might expect, the largest LIP accumulations are found on slow moving plates (e.g. Kerguelen Plateau: Erba *et al.* 2015). When plumes penetrate fast-moving plates, they typically form large, long-lived, hotspot tracks (e.g. Ninety East Ridge). The break-up of large oceanic plateaus, such as the Manihiki and Hikurangi plateaus (120 Ma), can provide important constraints on plate evolution (Seton *et al.* 2012).

LIPs have had an important effect on palaeoclimate and evolution. There is extensive literature describing the relationship between these massive volcanic eruptions and global warming (Larson 1991a, b; Godd  ris *et al.* 2012; Kidder and Worsley 2012; Ernst and Youbi 2017; McKenzie and Jiang 2019; Scotese *et al.* 2021; Percival *et al.* 2024), as well as, the correlation between LIP eruptions and major extinction events (Rampino and Stothers 1988; Wignall 2001, 2015; Morgan *et al.* 2004; Kidder and Worsley 2010; Bond and Wignall 2014; Rampino and Self 2015; Bond and Grasby 2017; Ernst and Youbi 2017; Clapham and Renne 2019; Schobben *et al.* 2019; Suarez *et al.* 2019).

Palaeobiogeography

Palaeobiogeography describes the past geographical distribution of various fossil taxa. Modern biogeographical patterns are complex, and are controlled by a variety of factors including temperature, geographical barriers, ocean currents and dispersal history (vicariance). Palaeobiogeography provides important constraints for pre-Pangaea plate tectonics (Fig. 13) (Middlemiss *et al.* 1971; Hallam 1973; Hughes 1973; McKerrow and Scotese 1990; Harper and Servais 2013; Harper *et al.* 2013; Torsvik and Cocks 2017; Cocks and Torsvik 2021; Harper *et al.* 2023; Servais *et al.* 2023) but is less diagnostic for Mesozoic and Cenozoic plate movements. McKenna (1973), Briggs (1987) and Brown and Lomolino (1998) provide a good overview of the general principles of biogeography, and Lieberman (2000, 2003) discusses the how fossils and evolutionary theory are applied to the subject of palaeobiogeography.

Cretaceous palaeobiogeography can be divided into the study of terrestrial and marine realms. The most useful terrestrial components are dinosaurs and land plants. Dinosaurs were strictly terrestrial and could not easily cross wide bodies of water (>200 km). They were, however, highly mobile and could migrate across vast tracks of land in relatively short time intervals (thousands of years). Consequently, early dinosaurs and other reptile groups (Lystrosaurus and Cynognathus: Colbert 1973) were widely distributed across Pangaea prior to the formation of the Atlantic and Indian oceans.

Throughout most of the Jurassic, the dinosaurs of North America–Europe, Asia and Gondwana were recognizably different (Kraus *et al.* 2019). As the oceans widened during the Late Jurassic and Early Cretaceous, dinosaurs became progressively isolated and distinct regional groups were established (Upchurch *et al.* 2002). The dinosaurs of East Gondwana (India–Australia–Antarctica) had become distinct from the dinosaurs of West Gondwana (Africa–South America) by the Valanginian (c. 130 Ma). As the South Atlantic Ocean widened the dinosaurs of Africa and South America became endemic by the mid-Cretaceous (Albian, 110–100 Ma: Upchurch *et al.* 2002). The migration of Cretaceous dinosaurs was somewhat restricted by different climatic regimes (K  ppen belts), as well as by oceanic barriers (Dunhill *et al.* 2016). Theropods and ornithischians seemed to have preferred middle and high latitudes, whereas sauropods showed a preference for warmer subtropical latitudes (Chiarenza *et al.* 2022).

Although deep, widening ocean basins provided barriers to dinosaur migration, changes in sea level were probably more effective, although more short-term, barriers (Jabri *et al.* 2010). For example, the

Table 8. Cretaceous hotspots, LIPS and hotspot tracks

| ID # | Hotspot name | Location when active | | Principal volcanic feature | Location | Old age (Ma) | Young age (Ma) | Area (×10 ⁶ km ²) | Associated hotspot track | Sources |
|------|--------------------------------|----------------------|-----------|--|-------------------|--------------|----------------|--|---------------------------------|--|
| | (bold = still active) | Latitude | Longitude | (bold = LIP (>0.5 × 10 ⁶ km ²)) | | | | | | |
| 1 | <i>A. Atlantic Ocean</i> | | | | | | | | | |
| | Iceland | 65° N | 20° W | Alpha–Mendeleev Ridge | Arctic | 150 | 120 | 1.3 | Alpha–Mendeleev Ridge | |
| | Iceland | 65° N | 20° W | Baffin Bay–Disko Island | North Atlantic | 108 | 70 | 0 | Baffin Bay–Disko Island–Iceland | Johnston and Thorkelson (2000) |
| 2 | Bermuda | 30.5° N | 42.4° W | Bermuda | Central Atlantic | 72 | 68 | 0 | None | |
| 3 | Great Meteor | 30° N | 29° W | New England Seamounts | Central Atlantic | 100 | 75 | 0.1 | New England seamounts | Condie (2001) |
| | Great Meteor | 30° N | 29° W | Corner and Sohm seamounts | Central Atlantic | 75 | 60 | 0.1 | Corner and Sohm seamounts | |
| 4 | Cabo Verde | 15°N | 24° W | East Bahamas Platform | Central Atlantic | 144 | 130 | 0.2 | Bahamas Platform | |
| | Cabo Verde | 15°N | 24° W | Central Bahamas Platform | Central Atlantic | 153 | 144 | 0.4 | Bahamas Platform | |
| 5 | Caribbean | 11° N | 73° W | Caribbean–Colombian | Caribbean | 95 | 85 | 1.1 | None | Kerr et al. (1997) |
| 6 | Sierra Leone–Ceara | 1.2° N | 28° W | Sierra Leone–Ceara seamounts | South Atlantic | 70 | 68 | 0.7 | None | Kumar et al. (2007) |
| 7 | Tristan da Cunha | 37° S | 12° W | Parana Flood Basalts | Brazil–Argentina | 140 | 129 | 1 | Rio Grande Rise | Peate (1997) |
| | Tristan da Cunha | 37° S | 12° W | Rio Grande Rise | South Atlantic | 115 | 78 | 0.7 | Rio Grande Rise | |
| | Tristan da Cunha | 37° S | 12° W | Entendeka Basalts | Namibia–Angola | 140 | 129 | 1 | Walvis Ridge | Peate (1997) |
| 8 | Discovery | 50° S | 18° W | Discovery Seamount | SW South Atlantic | 66 | 58 | 0.1 | None | |
| 9 | Orcadas–Meteor | 55° S | 14° W | Islas Orcadas Rise | SW South Atlantic | 66 | 58 | 0.1 | None | |
| | Orcadas–Meteor | 55° S | 14° W | Meteor Rise | SE South Atlantic | 66 | 58 | 0.1 | None | |
| 10 | Agulhas–Georgia | 58° S | 1° W | NE Georgia Rise | SW South Atlantic | 103 | 92 | 0.1 | None | |

| | | | | | | | | | | |
|----|-------------------------|---------|----------|---|-------------------------------|-----|-----|-----|--------------------------------------|---------------------------------------|
| | Agulhas– Georgia | 58° S | 1° W | Agulhas Plateau | SE South. Atlantic | 103 | 92 | 0.5 | None | |
| | <i>B. Indian Ocean</i> | | | | | | | | | |
| 1 | Reunion | 21° S | 56° E | Deccan | India | 66 | 65 | 1.8 | Mascarene–Chagos–Laccadive | |
| 2 | Roo | 40° S | 81° E | Roo Rise | East Indian Ocean | 130 | 120 | 0.1 | None | |
| 3 | Wallaby | 44.8° S | 69.8° E | Wallaby Plateau | East Indian Ocean | 124 | 120 | 0.1 | None | Direen et al. (2017) |
| 4 | Mozambique– Astrid | 46° S | 3° E | Astrid Ridge | Antarctica | 154 | 118 | 0.4 | Mozambique Ridge | |
| | Mozambique– Astrid | 46° S | 3° E | North Mozambique Ridge | SW Indian Ocean | 136 | 130 | 0.2 | Mozambique Ridge | |
| | Mozambique– Astrid | 46° S | 3° E | Central Mozambique Ridge | SW Indian Ocean | 130 | 124 | 0.2 | Mozambique Ridge | |
| | Mozambique– Astrid | 46° S | 3° E | South Mozambique Ridge | SW Indian Ocean | 124 | 114 | 0.2 | Mozambique Ridge | |
| 5 | Marion | 47° S | 37.8° E | Madagascar Plateau–del Cano Rise | SW Indian Ocean | 95 | 58 | 1.6 | Madagascar Plateau– del Cano Rise | Storey et al. (1997) |
| 6 | Cuvier | 47° S | 66° E | Cuvier Plateau | East Indian Ocean | 138 | 131 | 0.1 | None | |
| 7 | Kerguelen | 49° S | 63° E | South Kerguelen | SE Indian Ocean | 110 | 96 | 0.5 | South Kerguelen | Kent et al. (1997) |
| | Kerguelen | 49° S | 63° E | Central Kerguelen– Broken Ridge | SE Indian Ocean | 96 | 84 | 1.5 | Central Kerguelen–Broken Ridge | |
| | Kerguelen | 49° S | 63° E | North Kerguelen | SE Indian Ocean | 84 | 0 | 0.5 | Ninetyeast Ridge | |
| 8 | Conrad | 53° S | 35° E | Conrad Rise | SW Indian Ocean | 88 | 80 | 0.4 | Madagascar Plateau–Conrad Rise | |
| 9 | Rajmahal | 53.4° S | 48.4° E | Rajmahal Traps | East India | 134 | 120 | 2.3 | None | |
| 10 | Bovet | 54° S | 3.5° E | Maud Rise | Southern South Atlantic | 120 | 114 | 0.1 | None | |
| 11 | Bunbury | 57.7° S | 57.2° E | Bunbury volcanics | SW Australia | 136 | 130 | 0 | None | Direen et al. (2017) |
| | <i>C. Pacific Ocean</i> | | | | | | | | | |
| 1 | Hawaii | 19.3° N | 155.4° W | Hawaiian– Emperor | North Pacific | 70 | 0 | 0.2 | Hawaiian–Emperor | |
| 2 | Lynn | 2° S | 137° W | Line Island–Hess | North Pacific | 115 | 70 | 0.1 | Line Island–Hess | Henderson (1985) |
| 3 | Hess | 5° S | 135° W | Hess | North Pacific | 124 | 112 | 0.8 | None | Vallier et al. (1983) |
| 4 | Wilkes | 8° S | 125° W | Line Island–Hess | North Pacific | 115 | 70 | 0.1 | Line Island–Hess | Henderson (1985) |
| 5 | Shatsky | 12° S | 152° W | Shatsky–Tamu | North Pacific | 155 | 140 | 1 | None | |

(Continued)

Table 8. *Continued.*

| ID # | Hotspot name | Location when active | | Principal volcanic feature | Location | Old age (Ma) | Young age (Ma) | Area ($\times 10^6 \text{ km}^2$) | Associated hotspot track | Sources |
|------|--------------------------|----------------------|-----------|--|-----------------|--------------|----------------|-------------------------------------|-------------------------------------|--|
| | (bold = still active) | Latitude | Longitude | (bold = LIP ($>0.5 \times 10^6 \text{ km}^2$)) | | | | | | |
| 6 | Somoa | 14° S | 170° W | Magellan Seamounts | North Pacific | 70 | 0 | 0.1 | Magellan Seamounts | Henderson (1985) |
| 7 | Tahiti | 18° S | 150° W | Gilbert–Mid-Pacific Seamounts | North Pacific | 90 | 0 | 0.1 | Gilbert–Mid-Pacific Seamounts | Henderson (1985) |
| 8 | Mid-Pacific | 21° S | 130° W | Mid-Pacific Mountains | Central Pacific | 140 | 114 | 1.1 | Mid-Pacific Mountains | Coffin and Eldholm (1991) |
| 9 | Pitcairn–Tuamotus | 26° S | 130° W | Austral–Tuvalu–Gilbert | Central Pacific | 115 | 0 | 0.1 | Austral–Tuvalu–Gilbert | Steinberger and O’Connell (1998) |
| 10 | Easter | 27° S | 109° W | Tuamotus–Line–Mid-Pacific Seamounts | Central Pacific | 115 | 0 | 0.1 | Tuamotus–Line–Mid-Pacific Seamounts | Henderson (1985) |
| 11 | Macdonald | 30° S | 140° W | Society–Austral–Cook | Central Pacific | 115 | 0 | 0.1 | Society–Austral–Cook | Henderson (1985) |
| 12 | Ontong Java | 40° S | 161° W | Ontong Java | Central Pacific | 122 | 119 | 4.3 | None | Neal <i>et al.</i> (1997) |
| 13 | Manihiki | 44° S | 110° W | Manihiki | Central Pacific | 122 | 119 | 0.9 | None | |
| 14 | Louisville | 51° S | 141° W | Louisville Ridge | South Pacific | 90 | 0 | 0.1 | Louisville Ridge–Gilbert–Marshall | Steinberger and O’Connell (1998); Sager (2007) |
| 15 | Whitsunday | 70° S | 131° E | Whitsunday | Queensland | 120 | 90 | 0.2 | None | Bryan <i>et al.</i> (2000) |
| 16 | Hikurangi | 78° S | 97° W | Hikurangi | SW Pacific | 121 | 119 | 0.4 | None | |

485 Ma

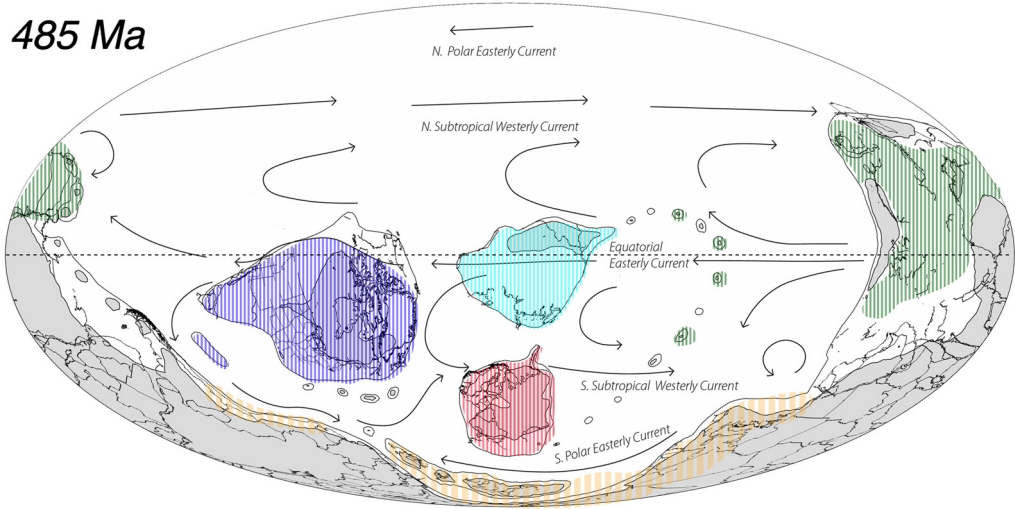


Fig. 13. Early Ordovician palaeobiogeography with ocean currents. Faunal provinces: blue, Laurentian; red, Baltic; cyan, Siberian; green, China–Australia; orange, NW Africa–central Europe–Avalonia. Brachiopod provinces are defined by temperature (latitude) and ocean currents. Source: after Harper *et al.* (2013); see also Harper *et al.* (2023) and Servais *et al.* (2023).

Cretaceous mid-Continent Seaway divided North America into western (Laramidia) and eastern (Appalachia) landmasses. Laramidia shared many taxa with eastern Asia during the Cretaceous because a land bridge extended across the Bering Sea, whereas Appalachia developed a less diverse, endemic dinosaur fauna. In a few special cases, hot-spot tracks and large volcanic edifices (e.g. Kerguelen Plateau: Ali and Krause 2011; Kraus *et al.* 2019) created land bridges linking continental landmasses across widening ocean basins.

Plants were the other important component of the Cretaceous terrestrial realm. The first flowering plants appeared in the Early Cretaceous (c. 140 Myr ago: Willis and McElwain 2002). Their rapid diversification during the mid and Late Cretaceous transformed the ecosphere and led to their global dominance by the end of the Cretaceous. Because plants are not locomotive, they do not easily spread from one place to another and are primarily adapted to local climatic conditions. The phytogeography of the Cretaceous can be described by seven global plant biomes: tropical ever-wet, tropical summer-wet, subtropical desert, winter-wet, mid-latitude desert, warm temperate and cool temperate (Horrell 1991; Upchurch *et al.* 1999). There was no tundra or subpolar plant assemblage during the Cretaceous.

The marine faunas of the Cretaceous have long been subdivided into a warm-water ‘Tethyan’ realm and a cool-water ‘Boreal’ realm (Casey and Rawson 1973). These biogeographical differences

were recognized well before the advent of plate tectonics. Recent investigations of planktonic coccolithophorid taxa (*Braarudisphaera bigelowii*) have hypothesized that distinct Cretaceous marine provinces were segregated by both temperature and evolving ocean currents (de Lurdes Fonseca *et al.* 2019) (Fig. 14).

Palaeoclimate

The advent of supercomputers has made global palaeoclimate simulations more practicable, if not routine (e.g. Lunt *et al.* 2016, 2023; Valdes *et al.* 2017; Haywood *et al.* 2019; Li *et al.* 2022). The increase in the number of simulations means that we now have multiple palaeoclimate simulations for each stage of the Cretaceous. These simulations now provide a baseline for modelling Cretaceous environments (Köppen Zones: Fig. 2c), as well as quantitative estimates of, for example, global temperature (Fig. 3a), precipitation (Fig. 3b), runoff, ocean circulation (Fig. 3c) and upwelling. For the most part, the results of these palaeoclimatic models compare favourably with the geological record of coals, bauxites, evaporites, calcretes, glendonites, dropstones and tillites (Boucot *et al.* 2013; Bao and Hu 2024; Burgener *et al.* 2023; Rogov *et al.* 2023). The latitudinal distribution of climatically sensitive lithologies (Boucot *et al.* 2013) and the reconstruction of past Köppen belts can often provide an important test of palaeomagnetic estimates of

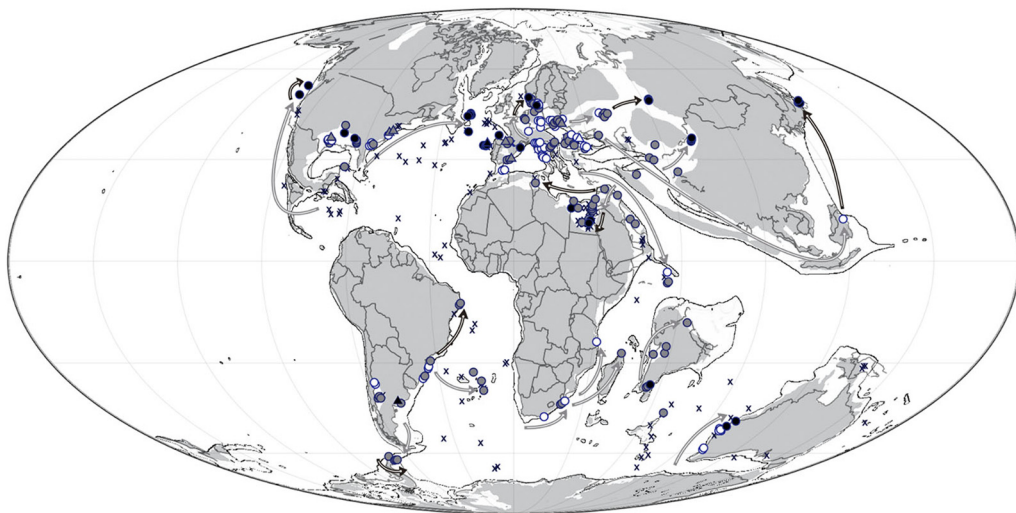


Fig. 14. *Braarudisphaera bigelowii* migration paths during the Maastrichtian. Reliability (weak to very good) depends on the number of supporting observations. Source: from de Lurdes Fonseca *et al.* (2019).

palaeolatitude (Bao and Hu 2024; Burgener *et al.* 2023).

True polar wander

The continents move across the face of the globe because they are motivated by plate tectonics. It is also possible, however, that a component of their latitudinal motion may be due to the rotation of the entire Earth beneath the spin axis. This rotation of the entire Earth relative to the spin axis might have been called ‘whole Earth rotation’ or ‘global rotation’; however, for historical reasons it was called true polar wander (Goldreich and Toomre 1969). The term ‘true polar wander’ (TPW) was coined to contrast it with ‘apparent polar wander’: apparent polar wander refers to the palaeomagnetic estimate of the motion of the spin axis (north and south geographical poles) relative to a specific continent (Creer 1954) (see Fig. 10). Each continent has its own, unique apparent polar wander (APW) path (see Table 5). If the entire Earth rotates with respect to the spin axis, then this component of motion is shared by all the continents, hence it is ‘true polar wander’ (TPW). Palaeomagnetic measurements cannot be easily used to differentiate between continental motions due to plate tectonics and continental motions due to TPW because palaeomagnetic data lack the precision to do so.

A small amount of TPW undoubtedly occurs because the distribution of dense material within the Earth (i.e. subduction zone graveyards) constantly changes. This redistribution of dense material affects the Earth’s instantaneous moment of inertia,

which causes the Earth to shift slightly to rebalance the load (Gold 1965). Over tens or hundreds of millions of years these global readjustments may add up to hundreds of kilometres (Steinberger and Torsvik 2010; Vaes 2023).

In summary, the average rate of TPW (mm a^{-1}) is a fraction of the average rate of plate movement (cm a^{-1}) and is likely to be below the resolution of palaeomagnetic data (Vaes 2023). The large, rapid and often recursive episodes of TPW that have been proposed by some researchers (Kirschvink *et al.* 1997; Evans 2003; Steinberger and Torsvik 2010; Muttoni *et al.* 2013; Eglington *et al.* 2017; Muttoni and Kent 2019; Evans *et al.* 2021; Le Pichon *et al.* 2023), we believe, are based on an insufficient number of palaeopole determinations ($N < 50$).

Geological and geophysical evidence used to map ancient palaeogeography

In its strictest sense, the term palaeogeography describes not only the past positions of the continents but also the location of ancient shorelines, shallow seas, deep oceans, land and mountains. A complete palaeogeographical map also models the palaeotopography of the land surface and palaeobathymetry of the ocean basins (Fig. 2b). The digital basis of the palaeogeographical maps shown here is a palaeodigital elevation model or palaeoDEM (Scotese and Wright 2018). Each palaeoDEM is composed of more than six million grid cells that capture digital elevation information at a 10×10 km horizontal

resolution and 40 m vertical resolution. Palaeo-DEMs allow us to visualize and analyse the changing surface of the Earth using GIS software and other computer modelling techniques. For example, we can use a palaeoDEM to calculate the average elevation of the land surface, the average depth of the ocean floor, the area of the continents flooded by the ocean or the relative area of continental v. oceanic crust. The palaeoDEMs that are the basis of the Cretaceous palaeogeographical maps are provided in the [Supplementary material](#).

To construct an ancient palaeogeography, the geological lithofacies that define the ancient depositional environments must be mapped. For example, a thick sequence of pure limestones might represent warm, shallow-water environments like the Bahamas Platform or a vast epeiric sea. Extensive sets of massive, cross-bedded sandstones may once have been wind-blown, desert dunes. A terrane composed of andesite and granodiorite may have been a continental arc or Andean mountain range. [Table 9](#) ([Ziegler *et al.* 1985](#)) summarizes the lithofacies and rock types that correspond to the depositional environments that have been used to interpret the ancient topography and bathymetry.

Geologists have been collecting lithological information and producing lithofacies and palaeoenvironmental maps for more than 200 years ([Smith 1815](#)). During the late 1970s and early 1980s, the Paleogeographic Atlas Project, under the leadership

of Prof. A.M. Ziegler, in the Department of Geophysical Sciences, University of Chicago, compiled a database of more than 125 000 lithological and palaeoenvironmental records for the Mesozoic and Cenozoic ([Ziegler *et al.* 1985](#)). This database – supplemented by the Phanerozoic reef database of [Flügel and Kiessling \(2002\)](#) and [Kiessling *et al.* \(2002\)](#), [Kiessling and Flügel \(2002\)](#), a database of climatically sensitive lithofacies ([Boucot *et al.* 2013](#)), and environmental information from the Paleobiology database ([Alroy *et al.* 2008](#)) – was used to produce the Cretaceous palaeogeographical maps in this paper. This digital palaeogeographical information was supplemented by more than 50 sources that feature Cretaceous palaeogeographical maps ([Table 10](#)).

Information from these four lithological databases was standardized, sorted by time interval and plotted in the simplified fashion shown in [Figure 15](#) ([Scotese 2021](#)). These maps show the control points for palaeogeographical interpretations. In these simplified maps, the palaeocoastlines (black lines) weave their way between geological data, indicating marine environments (circles) or terrestrial environments (plus signs). The size of the symbol is proportional to the duration of the stratigraphic interval (i.e. small symbols are better dated than large symbols).

Lithological data can only be used to map palaeogeographical environments where the rock record is fairly complete. However, there are many instances

Table 9. Elevation, environments and geological evidence

| Code | Elevation | Environments | Geological evidence |
|------|-----------------------|--|---|
| 9 | 10 000–4000 m | Collisional mountains | High-temperature, high-pressure metamorphics |
| 8 | 4000–2000 m | Andean-type mountains | Andesites/granodiorites in a continental setting |
| 7 | 2000–1000 m | a. Island arc volcanos b. Intra-continental rift shoulders | Andesites/granodiorites in a marine setting Adjacent fanglomerates |
| 6 | 1000–200 m | a. Rift valley b. Some forearc ridges | Basalts, lake deposits in graben Tectonic mélanges |
| 5 | 200 m to sea level | a. Coastal plains b. Lower river systems c. Delta tops | Alluvial complexes Major floodplain complexes Swamps and channel sands |
| 4 | Sea level to –50 m | a. Inner shelves b. Reef-dammed shelves c. Delta fronts | Heterogeneous marine sediments Bahamian-type carbonates Topset silts and sands |
| 3 | –50 to –200 m | a. Outer shelves b. Some epeiric basins c. Prodelta | Fine sediments, most bioproductites Fine clastics or carbonates Foreset silts and proximal turbidites |
| 2 | –200 to –4000 m | a. Continental slope/rise b. Mid-ocean ridges c. Prodelta fans | Slump/contourite facies Oceanic crust less than 60 Myr old Bottomset clays and distal turbidites |
| 1 | –4000 to –6000 m | Ocean floors | Pelagic sequences on oceanic crust |
| 0 | –6000 to –12 000 m | Ocean trenches | Turbidites on pelagic sequences |

Table 10. Bibliography of sources for Cretaceous palaeogeographical maps

Explanation: Each bibliographical citation is followed by the region of the world, the total number of maps and the Cretaceous time intervals

For example: Dercourt, J., Ricou, L.E., and Vrielynck, B. 1993/Tethys region from northern Australia to North America/14 Maps/Cretaceous (Early Aptian, Late Cenomanian, Late Maastrichtian)

Blakey, R.C. (2002)/Global/31 Maps/Aptian (120 Ma), Albian (105 Ma), Cenomanian–Turonian (90 Ma), Maastrichtian (65 Ma)

Blakey, R.C. (2008)/Gondwana/18 Maps/Early Cretaceous (120 Ma), mid-Cretaceous (105 Ma), Late Cretaceous (90 Ma), Late Cretaceous (75 Ma)

Blakey, R.C. (2011)/Western Europe/26 Maps/Early Cretaceous (125 Ma), Late Cretaceous (100 and 75 Ma)

Blakey, R.C. (2013)/Western Europe/37 Maps/Early Cretaceous (130, 115 and 105 Ma), Late Cretaceous (92, 85 and 72 Ma)

Boucot, A.J., Xu, C., Scotese, C.R. and Fan, J.X. (2009)/Global/27 Maps/Early Cretaceous (120 Ma), early Late Cretaceous (100 Ma), late Late Cretaceous (80 Ma)

Bozhko, N. A. and Khain, V. E. (1987)/Africa, South America, Arabia, Madagascar, India, Antarctica, Australia/22 Maps/Late Jurassic–Early Cretaceous (160 Ma), Late Cretaceous (65 Ma)

Cook, P. J. (1990)/69 Maps/Cretaceous (11 Maps)

Cook, T. D. and Bally, A. W. (1975)/North America/42 Maps/Cretaceous (top Jurassic–mid Aptian, mid Aptian–mid Cenomanian, mid Cenomanian–top Turonian, Coniacian–Santonian, Campanian–Maestrichtian)

Cope, J.C.W., Ingham, J.K. and Rawson, P.F. (1992)/Great Britain and the North Sea/c. 80 Maps/Cretaceous (Berriasian, Mid Hauterivian, Late Aptian, Latest Albian, Early Cenomanian, Late Campanian)

Dercourt, J., Ricou, L.E. and Vrielynck, B. (1993)/Tethys from northern Australia to eastern North America/14 Maps/Cretaceous (Early Aptian, Late Cenomanian, Late Maastrichtian)

Dercourt, J., Gaetani, M., Vrielynck, B., Barrier, E., Biju-Duval, B., Brunet, M.F., Cadet, J.P., Crasquin, S. and Sandulescu, M. (2000)/CGMW, 24 Maps and explanatory notes, 269 pp., Paris./Western Tethys from Caspian Sea to Grand Banks/24 Maps/Cretaceous (Early Hauterivian, Early Aptian, Late Cenomanian, Early Campanian, Late Maastrichtian)

Evans, D., Graham, C., Armour, A. and Bathurst, P. (2003)/Central North Sea/>46 Maps/Early Cretaceous (late Ryazanian–early Valanginian, late Valanginian–late Barremian, early Aptian–early Albian), Late Cretaceous (Campanian–Maastrichtian)

Furon, R. (1941)/Global/15 Maps/Cretaceous (early–middle, late)

Golonka, J., Ross, M.I. and Scotese, C.R. (1994)/Global/29 Maps/Cretaceous (Valanginian, Aptian, Albian, Cenomanian, Coniacian, Maastrichtian)

Golonka, J. (2000)/Global/31 Maps/latest Jurassic–earliest Cretaceous, Cretaceous (Early, Early–earliest Late, Late), Late Cretaceous–earliest Paleogene

Hambrey, M.J. and Harland, W.B. (1981)/Global/>50 Maps/pre-Pleistocene

Hutchison, C.S. (1989)/South-East Asia/8 Maps/Late Jurassic–mid Cretaceous, mid Cretaceous–Neogene

Hulver, M. (1985)/Africa/5 Maps/Cretaceous (Valanginian, Aptian, Ceno Manian, Coniacian, Maastrichtian)

Kazmin, V.G. and Natapov, L.M. (1998)/Northern Eurasia/26 Maps/70 Ma (Maastrichtian), 80 Ma (Santonian and Campanian), 90 Ma (Cenomanian, Turonian and Coniacian), 100 Ma, (LATE Albian), 110 Ma (early Albian), 120 Ma (Aptian), 130 Ma (Hauterivian and Barremian), 140 Ma (Berriasian and Valanginian)

Khain, V.Ye., Ronov, A.B. and Balukhovskiy, A.N. (1976)

Kriest, J. (1991)/Global/27 Maps/Hauterivian (135 Ma), Aptian (120 Ma), Albian (105 Ma), Cenomanian/Turonian (90 Ma), Campanian/Maastrichtian (75 Ma)

Kiessling, W. (2001)/Phanerozoic Reef Paleolatitudes

Kiessling, W., Flügel, E. and Golonka, J. (2002)/Global/>40 Maps/Cretaceous (Berriasian, late Valanginian–early Aptian, late Aptian–middle Ceno Manian, late Ceno Manian–Santonian), Campanian–Danian

Mallory, W.W. (1972)/Rocky Mountain States/>62 Maps/Cretaceous (Neocomian–Aptian, early Albian, middle–late Albian, late Skull Creek, latest Albian, early Belle Fourche, middle Greenhorn, middle Carlisle, early Niobrara, middle Niobrara, Telegraph Creek, latest Eagle, early Claggett, middle Judith River, middle Bearpaw, early Fox Hills, latest Cretaceous)

McCrossan, R.G., Glaister, R.P., Austin, G.H. and Nelson, S.J. (1964)/western Canada/>45 Maps/Cretaceous (Aptian–lower Albian, lower–middle Albian, upper Albian, Ceno Manian–lower Campanian, middle Campanian, upper Campanian–early Maastrichtian)

Moore, T.L. and Scotese, C.R. (2012)/Global/24 Maps/KT Boundary (65.5 Ma), Maastrichtian (68 Ma), Early Campanian (80.3 Ma), Turonian (91.1 Ma), late Albian (101.8 Ma), early Albian (110.0 Ma), early Aptian (121.8 Ma), Hauterivian (132.0 Ma), Berriasian (143.0 Ma)

Mossop, G. and Shetson, I. (1994)/Western Canada/>52 Maps/Cretaceous (latest Jurassic–earliest Cretaceous, Berriasian, Berriasian–Valanginian, latest Barremian–early late Aptian, late Aptian, earliest Albian, early Albian, late early Albian, middle Albian, Cenomanian, Turonian, early Campanian, late early Campanian, middle Campanian, late Campanian, middle Maastrichtian)

Ronov, A.B., Khain, V.Ye. and Balukhovskiy, A. (1989)/Global/13 Maps/Early Cretaceous, Late Cretaceous

The Cretaceous world

- Schandelmeier, H. and Reynolds, P.O. (1997)/Northeast Africa and Arabia/17 Maps/Cretaceous (Valanginian, Aptian, Campanian–Maastrichtian)
- Schuchert, C. (1955)/North America/84 Maps/Lower Cretaceous (Lower Comanchean, Middle Comanchean, Upper Comanchean), Lower Upper Cretaceous (Turonian), Upper Cretaceous (Lower Senonian–Niobrarian, Campanian) High Upper Cretaceous (Upper Maastrichtian and ?Danian)
- Scotese, C.R. (1998)/Global/40 Maps/Berriasian–Barremian (140 Ma), Aptian (120 Ma), Albian (100 Ma), Ceno Manian–Turonian (90 Ma), early Campanian (80 Ma), Maastrichtian (70 Ma)
- Scotese, C.R. (2001*b*)/Global/16 Maps/Late Cretaceous, KT Boundary
- Scotese, C.R. (2004)/Global/18 Maps/Cretaceous(Berriasian, Barremian–Aptian, Albian–Cenomanian, Turonian, Campanian, middle Maastrichtian)
- Scotese, C.R. (2014)/Global/7 Maps/Map 16 K/T Boundary (latest Maastrichtian, 65.5 Ma), Map 17 Late Cretaceous (Maastrichtian, 68 Ma), Map 18 Late Cretaceous (Late Campanian, 73.8 Ma), Map 19 Late Cretaceous (Early Campanian, 80.3 Ma), Map 20 Late Cretaceous (Santonian and Coniacian, 86 Ma), Map 21 Mid Cretaceous (Turonian, 91.1 Ma), Map 22 Mid Cretaceous (Ceno Manian, 96.6 Ma)
- Scotese, C.R. (2014)/Global/14 Maps/Map 23 Early Cretaceous (late Albian, 101.8 Ma), Map 24 Early Cretaceous (middle Albian, 106 Ma), Map 25 Early Cretaceous (early Albian, 110 Ma) Albian Supersequence Boundary and Transgressive System Tract, Map 26 Early Cretaceous (late Aptian, 115.2 Ma), Map 27 Early Cretaceous (early Aptian, 121.8 Ma), Map 28 Early Cretaceous (Barremian, 127.5 Ma), Map 29 Early Cretaceous (Hauterivian, 132 Ma), Map 30 Early Cretaceous (Valanginian, 137 Ma) Barremian–Hauterivian Supersequence boundary and Transgressive Systems Tract, Map 31 Early Cretaceous (Berriasian, 143 Ma) Berriasian Supersequence boundary and Maximum Flooding Surface
- Scotese, C.R. and Golonka J. (1992)/Global/28 Maps/Cretaceous (Valanginian, Aptian, Cenomanian, Coniacian, Maastrichtian)
- Scotese, C.R. and Winn, K. (1987)/Global/14 Maps/Cretaceous (Cenomanian, Maastrichtian)
- Smith, A.G., Smith, D.G. and Funnell, B.M. (1994)/Global/31 Maps/Cretaceous (Valanginian–Berriasian, Barremian–Hauterivian, Aptian, Albian, Cenomanian, Turonian, Coniacian, Santonian, Campanian, Maastrichtian)
- Ulmishek, G.F. and Klemme, H.D. (1990)/Global/6 Maps/Middle Cretaceous
- Veevers, J.J. (1984)/Australia/44 Maps/Cretaceous (earliest, early, Aptian, Aptian–Albian, Albian, Cenomanian, Turonian, Campanian, Maastrichtian)
- Veevers, J.J. (2000)/Australia, Antarctica, South Africa, S. South America/41 Maps/Cretaceous(Neocomian–Aptian, Aptian, Aptian–Albian Cenomanian, Turonian–Campanian, Campanian)
- Vinogradov, A.P., Vereshchagin, V.N., Nalivkin, V.D., Ronov, A.B., Khabakov, A.V. and Khain, V.E. (1968)/26 Maps/Valanginian, Hauterivian, Barremian, Aptian, Albian, Cenomanian, Turonian, Coniacian, Santonian, Campanian, Maastrichtian
- Vrielynck, B. and Bouyessse, P. (2001)/Global/19 Maps/Cretaceous (Cenomanian, Maastrichtian)
- Walsh, D.B. (1996)/South Atlantic/9 Maps/Cretaceous (Valanginian, Aptian, Albian, Cenomanian, Coniacian–Turonian–Santonian, Maastrichtian)
- Wang Hongzhen (1985)/China/41 Maps/Precambrian Cretaceous (early Early, late Early, Late)
- Wilford, G.E. (1979)/Australia/20 Maps/middle Jurassic–early Cretaceous, Cretaceous (early, late)
- Willis, K.J. and McElwain, J.C. (2002)/Global Biome Maps/9 Maps/Maastrichtian
- Ziegler, A.M., Scotese, C.R. and Barrett, S.F. (1983)/Global/7 Maps/Cretaceous (Cenomanian, Maastrichtian)
- Ziegler, P.A. (1982)/Western and Central Europe/21 Maps/Cretaceous (Berriasian–Barremian, Aptian–Albian), Cretaceous–Tertiary Boundary (Cenomanian–Danian)
- Ziegler, P.A. (1988)/North Atlantic, Arctic, and western Tethys/20 Maps/Cretaceous (Berriasian–Barremian, Aptian–Albian, Turonian–Campanian)
- Ziegler, P.A. (1990)/Western and Central Europe/28 Maps/Cretaceous (Berriasian–Valanginian, Hauterivian–Barremian, Aptian–Albian, Cenomanian–Turonian), Cretaceous–Tertiary Boundary
- Zonenshain, L.P., Kuzmin, M.I. and Natapov, L.M. (1990)/Europe and USSR/18 Maps/Cretaceous (Early, Mid, Late), Cretaceous–Tertiary Boundary

where the rock record has been eroded, destroyed by tectonic processes or covered by younger strata. For these areas, a second, more interpretive, approach was taken to restore the palaeogeography. In these instances, the palaeoenvironments and palaeogeography must be inferred from the tectonic history of a region. As discussed earlier, the PALEOMAP Global Plate Tectonic Model (Scotese 2016*b*) provides the tectonic framework required to make these inferences and interpretations. The plate

tectonic reconstructions (Scotese and Elling 2017; Scotese 2018) are used to ‘model’ the expected changes in topography and bathymetry caused by plate tectonic events, such as seafloor spreading, continental rifting, subduction along active margins and continental collision, as well as other isostatic events such as glacial rebound (Peltier 2004). For example, to produce a palaeogeographical map for the Early Cretaceous, young tectonic features, such as recent uplifts or volcanic eruptions (e.g. Mid-

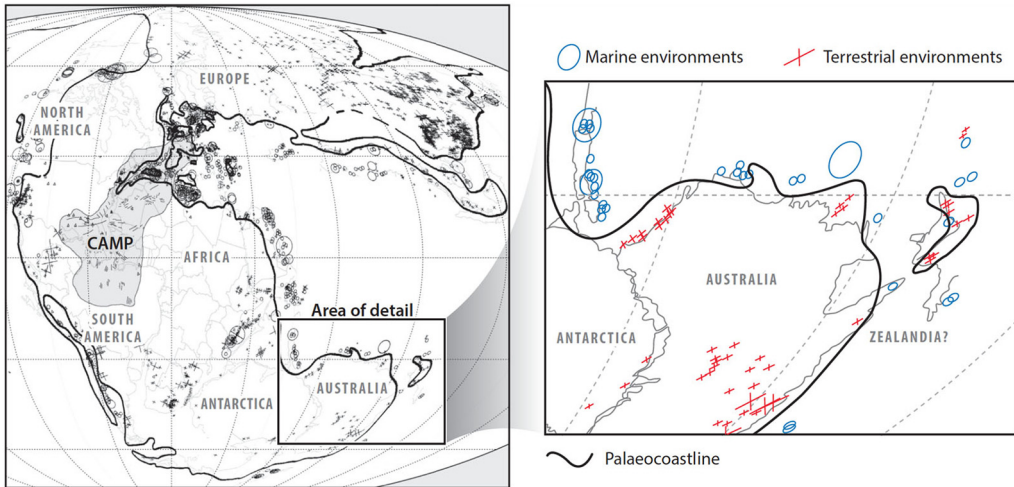


Fig. 15. Control points used to map the location of the palaeocoastline during the Early Jurassic (200 Ma): blue circles, marine deposits; red plus signs, terrestrial deposits. Smaller symbols have better age constraints. CAMP, Central Atlantic Magmatic Province. Source: from [Scotese \(2021\)](#).

African Rift), must be removed or reduced in size, whereas older tectonic features, such as ancient mountain ranges (e.g. Appalachian mountains), must be restored to their former extent. This approach is similar to the more recent dynamic techniques described by [Baatsen *et al.* \(2015\)](#), [Vérard *et al.* \(2015\)](#), [Markwick \(2019\)](#), [Vérard \(2019\)](#), [van der Linden *et al.* \(2020\)](#), [Poblete *et al.* \(2021\)](#), [Torsvik *et al.* \(2021\)](#) and [Boschman \(2022\)](#).

In a similar manner, the palaeobathymetry of the ocean floor must be restored back through time. As the ocean floor moves away from a spreading ridge, it cools and subsides. In many respects restoring the past bathymetry of the ocean floor is much easier than estimating the elevation of ancient mountain ranges ([Rowley *et al.* 2001](#); [Rowley and Currie 2006](#); [Rowley and Garzone 2007](#)). The amount that the seafloor subsides through time follows a regular mathematical rule where the amount of thermal subsidence is inversely proportional to the square root of the age of the oceanic crust ([Parsons and Sclater 1977](#); [Sclater *et al.* 1980](#)). To restore the ancient ocean floor to its former depths, the bathymetry of the ocean floor was adjusted using the depth–age relationship originally published by [Stein and Stein \(1992\)](#) and later updated by [Rowley \(2018\)](#).

Once the palaeogeography for each time interval has been mapped and corrections to the topography and bathymetry have been duly noted, this information was converted into the aforementioned elevation model or ‘palaeoDEM’ ([Scotese and Wright 2018](#)). By substituting a modified colour look-up table, the palaeogeography can also be subtly modified to represent eustatic changes in sea level ([Vail *et al.*](#)

[1977a, b](#); [Hallam 1984a, b](#); [Ross and Ross 1985](#); [Haq *et al.* 1987, 1988](#); [Algeo and Sclavinsky 1995](#); [Miller *et al.* 2005a, b](#); [Müller *et al.* 2008a, b](#); [Haq and Schutter 2009](#); [Snedden and Liu 2010, 2011](#); [Simmons 2012, 2020](#); [Haq 2014](#); [Vérard *et al.* 2015](#); [van der Meer *et al.* 2017, 2022](#); [Davies and Simmons 2023](#)).

For a more detailed discussion of the data and methods used to produce palaeogeographical maps, see [Scotese \(2021\)](#). A series of tutorials that describe how to build digital palaeogeographical maps from scratch can be found in the [Supplementary material](#).

Eustatic changes in sea level derived from estimates of continental flooding

Introduction

In general, sea level was much higher during the past ([Simmons 2012, 2020](#)). The modern era is characterized by recent continental collisions (e.g. India–Asia, Africa–southern Europe, Arabia–Turkey and Iran) that have raised the landscape, and by large continental ice sheets that have removed water from the ocean basins and dropped the sea level. During the Cretaceous, based on our estimates, sea level was relatively low (+50–70 m) during the earliest and latest parts of the period, and highest during the mid-Cretaceous (Cenomanian–Turonian, +150 m: this study). Changes in sea level can drastically change the palaeogeography of a continent. This section

The Cretaceous world

describes the methodology used to estimate changes in sea level during the Cretaceous.

The surface of the continents, however, is not flat. It gently slopes upwards from the coastline across the broad continental interiors ($c. 0.4 \text{ m km}^{-1}$) and then rises rapidly in the foothills of mountains ($c. 1.2 \text{ m km}^{-1}$). Figure 16 is a simplified diagram that shows how the average slope of the present-day continents varies from about $c. 400 \text{ m}$ above sea level to $c. 400 \text{ m}$ below sea level. This brackets the likely range of potential sea-level change during the Phanerozoic.

The vertical axis in Figure 16 is sea level. Zero metres indicates the location of the present-day coastline. Note that the horizontal axis is not distance but, rather, the percentage of the global surface area that is land. As sea level rises, continents are progressively flooded. For the modern world, land covers $c. 30\%$ of the globe. If we were to completely melt both the Greenland and Antarctic ice caps, sea level would rise by $c. 70 \text{ m}$ (Clark *et al.* 2016) and the global land area would be reduced to $c. 26.5\%$. During the height of the last ice age (Last Glacial Maximum, 20–18 ka), massive continental ice sheets withdrew $60 \times 10^6 \text{ km}^3$ of water from the oceans, enough to drop the sea level by 120 m (Gornitz 2008). Correspondingly, at that time, land covered $c. 33\%$ of the Earth's surface (Fig. 16). During the past 540 Myr, according to our palaeogeographical models, the percentage of land area has varied

from a minimum of $c. 14\%$ during the Early–Middle Paleozoic (500–400 Ma) to a maximum of $c. 33\%$ during the Last Glacial Maximum (20 ka).

The solid line in Figure 17 (Kocsis and Scotese 2020) plots the changing percentage of land area during the last 540 Myr. The dashed line, which is the mirror image of land area, is the percentage of the continents covered by shallow sea. There are four other time intervals when the continents were as emergent as they are today: the Early–Middle Triassic (250–220 Ma), the Middle Jurassic (180–160 Ma), the Early Cretaceous (140 Ma) and the Eocene–early Miocene (45–15 Ma). It is interesting to note that though sea level fell rapidly during the Permo–Carboniferous Ice Age, the global sea level was relatively high ($c. +80 \text{ m}$) when compared to the present day.

In this regard, the present is not the key to the past. During the past 540 Myr the continents, more often than not, have been flooded by the oceans. According to the model, the times of relatively high continental flooding were: throughout the early and middle Paleozoic (500–400 Ma), the Aptian–Albian (130–110 Ma), the mid-Cretaceous (100–80 Ma) and the early–middle Paleogene (66–50 Ma). It is interesting to note that an important cross-over occurred 360 Myr ago (Fig. 17). At that time the shallow seas began to drain away from the continents and the percentage of land gradually increased. It is probably no coincidence that this late Devonian transition

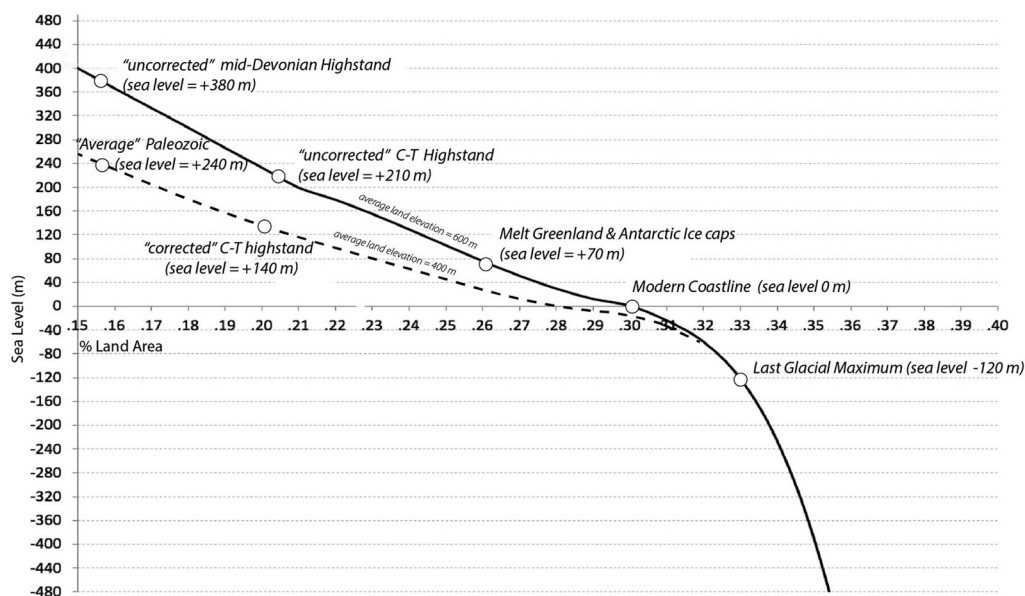


Fig. 16. Continental flooding curve. The solid black line represents the modern continental gradient. The dashed black line represents the reduced continental gradient during the Devonian (middle Paleozoic). This curve is similar to a hypsometric curve that plots the area of the Earth represented by various elevations.

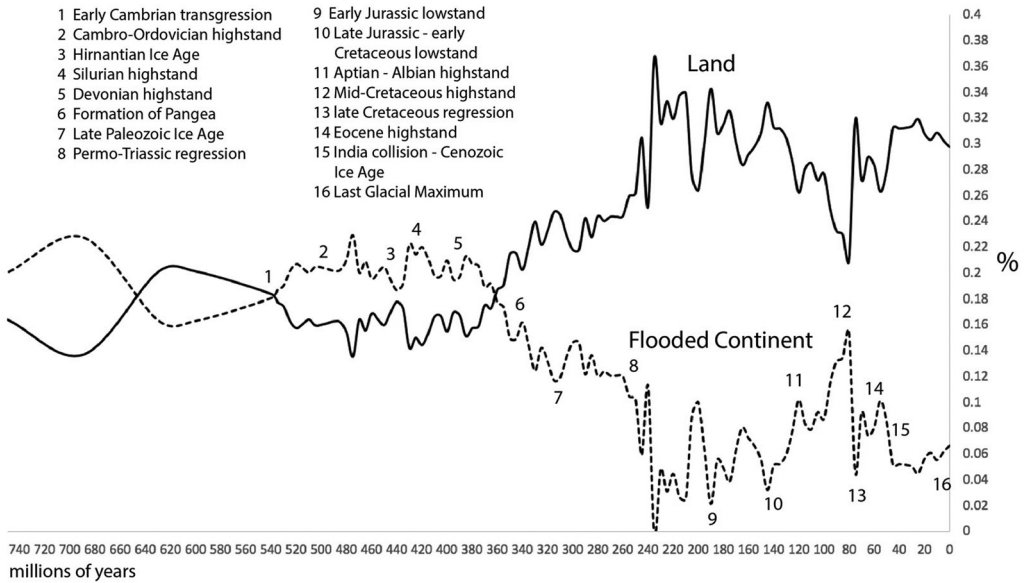


Fig. 17. Continental flooding. The percentage of global area that is land (solid line) and continent covered by shallow seas (dashed line). Important eustatic events are labelled with numbers 1–16.

also marks the evolution of land-dwelling tetrapods, the first extensive tropical rainforests and the rapid expansion of the terrestrial ecosystem.

Estimating past sea levels from changes in continental flooding

The seas go in and the seas go out because the level of the oceans (i.e. sea level) changes with respect to the land. Although most of these forces act regionally, their combined effect is global. A global change in sea level is called ‘eustasy’ (Chamberlin 1898, 1906, 1909; Suess 1908; Grabau 1924; Wagreich *et al.* 2014). Eustatic changes in sea level are globally contemporaneous and provide an important stratigraphic calibration tool. The episodic pattern of the seas coming in and the seas going out provides a standard that allows us to correlate far-flung geological and evolutionary events. This recurrent change in sea level is at the core of the study of stratigraphy, biostratigraphy and sequence stratigraphy (Sloss 1963; Vail *et al.* 1977a, b; Simmons 2012, 2020; Davies and Simmons 2023); long-term eustatic sea-level change may be the most important driver of global climate change (Fischer 1981, 1982, 1984; Berner *et al.* 1983; Berner 1994, 2004; Berner and Kothavala 2001).

One approach to estimating changing sea level would be to model all of the various factors that can cause a sea-level to rise or fall. This approach, however, is fraught with difficulties, uncertainties and complexities (Simmons 2012, 2020). We have

chosen a simpler, more direct way to estimate sea-level change. High sea level, whatever the cause, floods the continents. If we can accurately measure the amount of continental flooding through time, then we can use this measurement to retrodict past sea levels. This section of the paper describes how we used continental flooding to produce a novel Phanerozoic sea-level curve.

As illustrated in Figure 16, there are several sea-level calibration points along the modern continental flooding curve (solid black line): Last Glacial Maximum (−120 m, 33% land), present-day sea level (0 m, 30% land) and no polar ice caps (+70 m, 26% continental area). We can use measurements of land area obtained from the palaeogeographical maps to estimate past sea levels. For example, during the Late Cretaceous (80 Ma), shallow seas covered most of the continents and the land area was reduced to c. 21%. Using the modern continental flooding (i.e. hypsometry) curve, this change in land area corresponds to a sea-level rise of c. 220 m (Fig. 16). Maximum continental flooding occurred during the early and middle Paleozoic (500–400 Ma). At that time, land areas accounted for only 16% of the Earth’s surface. If we used the present-day flooding curve, we would predict that the sea level during the early and middle Paleozoic was nearly 400 m higher than the present-day sea level! This, however, is clearly an overestimate. We need to improve our predictions of past sea level by taking into account how the average elevation of the continents has changed through time.

The Cretaceous world

The Earth's surface is constantly changing. Mountain-building pushes the continents upwards, which steepens the continental flooding curve; rift and drift processes stretch the continents, which flattens the continental flooding curve. Today's topography, unfortunately, is not a good analogue for past topographies. The continents have been recently uplifted by Andean-style mountain building and a series of Cenozoic continent–continent collisions. The average elevation of the present-day land surface is nearly 600 m (Fig. 19). This is as high as or higher than any other time during the last 540 Myr. In order to use continental flooding to estimate past sea levels, we need to produce continental flooding curves that better match the continental topographies of these past times.

The best estimate of past continental topography is the changing average elevation of continental land areas through time. The average elevation of the land surface through time can be directly measured from the palaeogeographical maps and the corresponding palaeoDEMs. Figure 18 illustrates the average elevation above sea level of the continents during the Phanerozoic.

Major peaks occur during times of continental collision and most of the sharp drops take place during times of continental extension associated with

the early phases of ocean basin formation. This curve has two peaks. Present-day topography is the highest peak (c. 600 m). A second peak spans 100 Myr, and represents the uplift of the continents due to the continent–continent collisions that formed Pangaea (380–280 Ma). Prior to the formation of Pangaea, continental topography was much more subdued. During the early and mid-Paleozoic (540–400 Ma) and during most of the Mesozoic, the average height of the land surface was only c. 400 m, two-thirds of the present-day value. During the Cenozoic, continental elevations trended steadily higher, peaking in the last 30 Myr following the collision of Africa with Europe, and India with Asia.

As noted earlier, the dashed line in Figure 16 is the continental flooding curve based on the topography of the continents during the mid-Paleozoic. The mid-Paleozoic flooding curve is similar in shape to the modern continental flooding curve but the curve crosses zero metres (the coastline) at a level that corresponds to a land area of 26%, rather than 30%. In the mid-Paleozoic, because the continents were so low lying, even a modest rise in global sea level was sufficient to inundate much of the continents. For example, a 200 m rise in sea level during the mid-Paleozoic would have been sufficient to further reduce the land area to 15% (Fig. 16).

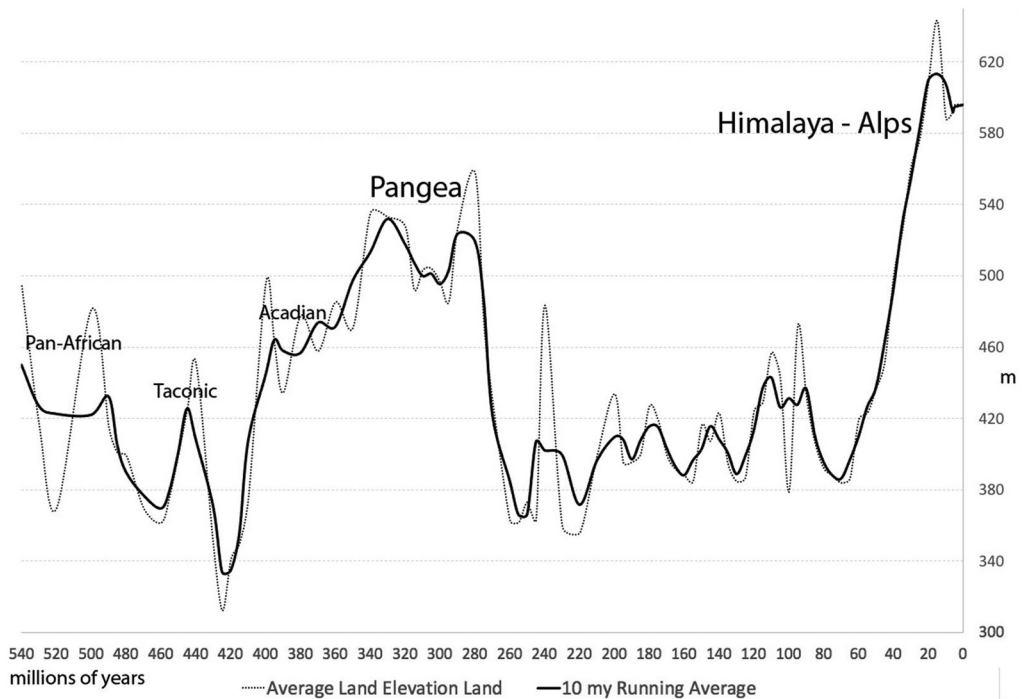


Fig. 18. Average elevation of the land surface above sea level during the Phanerozoic. The solid black line is the 10 Myr moving average.

The modern continental flooding curve and the middle Paleozoic flooding curve bracket the range of expected palaeotopographical variation of continental lowland areas during the Phanerozoic. We have used these maximum and minimum limits to construct a Phanerozoic global sea-level curve (Fig. 19). By taking into account the reduced topography of earlier time periods, the amount of sea-level change required to flood the continents is greatly reduced. For example, during the mid-Cretaceous, the average elevation of the continents was *c.* 400 m, or *c.* 66% of the modern average elevation. This means that the amount of sea-level rise during the mid-Cretaceous that was required to flood the same continental area was reduced from 210 to 140 m (a 33% reduction).

In a similar fashion, because of the reduced Paleozoic topography, the predicted mid-Paleozoic sea-level maximum of 400 m was reduced to a more plausible, but still elevated, level (+260 m). Taking into account the changing elevation of the continents (Fig. 18), we have estimated changes in the Phanerozoic sea level (Fig. 19) predicted by the changing degree of continental flooding (Fig. 16).

In Figure 20, the Phanerozoic sea-level curve derived from the palaeogeographical maps is

compared to other published sea-level curves estimates (Vail *et al.* 1977a, b; Hallam 1984a, b; Algeo and Selslavinsky 1995; Miller *et al.* 2005a, b; Müller *et al.* 2008a; Snedden and Liu 2010, 2011; van der Meer *et al.* 2014, 2022; Vérard *et al.* 2015). All of the Phanerozoic sea-level curves can be described as double humped, with peaks in the early–middle Paleozoic and the Cretaceous–early Cenozoic. The lowest sea level occurs during the Triassic and Jurassic between 240 and 160 Ma (<100 m) and the late Cenozoic (50–0 Ma).

Our estimate of Cretaceous sea level is in good agreement with the Miller *et al.* (2005a, b) and Müller *et al.* (2008a) sea-level curves. These curves represent the most conservative estimate of sea-level change (<200 m) during the last 200 Myr. Our curve is in the mid-range of the other curves for the Triassic lowstand. The Paleozoic portion of our curve is similar to the Vail *et al.* (1977a, b) curve, and substantially higher than all other curves except Hallam (1984a, b).

In summary, our estimate of Cretaceous sea-level change based on the degree of continental flooding suggests that sea level was highest (+150 m) during the Cenomanian–Turonian (90–80 Ma), with a subsidiary highstand during the early Aptian (120 Ma).

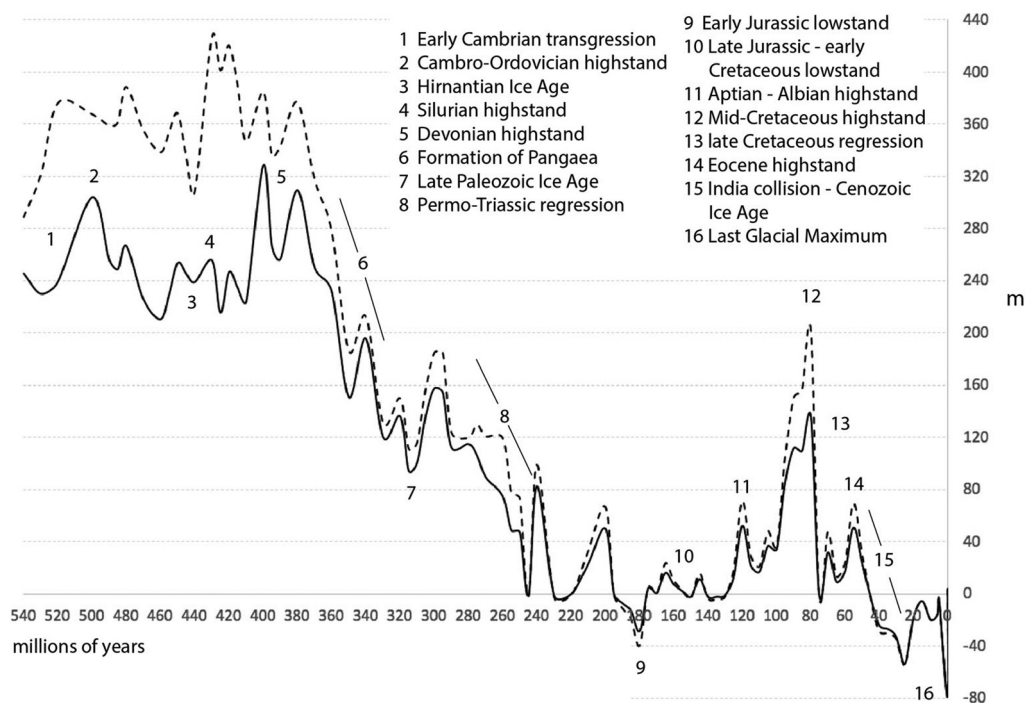


Fig. 19. Phanerozoic global sea level derived from continental flooding and the changing elevation of the continents. The dashed line is an estimate of sea-level change based on modern hypsometry. The solid line is an estimate of sea level that takes into account reduced continental hypsometry.

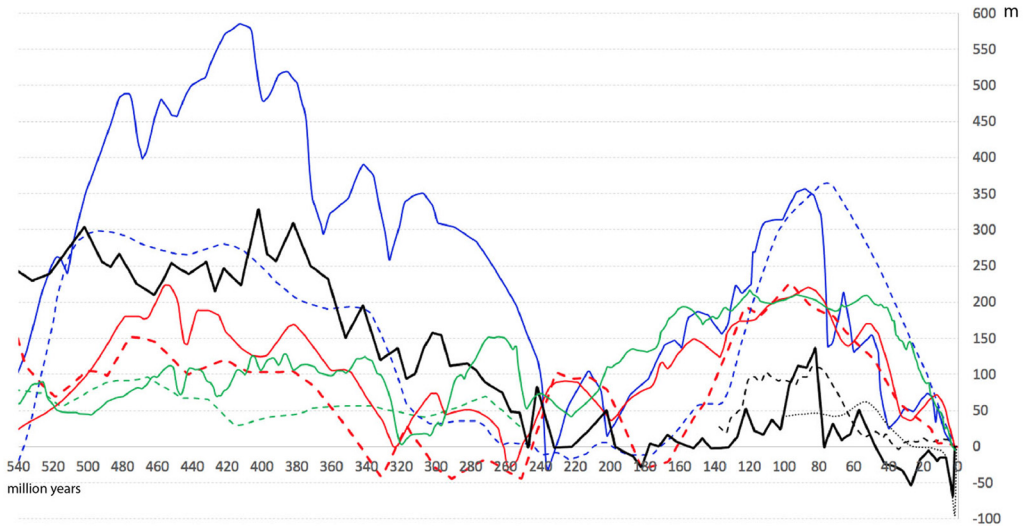


Fig. 20. A comparison of Phanerozoic sea-level curves: blue, Hallam (1984a, b); blue dashes, Vail *et al.* (1977a, b); green, van der Meer *et al.* (2022); green dashes (540–250 Ma), Algeo and Sessler (1995); red, Snedden and Liu (2010), red dashes, V  rard *et al.* (2015); black dashes (140–0 Ma), M  ller *et al.* (2008a, b); black dots (100–0 Ma), Miller *et al.* (2005a, b); black, this study.

Sea level was lowest during the earliest Cretaceous (+10 m) and at the end of the Cretaceous (+25 m).

Modelling Cretaceous palaeoclimate: computer simulations and lithological indicators of climate

Introduction

Cretaceous palaeoclimate simulations have progressed a long way from the first computer models of Barron *et al.* (1981), Barron and Washington (1982a, b, 1984, 1985) and Barron (1983, 1984). During the intervening 40 years, a multitude of simulations of Cretaceous climate have been run: for example, Schneider *et al.* (1985), Crowley *et al.* (1986), Horrell (1991), Barron *et al.* (1995), Valdes *et al.* (1996), Bush and Philander (1997), Herman and Spicer (1997), Price *et al.* (1998), Sloan and Pol-lard (1998), Barrera and Johnson (1999), DeConto *et al.* (1999), Poulsen *et al.* (1999, 2001, 2007), Upchurch *et al.* (1999), Beerling and Woodward (2001), Markwick (2004), Scotese *et al.* (2007, 2008), Sewall *et al.* (2007), Hunter *et al.* (2008), Zhou *et al.* (2008), Fl  gel *et al.* (2011), Hasegawa *et al.* (2012), Hay and Fl  gel (2012), Donnadieu *et al.* (2016), Ladant *et al.* (2020) and Landwehrs *et al.* (2021). These advances are attributable to a better understanding of the complexities of the Earth's climate system, a substantial increase in computer processing power (Moore's law), a wealth of digital

measurements of the modern climate and a growing community of scientific researchers using advanced global climate simulations (IPCC 2007, 2018, 2019).

These advances in computational climate modelling are now complemented by a growing database of lithological indicators of past climates such as coals, bauxites, coral reefs, evaporites, calcretes, tillites, glendonites and dropstones (Habicht 1979; Hallam 1984a, b; Ziegler *et al.* 1987; Frakes *et al.* 1992; Sellwood *et al.* 1994; Chumakov *et al.* 1995; Chumakov 1997; Parrish 1998; Markwick 2007; Boucot *et al.* 2013; Burgener *et al.* 2023). In addition, geochemical proxies for palaeotemperature (Veizer and Hoefs 1976; Veizer 1995; Veizer *et al.* 1999; Prokoph *et al.* 2008; Grossman 2012a, b; Veizer and Prokoph 2015; Henkes *et al.* 2018; Grossman and Joachimski 2020, 2022; Gaskell *et al.* 2022; Judd *et al.* 2022) and estimates of the ancient atmospheric concentration of the greenhouse gas CO₂ (Royer *et al.* 2004; Foster *et al.* 2017; Mills *et al.* 2019; Rae *et al.* 2021; H  nisch *et al.* 2023), in combination with novel statistical techniques (Bayesian statistics: Tierney and Tingley 2014, 2015; Judd *et al.* 2022; Burgener *et al.* 2023), are providing a clearer vision of climate change in deep time.

Computer simulations of palaeoclimate

The estimates of past temperature, precipitation and oceanic circulation presented in this study were produced by the Hadley Centre Model (HadCM3) developed by Paul Valdes at the University of Bristol

(Valdes *et al.* 2017, 2021). HadCM3 is a coupled atmosphere–ocean–vegetation model with a horizontal resolution of 3.75° (longitude) \times 2.5° (latitude). The atmospheric simulation has 19 levels and the oceanic simulation has 20 levels. A more detailed description of the workings of the HadCM3 model can be found in Gordon *et al.* (2000), Pope *et al.* (2000) and Valdes *et al.* (2017). Recent computer simulations of Cretaceous climate are also available for review (Lunt *et al.* 2016, 2023; Valdes *et al.* 2017, 2021; Haywood *et al.* 2019; Li *et al.* 2022; Willeit *et al.* 2022).

In order to simulate Cretaceous climates, the HadCM3 model requires four additional input parameters (Valdes *et al.* 2021): (1) the topography of the land surface and the bathymetry of the ocean floor during the Cretaceous; (2) an estimate of the amount of insolation received by the Earth during the Cretaceous; (3) an estimate of the changing amount of atmospheric CO₂ during the Cretaceous (Foster *et al.* 2017; Scotese *et al.* 2022); and (4) the pre-industrial concentration of ozone, which varies as a function of latitude (Beerling *et al.* 2011). One should also note that the HadCM3 model conserves the combined volume of water in the atmosphere and in the oceans.

Palaeogeography. The 17 Cretaceous palaeogeographical maps used in the HadCM3 simulations are derived from the PALEOMAP Palaeogeographic Atlas (Scotese 2016a, b, 2021; Scotese and Wright 2018). The original high-resolution elevation grid ($0.1^\circ \times 0.1^\circ$) was reduced to a $c. 111 \times c. 111$ km ($1^\circ \times 1^\circ$) grid. These data were regridded to $3.75^\circ \times 2.5^\circ$ resolution that matched the GCM using a simple area- or volume-conserving algorithm. The bathymetry was lightly smoothed using a simple binomial filter to ensure that the ocean properties were numerically stable. The areas at high latitudes had this filter applied multiple times. This gridding procedure sometimes produced single oceanic grid points surrounded by land grid points, particularly along complicated coastlines. These oceanic singletons were removed manually. Similarly, important ocean gateways were sometimes widened to ensure that the regridded coastlines permitted the free-flow of ocean waters.

The palaeogeographical reconstructions also include an estimate of the land ice area (Scotese and Wright 2018). These were converted to GCM boundary conditions assuming a simple parabolic shape to estimate the ice sheet height (Valdes *et al.* 2021). Unlike the Cretaceous palaeoclimate simulations of Lunt *et al.* (2016), which had no polar ice caps, the Cretaceous reconstructions in this study suggest that there may have been small areas of polar land ice during the earliest Cretaceous ($<4 \times 10^6$ km², about twice the area of Greenland).

Insolation. The amount of energy received from the Sun during the Cretaceous was approximately 98.4% of the modern value. This is based on the model of Gough (1981), which estimates that solar insolation has increased 30% since the formation of the solar system at a rate of 1.5°C per 100 Ma. Owing to the lower level of insolation, the mid-Cretaceous should have been 1.6°C cooler than the present day. This, of course, was not the case because levels of atmospheric CO₂ were, on average, three times higher during the Cretaceous (Cretaceous CO₂ = 1140 ppm, pre-industrial CO₂ = 380 ppm: Mills *et al.* 2019; Scotese *et al.* 2022).

Atmospheric CO₂. Global climate models, such as CESM (UCAR) and the HadCM3 (University of Bristol, UK), require estimates of atmospheric CO₂ to modulate the temperatures produced by these simulations. Therefore, an accurate estimate of the ancient concentration of atmospheric CO₂ is essential to successfully model past climates.

There have only been a few studies that have attempted to describe the variation in atmospheric CO₂ over the past 540 Myr. Figure 21 illustrates estimates of the changing levels of CO₂ during the Phanerozoic (Foster *et al.* 2017; Scotese *et al.* 2022), with two additional high-resolution curves for the Cenozoic (Rae *et al.* 2021; Hönisch *et al.* 2023). The Phanerozoic CO₂ curves suffer from gaps in the CO proxy record and time intervals when the range of CO₂ proxy estimates varies widely.

These data gaps are especially large in the early and middle Paleozoic (460–320 Ma), the late Permian and Early Triassic (270–230 Ma), and the Mid-Jurassic (180–150 Ma). During the Cambrian and Early Ordovician (540–460 Ma), there were no land plants and only a few types of plankton. For these reasons, there are no reliable proxy data for early Paleozoic. It should be noted that proxy values for CO₂ are quite variable during the early Permian (360–1440 ppm), the Triassic (400–3240 ppm) and the Paleocene (360–1200 ppm) (Foster *et al.* 2017).

In order to improve the estimates of the changing levels of atmospheric CO₂, we have used our growing understanding of the temperature history of the Phanerozoic (Scotese *et al.* 2021) to refine and update the Foster CO₂ curve. The sequence of black and white intervals along the time axis refers to times of relative global warming (black) and global cooling (white). Only 50% of the CO₂ peaks in the Foster curve correspond with warm intervals. Assuming CO₂ is the predominant cause of global warming, it is reasonable to make minor adjustments to the CO₂ curve so that peaks in the CO₂ curve correspond with times of maximum warming.

Using our updated estimate of Phanerozoic temperatures (Scotese *et al.* 2021), we can now fill in the gaps and reject contradictory CO₂ data. For

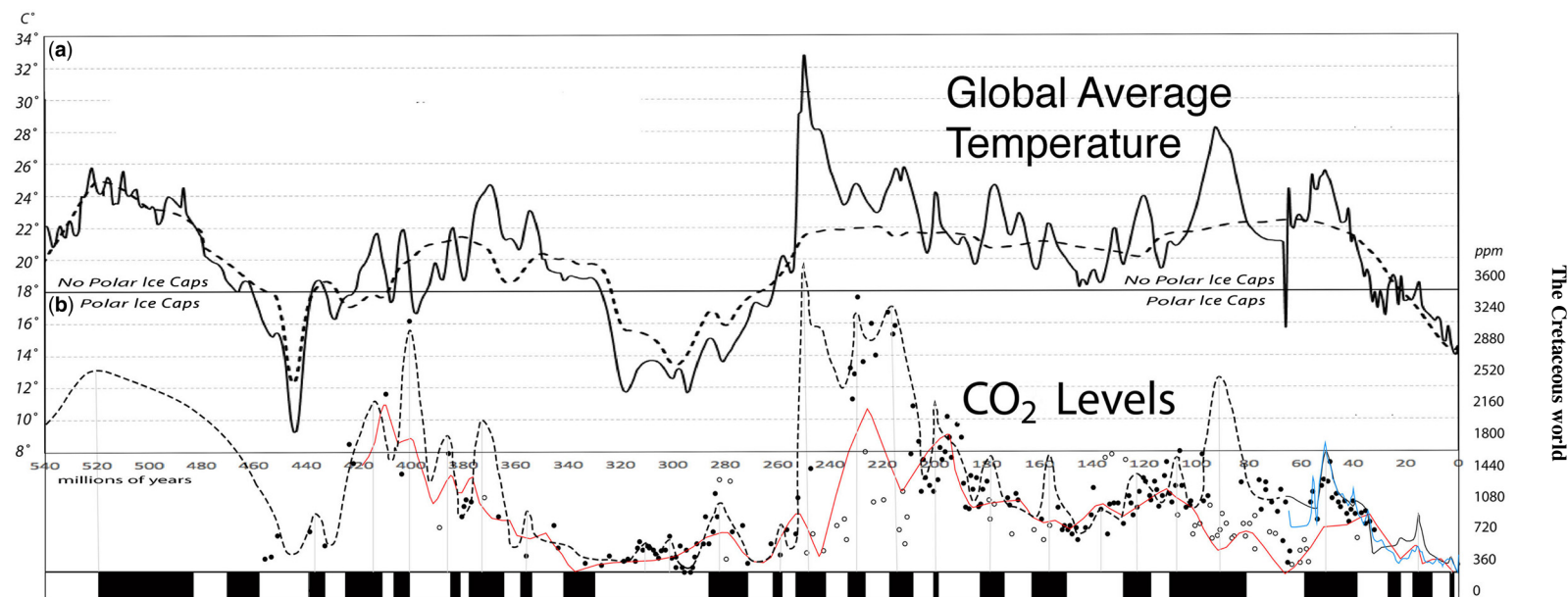


Fig. 21. Comparison of Phanerozoic global average temperature with Phanerozoic CO₂ levels. (a) Solid line, global average temperature (GAT); dashed line, 40 Myr running average. (b) Estimates of atmospheric level of CO₂: dotted line, *Scotese et al. (2022)*; red line, *Foster et al. (2017)*; thin black line (Cenozoic only), *Rae et al. (2021)*; thin blue line (Cenozoic only), *Hönisch et al. (2023)*; black dots, CO₂ proxy data binned in 1 Myr intervals; open black dots, rejected proxy data. The rectangles at the bottom of the figure indicate alternating warmer (black) and cooler (white) global temperature intervals. This vertical grey line connects CO₂ peaks with warmer intervals (*Scotese et al. 2021*).

example, during the Triassic and the Late Cretaceous the CO₂, estimates of less than *c.* 1080 ppm were rejected (open circles in Fig. 21). At first, this may seem like circular reasoning. No CO₂ proxies, however, were used to determine the cool and warm intervals (Scotese *et al.* 2021). We are simply redrawing the CO₂ curve so that it conforms to what we independently know about global temperature change. These adjustments significantly improve the fit between the revised CO₂ curve and the CO₂ proxy data.

There are still large gaps in the CO₂ proxy record; consequently, the estimation of CO₂ concentration is speculative (e.g. Cambrian, Early Triassic and Cenomanian–Turonian). This curve, however, represents a testable hypothesis that awaits confirmation or rejection with additional proxy data.

In recent years, a new modelling approach has been developed with regard to the use of CO₂ in computer simulations (Li *et al.* 2022; Lunt *et al.* 2023). Rather than relying on estimates of CO₂ based on proxy data (Fig. 21), the CO₂ level is derived or tuned from the expected global temperature. In other words, the global average temperature is assumed to be known and the level of CO₂ required in order to achieve that temperature is then derived, secondarily. This reverse engineering of CO₂ levels requires a well-established and credible Phanerozoic temperature curve (Fig. 21a) (Scotese *et al.* 2021).

Lithological indicators of climate and Köppen belts

An alternate approach to palaeoclimate modelling uses geological and palaeontological data to directly reconstruct the climate of the past (Habicht 1979; Ziegler *et al.* 1979, 1981; Parrish *et al.* 1982; Sellwood and Price 1994; Parrish 1998; Hart 2000; Gibbs *et al.* 2002; Rees *et al.* 2002; Sellwood and Valdes 2006; Markwick 2007; Boucot *et al.* 2013; Scotese *et al.* 2021; Burgener *et al.* 2023). The simplest approach uses lithological indicators of climate (e.g. coals, bauxite, coral reefs, evaporites, calcretes, kaolinites, tillites, glendonites and dropstones: see Boucot *et al.* 2013 for more information) to map ancient climatic belts.

Using modern temperature and rainfall records, we can map five major and eight minor climatic zones called ‘Köppen climate belts’ (Fig. 22). The Köppen climate belts are largely defined by seasonal variations in temperature and precipitation (Köppen 1918, 1936). These variations give rise to regional climates and create the mosaic of diverse environments that cover the Earth. These environments include: (A) tropical rainforests near the Equator (dark green); (B) desert belts at subtropical latitudes (yellow-tan) that transition into (C) warm temperate grasslands and forests (light green). In the modern world, as we move polewards, warm-temperate regions are replaced by (D) seasonally warm/cold

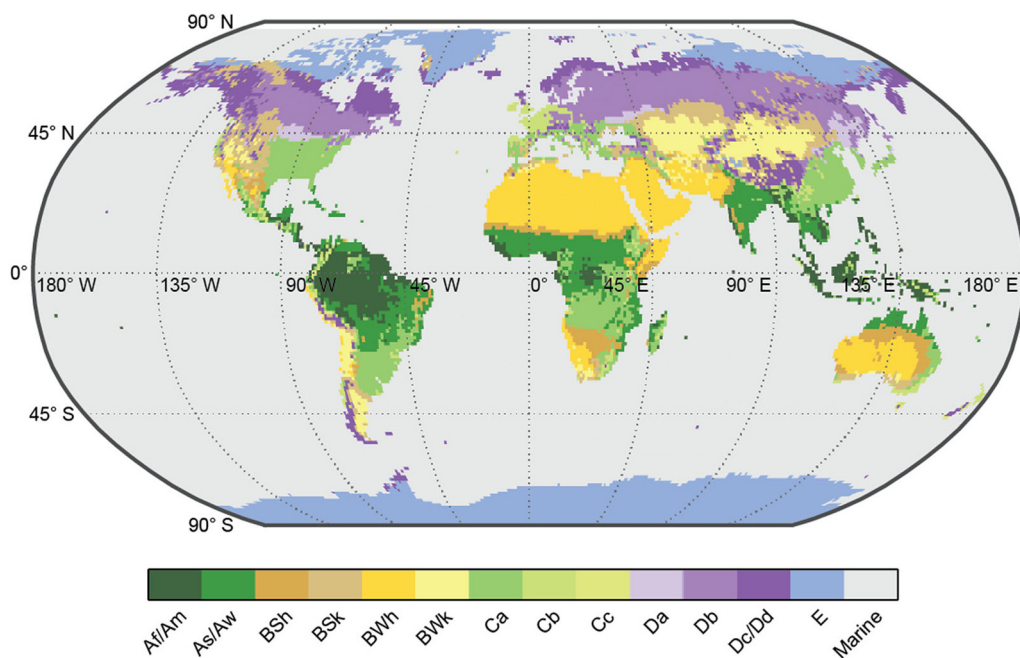


Fig. 22. Modern Köppen belts: Source: Burgener *et al.* (2023).

The Cretaceous world

temperate regions (purple) and finally (E) frigid polar regions (blue). Each of these climatic zones is characterized by a distinctive flora, fauna, land-cover and depositional environments.

The principal lithological indicators of climate – coals, evaporites and glacial deposits – can be used to map palaeo-Köppen climate belts for ancient time periods (Ziegler *et al.* 2003; Boucot *et al.* 2013). Other important lithological indicators of climate are: soil minerals such as bauxite, an aluminium ore that forms in warm, wet climates; calcrete, or caliche, which forms in semi-arid regions; and kaolinite, which forms in regions with climates that are sometimes wet and sometimes dry (Warm

Temperate climate belt). Dropstones, such as tillites, are important indicators of frozen lakes or sea ice. A glendonite (Rogov *et al.* 2023) is a pseudomorph of ikaite, a low-temperature, hydrated polymorph of CaCO_3 that forms at temperatures at less than 4°C . The legend inset in Figure 23 summarizes the association of the various lithological indicators of climate with warm/cool and wet/dry environmental conditions.

The palaeogeographical distribution of bauxites, in particular, helps us to understand Cretaceous climates. Bauxites, as a general rule, reflect tropical–subtropical humid, monsoonal conditions. Their modern occurrence is almost entirely restricted to

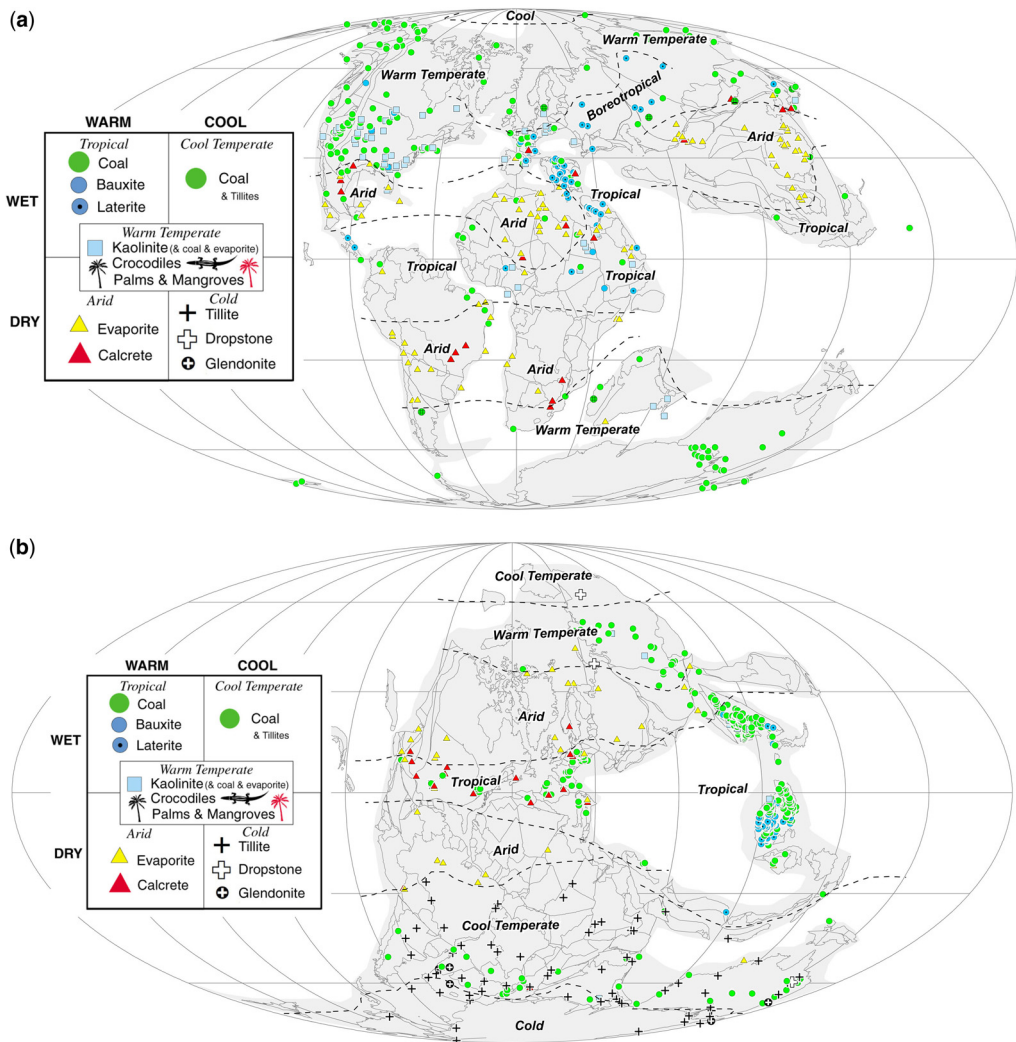


Fig. 23. (a) Mid-Cretaceous (100 Ma) and (b) Early Permian (280 Ma) lithological indicators of climate and palaeo-Köppen belts. Source: Boucot *et al.* (2013).

the Equatorial Wet belt. The occurrence of bauxite deposits in northern Europe and Siberia during Late Jurassic, Cretaceous, Paleocene and Eocene times (Boucot *et al.* 2013) is one of the strongest geological indications of warm and wet conditions at high latitudes.

Over the past 20 years, a global database of more than 15 000 lithological indicators of climate has been assembled (Boucot *et al.* 2013; see also the [Supplementary material](#)). For a thorough discussion of both the lithological and biological indicators of climate, see Parrish (1998), Boucot *et al.* (2013) and Cao *et al.* (2019).

An icehouse world is simply defined as a time when the Earth is covered by permanent ice at either pole. For permanent ice to accumulate in the polar regions ($>67^\circ$ N and S), the temperatures must remain below freezing during the summer months. In other words, the global average temperature (GAT) must be less than 18°C and the average annual temperature of the polar region must be below -10°C . Although the tropics remain warm (26°C) in an icehouse world, the polar regions are frigid (-50 to -10°C).

There also have been times in the past when there was no ice above the polar circle – even during the winter (e.g. Late Cretaceous; Fig. 23b). During these hothouse times, the average temperature of the Earth was generally above 20°C (68°F), and the polar regions were relatively warm (5 – 15°C), and no ice could accumulate. It is a well-established fact that no polar ice existed during the Cenomanian–Turonian Thermal Maximum (93 Ma; Ziegler *et al.* 1985) or the Paleocene–Eocene Thermal Maximum (55.6 Ma; McInerney and Wing 2011).

Despite these limitations, the Köppen approach does provide another important piece of information. This procedure describes how the pole-to-equator temperature gradient has changed through time. The relative widths of the Equatorial Wet belt and the Subtropical Arid belt do not change significantly through time because they are controlled by Hadley cell circulation (Ziegler *et al.* 2003). The changing pole-to-equator temperature gradient is due almost exclusively to the changing width of the Warm Temperate, Cool Temperate and Polar belts.

In icehouse worlds, like the present day, the pole-to-equator temperature gradient is very steep. The temperature falls 0.75 – 1°C per degree of latitude as we move towards the pole (e.g. if we start at 30°C at the Equator, we end up with temperatures of -60 to -40°C at the pole). During hothouse worlds (e.g. Cenomanian–Turonian Thermal Maximum, 93 Ma), the pole-to-equator temperature gradient was much shallower, approximately 0.20 – 0.33°C per degree of latitude. This means that if we start out at 30°C at the Equator, the temperature at the pole would still be well above freezing (0 – 12°C).

Combining lithological indicators of climate with quantitative palaeoclimate proxies

Recently, a more quantitative approach has been taken to estimate the actual range of palaeotemperatures and palaeoprecipitation (Tierney and Tingley 2014, 2015; Judd *et al.* 2022; Burgener *et al.* 2023). This approach assigns a precise numerical range of temperature and precipitation to specific lithological indicators of climate (Zhang *et al.* 2016) and combines them with more traditional quantitative palaeoclimate proxies such as various isotopic and molecular systems (e.g. $\delta^{18}\text{O}$, clumped isotopes and TEX_{86} ; Veizer *et al.* 1999; Grossman 2012a, b; Veizer and Prokoph 2015; O'Brien *et al.* 2017; Henkes *et al.* 2018; Song *et al.* 2019; Grossman and Joachimski 2020, 2022; Gaskell *et al.* 2022; Judd *et al.* 2022).

Using Bayesian statistics, the lithological indicators of climate and the geochemical proxy data are integrated to estimate the mean annual temperature (MAT), the warmest mean monthly temperature (WMMT) and the mean annual precipitation (MAP). The MAT, MAP and WMMT form the basis of the palaeo-Köppen map shown in Figure 2c (Burgener *et al.* 2023).

The three methods used to produce palaeoclimatic reconstructions – computer simulation (e.g. HadCM3 and CESM), lithological indicators of climate (Boucot *et al.* 2013) and a Bayesian analysis of palaeoclimatic proxies (Burgener *et al.* 2023) – give subtly different results. The best way to compare and contrast these different methods is to compare the pole-to-equator gradient diagrams produced by these methods. Figure 24 illustrates the pole-to-equator gradients for the Hauterivian–Barremian (Fig. 24a), the Albian (Fig. 24b) and the Turonian (Fig. 24c). The grey curve in each diagram is the modern pole-to-equator gradient. In the present-day world, the average temperature near the Equator is $c. 26^\circ\text{C}$. The temperature remains nearly constant in the subtropics (0° – 15° N and S latitude) and then begins to decrease rapidly. Freezing temperatures are reached at 60° latitude; falling to below -35°C at the poles.

The modern pole-to-equator temperature curve lies well below the curves for the Cretaceous.

This is not a surprise. The modern GAT is 14.5°C , whereas estimates of the GAT for the Cretaceous range from 18 to 28°C . The computer simulations (blue lines in Fig. 24) are similar to each other, and the two methods based on geological evidence are likewise similar. There are a few other general tendencies. The computer simulations tend to produce warmer tropical temperatures. The exception to this is the Turonian, when all models produced equally high tropical temperatures ($c. 30^\circ\text{C}$). Conversely, the mid- to high-latitude temperatures observed in

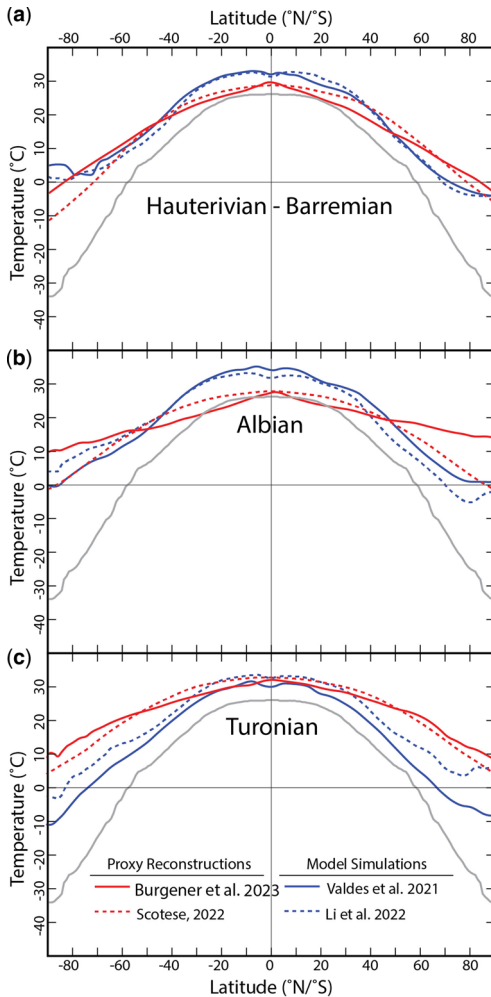


Fig. 24. Pole-to-equator temperature gradients during the Cretaceous. **(a)** Hauterivian–Barremian, **(b)** Albian and **(c)** Turonian. A comparison of pole-to-equator global surface temperature gradients from two proxy-based models (dashed red line, Scotese *et al.* 2021; solid red line, Burgener *et al.* 2023) and two computer simulations (solid blue line, Valdes *et al.* 2021; dashed blue line, Li *et al.* 2022). The modern average pole-to-equator gradient (grey line) is shown for comparison (Legates and Willmott 1990).

computer simulations are 10–20°C cooler than the results from the proxy methods. The exception is the Hauterivian–Barremian result. During this cooler period, the mid- and high-latitude temperatures obtained from all methods are roughly equivalent.

Although we can be encouraged by the similar results obtained from all three disparate methodologies, interesting anomalies still persist. The Bayesian method displays an unlikely flat gradient during the

Albian, with unsustainably warm temperatures at moderate and high latitudes. At polar latitudes, the computer simulations display a strange tendency towards increased warming, unlike modern polar temperatures.

Modelling Cretaceous palaeorivers

Drainage system and palaeorivers

Thanks to the palaeoDEMs (quantified topography: Scotese and Wright 2018), it has been possible to model drainage systems and palaeorivers during the Phanerozoic. The drainage systems were initially established without considering precipitation, and thus provide metrics about how water would flow given sufficient rainfall. The palaeorivers that were filled with water were mapped once the amount of precipitation generated by HadCM3 climate model of Valdes *et al.* (2021) was applied. Other researchers have taken a similar approach using the PALEO-MAP palaeoDEMs to model landscape dynamics on a global scale (Salles *et al.* 2023).

Method

We used the Hydrology tools of the ArcGIS® software both to produce the drainage maps and to predict the location of palaeorivers for each stage of the Cretaceous. Emerged land areas were mapped using the Cretaceous palaeoDEMs. Land surfaces were then prepared using the Fill function of ArcGIS®, which removes spurious sinks or peaks, and flow directions were computed and forced to flow down the topographical gradient. Note that all basins below sea level but not in contact with ocean basins were considered to be lakes and were filled up using the Fill function of ArcGIS®. The Basin function of ArcGIS® was used to delineate drainage basins by identifying the drainage divide between basins. The corresponding raster files were then converted into polygons and the basin sizes (geodetic surfaces) were computed. The Flow Length tool of ArcGIS® calculated the linear distance from any given pixel along the drainage system to the river mouth. In other words, the flow length map shows how far a drop of rainwater would need to travel to reach the shoreline, presumably a river delta.

The Cretaceous palaeorivers (Fig. 25) were mapped by calculating the flow accumulation (Flow Accumulation tool of ArcGIS®) weighted from the precipitation maps of Valdes *et al.* (2021). Using HadCM3BL-M2.1Da, a variant of the Hadley Centre HadCM3 model (http://www.ipcc-data.org/sim/gcm_clim/SRES_TAR/hadcm3_info.html), simulations were run for every Cretaceous time slice (Table 1). Note that runoff was then merely taken

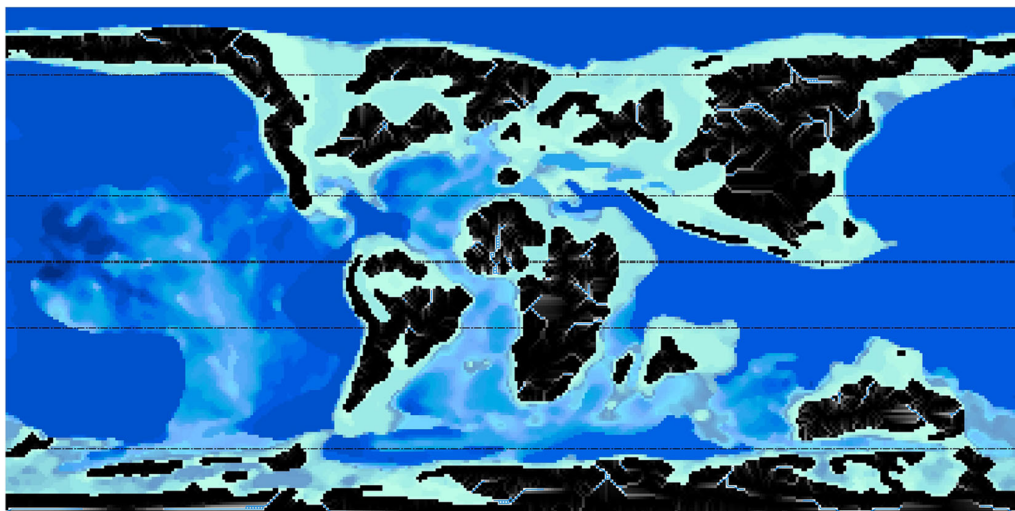


Fig. 25. Early Campanian (80 Ma) drainage pattern and palaeorivers. The thickness of the lines representing the palaeorivers is proportional to the river discharge.

into account by bringing a quantity of water (precipitation) to the nearest ocean (as the crow flies) and not by following the drainage system (the palaeorivers) as defined here. For the sake of clarity, a conditional rule was set to only select and display the palaeorivers with the largest flux.

Flow length

In each time slice, there are many small basins and only few large basins. The distribution is

exponential. The same is true regarding flow length, which represents the average river length. The mean values of the river length (and associated standard deviation) were calculated on the basis of their logarithmic (\log_{10}) values, which approximates a Gaussian distribution.

In general, the average river length during the Phanerozoic responds inversely to sea-level change (Fig. 26). During the Cretaceous, the average river length decreases from a Cretaceous high at 145 Ma to an all-time low at 80 Ma. The average river length

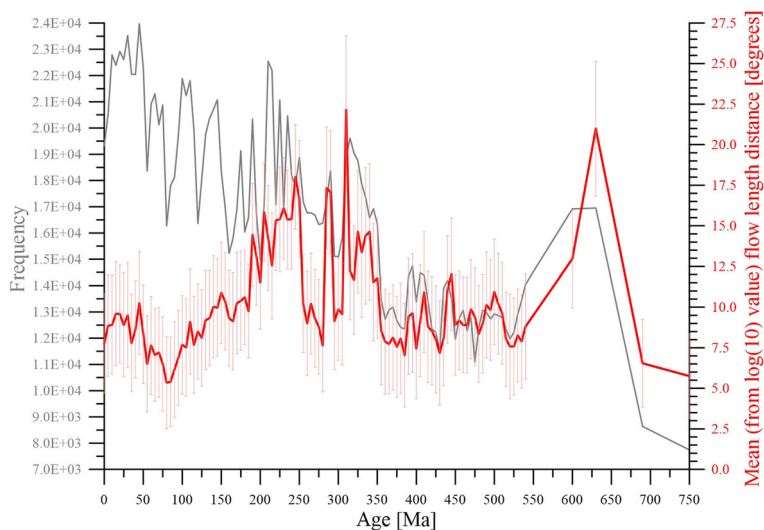


Fig. 26. Drainage basin size (grey line) and mean flow length (red lines) during the Phanerozoic.

then increases towards the end of the Cretaceous. As the dispersal or aggregation of continents is not the major factor over this time interval, it is clear that the length of rivers changed due to rising and falling sea level.

Chronological review of plate tectonics, palaeogeography and palaeoclimate during the Cretaceous

Plate tectonics during the Cretaceous

Overview

This section reviews plate tectonic events for four intervals during the Cretaceous: the earliest Cretaceous (Berriasian–Barremian), the Early Cretaceous (Aptian–Albian), the mid-Cretaceous (Cenomanian–Turonian) and the Late Cretaceous (Coniacian–Maastrichtian). To better understand the complex series of Cretaceous plate tectonic events, the reader is referred to [Figures 28–44](#), as well as additional plate tectonic reconstructions in the [Supplementary material](#). While reading the text, the reader should simultaneously review the animation of Cretaceous plate motions ('Plate tectonics: 200 million years–today' provided in the [Supplementary material](#). Scrolling backwards and forwards through the animation will give the reader a much better understanding of the dynamic nature of Cretaceous plate tectonics.

Although the initial break-up of Pangaea began in the Early–Middle Jurassic (200–170 Ma: [Scotese and Schettino 2017](#)), most of the modern ocean basins formed by successive rifting events during the Cretaceous. North America continued to separate from NW Africa during the Cretaceous, widening the Central Atlantic. Simultaneously, East Gondwana (Madagascar, India, Australia and Antarctic) rifted away from West Gondwana (Africa and South America), widening the western Indian Ocean. In the South Atlantic, Africa and South America were fully separated by the Albian (110–105 Ma). Shortly thereafter (*c.* 95 Ma, Cenomanian), India separated from Madagascar and Australia slowly rifted away from East Antarctica. North America remained connected to northern Europe during the Cretaceous, although the Labrador Sea had partially opened, and multiple zones of extension had appeared between East Greenland and Rockall Bank (northwestern Europe).

Other significant Cretaceous tectonic events include: the collisions of Stikinia and Wrangellia along the western margin of North America (143 and 100 Ma, respectively), the opening of the Circum-Arctic Ocean (145–125 Ma), the insertion of the Caribbean Plate between North and South

America (95–45 Ma), and the rifting of Zealandia from eastern Australia, which opened the Tasman Sea (85–55 Ma), as well as the complex development of the Pacific, Farallon, Izanagi and Phoenix oceanic plates ([Nakanishi *et al.* 2015](#)). Two major subduction zone systems dominated the Cretaceous world: the Circum-Panthalassic subduction zone, and the northward-dipping Tethyan subduction zone. This complex series of Cretaceous rifting events is illustrated on the tectonic timeline ([Fig. 27](#)). Each major Cretaceous rifting event is indicated by a split in the tectonic tree.

Earliest Cretaceous (Berriasian–Barremian, 145–125 Ma)

Intra-Pangaean Ocean basins. Seven of the 11 intra-Pangaean ocean basins had opened by the start of the Cretaceous (145 Ma): the Central Atlantic, the Gulf of Mexico, the proto-Caribbean Ocean, the South Atlantic, the western Indian Ocean, the NE Indian Ocean (Argo Sea) and the Canada Basin. An intra-Pangaean ocean basin is defined as an ocean basin formed by the break-up of the encircling Pangaean supercontinent.

The Central Atlantic, which had opened in the Early–Middle Jurassic (*c.* 175 Ma: [Scotese and Schettino 2017](#)), was *c.* 1500 km wide by the early Aptian (125 Ma). The Bahamas Platform hotspot track divided the Central Atlantic Basin from the proto-Caribbean Ocean and Gulf of Mexico basins. Rifting in the Gulf of Mexico, which had opened synchronously with the Central Atlantic, was finished by the earliest Berriasian (144 Ma: [Pindell *et al.* 1988, 2005; Ross and Scotese 1988; Pindell and Barrett 1990; Pindell and Kennan 2009](#)). Most of the Gulf of Mexico is underlain by hyper-attenuated continental crust; however, a small crescent of oceanic crust lies at the centre of the basin ([Buffler and Sawyer 1983](#)) (see [Figs 28–32](#)).

The proto-Caribbean Ocean Basin was divided into two parts by the Yucatan Peninsula. The triangular-shaped eastern proto-Caribbean Ocean Basin lay between the Bahamas Platform, the northern coast of Venezuela and the eastern shores of Yucatan. The western half of the proto-Caribbean Ocean Basin was located between western Colombia and eastern Honduras. Both halves of the proto-Caribbean Ocean Basin opened as North America pulled away from South America, together with Africa, in the Late Jurassic and Early Cretaceous.

Portions of the volcanic islands of Cuba and Hispaniola (Greater Antilles) formed the southwestern margin of the proto-Caribbean Ocean Basin. The Greater Antilles were originally a continental island arc that was continuous with the Andean margins of Mexico and South America.

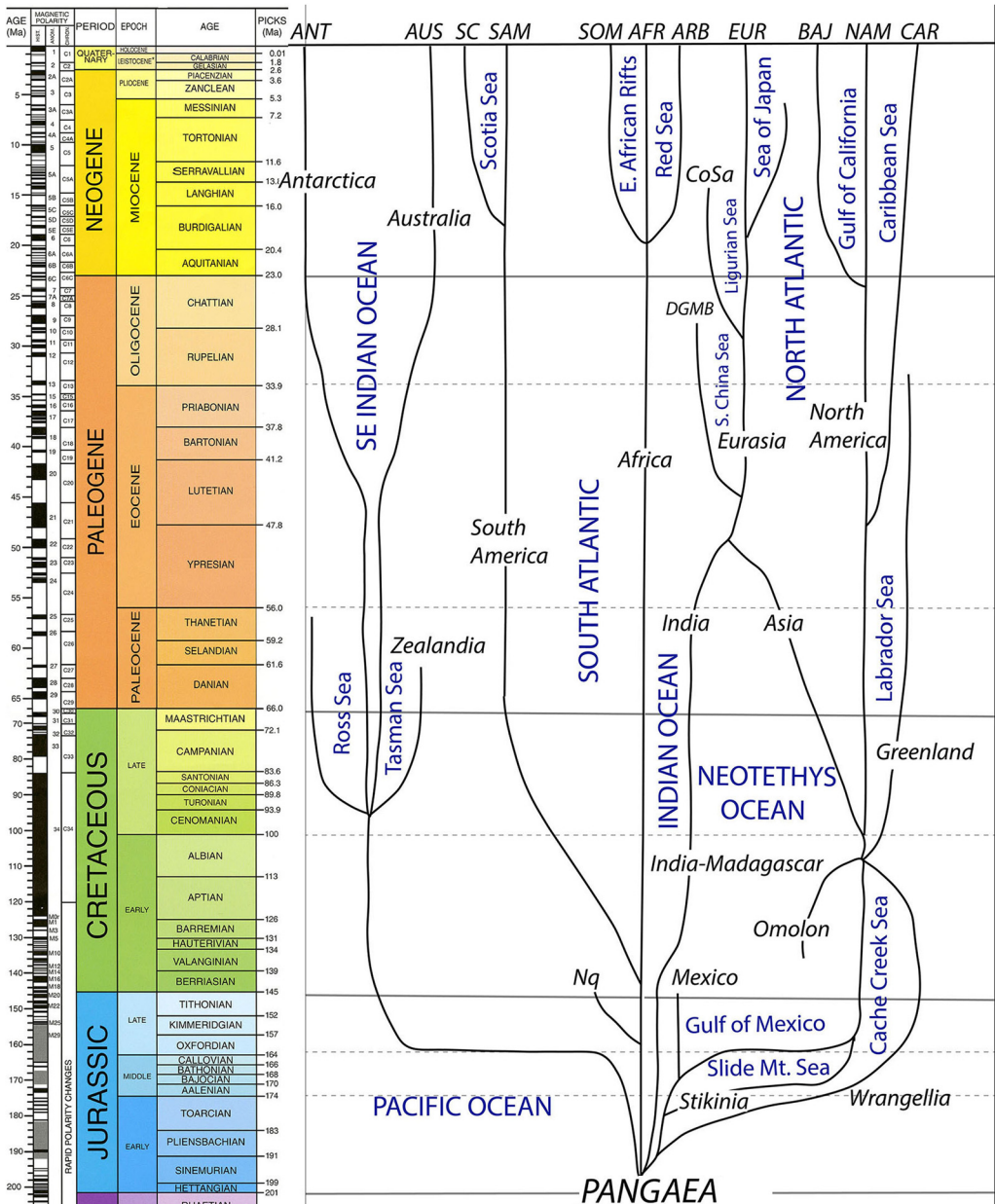


Fig. 27. Plate tectonic tree diagram for the Mesozoic and Cenozoic. Branches represent rifting events that form new ocean basins (blue lettering). Coalescing root-like structures indicate continent–continent collisions (e.g. India–Asia). Continents and continental terranes are labelled with black italic lettering. The abbreviations in capital letters across the top of the diagram are the modern plates: AFR, Africa; ARB, Arabia; ANT, Antarctica; AUS, Australia; BAJ, Baja California; CAR, Caribbean; EUR, Europe; NAM, North America; SAM, South America; SC, Scotia Sea; SOM, Somalia. Other abbreviations are: CoSa, Corsica and Sardinia; DGMB, Dangerous Grounds and Macclesfield Bank; Nq, Neuquen Basin.

By the Berriasian (140 Ma), the South Atlantic had just begun to open. The eruption of the Páramo–Entendeka flood basalts (130–138 Ma)

occurred during the early rift phase. Oceanic crust (early drift phase) had just begun to form in the portion of the South Atlantic south of the Rio Grande

The Cretaceous world

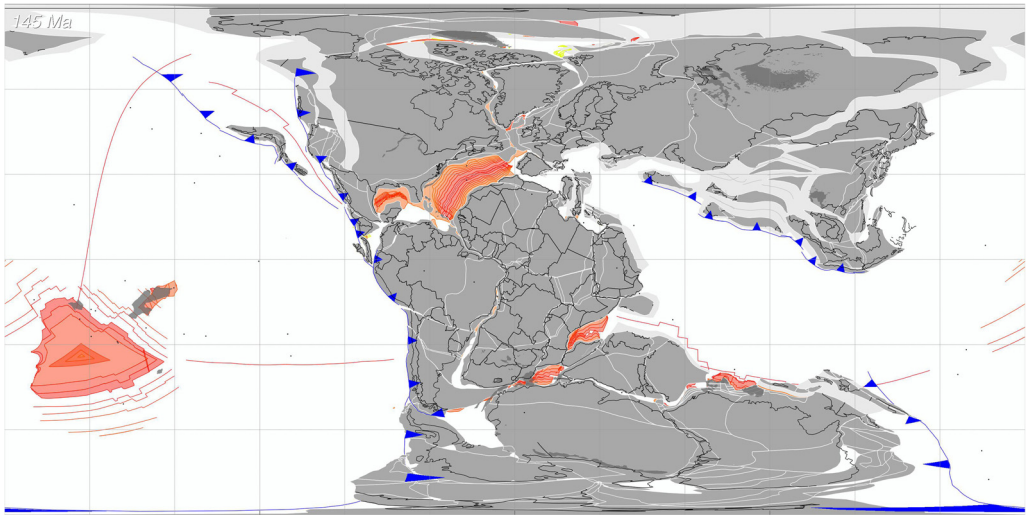


Fig. 28. Jurassic–Cretaceous Boundary (145 Ma); see [Figure 2a](#) for the legend.

Rise–Walvis Ridge hotspot track. The central portion of the South Atlantic from the São Paulo Plateau to the Benue Trough was characterized by rift lakes and crustal extension similar to that in the present-day East African Rift System. The northern segment of the South Atlantic margin, from the Benue Trough to the Guinea Plateau/Demerara Rise, had yet to experience significant extension. As Africa separated from South America, some of the deformation was taken up by right-lateral transtensional deformation in southern South America that created rift

basins in the vicinity of the Rio de le Plata and south of the Rio Negro.

The Somali Basin, Mozambique Basin and Weddell Sea were actively opening during the earliest Cretaceous. East Gondwana (Madagascar, India, Antarctic and Australia) drifted southwards, away from West Gondwana (Africa and South America). Madagascar slid past northeastern Mozambique along the Davie Fracture Zone, while Queen Maud Land slid past the eastern tip of the Falkland Plateau along the Mozambique Escarpment. This strike-slip

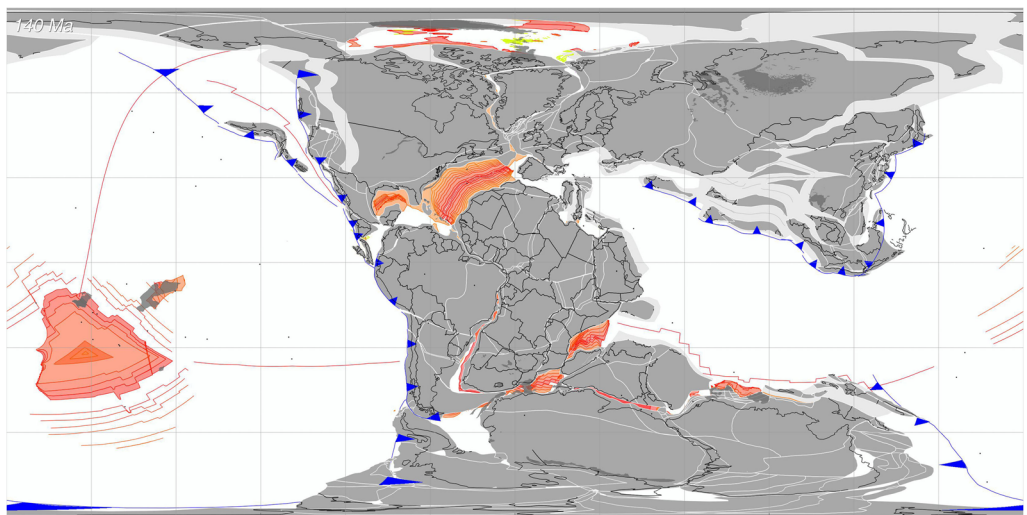


Fig. 29. Early Cretaceous (latest Berriasian, 140 Ma); see [Figure 2a](#) for the legend.

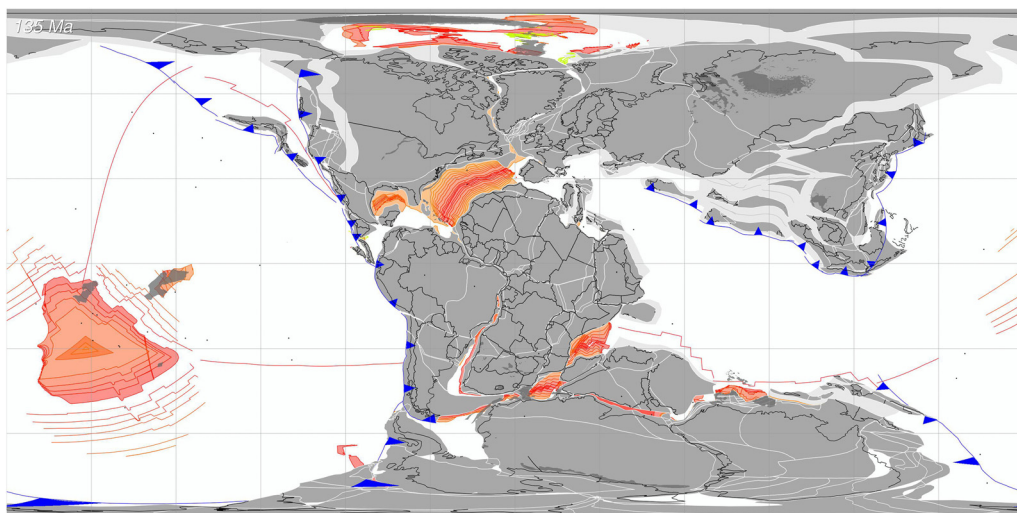


Fig. 30. Early Cretaceous (Valanginian, 135 Ma); see Figure 2a for the legend.

separation of East and West Gondwana created three narrow ocean basins: the Somali Basin in the north, the Mozambique Basin in the centre and the Weddell Sea in the south.

Although most of East Gondwana (Madagascar, India–Greater India, Australia and Antarctica) remained intact during the earliest Cretaceous, by 125 Ma (latest Barremian) a small ocean basin had opened between India and East Antarctica (Queen Maud Land) and where the eastern face of Greater India abutted against western Australia. Plate

stresses in this region appear to have been erratic during this time period and the location of the mid-ocean ridges in the Perth Basin and Gascoyne Plain jumped to the NW on several occasions (Powell *et al.* 1988).

Extra-Pangaeian ocean basins. The splintering remnants of Pangaea were surrounded by five distinct ocean basins: the Pacific Ocean, the Tethys Sea, the Amurian Seaway, the Angayucham Ocean and the Wrangellian back-arc basin, also called the Cache Creek Sea. The largest of these ocean basins was the Pacific Ocean, which was a direct

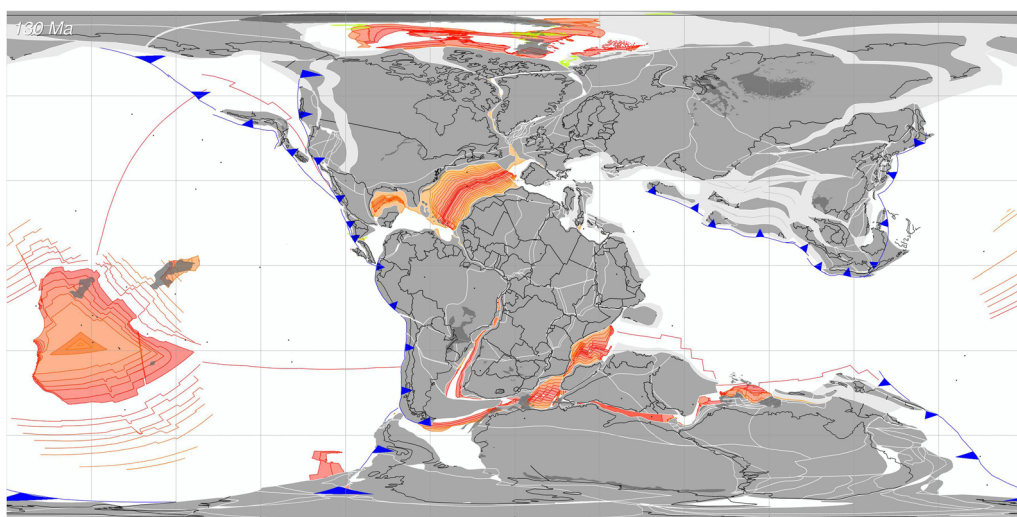


Fig. 31. Early Cretaceous (early Hauterivian, 130 Ma); see Figure 2a for the legend.

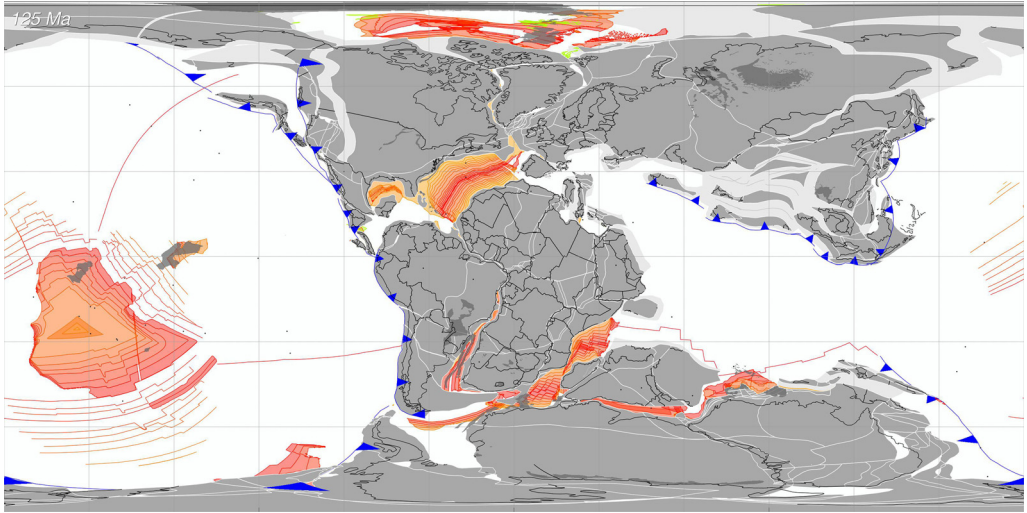


Fig. 32. Early Cretaceous (earliest Barremian, 125 Ma); see [Figure 2a](#) for the legend.

descendent of the Paleozoic and early Mesozoic Panthalassic Ocean. Four oceanic plates – the Pacific Plate, the Farallon Plate, the Phoenix Plate and the Izanagi Plate – continued to grow during the earliest Cretaceous ([Wright *et al.* 2016](#)). These four plates had emerged from the expansion of a triple-triple junction that formed in the SW Pacific during the early part of the Jurassic (c. 190 Ma), which is most likely to have been due to a massive mantle plume that also generated the thick basaltic crust underlying the Caribbean Plate.

The recumbent, V-shaped Tethys Ocean separated the northern continents of Laurasia (North America and Eurasia) from the southern hemisphere continents that were located along the Afro-Indian–Australian margin of Gondwana. Two mid-ocean ridges (North Tethys Ridge and South Tethys Ridge) divided the Tethys Sea into three oceanic plates: a small Palaeotethys Plate to the north, a large Mesotethys oceanic plate in the middle and the nascent Neotethys Plate to the south.

The North Tethyan Ridge formed along the northern margin of Indo-Australian Gondwana during the Early Jurassic. Beginning in the Late Jurassic and continuing into the earliest Cretaceous, a mysterious continental fragment (Argoland; [Audley-Charles 1988](#); [Powell *et al.* 1988](#)) rifted away from the northwestern shelf of Australia (Argo Sea). We do not know precisely where this continental fragment ended up. Some authors believe that it is now part of SE Asia ([Metcalf 1984, 1993, 1999](#); [Zahirovic *et al.* 2014](#); [Vérard *et al.* 2017](#); [Advokaat and van Hinsbergen 2024](#)). By the Berriasian, the North Tethyan Ridge had migrated northwards to a position off the southern coast of Central Asia.

During the Early Cretaceous, the North Tethyan Ridge was progressively subducted beneath Eurasia and the last remnants of the Palaeotethys Plate was subducted by the early Aptian (125 Ma).

The South Tethyan Ridge was initially a slow spreading ridge that formed along the northern margin of the Indo-Australian margin of Australia and directly connected to the mid-ocean ridges in the Somali and Mozambique basins. The South Tethyan Ridge separated NW India and Greater India from a thin sliver of continental crust that would later become the Lut Block of eastern Iran. During the Early Cretaceous, the South Tethyan Ridge coincidentally aligned with the Pacific–Izanagi mid-ocean ridge, although the precise nature of plate boundaries in the easternmost Tethys is speculative.

Active subduction zones bordered the expanding frontiers of Pangaea during the earliest Cretaceous. In several areas, back-arc basins opened along margins that were previously Andean-type subduction zones (e.g. the Qiang Tang back-arc basin along the northern margin of Tethys). In other places, back-arc basins that had opened in the Triassic and Jurassic collapsed and were converted into compressional, foredeep environments (Neuquen Basin, western Argentina; [Uliana and Leggarreta 1993](#); [Cobbold and Rossello 2003](#)). Along the North American margins of the NE Pacific Ocean were two notable back-arc basins: the Angayucham Sea and the Cache Creek Sea. The Angayucham Sea ([Nokleberg *et al.* 2001](#); [Scotese *et al.* 2005](#)) began to close in the earliest Cretaceous, as the North Slope terrane rotated counter-clockwise away from the Arctic Islands of Canada, opening the Canada Basin. The Wrangellian back-arc basin, which had opened in the Mid-

Triassic (c. 230 Ma), closed in the mid-Cretaceous (c. 110 Ma; [Nokleberg *et al.* 2001](#)).

The Cretaceous was nearly devoid of continent–continent collisions. The one exception was the closure of the Amurian Seaway in the Late Jurassic and earliest Cretaceous. The Amurian Seaway diachronously closed (west to east) as a collage of recently assembled continental terranes (Amuria, North China, Tarim, South China, Indochina and Sibumasu) collided with Mongolia and southeastern Siberia along the Mongol–Okhotsk suture ([Zonenshain *et al.* 1990](#)). The Amurian Seaway was completely closed by the Barremian (125 Ma).

Early Cretaceous (Aptian–Albian, 125–100 Ma)

NW sector of Pangaea. By the mid-Early Cretaceous (125 Ma), Pangaea had divided into three major continental groupings: (1) Laurasia (North America, northern Europe and Asia) to the NW; (2) West Gondwana (Africa, Iberia, Southern Europe, Arabia, and South America) in the centre; and (3) East Gondwana (Madagascar, India, Greater India, Antarctica, Australia and Zealandia) to the SE. During the Aptian–Albian, each of these continental groupings began to subdivide.

In the NW sector, Laurasia slowly began to break apart. Iberia, which was attached to NW Africa (Morocco), rifted away from western France, slowly opening the Bay of Biscay (125–90 Ma). Rifting propagated northwards into the North Atlantic, stretching the continental crust between Greenland, Rockall Bank and western Europe.

The proto-Caribbean Ocean Basin continued to open as South America, together with Africa, pulled away from North America. The proto-Caribbean Ocean Basin would continue to widen until the mid-Albian (105 Ma). By that time South America was completely separate from NW Africa and had begun to move in concert with North America. The proto-Caribbean Ocean stopped widening because relative motion between the North American and South American plates had essentially ceased (see [Figs 32–37](#)).

Cuba and Hispaniola (Greater Antilles) formed the southwestern margin of the proto-Caribbean Ocean Basin during the Aptian–Albian. The Greater Antilles were originally a continental island arc that was continuous with the Andean margins of Mexico and northern South America.

To the far north, during the latest Jurassic and Early Cretaceous (155–125 Ma), the Canada Basin opened as the North Slope of Alaska rifted away from the Arctic margin of Canada ([Lawver and Scotese 1990](#); [Nokleberg *et al.* 2001](#); [Scotese 2008](#)). The opening of the Canada Basin stopped when the North Slope/Chukotka Block collided with the continental backstop made up of central Alaska and NE Siberia ([Lawver and Scotese 1990](#)). This collision of the North Slope Block along the Brooks Range closed the Angayucham Ocean (Barremian, 125 Ma).

Central sector of Pangaea. In the central sector, Africa and South America did not break apart as two rigid continental blocks. Rather, there was a period of diachronous separation (150–110 Ma) as the rift zone between Africa and South America propagated northwards, facilitated by crustal weaknesses caused

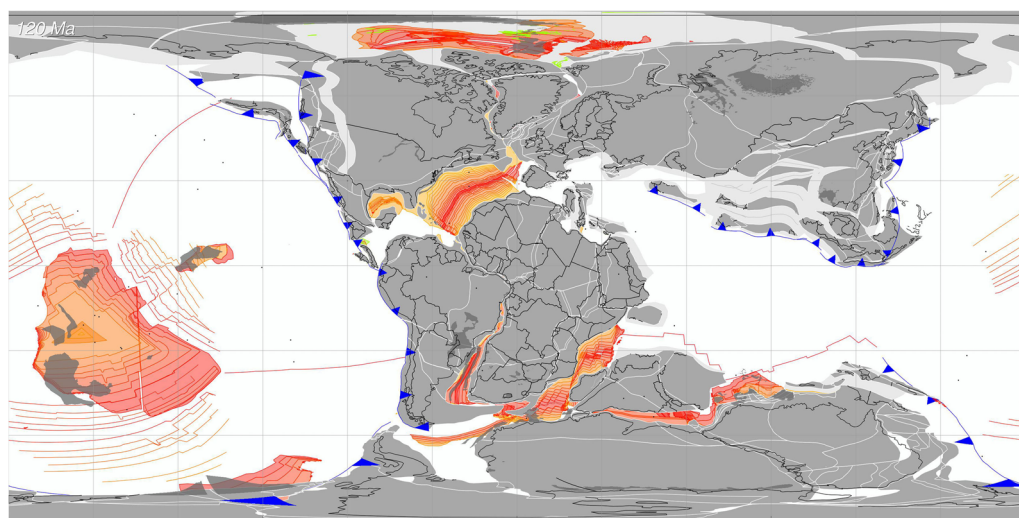


Fig. 33. Early Cretaceous (early Aptian, 120 Ma); see [Figure 2a](#) for the legend.

The Cretaceous world

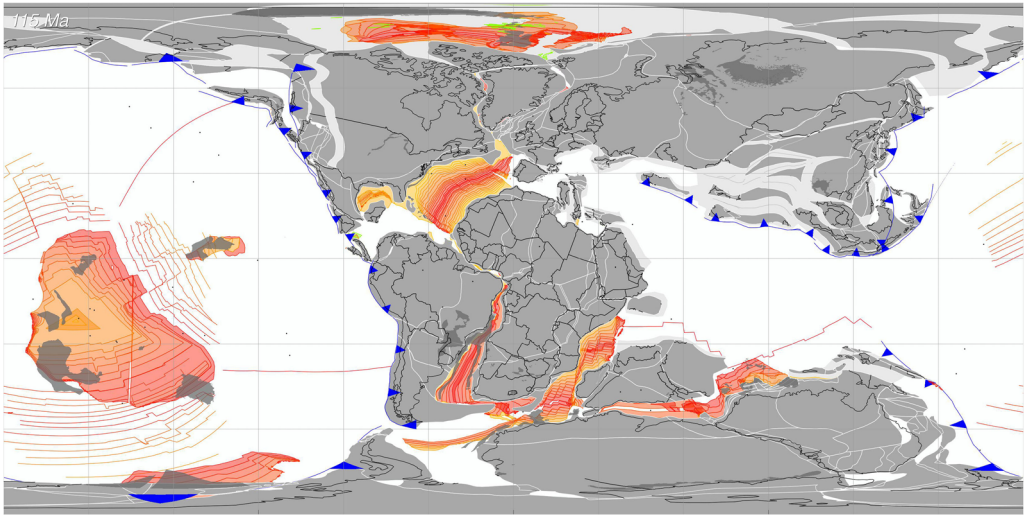


Fig. 34. Early Cretaceous (late Aptian, 115 Ma); see [Figure 2a](#) for the legend.

by the Tristan da Cunha (Entendeka and Párama LIPs, 130–135 Ma) and the Bahamas hotspots. The oldest datable magnetic anomalies in the far South Atlantic are M11 (133 Ma), whereas the oldest magnetic anomaly in the central South Atlantic is M3 (c. 125 Ma).

This diachronous pattern of rifting resulted in considerable transtensional deformation in southeastern South America (150–125 Ma) and later in central Africa (120–110 Ma). The extension in southeastern South America took place primarily in

the Salado and Rio Negro basins. Hypothetical right-lateral shear zones separated the more rigid part of the South American Plate (Amazonia) from the more deformable Paranaíba, Rio de la Plata and Patagonian blocks ([Fig. 4](#)). During the Aptian and Albian (120–110 Ma), right-lateral transtension along the Central African Shear Zone produced continental rifting in Niger and southern Sudan ([Fairhead 1988](#); [Unternehr *et al.* 1988](#)).

The likely explanation for this unzipping of the South Atlantic can be found along the northern

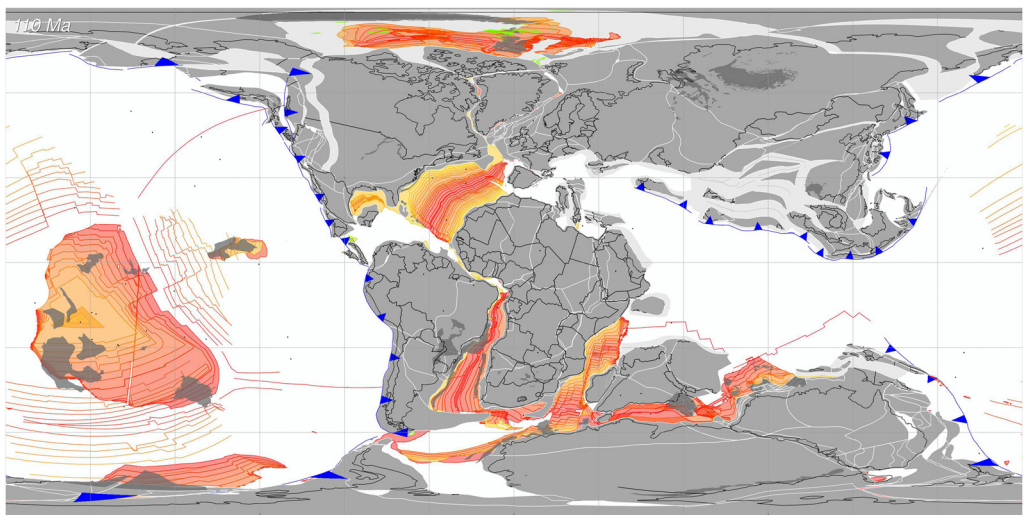


Fig. 35. Early Cretaceous (early Albian, 110 Ma); see [Figure 2a](#) for the legend.

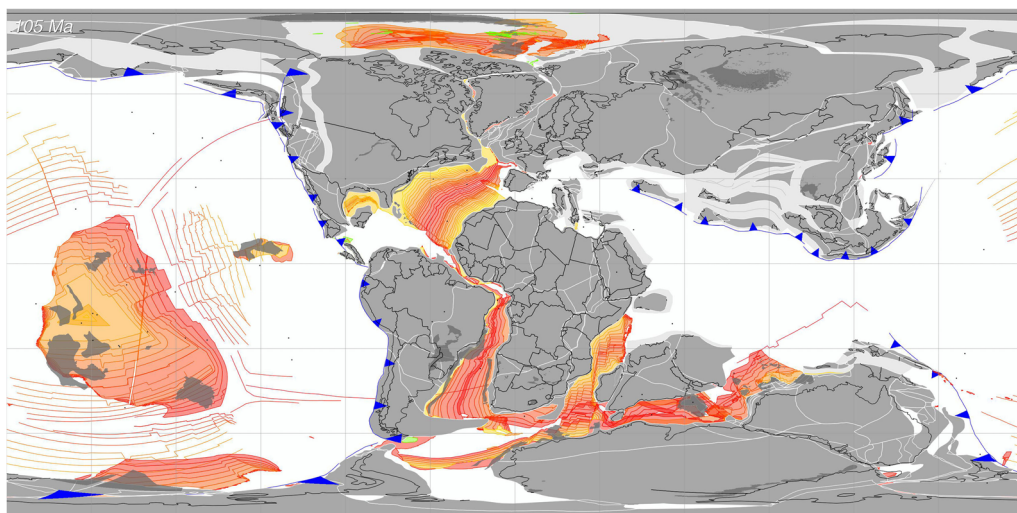


Fig. 36. Early Cretaceous (middle Albian, 105 Ma); see Figure 2a for the legend.

boundary of the African Plate. Starting in the latest Jurassic (*c.* 150 Ma), the southern boundary of the Palaeotethyan Plate, the North Tethyan Ridge, began to be subducted beneath southern Eurasia. The subduction of the North Tethyan Ridge was diachronous, starting in the west beneath Iran and progressing eastwards towards Sibumasu. As a consequence, the African Plate, for the first time, began to be subducted northwards beneath Eurasia. Gradually, as more and more of the African Plate was subducted, increasing slab-pull forces pulled

Africa, together with India, away from South America.

The widening South Atlantic separated the Santos and Campos basins of eastern Brazil from the Gabon and Kwanza basins of west Africa. What were once rift lakes became narrow, deep marine basins floored by attenuated continental crust (São Paulo Plateau) and filled with salty brines that would become thick Aptian salt deposits. These salt basins, which formed in the arid subtropics, were isolated from the southernmost South Atlantic

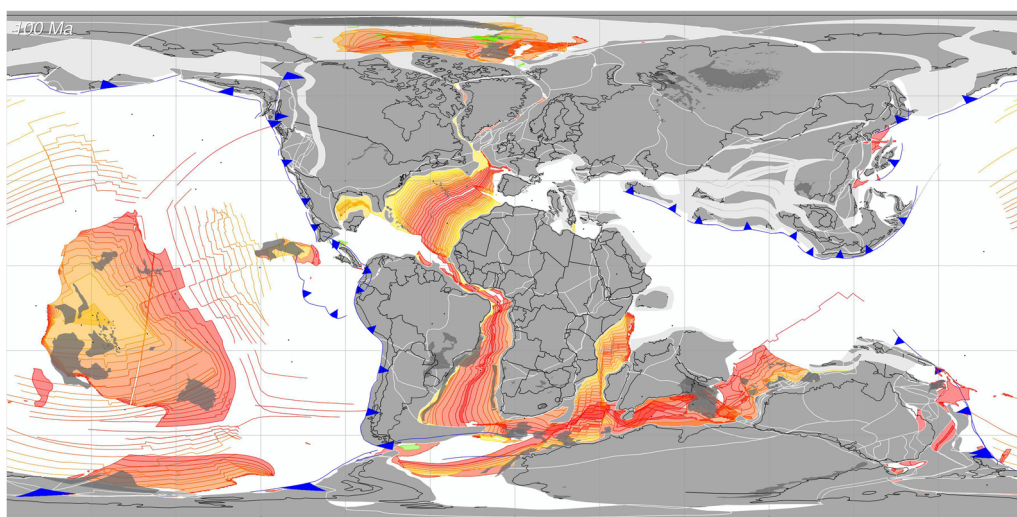


Fig. 37. Early Cretaceous (latest Albian, 100 Ma); see Figure 2a for the legend.

by a massive submarine volcanic escarpment formed by the Rio Grande Rise–Walvis Ridge hotspot track.

SE sector of Pangaea. During the Early Cretaceous, in the SE sector, East Gondwana rifted apart as the western portion, India together with Madagascar, separated from the combined Antarctica–Australia continent. Starting at *c.* 140 Ma, the NE coast of India (Eastern Ghats) diachronously (east to west) rifted away from the Enderby Land margin of East Antarctica. At *c.* 112 Ma, final separation took place as Sri Lanka tore away from the socket formed by the Gunnerus Ridge. The Cauvery Basin (Straits of Mannar), which now separates Sri Lanka from mainland India, was produced during this final phase of rifting. The eruption of the Rajmahal flood basalts in Assam (*c.* 120 Ma) is associated with the rifting of India from Antarctica. The Rajmahal flood basalts mark the initiation of the Kerguelen hotspot, which would generate the Kerguelen Plateau and Ninety East Ridge during the Late Cretaceous and Cenozoic.

During the mid-Cretaceous (*c.* 110 Ma), seafloor spreading ceased in the Somali Basin. As a consequence, Madagascar became fixed to the African Plate (Segoufin and Patriat 1981; Coffin and Rabino-witz 1988). Seafloor spreading in the Mozambique Basin, however, continued and the SW Indian Ocean and the Weddell Sea widened. The east–west-trending mid-ocean ridge in the Mozambique Basin slid past the eastern edge of the Mozambique Escarpment. When the ridge cleared the southern end of the escarpment, it jumped northwards, forming the series of stair-step offsets characteristic of the modern Southwest Indian Ridge.

Although Australia and Antarctica remained together throughout the Early Cretaceous, the Wharton Basin between western Australia and Greater India continued to widen. During the Early Cretaceous, the south-central Indian Ocean became wider; however, the Kerguelen hotspot land bridge may have linked India with East Antarctica.

At *c.* 110 Ma (early Albian), seafloor spreading in the Somali Basin and along the South Tethyan mid-ocean ridge simultaneously ceased. This resulted in the fusing of the Neotethys and Mesotethys plates. As a consequence, the Tethyan subduction zone continued to draw Africa northwards and, for the first time, the Tethyan subduction zone began to pull India northwards towards Asia.

Ocean basins exterior to Pangaea. During the Aptian–Albian, the ocean basins that were exterior to Pangaea (Neotethys and the Pacific Ocean) continued to contract as the interior ocean basins expanded (Atlantic and Indian oceans). The Pacific Plate continued to expand at the expense of the Farallon, Izanagi and Phoenix plates. During the Aptian (*c.* 120 Ma), a ‘superplume’ erupted in the Pacific Ocean Basin, covering the once relatively smooth

seafloor with more than 100 intraplate volcanic islands and seamounts. Most notable was the eruption of several large, submarine volcanic plateaus (Ontong Java Plateau and Manihiki Plateau, 123 Ma). The Ontong Java Plateau consists of more than $50 \times 10^6 \text{ km}^3$ of basaltic magma that forms a 30 km-thick plateau, which is equal in area to one-third of the USA (Tarduno *et al.* 1991). It has been proposed that tremendous outgassing of CO₂ associated with this volcanic event led to global warming and resulted in the early Aptian oceanic anoxic event (OAE1a) (Larson 1991a, b; Larson and Erba 1999).

In the NW Pacific, exotic terranes (Omolon and Kolyma) collided along the northeastern margin of Siberia, resulting in folding and thrusting in the Verkhoyansk mountain range (*c.* 120 Ma: Parfenov *et al.* 2010, 2011). These collisions were followed by the initiation (*c.* 100 Ma) of a new, west-dipping subduction zone (Okhotsk–Chukotka volcanic arc) (Nokleberg *et al.* 2001).

Eastwards along the Pacific margin of North America, the Wrangellian Seaway had closed by the late Albian (*c.* 100 Ma). This collision is marked by the Gravina–Nutzotin orogenic collage (Friedman 1983; Monger 2008). Palaeomagnetic data indicate that during the Cretaceous, Wrangellia moved northwards by *c.* 2000 km outboard of the western margin of North America. It collided with North America (British Columbia/Yukon) 850 km south of its present-day location. During the Paleocene and Eocene, it was displaced northward along continuous, right-lateral strike-slip faults (Tintina and Rocky Mountain Trench faults).

To the south, off the coast of Central America, the easternmost portion of the Farallon Plate closely approached the eastward-dipping Greater Antilles volcanic arc. The collision of this thickened oceanic crust (*c.* 100 Ma) flipped the polarity of the Greater Antilles subduction zone, resulting in the insertion of the Caribbean Plate between North and South America.

Mid-Cretaceous (Cenomanian–Turonian, 100–90 Ma)

Although only 10 Myr in duration (100–90 Ma), the Cenomanian–Turonian was a tectonically active time (see Figs 37–39). Five of the eight intra-Pangaean ocean basins had opened by the beginning of the Cenomanian–Turonian: Central Atlantic, proto-Caribbean, South Atlantic, western Indian Ocean and south-central Indian Ocean. The Central Atlantic, the oldest of these ocean basins, was now more than 4500 km wide. The proto-Caribbean Ocean Basin, located to the SW of the Central Atlantic, was at its maximum extent during the early Cenomanian. However, at some time during the

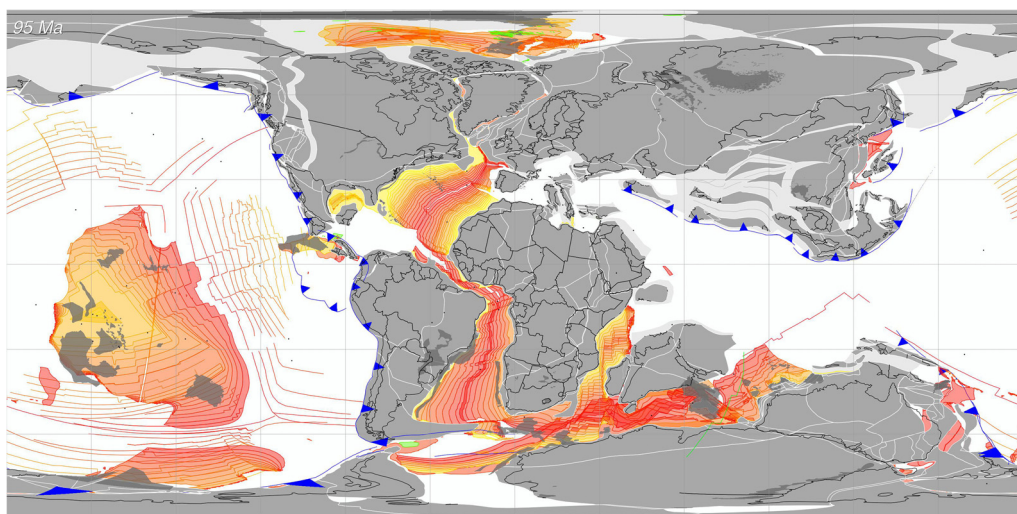


Fig. 38. Mid-Cretaceous (Cenomanian, 95 Ma); see Figure 2a for the legend.

Cenomanian and Turonian, a new subduction zone, dipping to the west beneath the Greater Antilles island arc (Cuba, Hispaniola and Puerto Rico), began to consume and override the proto-Caribbean ocean floor. This reversal of subduction direction was triggered by the arrival of the thick, basaltic, oceanic lithosphere that was to become the Caribbean Plate.

The South Atlantic, which had progressively opened from north to south during the Early Cretaceous, had completely broken through to the Central Atlantic by the Cenomanian–Turonian, allowing a

free-flowing deep-water connection between the South Atlantic and Central Atlantic. Similarly, relatively wide oceanic gateways linked the South Atlantic, Weddell Sea, southwestern Indian Ocean, western Indian Ocean and south-central Indian Ocean.

The three remaining intra-Pangaeian ocean basins began to rift open during the Cenomanian–Turonian: Madagascar Basin, SE Indian Ocean and North Atlantic (Labrador Sea: [Srivastava and Roest 1989](#)). India, with Madagascar attached, remained motionless with respect to Africa until the late

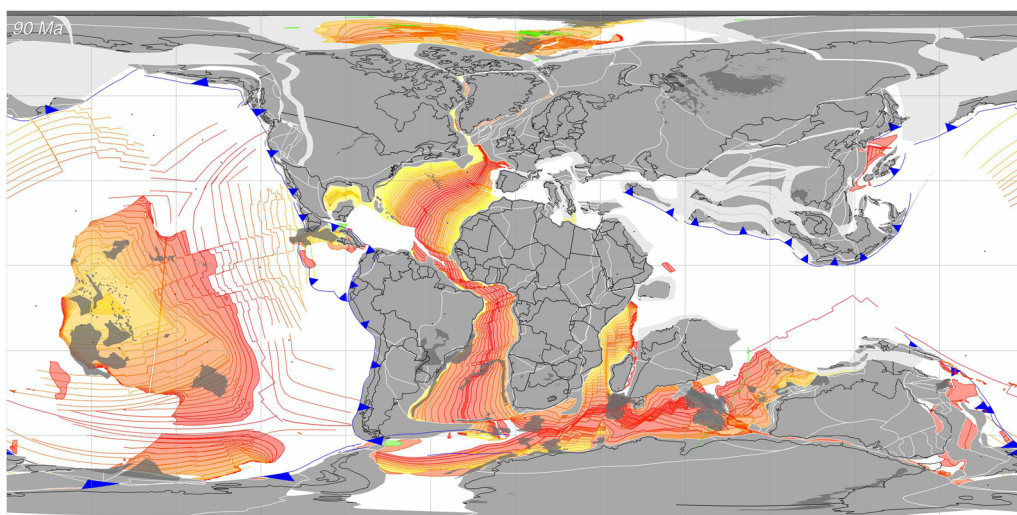


Fig. 39. Mid-Cretaceous (latest Turonian, 90 Ma); see Figure 2a for the legend.

Cenomanian (c. 100 Ma; Coffin and Rabinowitz 1988), when volcanic activity along the eastern coast of Madagascar signalled the start of India's northward journey towards Asia. It is notable how straight the east margin of Madagascar and the west margin of India are. This 1200 km-long boundary was undoubtedly the site of a major north–south strike-slip fault prior to the rifting of India from Madagascar. The timing of the strike-slip movement, the magnitude of the fault and the sense of offset (left-lateral v. right-lateral) are not well resolved. Our model shows a minimum amount of strike-slip movement between India and Madagascar.

During the Cenomanian–Turonian (95 Ma), the first phases of rifting began between Australia and Antarctica (Cande and Mutter 1982). Although no oceanic crust was generated, extensive crustal stretching resulted in the formation of a series of rift lakes. Further to the west, this slow, inexorable extension produced vast volcanic plateaus (Broken Ridge and Naturaliste Plateau) associated with the Kerguelen Plateau and hotspot. This phase of rifting was synchronous with the initiation of the separation of Zealandia (Luyendyk 1995; Matthews *et al.* 2015) from eastern Australia and the opening of the Tasman Sea.

The North Atlantic Ocean Basin has had a long history of pre-rift extension and stretching. In the Cenomanian–Turonian, two rift systems on either side of Greenland were in operation. Seafloor spreading was just beginning in the Labrador Sea to the west of Greenland in the late Cenomanian (c. 95 Ma). The West Greenland rift system passed up through the Labrador Sea and into Baffin Bay, and was bordered on either side by high rift shoulders that are still evident today. The Iceland hotspot passed down the length of the West Greenland rift system during the Late Cretaceous and, at 90 Ma, was located along the west coast of Baffin Island near Disko Island (70° N). On the other side of Greenland, the East Greenland rift system may have been active as early as the late Permian; seafloor spreading, however, did not begin in earnest until the late Paleocene. During the Cenomanian–Turonian, a broad zone of stretched continental and transitional lithosphere extended from the western margin of Ireland, across the Rockall Plateau and Hatton Bank, to the shores of SE Greenland.

The Pacific Ocean, Tethys Sea and Arctic Ocean surrounded the perimeter of the Cenomanian–Turonian continents. Along the eastern margin of the Pacific Ocean, the leading edge of the Farallon Plate continued to override the older oceanic lithosphere of the proto-Caribbean Plate. By the end of the Turonian (c. 90 Ma), a new eastward-dipping subduction zone had formed in the equatorial, eastern Pacific that clipped the Caribbean Plate from

the Farallon Plate. This proto-Mid America Trench linked the eastward-dipping subduction zones of Mexico, to the north, and Colombia and Peru, to the south.

During the Cenomanian–Turonian, the Pacific Plate continued to grow, while the Izanagi, Farallon and Phoenix plates continued to be subducted beneath an expanding Cretaceous Ring of Fire. In the far reaches of the South Pacific, during the late Albian (100 Ma), the Pacific–Phoenix mid-ocean ridge jumped to a new location closer to Antarctica. This was followed by a second ridge jump 10 Myr later that was caused by the oceanward retreat of the subduction zone dipping westwards beneath eastern Australia (van de Lagemaat *et al.* 2023). This rollback of the subduction zone resulted in the opening of the Tasman Sea and the isolation of the mostly submarine subcontinent, Zealandia, from the rest of Gondwana (Gaina *et al.* 1998a, b).

At some time during the late Albian or early Cenomanian (c. 100 Ma), a pair of back-arc basins opened along the NW rim of the Pacific Ocean: the Okhotsk–Bering back-arc basin (Parfenov *et al.* 2010, 2011; Vaes *et al.* 2019) and the Philippine back-arc basin. The Okhotsk–Bering back-arc basin was bounded on the east by the Kamchatka/Olyutorsky–Peninsular Alaska volcanic arc and on the west by NE Siberia (Kolyma, Omolon and Chukotka). We propose that the Philippine volcanic arc was initially located along the eastern margin of Asia between southern Japan and Taiwan. Both of these back-arc basins opened due to slab rollback, possibly triggered by the subduction of the oldest and densest portions of the Izanagi Plate.

Although active subduction zones consumed oceanic lithosphere along the western margins of the Americas, beneath the southern margin of Eurasia, beneath western Antarctica and New Zealand, and beneath the eastern margin of Asia, there were no continent–continent collisions during the Cenomanian–Turonian. There were, however, three episodes when island arcs collided and ophiolites were obducted onto continental margins (Oman, Troodos, Chortis and northern California: Metzler 2006).

Late Cretaceous (Coniacian–Maastrichtian, 85–65 Ma)

Overview. By the Late Cretaceous, all of the major ocean basins had fully opened, except for the North Atlantic that was still in its initial stage of rifting (see Figs 40–44). Like the modern world, the dominant subduction zone was the Circum-Pacific Ring of Fire, which produced Andean-style mountains along the eastern rim of the Pacific (North and South American Cordillera) and back-arc basins along the northwestern (Sea of Okhotsk,

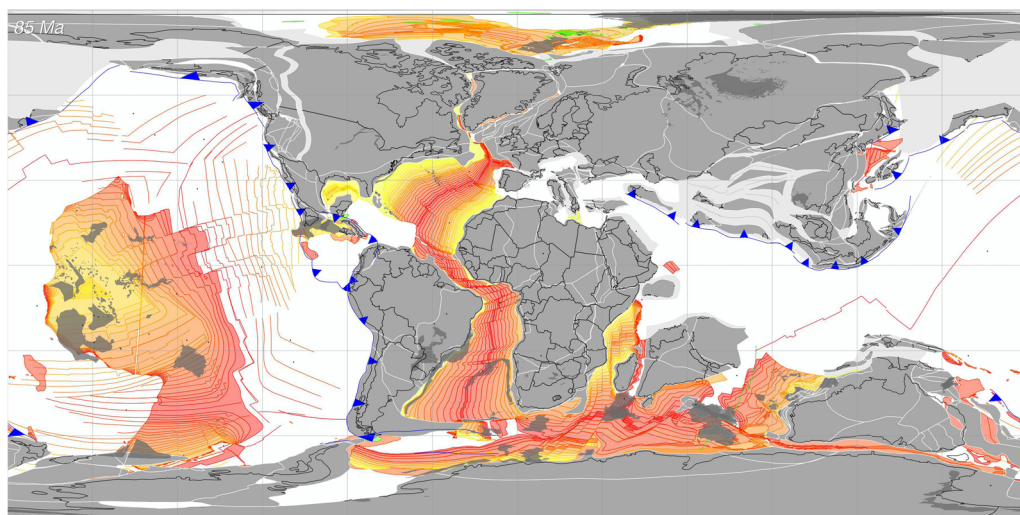


Fig. 40. Late Cretaceous (Coniacian – Santonian, 85 Ma); see [Figure 2a](#) for the legend.

Bering Sea and Philippine Sea) and southwestern margin of the Pacific (Tasman Sea). Subduction of the Neotethys Plate continued beneath the southern margin of Eurasia as India was drawn rapidly northwards by slab-pull forces. Throughout most of the Late Cretaceous there were no continent–continent collisions and there were no new continental rifts. The single exception is the Alpine collision between Adria, a promontory of northern Africa, and south-central Europe (AustroAlpine, Carnic–South Karawanken and Transdanubian regions), which began at the very end of the Cretaceous.

Circum-Arctic and North American Cordillera. During the Late Cretaceous, the Arctic region was quiescent ([Green *et al.* 1986](#)). The Amerasian Basin (Canada Basin and Makarov Basin) had opened by the mid-Cretaceous (c. 110 Ma: [Lawver and Scotese 1990](#); [Nokleberg *et al.* 2001](#)) and the Eurasian Basin had yet to open (60 Ma: [Srivastava 1985](#); [Rowley and Lottes 1988](#)). All the Late Cretaceous tectonic activity in the Circum-Arctic region took place in the Canadian Cordillera and in South-Central Alaska ([Monger and Nokleberg 1996](#)). The Wrangellia terrane, which had collided in the mid-

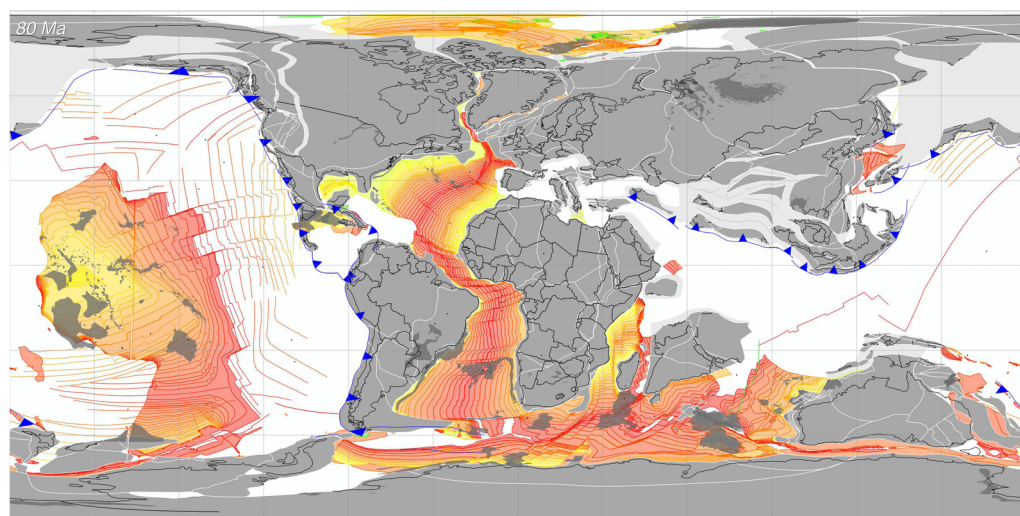


Fig. 41. Late Cretaceous (Early Campanian, 80 Ma), see [Figure 2a](#) for the legend.

The Cretaceous world

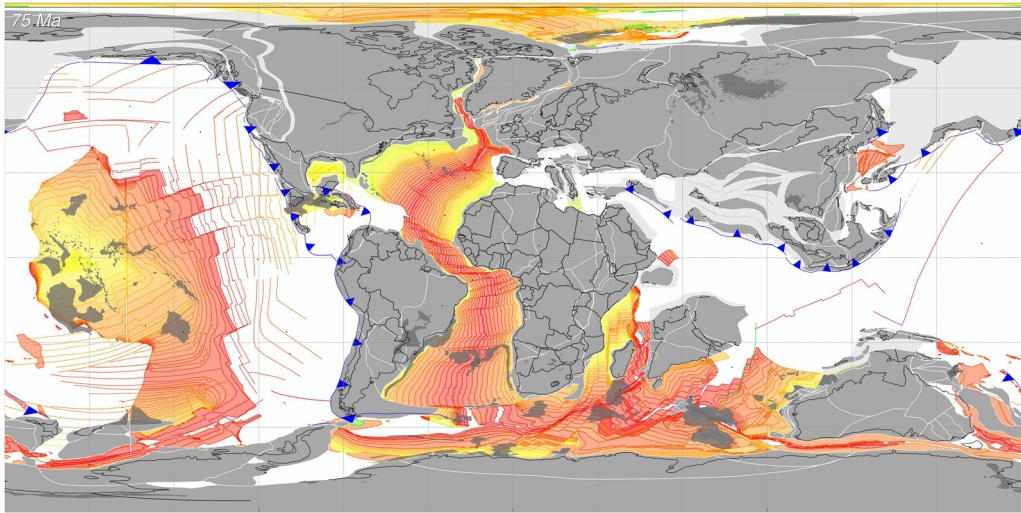


Fig. 42. Late Cretaceous (Late Campanian, 75 Ma); see Figure 2a for the legend.

Cretaceous (c. 110 Ma) with the Stikine Terrane, in the Late Cretaceous (<90 Ma) began to translate northwards with respect to cratonic North America along large (c. 700 km) right-lateral, strike-slip faults (Rocky Mountain Trench and Tintina Fault: [Engelbreton et al. 1985](#); [Monger and Nokleberg 1996](#); [Monger 2008](#)). This northward movement would continue until the middle of the Eocene.

North Atlantic and Europe. In the North Atlantic, the final phases of continental rifting were taking place between Greenland and northern Europe ([Srivastava and Tapscott 1986](#); [Rowley and Lottes 1988](#); [Ziegler 1988](#); [Skogseid et al. 2000](#)). Late

Cretaceous extension in the North Atlantic produced the Rockall and Hatton Bank microcontinents and the wide, stretched margins of East Greenland and central Norway (Vøring Plateau: [Skogseid et al. 2000](#)). The Labrador Sea and the southernmost part of the North Atlantic (the Rockall Trough and the Rockall–Hatton Basin: [Srivastava and Roest 1989](#)) were the only sites of seafloor spreading in the North Atlantic during the latest Cretaceous.

It is interesting to note that in the latest Cretaceous, rifting was taking place simultaneously on either side of Greenland. This is the only known case of two duelling rifts in Phanerozoic history.

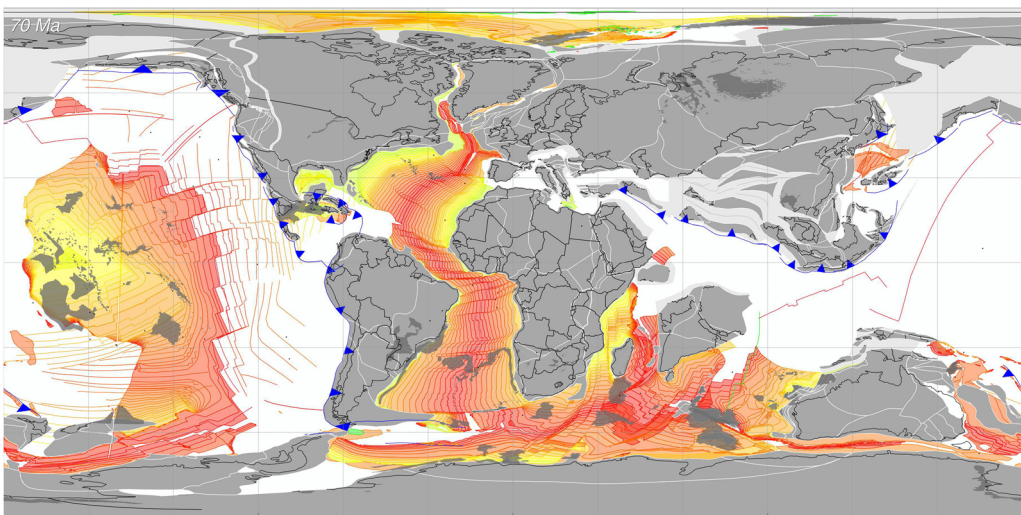


Fig. 43. Late Cretaceous (Maastrichtian, 70 Ma); see Figure 2a for the legend.

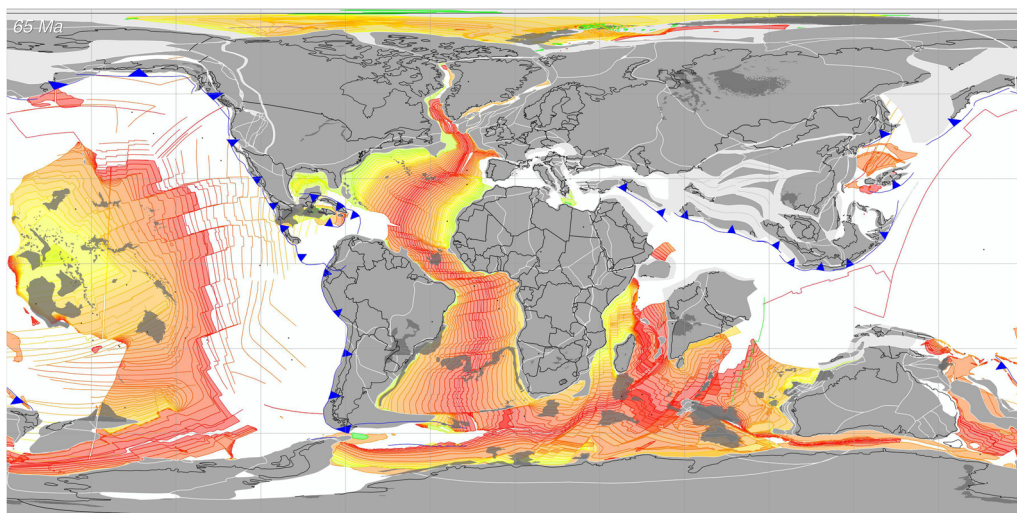


Fig. 44. Cretaceous–Paleogene boundary (65 Ma); see Figure 2a for the legend.

The location of the western rift, between Baffin Island and western Greenland, was probably due to the weakening of the continental lithosphere above the southward-moving Iceland hotspot (Scotese 2008). During the latest Cretaceous and Paleocene, the Iceland hotspot was located at the eastern edge of the Labrador Sea (Disko Island). Greenland's westward drift caused the hotspot to move below southern Greenland, emerging into the North Atlantic during the early Eocene (Lawver and Müller 1994). The arrival of the Iceland mantle plume, combined with highly attenuated continental lithosphere, would trigger massive volcanic eruptions in the North Atlantic region in the Paleocene.

In the Late Cretaceous, in southern Europe, the Adriatic Promontory (the northernmost extension of the African continent) had partially closed the Penninic Sea, and the Alps had begun to rise from the sea (Ziegler 1982, 1990; Dercourt *et al.* 1985, 1993, 2000; Yilmaz *et al.* 1996; Ziegler and Horvath 1996; Stampfli *et al.* 2001, 2004; Ziegler *et al.* 2001; Stampfli and Kozur 2006; Schettino and Turco 2011; Scotese and Schettino 2017; van Hinsbergen *et al.* 2020). Along the southern margin of Eurasia, due to the subduction of the Neotethyan Plate, an en echelon series of back-arc basins (Black Sea, southern Caspian Sea and Ladakh–Gangesi back-arc basin) opened sequentially from west to east during the Late Cretaceous. The Ladakh–Gangesi back-arc, which produced ophiolites of Late Cretaceous age (Metzler 2006), was the last back-arc basin to open along northern margin of Tethys.

Central Atlantic Ocean and Caribbean. During the latest Cretaceous (70 Myr ago), the Central Atlantic was approximately 60% as wide as it is

today. The Cruiser, Great Meteor and Corner seamounts had just erupted at a hotspot located along the Mid-Atlantic Ridge. The Great Meteor hotspot had produced the New England seamount chain and the White Mountain volcanics earlier in the Cretaceous.

The Late Cretaceous was a time of considerable plate tectonic activity in the Caribbean (Ross and Scotese 1988; Pindell and Barrett 1990; Pindell *et al.* 2005). As noted earlier, late in the Cretaceous, an extension of the Farallon Plate wedged itself between North and South America. The Greater Antilles island arc moved to the NE and continued to override the proto-Caribbean Plate. Approximately 90 Myr ago, this crustal extension was severed from the Farallon Plate, giving rise to an autonomous Caribbean Plate (Ross and Scotese 1988). The western edge of Cuba slid past the eastern margin of Yucatan, and the newly formed Panama volcanic arc rose from the ocean.

Several tectonic events are associated with the latest Cretaceous–early Paleogene collision of Cuba with the Bahamas Platform: (1) the opening of the Yucatan Basin between southern Cuba and the Cayman Ridge; (2) the start of rapid motion along the Motagua and Polochic faults as the Chortis Block slid eastwards along a series of sinistral strike-slip faults; and (3) the creation of the Aves Ridge, a proto-Lesser Antilles island arc that developed on the leading edge of the Caribbean Plate.

South Atlantic Ocean and SW Indian Ocean. At the end of the Late Cretaceous (66 Ma), the South Atlantic was approximately half its modern width (Cande *et al.* 1988; Fairhead 1988). In the central South Atlantic, the southwestern portions of the

Walvis Ridge were being generated by the Tristan da Cunha hotspot (Coffin and Eldholm 1994).

Between 72 (C32) and 64 Ma (C28), the motion of the African Plate shifted dramatically (Royer *et al.* 1988). Prior to Chron 32, the Southwest Indian Ridge was spreading in a NE–SW direction. Starting at 72 Ma, the spreading rate slowed and the spreading direction became more north–south (Royer *et al.* 1988). In the earliest Cenozoic (64 Ma), the spreading orientation reverted to a more NE–SW direction. These changes in spreading direction corresponded with a major ridge jump in the South Atlantic. In the latest Cretaceous–earliest Paleocene, the Bouvet Triple Junction, which had been located c. 1000 km to the SW of Africa in the Agulhas Basin, jumped to a new location adjacent to the Falkland Plateau. Volcanic leakage from this ridge jump generated the Meteor Rise (African Plate) and the Islas Orcadas Rise (South American Plate).

It is notable that this wobble in the movement of the African Plate can be seen along many of its margins. The equatorial fracture zones that linked Africa and South America underwent a compressive distortion that resulted in the uplift and inversion of sedimentary basins adjacent to the transform faults (Jubilee oilfield). Oceanic crust was obducted along the Arabian margin of NE Africa (Oman) as back-arc basins began to close. One could speculate that this adjustment in Africa's plate motion may have been caused by the resistance Africa encountered as a result of the continent–continent collision between northern Africa and southern Europe during the latest Cretaceous (Alpine Orogeny).

Western Indian Ocean, Madagascar and India.

As noted earlier, about 95 Myr ago rifting began between India and Madagascar as India began its northward movement towards Asia. India pulled away from Madagascar, opening the Madagascar Basin (Segoufin and Patriat 1981; Royer and Sandwell 1989; Royer *et al.* 1992a, b). The Seychelles, Laxmi Ridge, Mascarene Bank and Nazareth Bank represent small blocks of continental crust that were torn away from India during the initial rifting event. These continental blocks remained attached to the Indian Plate as the Madagascar Basin opened. They became separated from India in the early Paleocene as a result of a ridge jump from the Madagascar Basin to the Arabian Sea (c. 61 Ma).

During the Late Cretaceous, India moved northwards and the Neotethys narrowed (Patriat and Segoufin 1988; Royer and Sandwell 1989; Royer *et al.* 1992a, b). Chatterjee and Scotese (1999) suggested that in the latest Cretaceous India began to collide with island arcs that fringed the southern margin of Asia. The classical Himalayan ophiolites (Metzler 2006) represent the ocean floor that had formed in back-arc basins behind these island arcs. An alternate hypothesis (Burg 2011; V  rard *et al.*

2017) supposes that in the latest Cretaceous India collided with an archipelago that was the eastward extension of an island arc that collided with Arabia (Oman ophiolite) in the Late Cretaceous (80–70 Ma, Campanian). The ophiolitic remnants found on the island of Masirah, off the coast of Oman, may be an obducted portion of this island arc. In the Maastrichtian, the northward-moving Indian subcontinent collided with the eastward extension of this island arc. This collision created a temporary land bridge between Africa and India. This fleeting connection may explain the anomalous appearance of African dinosaurs in India during the Maastrichtian (Chatterjee and Scotese 1999).

An alternate hypothesis proposes that in the late Maastrichtian the leading edge of India collided with the Lut Block (eastern Iran). In the reconstruction of Gondwana presented here, the Lut Block lies nestled between southernmost Arabia and NW India. When India and Madagascar broke away from East Africa in the Jurassic, the Lut Block remained attached to Arabia. Later in the mid-Cretaceous, when a realignment of plate forces caused India to move northward towards Asia, the Lut Block similarly broke free.

It has long been noted that India set plate tectonic speed records during the Late Cretaceous and earliest Cenozoic (Molnar and Tapponnier 1975; Kumar *et al.* 2007). This rapid northward movement ($>20 \text{ cm a}^{-1}$) was due to the fact that India was attached to a large area of subducting oceanic lithosphere that produced powerful slab-pull forces. The eruption of the Deccan Large Igneous Province (Ernst 2014) at the Cretaceous–Paleogene boundary may have contributed to India's rapid movement by warming the base of the Indian Plate and thereby reducing mantle drag (Cande and Stegman 2011).

To the south of Madagascar, a broad volcanic, oceanic plateau (Madagascar Plateau) was generated by the Marion Dufresne hotspot (Duncan and Storey 1992; Coffin and Eldholm 1994). Just prior to the end of the Cretaceous, this hotspot crossed the Southwest Indian Ridge and began to generate the Conrad Rise. A little further to the east, starting at 90 Ma, the Kerguelen hotspot was creating an island chain that would become the Ninety East Ridge.

SE Indian Ocean, Australia and Zealandia.

The Late Cretaceous was a time of significant tectonic activity in the SE Indian Ocean and in Australia. During the mid-Cretaceous, Australia was separated from the rapidly moving Indian Plate by the long, north–south, dextral transform fault system (Larson 1975; Larson *et al.* 1979; Powell *et al.* 1988; Royer and Sandwell 1989) that ran parallel to the Ninety East Ridge (Duncan and Storey 1992). In the Late Cretaceous, Australia had separated from Antarctica (Wilkes Land; Cande and Mutter 1982), and very slow seafloor spreading ($<2 \text{ cm a}^{-1}$)

between Australia and Antarctica continued through the Maastrichtian and into the Paleogene. Australia and India joined together to form the Indo-Australian Plate (42 Ma) after the last major segment of the Neotethyan Ridge was subducted beneath Asia. The ocean floor attached to northern Australia was, for the first time, subducted into the Tethyan trench, pulling Australia northwards.

During the Late Cretaceous the Tasman Sea back-arc basin continued to open progressively from north to south along the eastern margin of Australia (Gaina *et al.* 1998a, b). In the latest Cretaceous, the northern segment of this rift system between the Queensland Plateau and the New Caledonia began to open. The Tasman Sea stopped opening in the Paleocene (c. 55 Ma).

It should be noted that initial seafloor spreading in the Tasman Sea (c. 90 Ma) was the westernmost extension of the Southwest Pacific mid-ocean ridge. When Australia began to move rapidly northwards in tandem with India, spreading in the Tasman Sea ceased and the Southwest Pacific Ridge (SE of Australia) and Southeast Indian Ridge (south of Australia) joined together (c. 50 Ma). This is when the Alpine Fault became active and split proto-New Zealand in two. The northwestern part of Zealandia, comprising North Island and the western half of South Island, remained fixed to Australia, while the southeastern part of Zealandia, made up of much of the South Island of New Zealand, Lord Howe Rise and the Campbell Plateau, began to move with the Pacific Plate.

Western Pacific and NE Asia. Only a fragmentary record exists of the plate tectonic history of the western Pacific and NE Asia (Sharman and Risch 1988; Parfenov *et al.* 2010, 2011; Vaes *et al.* 2019). The NE margin of Asia was an active margin with subduction beneath NE Siberia, the Sea of Okhotsk, Japan, the Yellow Sea, the South China Sea, eastern Borneo and the Philippines. A speculative model is proposed here regarding the tectonic evolution of the Philippine and the Olyutorsky volcanic arcs. Both arcs began as continental volcanic arcs along the northeastern margin of Eurasia. The Olyutorsky arc was originally located between the Koryak Peninsula and Sakhalin Island. The Philippine island arc was originally located between southern Japan and the modern location of Taiwan. It is proposed that during the Albian (c. 110 Ma) both volcanic arcs rifted away from NE Asia due to slab rollback. The Olyutorsky back-arc basin continued to widen during the Late Cretaceous and achieved its maximum width in the early Campanian (c. 80 Ma). Subduction resumed beneath NE Asia, drawing the arcs back towards Asia and collapsing the back-arc basin. The Olyutorsky Arc collided with NE Siberia in the Paleogene. After the Philippines rifted away from eastern Asia, the Philippine

back-arc basin continued to widen, forming the Philippine Sea during the latest Cretaceous–late Eocene (Chron 16).

Deccan flood basalts. Although strictly not a plate tectonic event, the eruption of the Deccan flood basalts in India (Courtilot *et al.* 1988, 1990; Duncan and Storey 1992; Coffin and Eldholm 1994; Courtilot 1999; Courtilot and Renne 2003) ranks as the most significant tectonic/volcanic event of the Late Cretaceous. The Deccan flood basalts erupted from fissures centred in west-central India 66 Myr ago. Lava flows were magnetized in both normal and reverse directions, corresponding to chrons C30, C29R and C29. Approximately 25% as large as the massive West Siberian flood basalts, the Deccan flood basalts covered more than 500 000 km² and buried India to a maximum depth of 2.5 km in the Western Ghats.

According to the best estimates, the eruption of the Deccan flood basalts predates the end of the Cretaceous by about 0.5 Myr (Miller *et al.* 2010; Renne *et al.* 2015; Schoene *et al.* 2019). Owing to the release of massive amounts of CO₂ into the atmosphere, there was a brief period of moderate global warming prior to the start of the Cenozoic (Olsson *et al.* 2002; Ravizza and Peucker-Ehrenbrink 2003).

One of the most interesting coincidences of geological history is the fact that the eruption of the Deccan flood basalts and the impact of the bolide at Chicxulub were nearly simultaneous. This has led some researchers to speculate that it was the Deccan flood basalts, not the Chicxulub impact event, that caused the end-Cretaceous mass extinction (Officer and Drake 1985; Courtilot *et al.* 1988; Keller *et al.* 2008). Others have suggested that the Deccan flood basalts were also triggered by a bolide impact in the vicinity of Mumbai (Bombay High: Chatterjee *et al.* 2006). Still others suggest that there may be a causal relationship between the Chicxulub impact event and the eruption of the Deccan flood basalts. Eugene Shoemaker (pers. comm. 1990) noted that the location of the Chicxulub impact site at 65.5 Ma (25° N, 70° W) was nearly antipodal to the location of the Deccan flood basalts (25° S, 55° E). It is proposed that, like a bullet piecing an apple, the shock waves from the impact site passed through the Earth's mantle and core, and were refocused on the other side of the Earth, enhancing eruptions that were already underway (Renne *et al.* 2015; Richards *et al.* 2015; Vanderkluyssen and Gibson 2015).

Palaeogeography during the Cretaceous

Overview

This section describes the mountains, landmasses, shallow seas, rivers, land bridges and oceanic

gateways that characterize the palaeogeography of the Cretaceous. These palaeogeographical features are intimately connected with the changing climate and plate tectonic activity of the Cretaceous.

There were no major continent–continent collisions during the Cretaceous. The lack of major mountain-building episodes, plus relatively fast episodes of seafloor spreading, during the Early Cretaceous resulted in high sea levels and extensive continental flooding by the mid-Cretaceous. Unlike the modern world, the continents of the Cretaceous world were flooded by warm, shallow (epeiric) seas. During much of the Cretaceous, sea level was approximately 50–150 m higher than the present-day sea level. During the Cretaceous, 11% of the continents were flooded, compared with the present-day figure of 7%. Small ephemeral ice caps may have covered the South Pole during parts of the Early and Late Cretaceous, contributing to numerous rapid episodes global sea-level change. Similarly, a precipitous, although short-lived, fall in sea level may have occurred at the end of the Cretaceous due to the Cretaceous–Tertiary (KT) impact winter and the growth of a very short-lived ice cap on Antarctica.

Cretaceous mountain ranges

Four distinct kinds of uplift characterize Cretaceous mountainous areas: (1) old collisional mountain belts, which were remnants of either late Paleozoic or the early Mesozoic collision and accretion; (2) Andean-style uplift due to subduction beneath a Circum-Pangaean Ring of Fire or along the northern margin of Tethys; (3) young rifted margins with elevated rift shoulders; or (4) LIPs and hotspot activity.

The most prominent old collision belts were: the Caledonides–Northern Appalachians, the remnants of the equatorial Central Pangaean Mountain Range, the Urals, the Tasman–Trans-Antarctic–Cape-Sierra de la Ventana ranges, and the multiple generations of Andean-type margins and collapsed back-arc basins in Central Asia (i.e. the Timanides, Tien Shan, Qinling–Qilian Shan, Songpan Ganze, Tien Shan and trans-Mongolian accretionary zone: Şengör *et al.* 1988, 1993, 2014a, b; Şengör and Natalin 1996; Ziegler *et al.* 1996; Windley *et al.* 2007).

The youngest collisional events that produced significant relief were the Cimmericides (Middle Triassic–Early Jurassic), the accretion of the Stikine (latest Jurassic) and the Wrangellia arc (late Albian, 100 Ma: Monger and Nokleberg 1996; Monger 2008), and the subsequent growth of the Early Cretaceous Canadian plutonic complex, the collapse of the Neuquen Basin in western Argentina (latest Jurassic–earliest Cretaceous) and the diachronous (west to east) closure of the Amurian Seaway (Triassic–Early Cretaceous: Zonenshain *et al.* 1990). Andean-

type subduction throughout the Cretaceous generated long, linear mountain chains (South America, Canadian Cordillera, eastern China and the northern margin of Tethys) or continental island arcs (e.g. Greater Antilles, Zealandia and Olyutorska–Peninsular Alaska arc) and oceanic volcanic arcs (Philippines).

Cretaceous sea level

We derived the changes in Cretaceous sea level illustrated in Figure 45 by measuring the amount of continental flooding on each of the palaeogeographical maps. This approach limits our temporal resolution, however. We cannot identify sea-level changes that take place over time intervals of less than 5 Myr. On average, the Cretaceous sea level was 70 m higher than the present-day sea level. The maximum sea level occurred during the mid-Cretaceous highstand (140–220 m), with a subsidiary peak (50–70 m) during the early Aptian. Sea level was relatively low (0–20 m) during the earliest part of the Cretaceous. There was a precipitous drop in sea level during the late Campanian and early Maastrichtian (c. 75 Ma). A table giving the exact sea-level values, as well as sea-level estimates for several other eustatic curves, is given in the [Supplementary material](#).

One of the outstanding puzzles of the Cretaceous is the cause and magnitude of the eustatic sea-level change. We can deconstruct the Cretaceous sea-level change into eight factors: (1) changes in the relative area of continental lithosphere and oceanic lithosphere; (2) changes in the volume of the ocean basin as a result of changes in the average age of the ocean floor; (3) the volume of oceanic crust produced by excess marine volcanism (e.g. seamounts and LIPs); (4) the relative length of mid-ocean ridges v. deep ocean trenches; (5) the number and size of back-arc basins; (6) the amount of sediment fill along passive continental margins; (7) the amount of water sequestered in continental aquifers; and, importantly, (8) the volume of continental ice caps. Wright *et al.* (2020) provided an excellent review of several of these factors – (2), (3), (5) and (6). They estimated that seafloor spreading in young back-arc basins may have contributed 120–150 m to sea-level rise; the addition of passive-margin sedimentary prisms and LIPs to the ocean basins may raise sea level by 75–165 and 45 m, respectively. A recent review of Phanerozoic eustasy by van der Meer *et al.* (2022) estimated the contribution of continental ice caps to sea-level change at c. 90 m.

Continental area. Figure 46 illustrates the changing area of continental lithosphere during the Phanerozoic. Changes in continental area are primarily controlled by plate tectonic processes that either

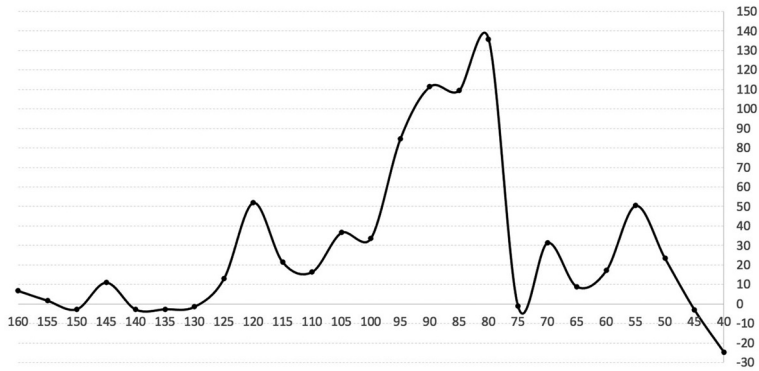


Fig. 45. Cretaceous sea level derived from continental flooding. The black dots are the control points. See [Davies and Simmons \(2023\)](#) for a discussion of alternative Cretaceous sea-level curves.

stretch or compress the continental lithosphere. The area of the continents increases during the pre-drift rifting phase, and decreases as a consequence of crustal shortening due to convergence along Andean-type margins and zones of collision. The changing area of the continents is a primary control on global sea level. If the area of the continents increases, then conversely the area and volume of

the ocean basins decreases and seawater is displaced onto the continents. Conversely, if the area of the continents shrinks, then water flows back into the enlarged ocean basins and sea level falls. Continental area, on average, steadily increased during the Paleozoic and into the Triassic ([Fig. 46](#)). A maximum continental area occurred during the Cretaceous, which contributed to a higher than average sea level during

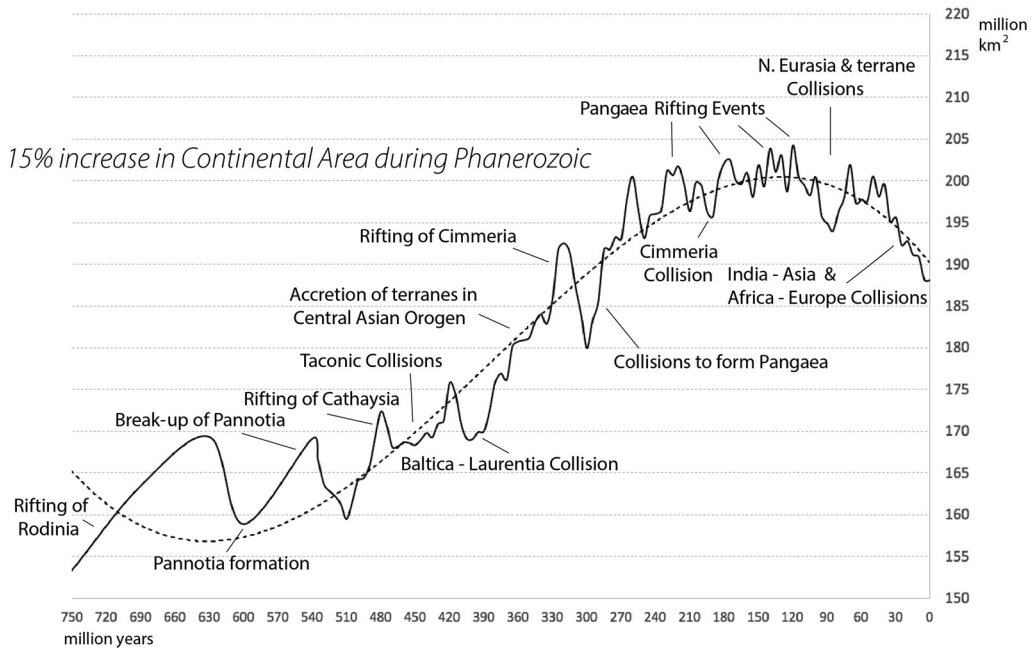


Fig. 46. The changing area of the continents during the late Neoproterozoic and Phanerozoic (750–0 Ma). The effects that rifting and terrane accretion (increase in area) and continental collisions (decrease in area) had on the continental area are labelled. The long-term trend is indicated by the dotted line.

The Cretaceous world

the Cretaceous with water being displaced out of the ocean basins and onto the continents.

An up and down sawtooth pattern of alternating continental extension and contraction characterizes the Cretaceous. These changes correlate reasonably well with alternating intervals of high and low sea level. On average, however, there was no long-term change in continental area during the Cretaceous. In contrast, continental area and sea level fell sharply during the Cenozoic due to a series of continent–continent collisions (e.g. India–Asia and Africa–Europe).

Mid-ocean ridge and trench length. Cretaceous sea-level changes can be viewed in the context of the changing length of mid-ocean ridges and the changing length of subduction zone trenches. Lithosphere production at mid-ocean ridges must be balanced by the amount of lithosphere removed by subduction (otherwise the Earth would either expand or contract). This implicit balance allows us to qualitatively estimate sea-level changes during the Cretaceous by comparing the relative length of mid-ocean ridges and subduction zones (Fig. 47).

The basic assumption is that the length of mid-ocean ridges should be in balance with the length of subduction zones. The modern ratio of mid-ocean ridges to subduction zones is approximately 2 : 1. The total length of mid-ocean ridges, including transform faults, is *c.* 100 000 km. The total length of subduction zones is *c.* 50 000 km. The rate of subduction is determined by the age of the subducting oceanic lithosphere. Old oceanic lithosphere is denser and heavier than young oceanic lithosphere and, therefore, old oceanic lithosphere subducts faster (12 cm a^{-1}) than young oceanic lithosphere ($<10 \text{ cm a}^{-1}$).

Therefore, all things being equal, an increase in the length of subduction zones would necessarily cause mid-ocean ridges to spread faster, which, in turn, would cause the global sea level to rise. Conversely, a decrease in the length of subduction zones would force mid-ocean ridges to slow down, producing a sea-level fall. In summary, the plate tectonic factors that most control sea level are the total length of oceanic trenches and the rate of subduction.

During the Early Cretaceous, Pangaea was just beginning to rift apart and there were few intra-Pangaean oceans. This requires that Early Cretaceous ridges in Panthalassa were spreading faster to balance the amount of subduction, which was nearly constant during the Cretaceous. Consequently, additional young ocean floor would have been produced in Panthalassa during the Early Cretaceous. Because there is a lag time of the order of tens of millions of years from the time when rapid seafloor spreading starts and the time when the average age of the ocean basins becomes substantially younger, the effects of this rapid seafloor spreading would not be seen until the mid-Cretaceous.

During the Cretaceous, rapid seafloor spreading in Panthalassa was gradually augmented by the appearance of numerous intra-Pangaean mid-ocean ridges. The appearance of these new rifts and mid-ocean ridges is the classic explanation that associates the break-up of supercontinents with global sea-level rise (supercontinent cycle: Pitman 1978; Fischer 1981, 1982, 1984; Nance *et al.* 1988, 2014; Nance and Murphy 2013).

Although it is not statistically significant, it is interesting to note that the lengths of mid-ocean ridges and subduction zones appear to have changed

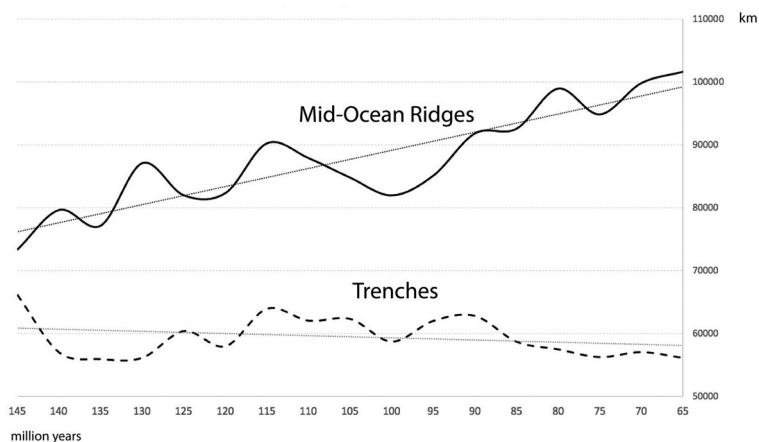


Fig. 47. Length of mid-ocean ridges (black line) and subduction zones (dashed line) during the Cretaceous. The y-axis is in kilometres; the x-axis is in millions of years.

in tandem between 125 and 90 Ma. An increase in trench length is immediately correlated with a corresponding increase in mid-ocean ridge length. This may suggest that mid-ocean ridges directly respond to subduction and reinforces the notion that slab-pull forces dominate the plate tectonic process. Finally, it should be noted that trench length was gradually reduced during the Late Cretaceous (90–65 Ma), suggesting that a global slowing of plate motion was at least partially responsible for the fall in sea level during the Cenozoic.

Continental ice. The Cretaceous has long been considered to be a hothouse world ($GAT = 22^{\circ}\text{C}$; Scotese *et al.* 2021). The average temperature in the polar regions ($>67^{\circ}\text{N}$ and S) was well above freezing. Throughout most of the Cretaceous, permanent ice only existed at latitudes greater than 85°N and 85°S (Fig. 48). During the Cenomanian–Turonian Thermal Maximum, there was no snow and ice at the poles, even during the winter months. However, cool polar temperatures may have prevailed during the Early Cretaceous (Berriasian–Hauterivian and Aptian) with a small polar ice cap in Antarctic extending down to 80°S and having an area of $c. 4 \times 10^6 \text{ km}^2$ (about the size of India). The waxing and waning of an ice cap this size could have caused sea-level fluctuations in the range of 15–25 m.

Cretaceous landmasses, land bridges and oceanic gateways

Introduction. The break-up of Pangaea resulted in both the destruction of land connections (land bridges) between the continents and the formation of new marine connections (oceanic gateways) between the world's oceans. These plate tectonic effects, combined with changing sea levels, produced an evolving mosaic of landmasses, shallow seas and deep ocean basins. In this section we chronologically describe the creation and destruction of land bridges and oceanic gateways during the Cretaceous. It is recommended that the reader review the animation 'Plate tectonics, palaeogeography and ice ages' that is provided with the [Supplementary material](#) while reading this section.

Early Cretaceous (145–100 Ma). Sea level was low during the Early Cretaceous, and as a consequence the land areas of the Earth were mostly connected (Fig. 49). However, a notable exception was the isolation of the landmasses of the northern hemisphere (Laurasia) from the southern hemisphere supercontinent (Gondwana). Europe was isolated from North Africa by the western Tethys Ocean, and North America was separated from Western Gondwana (South America and Africa) by the proto-Caribbean Sea. The closest approach between these

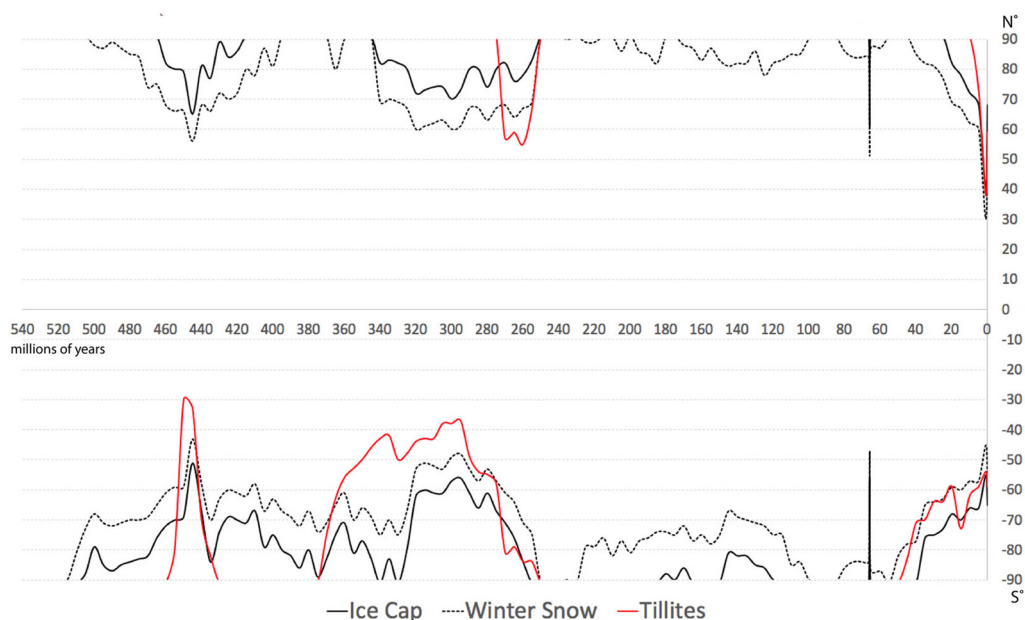


Fig. 48. Latitudinal limits of snow (dotted line) and ice (black line) during the Phanerozoic. The latitudinal limits of snow and ice were estimated from the global temperature model of Scotese *et al.* (2021). The 0° isotherm was used to map the winter snowline and the -10°C isotherm was used to map the limit of permanent ice. The red line indicates the latitudinal limit of glacial deposits (tillites and dropstones; Boucot *et al.* 2013).

two supercontinents was the narrow gap (115 km at 145 Ma) between southern Yucatan and northernmost South America. Some intercontinental migration may have occurred by island hopping along the Greater Antilles volcanic arc, Bahamas hotspot track, Azores hotspot track, and between southern Iberia and Morocco (Fig. 49).

Although the supercontinent of Laurasia remained intact throughout the Early Cretaceous, a rising sea level flooded the continent and produced short-lived, isolated landmasses. For example, the land areas of Europe and Asia, although connected during the Berriasian (145 Ma), were separated by the Straits of Turgai (also known as the Obik Sea, Ural Sea and West Siberian Sea) during most of the Early Cretaceous (140–c. 110 Ma: Figs 50–56).

During the entire Cretaceous, North America was connected to Asia across the Bering Sea land bridge. This connection was intermittent during the earliest Cretaceous (145–125 Ma) and was finally solidified after the collision of the North Slope of Alaska and the Chukotka Block during the early Albian (c. 110 Ma: Fig. 56). Also of note was the fact that Greater Britain (Britain plus Ireland) was an isolated island during most of the Cretaceous but was connected to North America via eastern Greenland during the earliest Cretaceous (145–130 Ma: Figs 49–52).

East Gondwana and West Gondwana were technically separate landmasses at the beginning of the Cretaceous (145 Ma: Fig. 49); however, they were only separated by a narrow (c. 70 km), shallow-water gap across the Davie Strait (≤ 500 m deep: Roche and Ringenbach 2022). During the Valanginian (c. 140 Ma), this shallow-water continental shelf was replaced by a deep oceanic separation (≥ 2000 m). The ocean between Madagascar and Africa widened during the remainder of the Early Cretaceous and achieved maximum width (500 km) when Madagascar stopped moving relative to Africa (105 Ma: Fig. 57).

The East Gondwana landmass composed of India, Madagascar, Australia, Antarctica and Zealandia remained intact throughout most of the Early Cretaceous (145–125 Ma: Figs 49–51). During the last half of the Early Cretaceous (Aptian–Albian, 120–100 Ma: Figs 54–58), a tenuous connection between Antarctica and India may have been maintained by island hopping along the Rajmahal–Kerguelen hotspot track.

Late Cretaceous (100–65 Ma). The early part of the Late Cretaceous (c. 100–85 Ma) was a tectonically active time. Australia and Antarctica began to break apart during the Cenomanian (95 Ma). During the Cenomanian–Turonian (95–90 Ma) a deep ocean trough separated the conjugate margins of Australia and Antarctica but the two continents were still connected by a land bridge in the vicinity of Tasmania (Figs 59 & 60). Although a shallow-water

connection was maintained across the Tasman Straits throughout the remainder of the Cretaceous, the Antarctic and Australian landmasses first became separated due to rising sea levels during the Coniacian–Santonian (c. 85 Ma: Fig. 61).

Zealandia (modern New Zealand) began to separate from eastern Australia during the Late Cretaceous (c. 100 Ma). Extensive continental stretching produced a wide shallow sea with only a small area of emergent volcanic land. The first oceanic lithosphere formed in the Tasman Sea c. 85 Myr ago (Fig. 61).

The partnership between India and Madagascar ended during the Cenomanian (c. 95 Ma). India, together with several small continental blocks (Seychelles, Laxmi Ridge, Mascarene Plateau and Nazareth Bank), rifted away and moved rapidly to the NNE (Figs 59–65).

Although South America and Africa had begun to rift apart during the earliest Cretaceous, they did not finally go their separate ways until the late Albian (105 Ma: Fig. 57). The last dinosaurs crossed the Amazon–Cape Palmas land bridge c. 110 Myr ago. The oldest ocean floor formed in this region of the South Atlantic, near the Romanche Fracture Zone, at c. 105 Ma (Cretaceous Quiet Zone). It is interesting to note that the South American continent remained as a single, contiguous landmass throughout the entire Cretaceous. Even during the high-stands of sea level from the Cenomanian through to the Santonian, it was possible for terrestrial fauna to migrate from the tip of Patagonia to the highlands of Venezuela. In contrast, for most of the Late Cretaceous, the flooded African continent was divided into two landmasses: (1) NW Africa and (2) Afro-Arabia. Beginning in the late Albian (c. 105 Ma: Fig. 57), the Trans-African Seaway crossed from Nigeria, northwards through Niger–Chad and across Libya into the Mediterranean Sea. This shallow-water seaway finally closed during the Campanian (c. 75 Ma: Fig. 63).

During the Late Cretaceous, a rising sea level divided North America into three separate landmasses: Laramidia, Appalachia and Greater Greenland. As mentioned previously, throughout the Cretaceous North America was connected to Asia via the Bering Sea land bridge. By the earliest Cenomanian (100 Ma: Fig. 58), Laramidia was separated from Appalachia by the Mid-Continent Seaway. During times of maximum sea level (90–80 Ma: Figs 60–62), the Trans-Hudson/Labrador Seaway isolated the northern half of Appalachia from Greater Greenland, which was made up of Greenland, the Arctic islands and the four-corners region of north-central Canada. A single North American landmass emerged when these seaways retreated from the continent during the Campanian (75–70 Ma: Fig. 63–64).

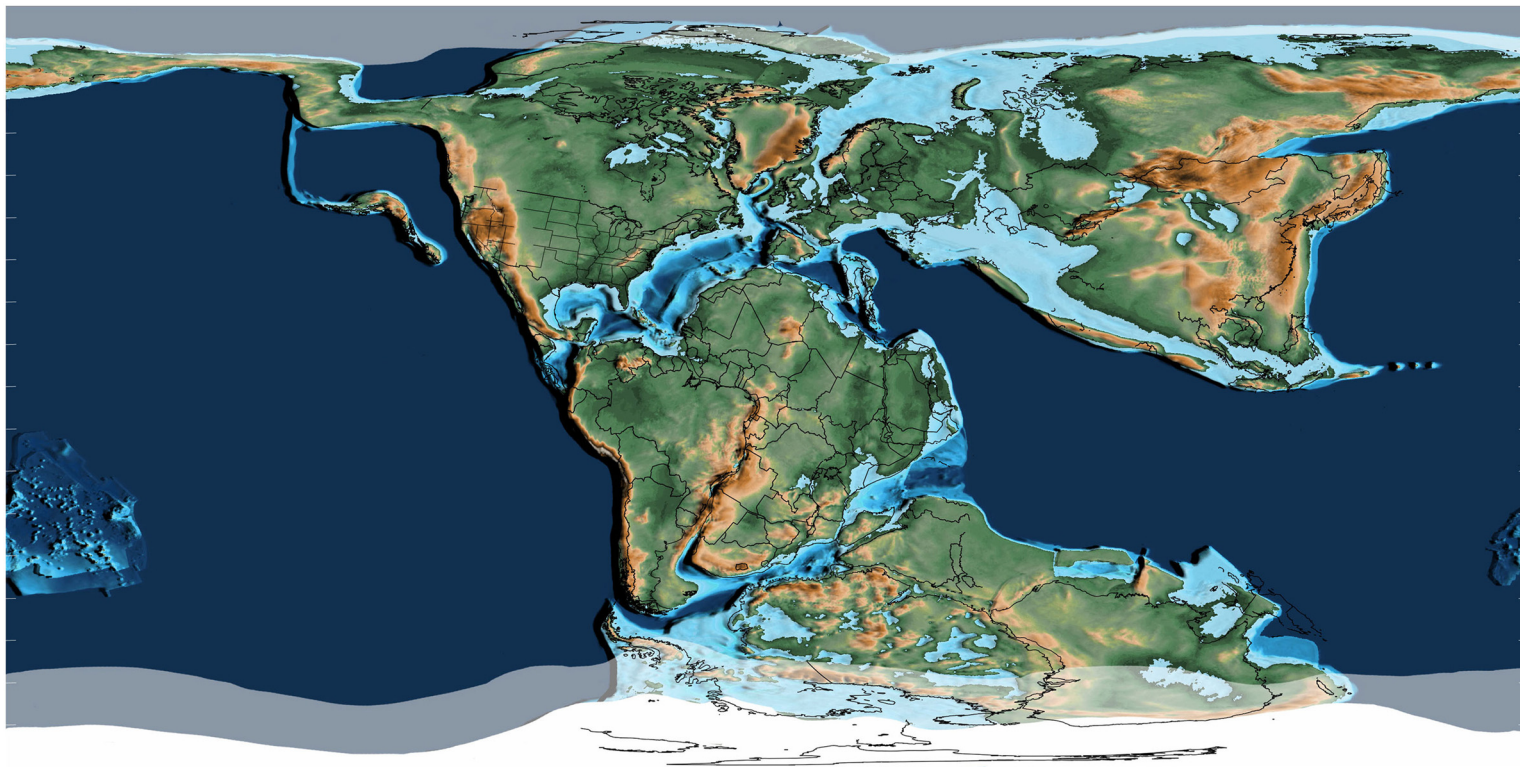


Fig. 49. Jurassic–Cretaceous boundary (145 Ma); see [Figure 2b](#) for the legend.

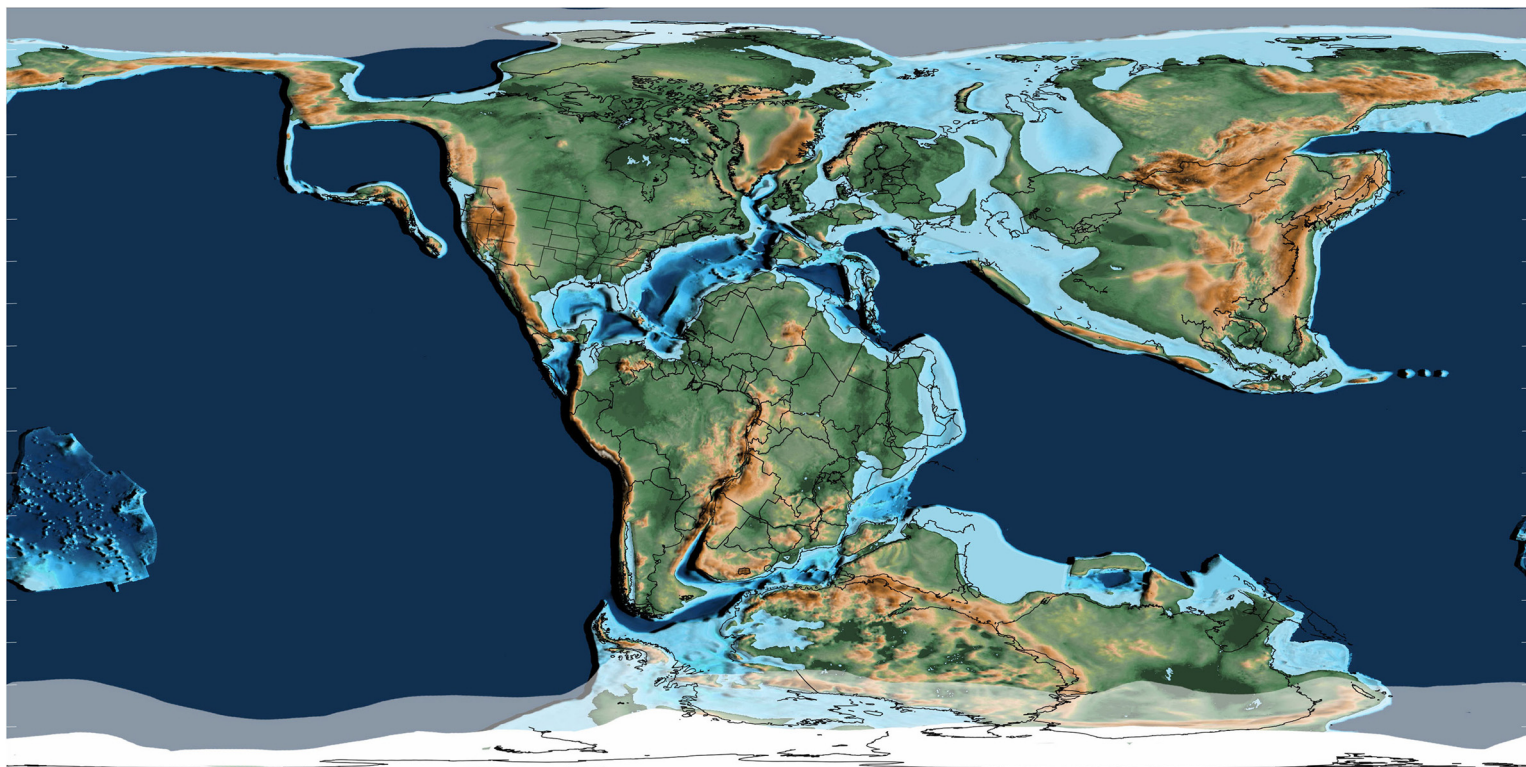


Fig. 50. Early Cretaceous (latest Berriasian, 140 Ma); see [Figure 2b](#) for the legend.

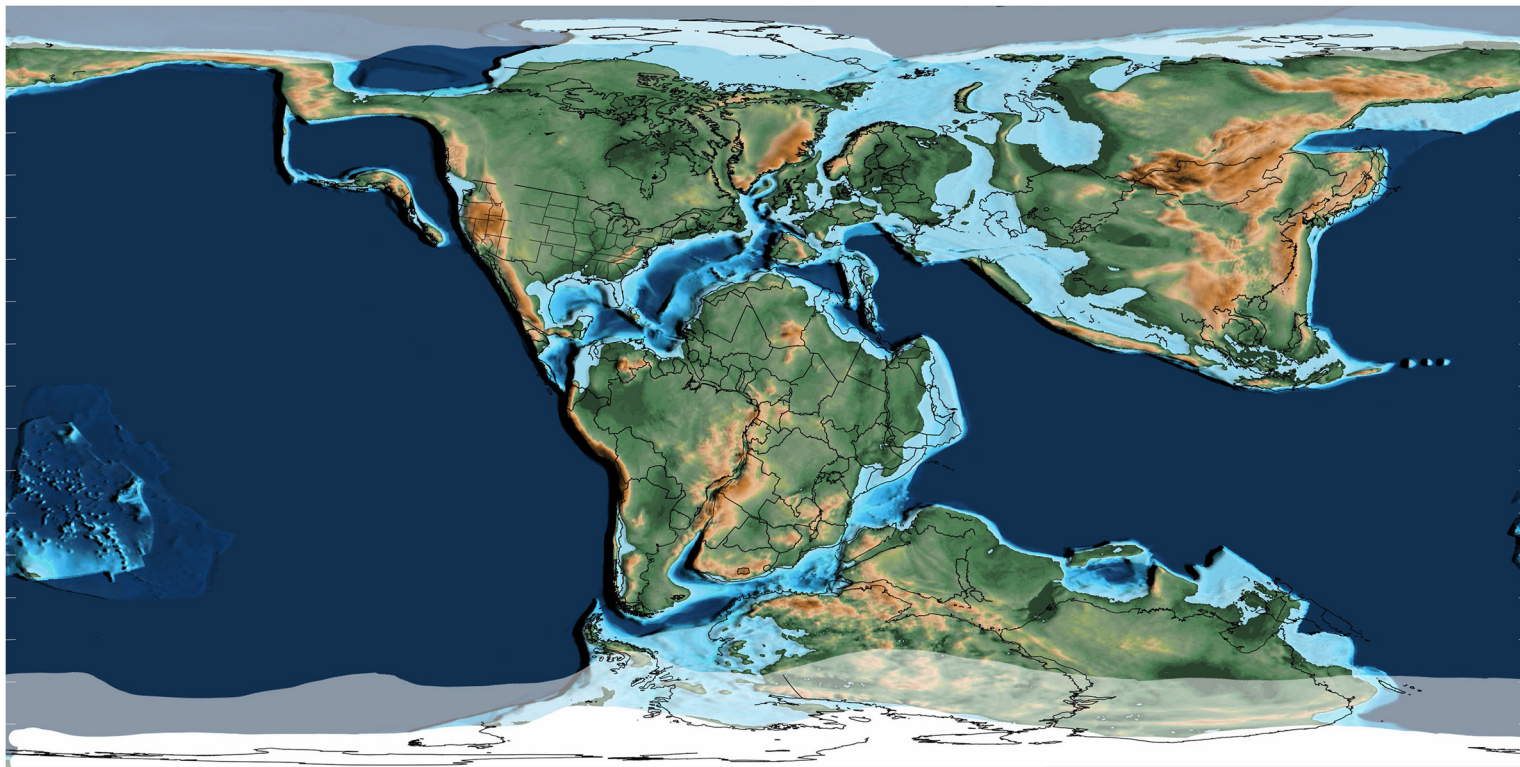


Fig. 51. Early Cretaceous (Valanginian, 135 Ma); see [Figure 2b](#) for the legend.

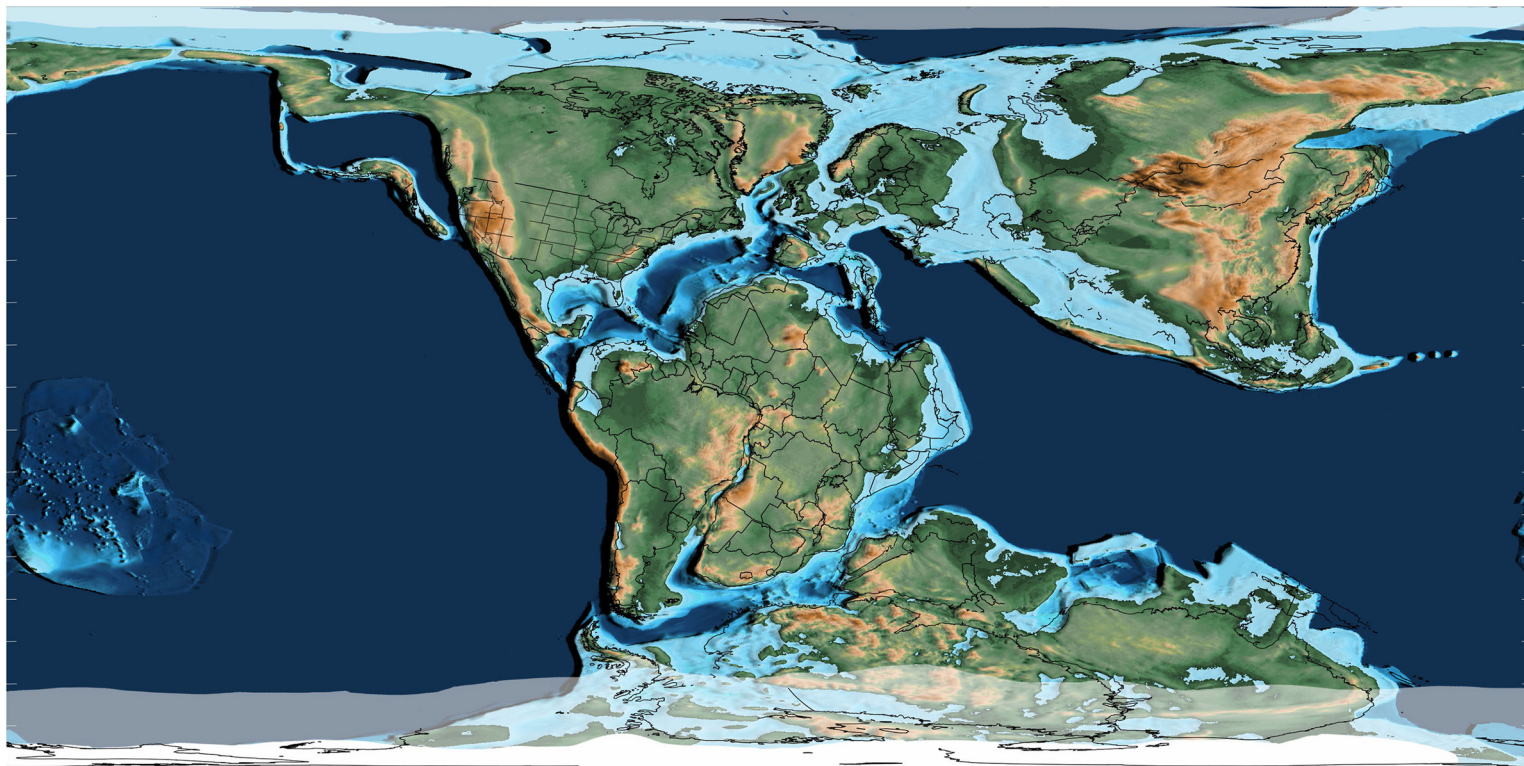


Fig. 52. Early Cretaceous (early Hauterivian, 130 Ma); see [Figure 2b](#) for the legend.

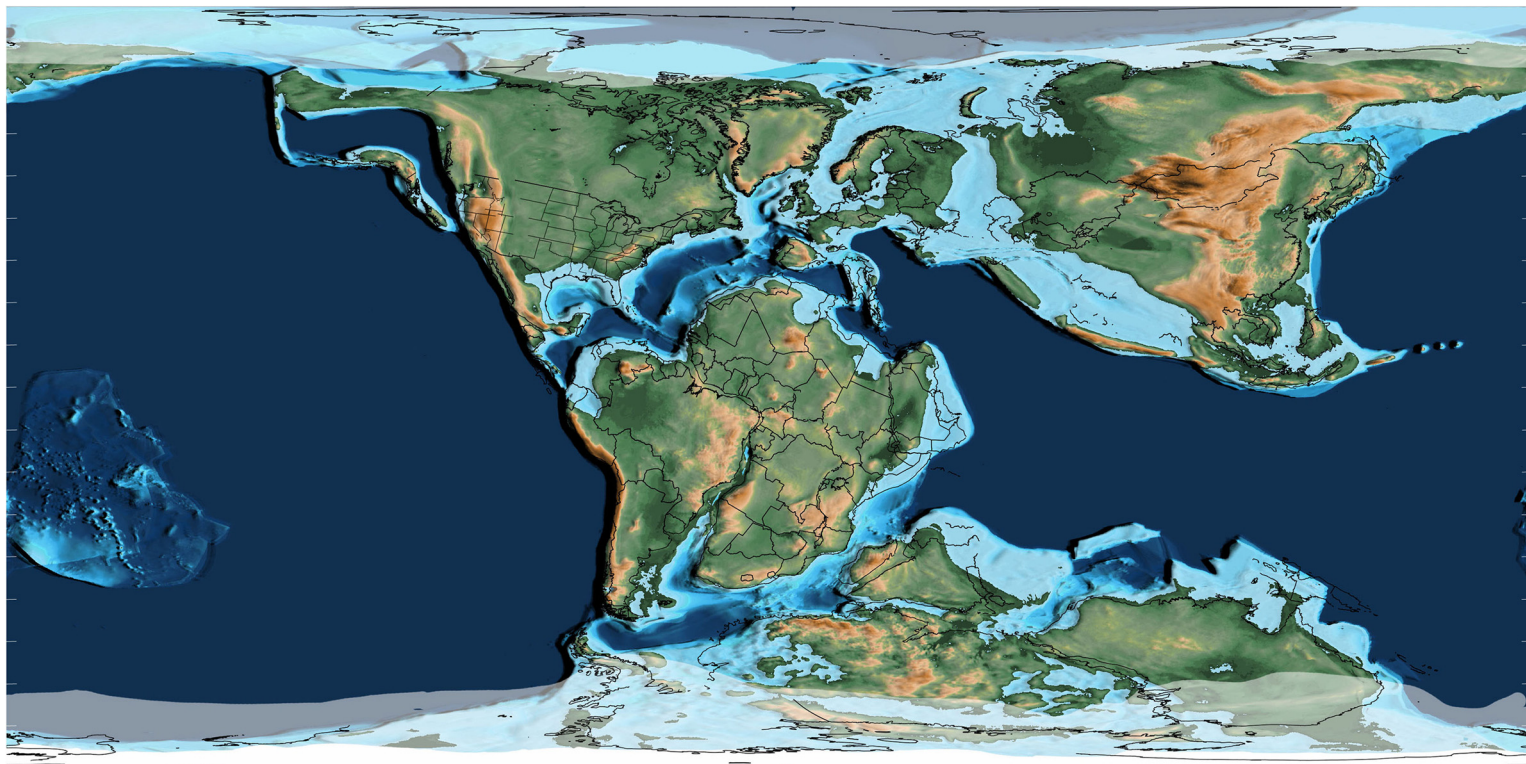


Fig. 53. Early Cretaceous (earliest Barremian, 125 Ma); see [Figure 2b](#) for the legend.

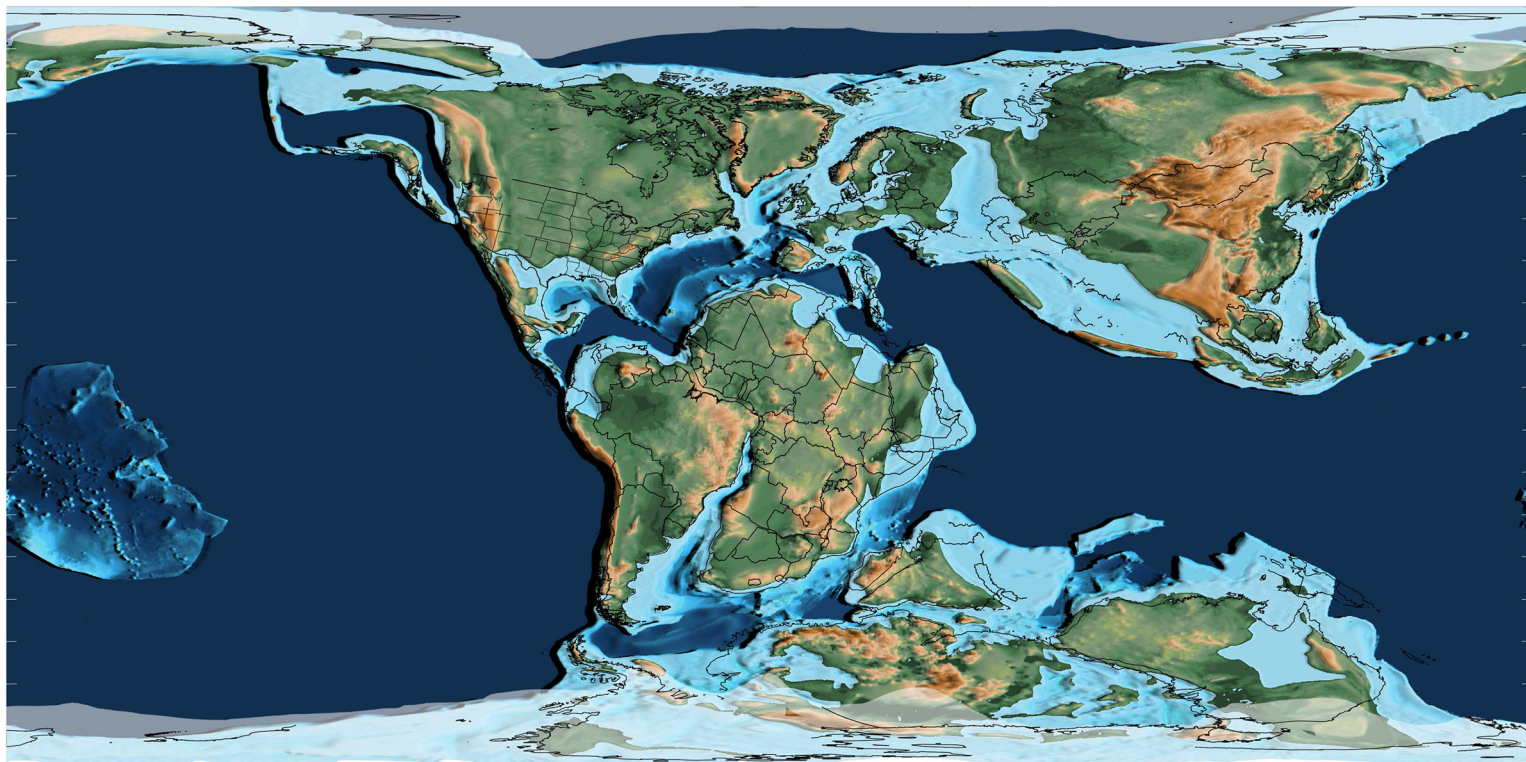


Fig. 54. Early Cretaceous (early Aptian, 120 Ma); see [Figure 2b](#) for the legend.

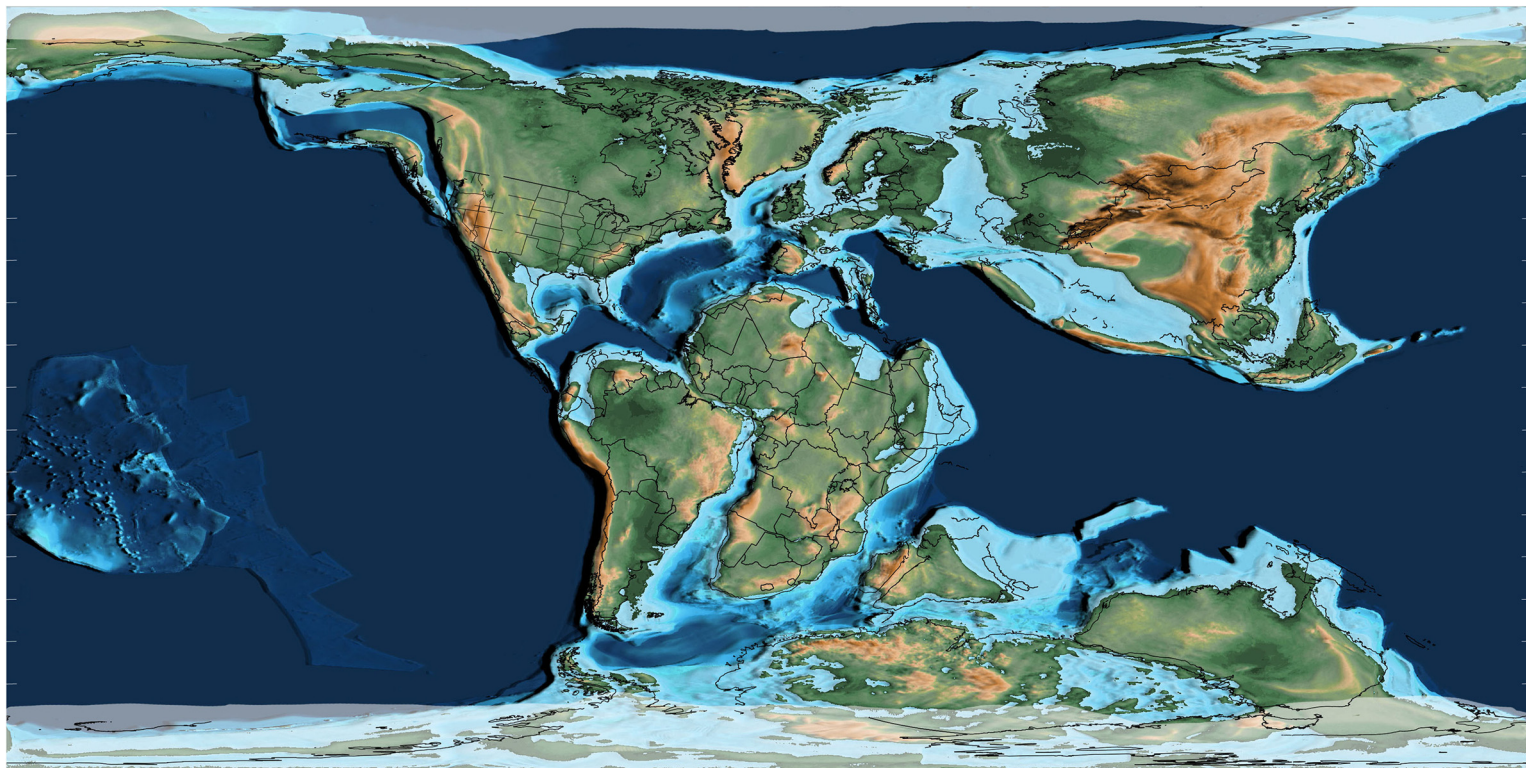


Fig. 55. Early Cretaceous (late Aptian, 115 Ma); see [Figure 2b](#) for the legend.

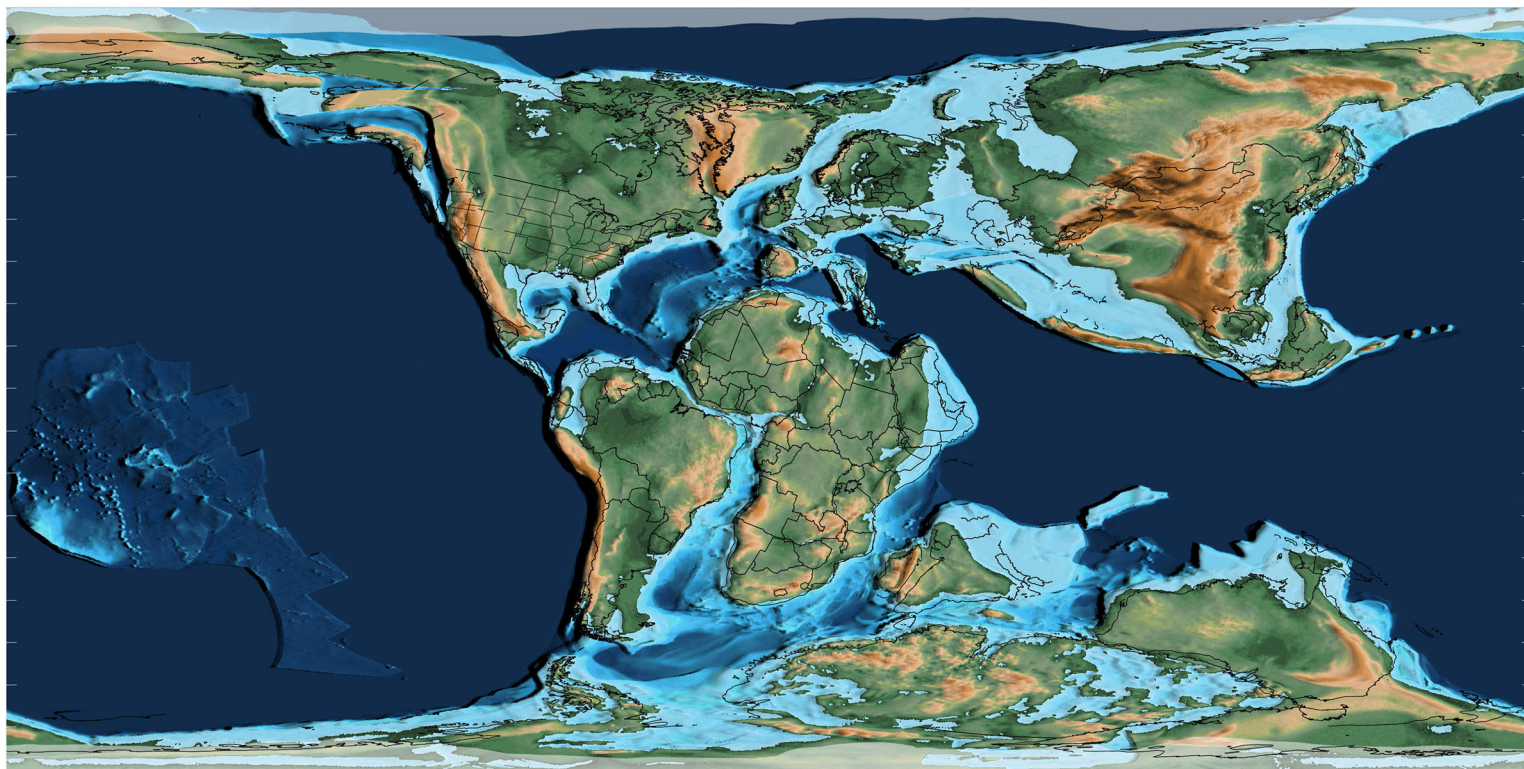


Fig. 56. Early Cretaceous (early Albian, 110 Ma); see [Figure 2b](#) for the legend.

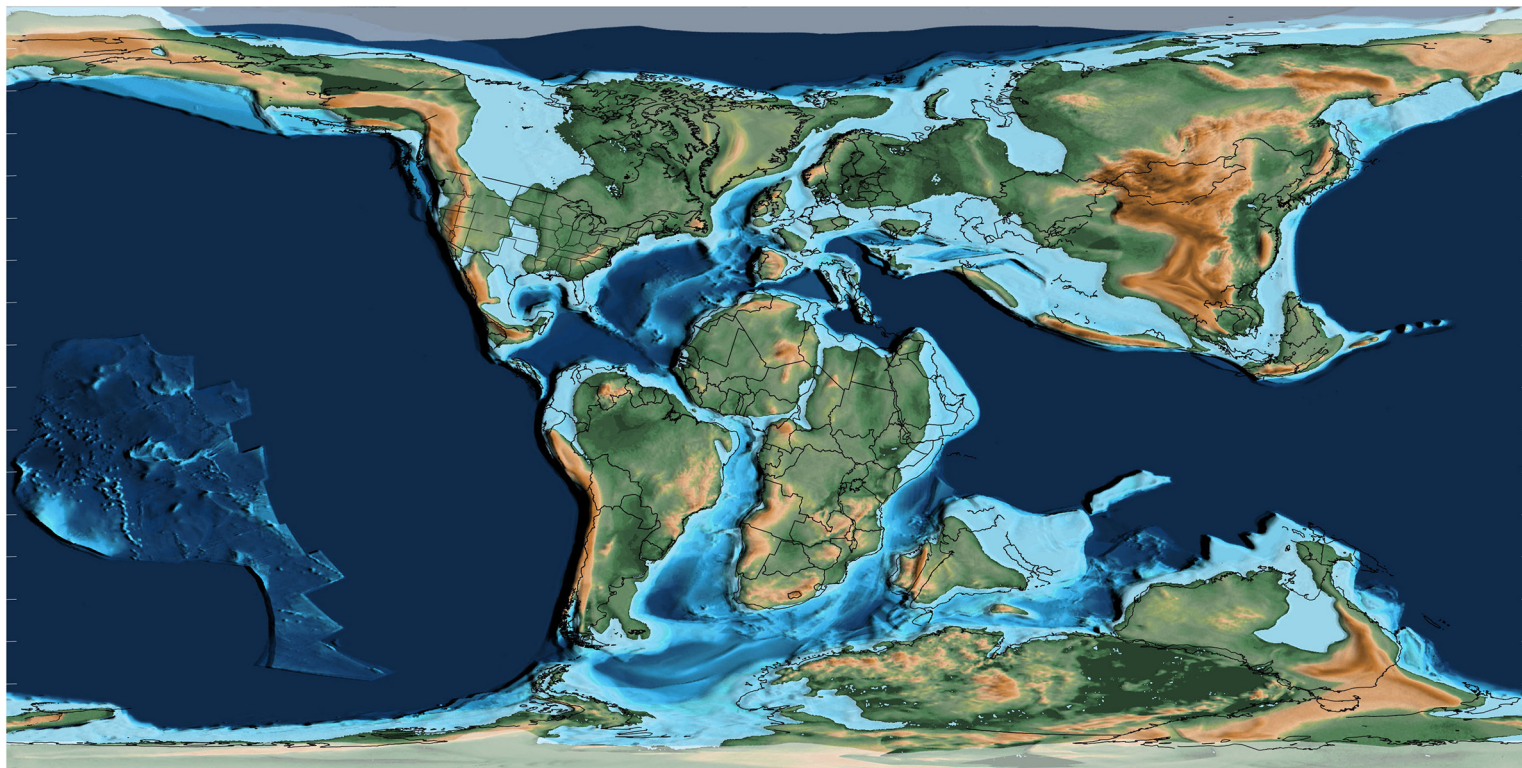


Fig. 57. Early Cretaceous (middle Albian, 105 Ma); see [Figure 2b](#) for the legend.

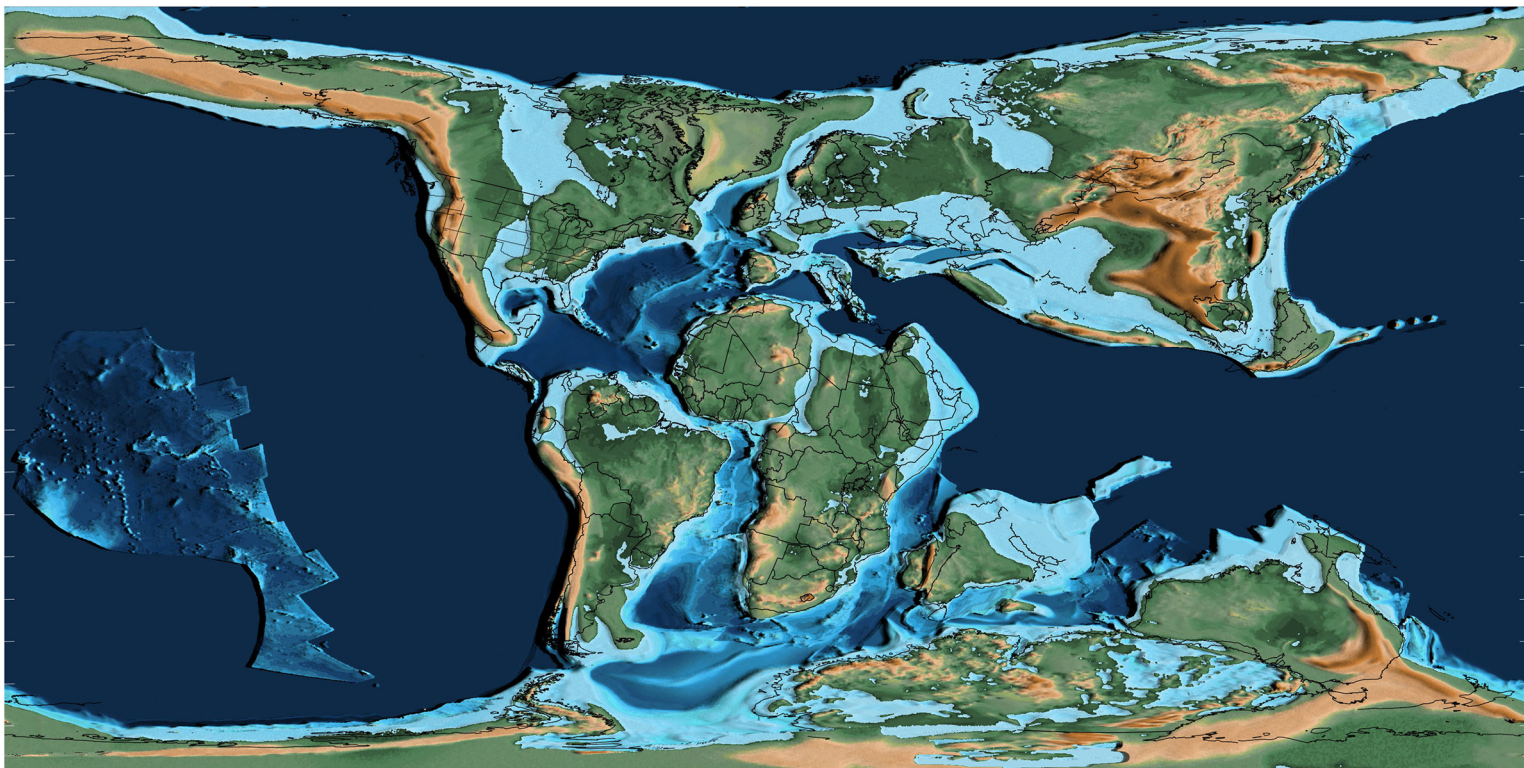


Fig. 58. Early Cretaceous (latest Albian, 100 Ma); see [Figure 2b](#) for the legend.

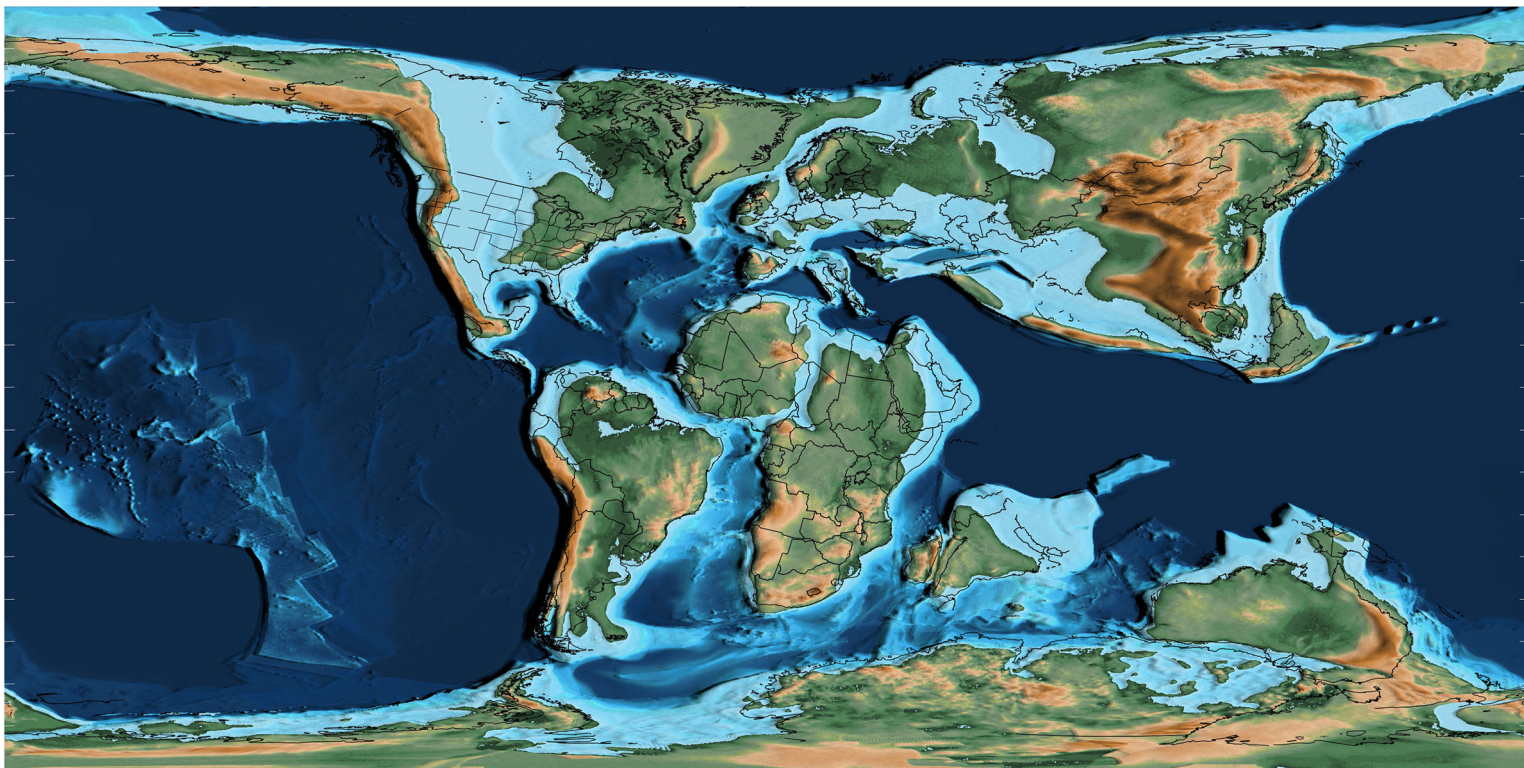


Fig. 59. Mid-Cretaceous (Cenomanian, 95 Ma); see [Figure 2b](#) for the legend.

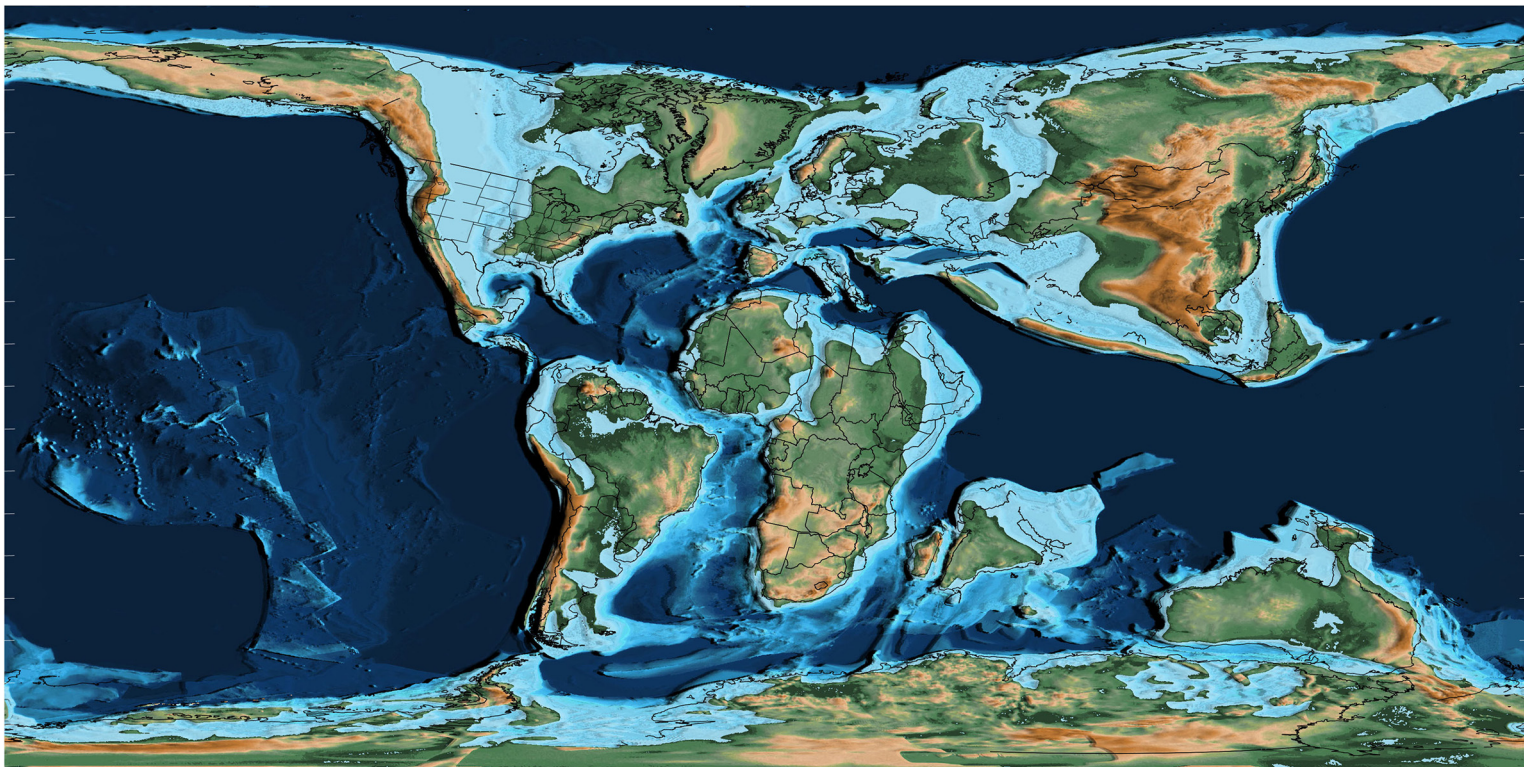


Fig. 60. Mid-Cretaceous (latest Turonian, 90 Ma); see [Figure 1b](#) for the legend.

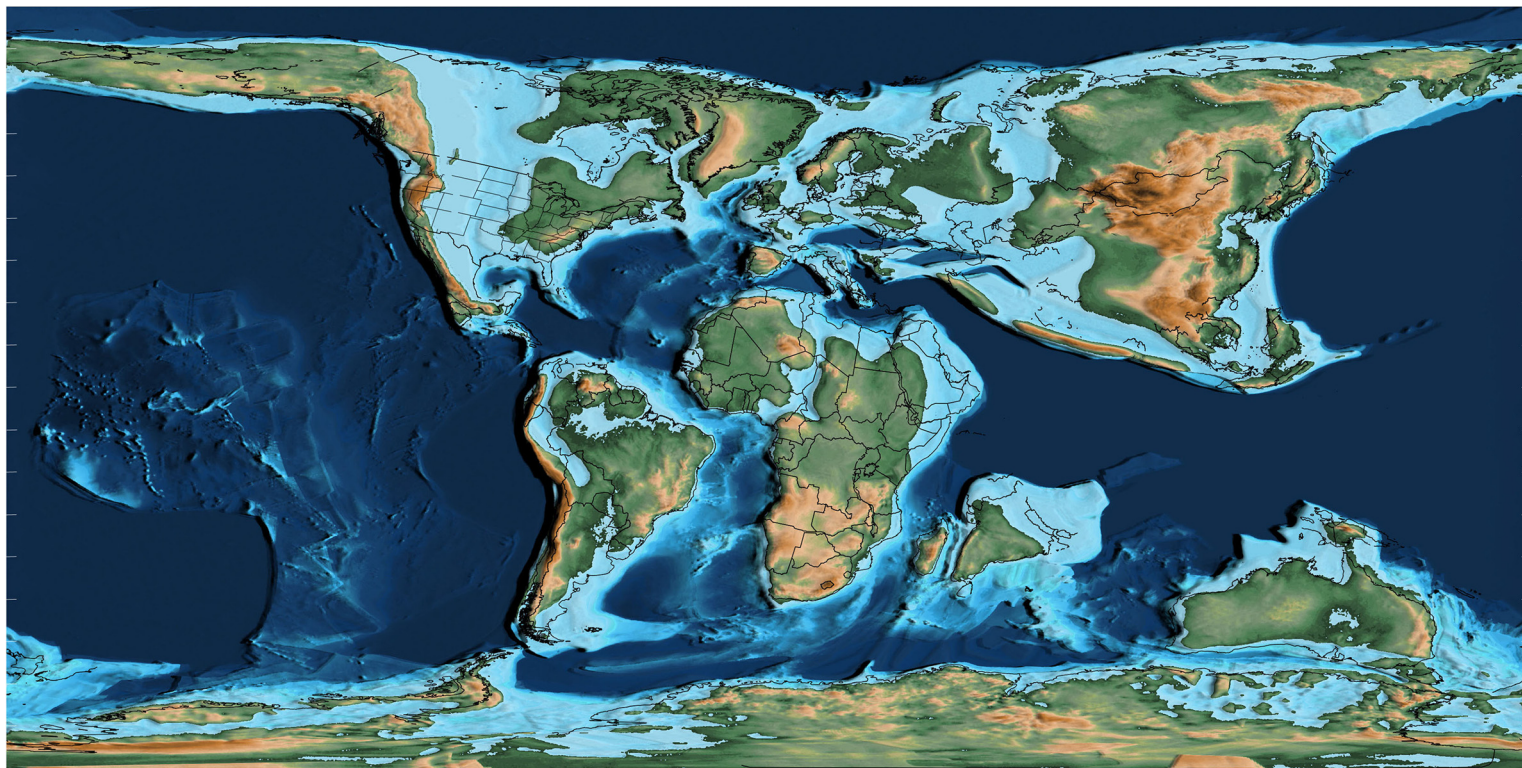


Fig. 61. Late Cretaceous (Coniacian – Santonian, 85 Ma); see [Figure 2b](#) for the legend.

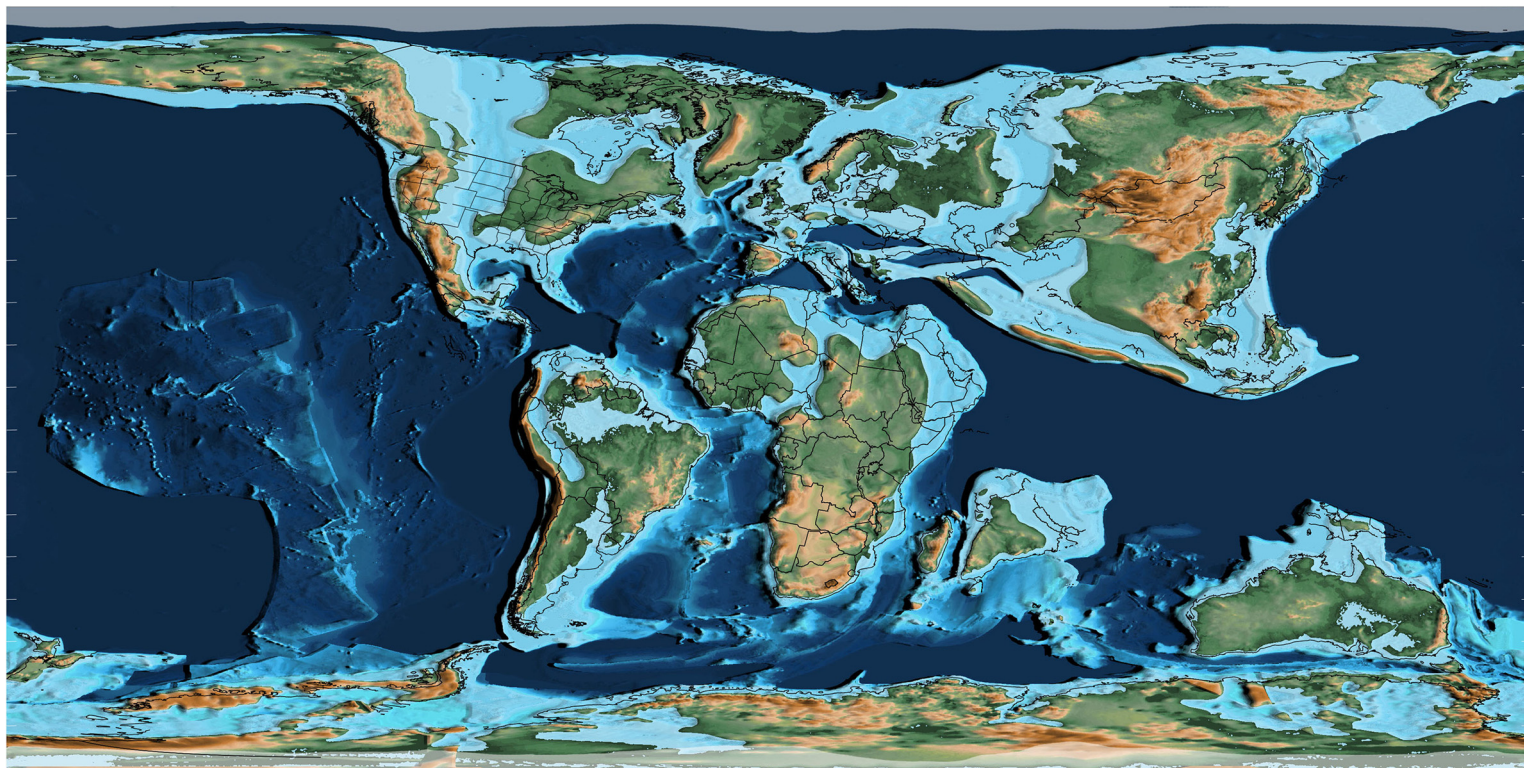


Fig. 62. Late Cretaceous (early Campanian, 80 Ma); see [Figure 2b](#) for the legend.

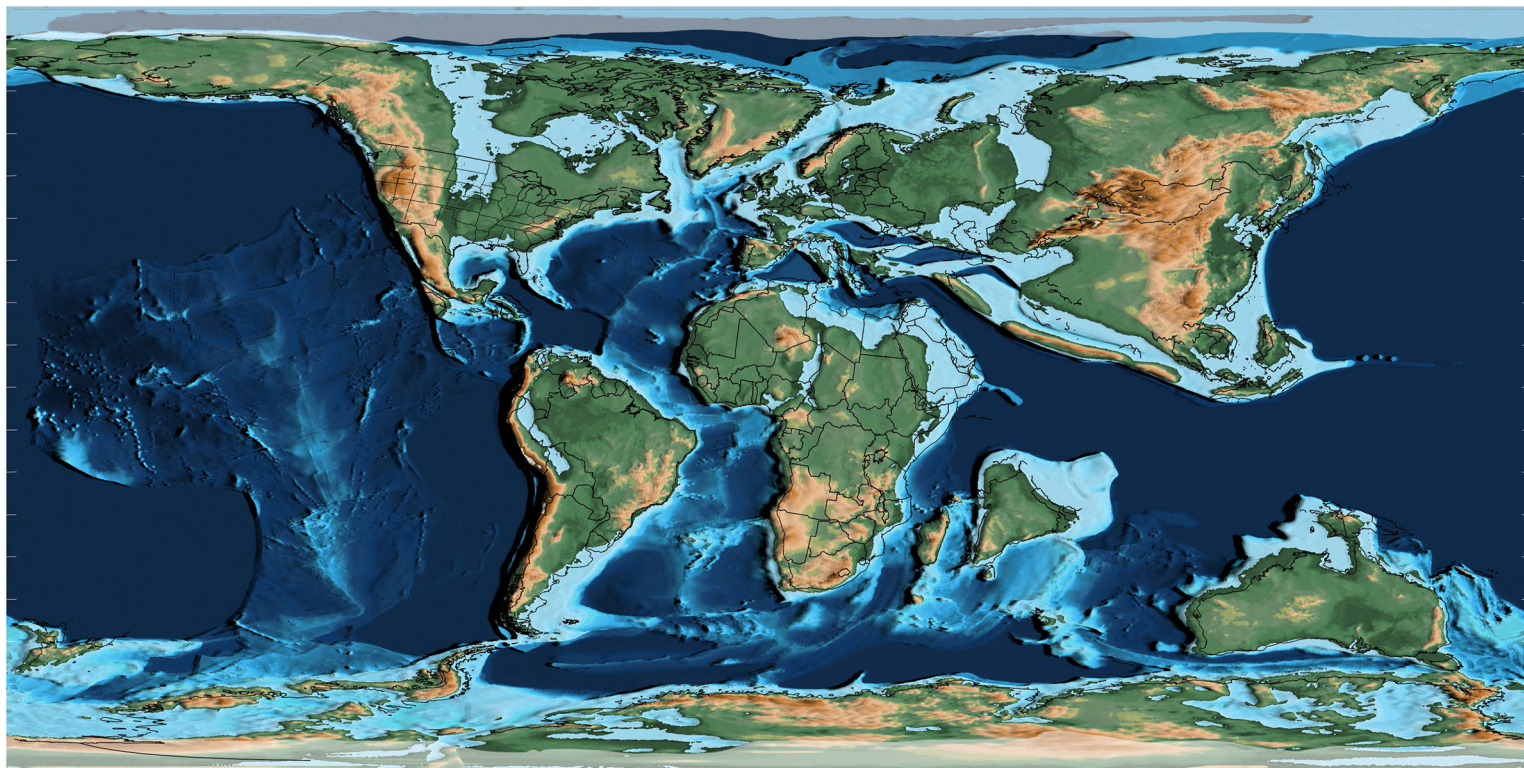


Fig. 63. Late Cretaceous (late Campanian, 75 Ma); see [Figure 2b](#) for the legend.

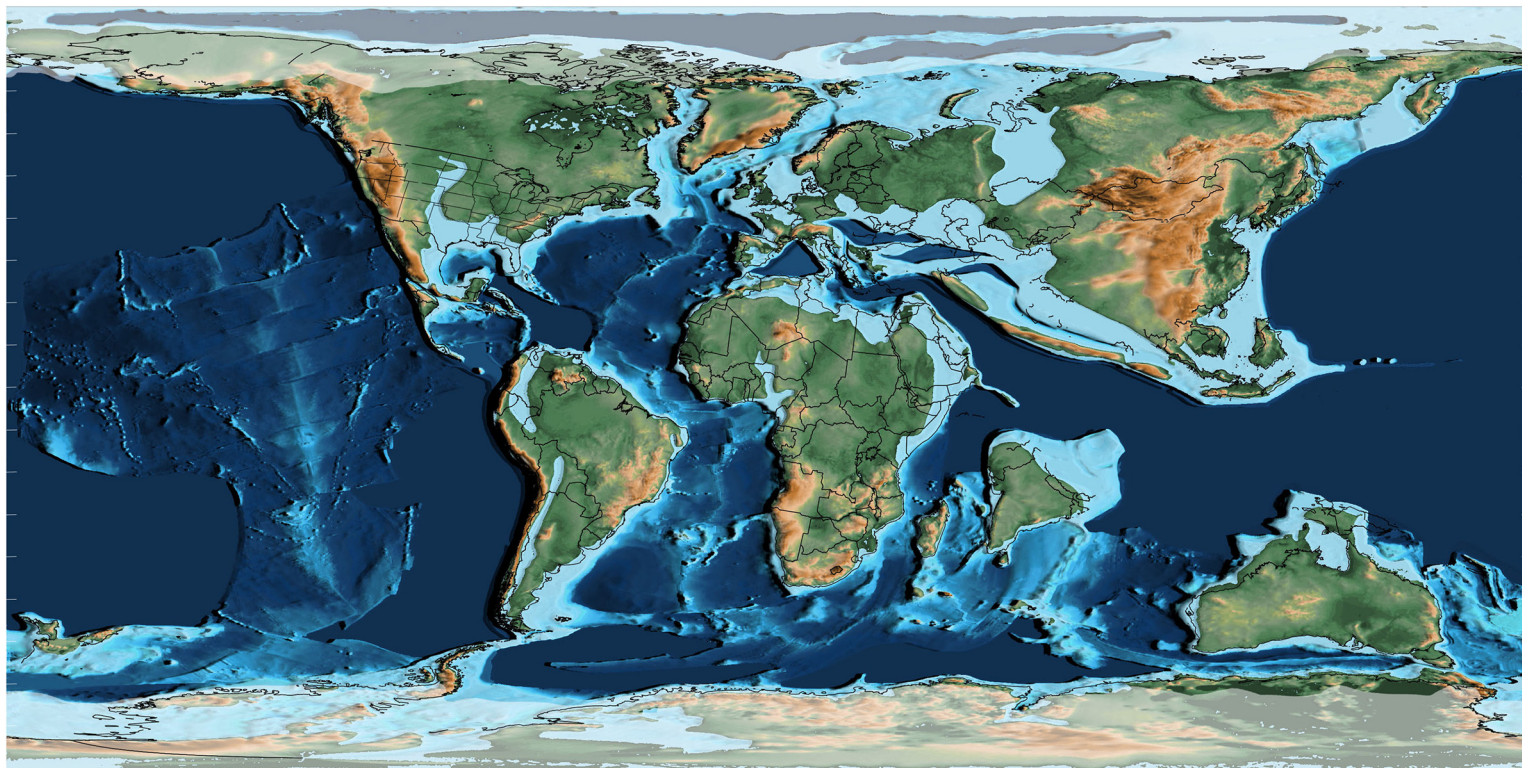


Fig. 64. Late Cretaceous (Maastrichtian, 70 Ma); see [Figure 2b](#) for the legend.

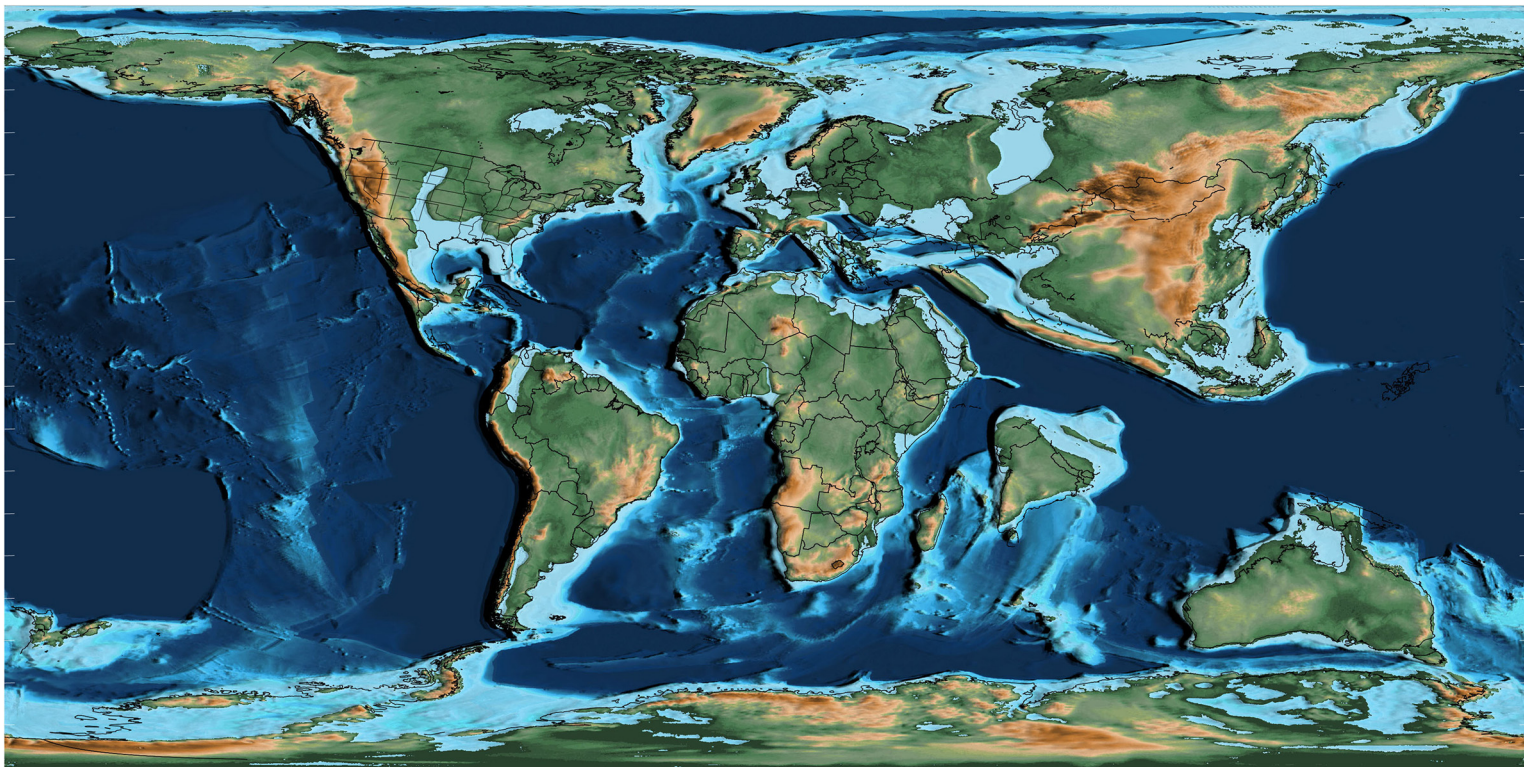


Fig. 65. Cretaceous–Paleogene boundary (65 Ma); see [Figure 2b](#) for the legend.

The Cretaceous world

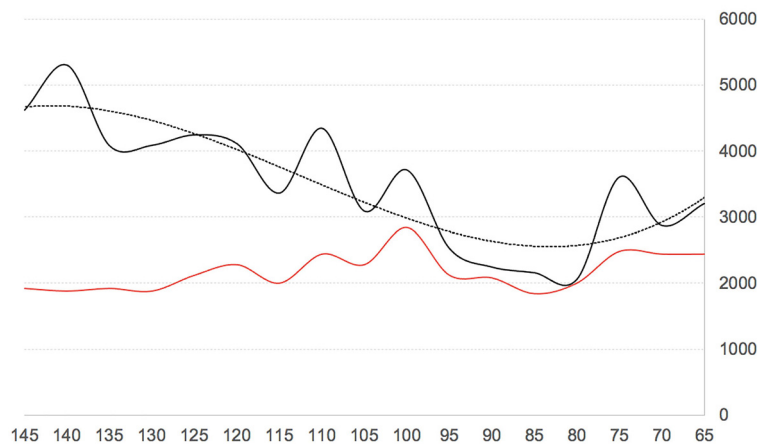


Fig. 66. Average river length (black line) and the number of rivers (red line) during the Cretaceous. x-axis, millions of years; y-axis, kilometres.

Cretaceous rivers

Overview. Rivers, especially at elevations greater than 200 m, are the great agents of erosion that level mountains and create continental peneplains. Although a vast amount of sediment is preserved in river deltas, evidence of the rivers that produced these accumulations are rarely preserved in the geological record. River lowlands, which are flooded and reworked during highstands of sea level, are the first to disappear. Ongoing continental flooding erases all but the most upland river systems. For these reasons, the Cretaceous river systems shown

in [Figures 67–82](#) are very speculative. They are derived entirely from the palaeoDEMs that are the basis of the palaeogeographical maps. No attempt has been made to ground-truth the predictions made by the simulation with evidence from the geological record.

As described previously, these palaeoDEMs can be used to recreate ancient drainage networks. These drainage networks represent potential river systems. To determine whether a drainage system will be filled with water, we must add the predictions of rainfall and runoff made by global climate models. The number and length of river systems are

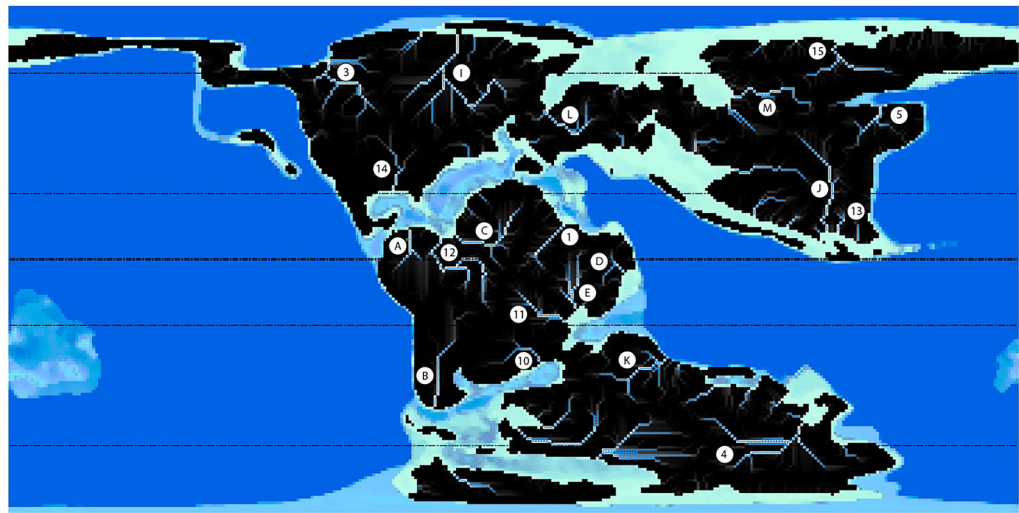


Fig. 67. Early Cretaceous drainage system and rivers, Jurassic–Cretaceous boundary (145 Ma), for the legend see [Table 11](#).

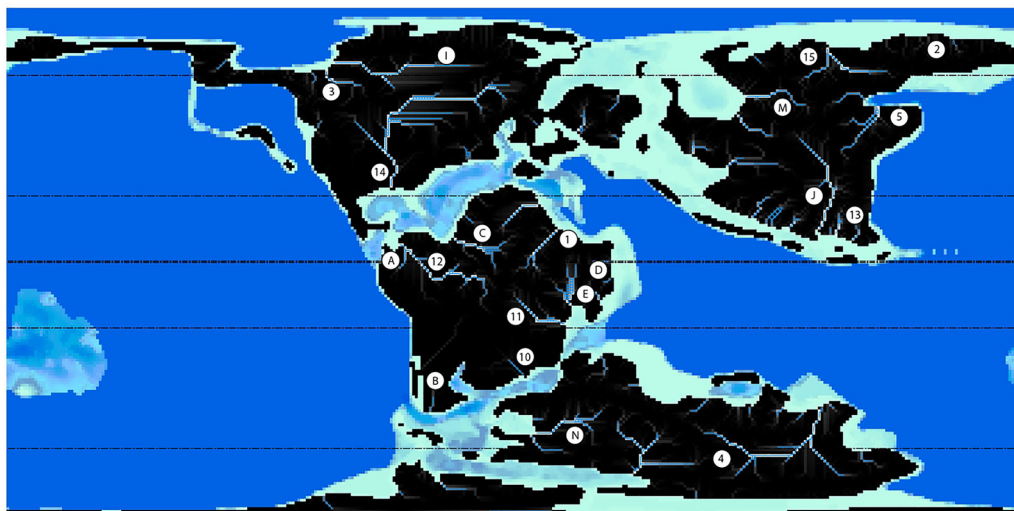


Fig. 68. Early Cretaceous (latest Berriasian, 140 Ma), for the legend see Table 11.

ultimately controlled by a combination of changes in topography and sea level.

The river systems presented here are unnatural, in the sense that they do not evolve through time. The geometry of actual rivers and drainage systems grows and changes in almost an organic fashion. Young upland rivers are straight and rapid; old rivers meander slowly across the plains. One river system may capture another river system, creating a mega-river network. None of these evolving patterns of river growth and maturity are shown on these maps. The rivers are each a unique representation of the specific topography. In this regard, the location

and pattern of rivers may change drastically from one stage to another (e.g. compare the rivers of the Berriasian and the Campanian). Nevertheless, there are some generalizations that can be made from the long-lived aspects of Cretaceous palaeogeography that have produced enduring river geometries. In the following sections we discuss average river length and the number of rivers during the Cretaceous, the effect of climate on river systems, the effect of plate tectonics on river basin geometry, and the Cretaceous origin of some of the modern rivers.

Average river length and the number of rivers. Figure 26 illustrates that during the Phanerozoic,

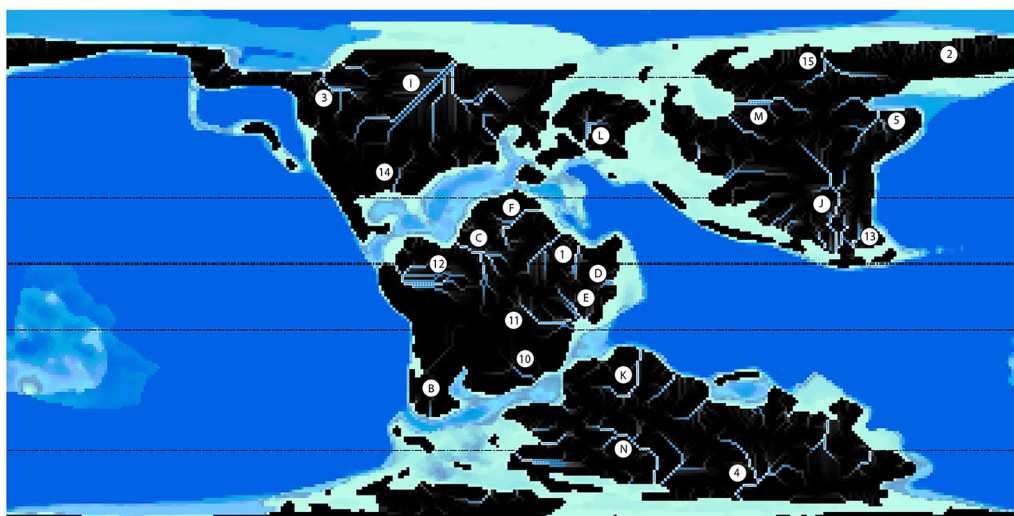


Fig. 69. Early Cretaceous (Valanginian, 135 Ma), for the legend see Table 11.

The Cretaceous world

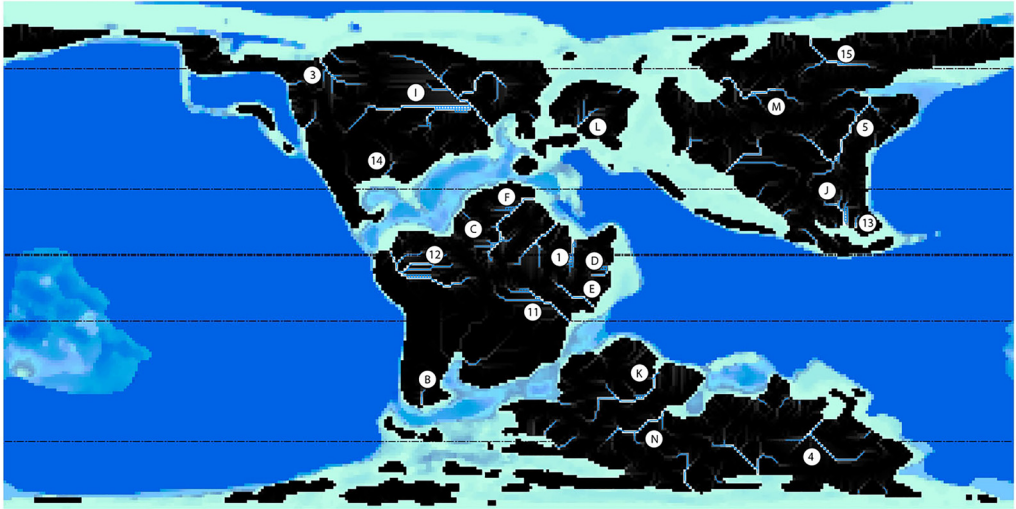


Fig. 70. Early Cretaceous (early Hauterivian, 130 Ma), for the legend see [Table 11](#).

when sea level is high, the average river length is reduced and, conversely, when sea level is low the average river length increases. The pattern holds true for the Cretaceous ([Fig. 66](#)). [Figure 66](#) plots the average length of major river systems (black line) during the Cretaceous. As expected, rivers are shorter during times of high sea level due to a reduce landmass area. Minimum river length (c. 2500 km) occurred during the mid-Cretaceous (Cenomanian–Santonian, 95–80 Ma). This interval corresponds with the peak in Cretaceous sea level (Turonian, c. 150 m; this study). Maximum river length occurred

during the earliest Cretaceous (c. 5000 km; Berriasian–Valanginian, 145–140 Ma) ([Figs 67–69](#)), a period of low sea level. [Figure 66](#) also plots the number of major river systems during the Cretaceous (shown as a red line). It is somewhat counterintuitive that the number of river systems remained relatively constant during the Cretaceous. During each stage of the Cretaceous, approximately 50 rivers longer than 250 km traversed the continents. The number of rivers is apparently independent of the landmass area; rivers simply become shorter as sea level rises and longer as sea level falls. This relationship can be

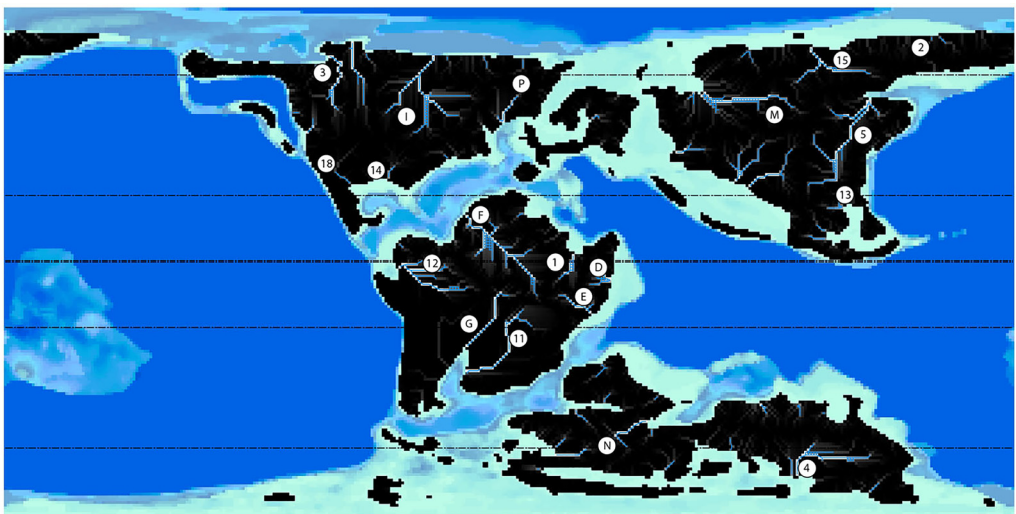


Fig. 71. Early Cretaceous (earliest Barremian, 125 Ma), for the legend see [Table 11](#).

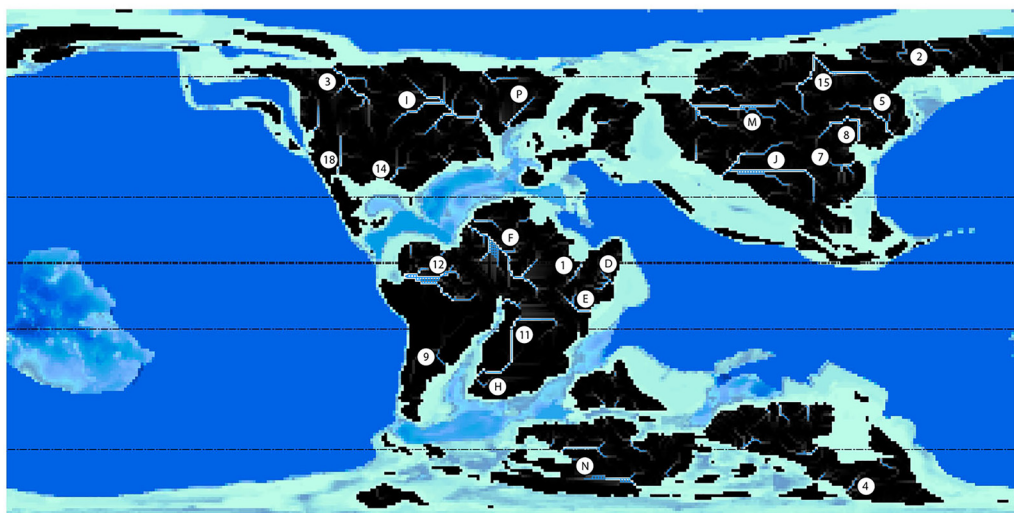


Fig. 72. Early Cretaceous (early Aptian, 120 Ma), for the legend see [Table 11](#).

seen by comparing Berriasian and latest Turonian maps.

Effect of climate on river systems. As stated previously, rivers exist where the prescribed drainage system is filled with water. The presence of water depends both on the amount of regional precipitation and the flow length of the river system. Flow length is directly proportional to the size of the drainage basin. The largest rivers, like the Amazon River, will be found in large drainage basins that lie within the ever-wet climate zone (Köppen Zone A). Major

ivers can also be found in the Warm Temperate and Cool Temperate Rainy belts.

As discussed in the section on ‘Computer simulations of palaeoclimate’, the HadCM3 climate model was used to predict the amount of precipitation during the Cretaceous. These estimates of precipitation are generally in good agreement with the Köppen climatic belts derived from lithological indicators of climate and palaeoclimate proxies ([Burgener *et al.* 2023](#)). However, the agreement between these two independent predictors of precipitation is not perfect.

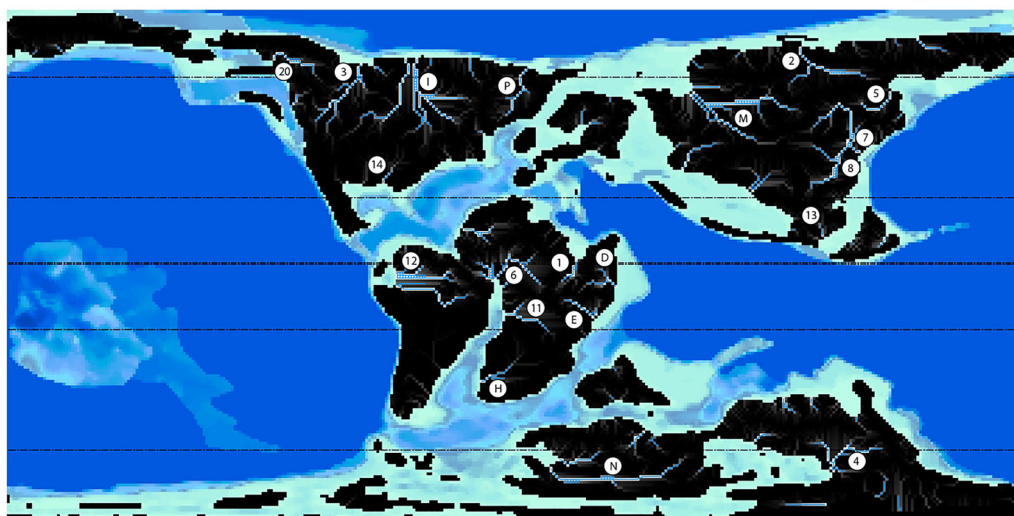


Fig. 73. Early Cretaceous (late Aptian, 115 Ma), for the legend see [Table 11](#).

The Cretaceous world

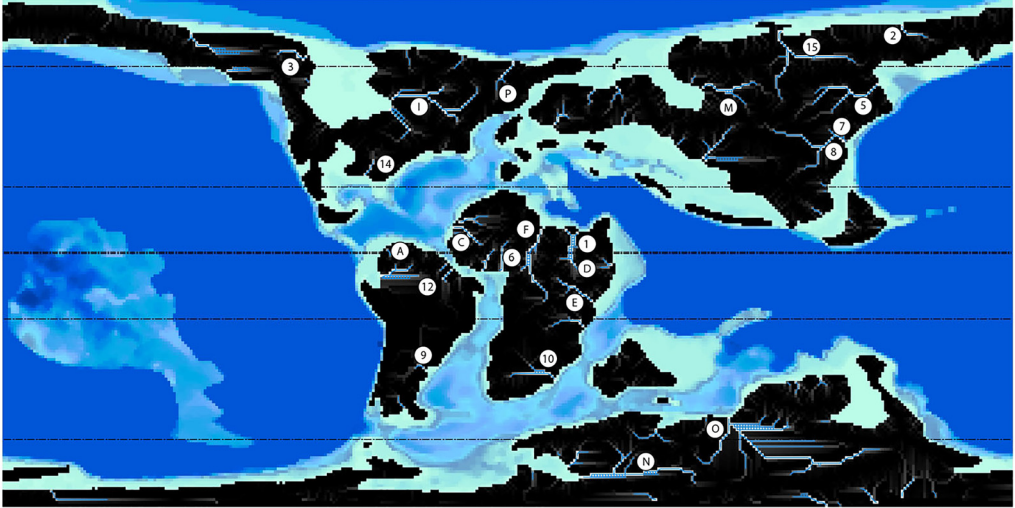


Fig. 74. Early Cretaceous (middle Albian, 105 Ma), for the legend see [Table 11](#).

Upon close inspection of palaeoriver maps, one may note several river systems that originate in regions that are predicted by the Köppen maps to be arid and therefore should be dry river beds. A good example of such a dry river system can be found in the arid zones surrounding the narrow South Atlantic and the northern arid belt of eastern China during the Aptian (120 Ma) (Figs 70–72).

Effect of plate tectonics on river systems. Rivers flow from high areas to low areas, therefore the quickest way to change the geometry of a river basin is to alter the gradient of the topography.

During the Cretaceous, several events profoundly affected palaeotopography. These events can be characterized as: the formation of Andean margins adjacent to subduction zones; continental collision; uplift associated with hotspot activity prior to continental rifting; and the formation of a medial rift valley and rift shoulders during the early phases of continental break-up (Figs 73–82).

During the Cretaceous, Andean margins were common along the western margins of the Americas and in eastern Asia. Rivers adjacent to these Andean margins tended to flow parallel to the mountain

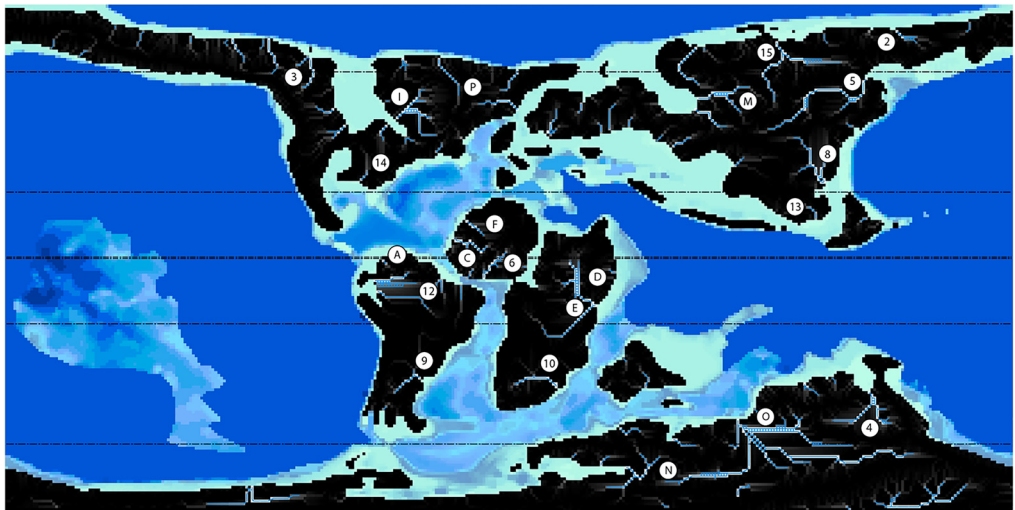


Fig. 75. Early Cretaceous (latest Albian, 100 Ma).

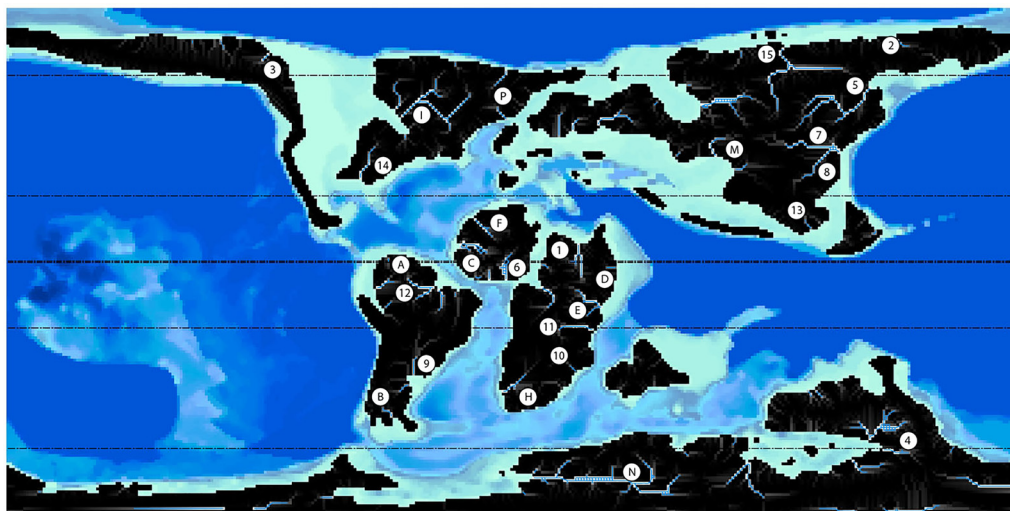


Fig. 76. Mid-Cretaceous (Cenomanian, 95 Ma), for the legend see [Table 11](#).

range in the depression (foredeep), caused by the thrusting of the mountain range over the adjacent craton. Examples of these mountain-parallel river systems are the MacKenzie, Orinoco, Patagonian and Amur rivers (see [Table 11](#)).

Although there were no major continental collisions during the Cretaceous, there were three minor collisions that affected the geometry of river basins. These tectonic events coincidentally took place in the Aptian (121–113 Ma). The Mongol–Okhotsk Ocean had closed by the Aptian, diverting the Amur River eastwards ([Figs 73 & 74](#)). Previously,

the Amur River had flowed south to north along the eastern margin of Asia ([Fig. 71](#)). In NE Siberia, the collision of Kolyma along the Verkhoyansk mountains created an elongate NW–SE foredeep through which the Lena River flowed into the Arctic Ocean ([Figs 73–75](#)). Finally, the North Slope Block collided with central Alaska during the late Aptian (115 Ma), creating the Yukon river system ([Fig. 73](#)).

During the Early Cretaceous (145–130 Ma: [Figs 67 & 70](#)), West Gondwana began to rift apart. Uplift in easternmost Brazil and central Africa created no

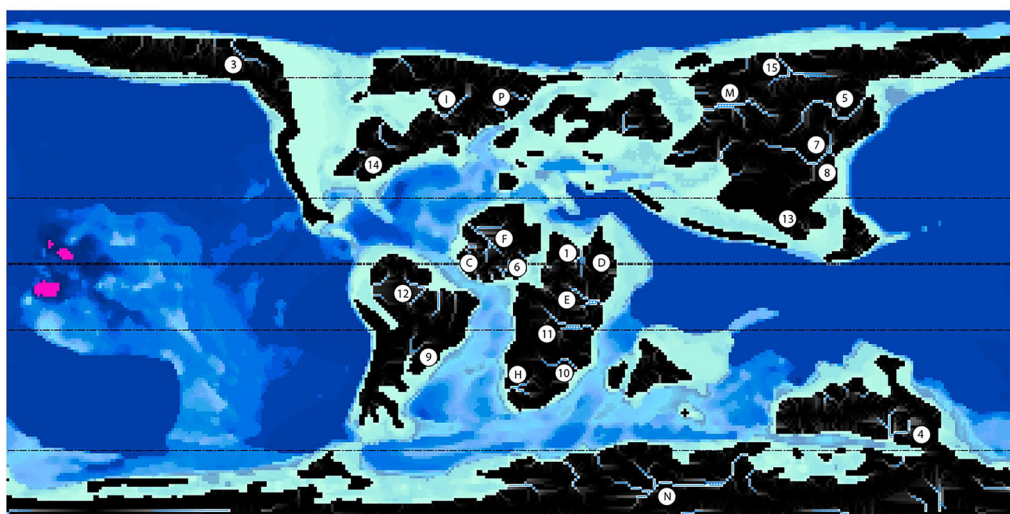


Fig. 77. Mid-Cretaceous (latest Turonian, 90 Ma), for the legend see [Table 11](#).

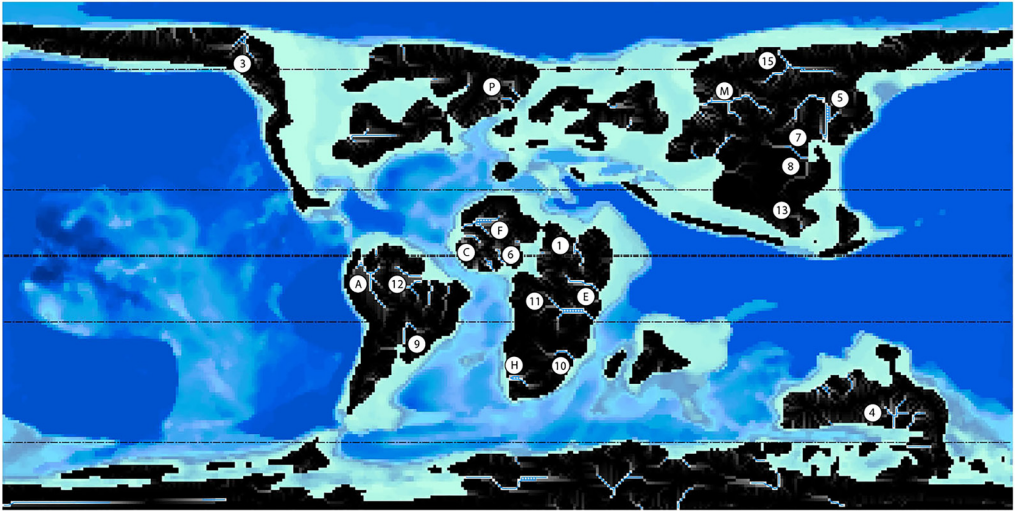


Fig. 78. Late Cretaceous (Coniacian – Santonian, 85 Ma), for the legend see Table 11.

less than eight major river systems (Fig. 69). These rivers radiated away from the core of West Gondwana (proto-Amazon, Senegal, Nile, trans-Saharan, Arabian, Lamu, Zambezi and Patagonian rivers). A similar phase of Early Cretaceous uplift between Australia and Antarctica created the proto-Darling–Murray river system (Fig. 73) and a vast, putative river system across eastern Antarctica (Fig. 74).

By the Barremian (125 Ma), a long, north–south river (Australis River) flowed down the rift valley that separated South America and Africa (Fig. 71). Within 10 Myr, emergent rift shoulders along the margins of the South Atlantic forced a new set of

ivers to flow westwards across South America (proto-Amazon and Parana rivers) and eastwards across Africa (proto-Congo and Namib rivers) (Fig. 73). It should be noted that these rivers flowed in directions that were opposite to their modern counterparts (Table 11).

Cretaceous origin of some modern rivers. Some of the rivers alluded to in the previous section are unique to the Cretaceous (e.g. Australis, trans-Saharan Arabian, Lamu, Namib and Patagonian). This is not surprising. Over the vastness of geological time, the topography of the continents has changed substantially, creating new drainage basins

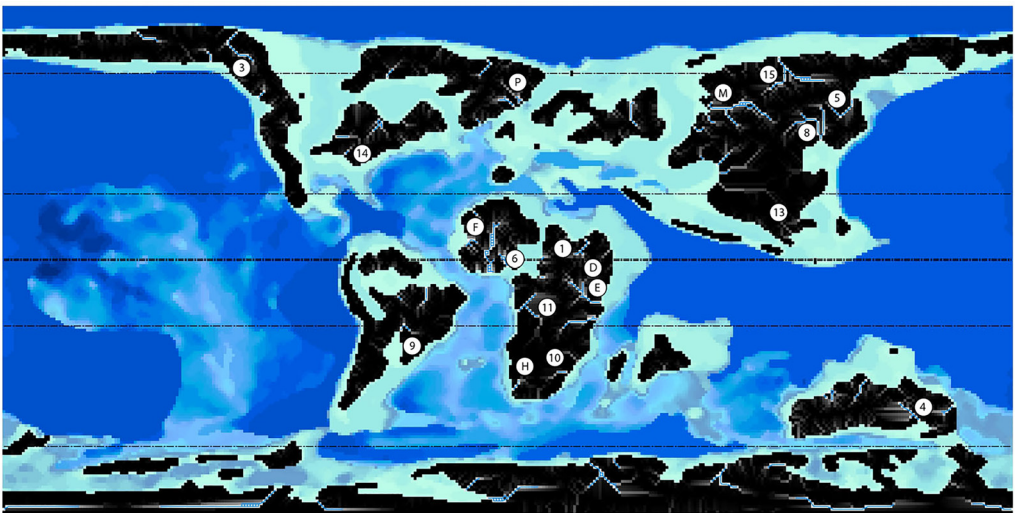


Fig. 79. Late Cretaceous (early Campanian, 80 Ma), for the legend see Table 11.

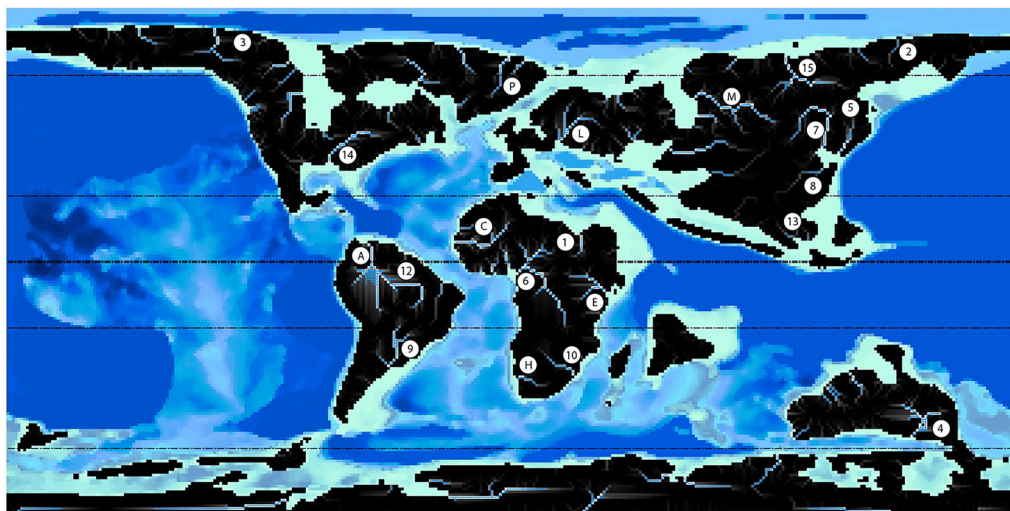


Fig. 80. Late Cretaceous (late Campanian, 75 Ma), for the legend see Table 11.

and rivers. It is a little surprising, however, that many of these Cretaceous rivers have modern counterparts (e.g. proto-Amazon, Amur, proto-Congo, Lena and MacKenzie).

Figure 83 illustrates some of the major modern river systems with lengths greater than 2500 km. Table 11 lists both the newly described Cretaceous rivers and Cretaceous rivers that have modern counterparts. A check mark, '✓', indicates that the named river can be found on the corresponding map. A simple naming convention has been used to describe important aspects of these rivers. The term 'proto-River name' implies that the mapped river may be

the ancestor of its modern counterpart but that the geographical location, extent and flow direction may be somewhat different. The suffix '-r' indicates that the geographical location of the palaeoriver is similar to its modern counterpart but the flow direction was reversed in the Cretaceous (e.g. Amazon-r). The suffix '-s' indicates that the geographical location and the flow direction are the same as its modern counterpart but the extent of the river system is much smaller (e.g. Mekong-s). The suffix '-f' indicates that the river system was flooded at that time. In a few cases the letters 'N, E, S and W' are used to indicate the direction that the palaeoriver flowed.

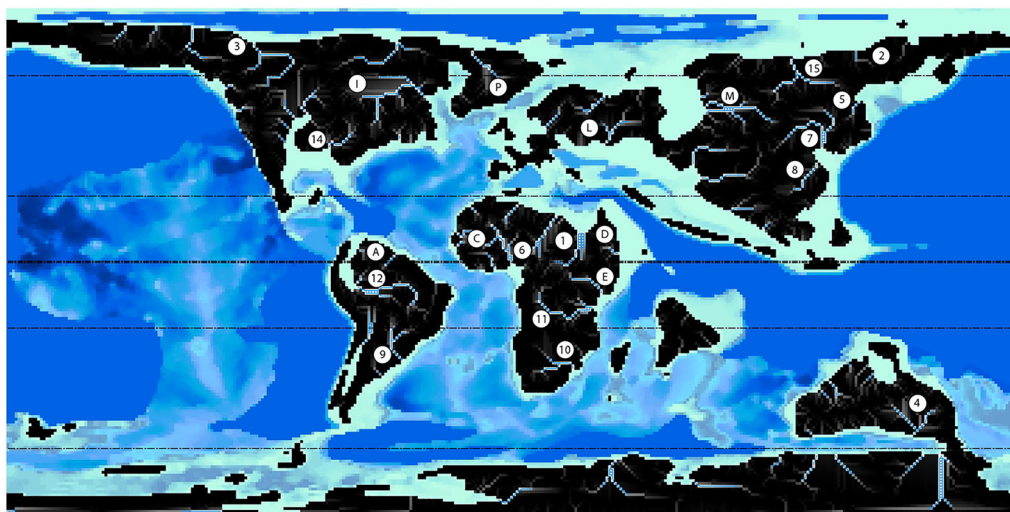


Fig. 81. Late Cretaceous (Maastrichtian, 70 Ma), for the legend see Table 11.

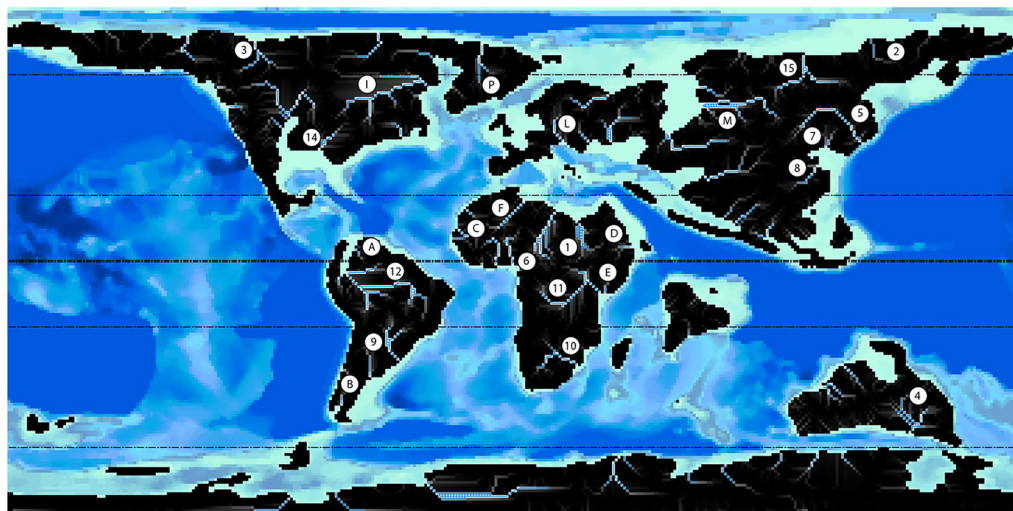


Fig. 82. Cretaceous–Paleogene boundary (65 Ma), for the legend see Table 11.

A quick review of Table 11 finds that more than half of the 35 longest modern river systems had counterparts during much of the Cretaceous. Most notable are the Nile, Amazon, Yangtze, Mississippi, Huang-He, Congo-r, Zambezi, Amur, Lena, Mac-Kenzie, Mekong, Niger and Murray–Darling.

The modern rivers that do not have Cretaceous counterparts fall into three categories: (1) rivers that occupied portions of the continents that were mostly flooded during the Cretaceous (e.g. Yenisey, Ob-Irtysh, Volga and Rio Grande); (2) rivers that were created in response to plate tectonic events during the Cenozoic (e.g. Danube, Rhone, Rhine, Loire, Tigres-Euphrates, Indus, Syr, Amu, Ganges, Brahmaputra, Columbia and Colorado); and (3) modern rivers in eastern South America that for most of the Cretaceous were located within the southern arid belt (Sao Francisco, Paraná and Paraguay–Uruguay) and, therefore, were not filled with water.

Some of the most intriguing and putative Cretaceous river systems that do not have any modern counterparts can be found in the Early Cretaceous (145–100 Ma: the Patagonian, trans-Asian, trans-Saharan, trans-Antarctic and trans-Indian rivers) and the Late Cretaceous (100–65 Ma: the Namib, Greenland and trans-Europe rivers). Four major river systems that have no modern equivalents span the entire Cretaceous: the Arabian, Lamu, trans-Hudson and trans-Siberian rivers.

Oceanic circulation during the Cretaceous

Introduction. In this final section on palaeogeography, we move from the continents to the ocean basins and discuss oceanic circulation during the

Cretaceous. The circulation of the surface of the ocean is primarily driven by the prevailing winds (Fig. 84). The tropical Easterlies and the temperate Westerlies push the ocean waters ahead of them. At the Equator, strong ocean currents generally move from east to west (Fig. 85). At mid-latitudes (35°–40° N and S), the ocean currents move predominantly from west to east. When an ocean current runs into a continent, it is deflected to the north or south depending on the hemisphere and the latitude. This deflection is due to the Coriolis force, which tends to drive the currents polewards.

At mid-latitudes in the northern hemisphere (*c.* 30° N), the gyres off the western coasts of continents spin clockwise; at high latitudes (55°–65° N) the gyres spin counter-clockwise; and polar gyres spin clockwise (Fig. 85). The opposite pattern is observed in the southern hemisphere: off the western coasts of southern continents a mid-latitude ocean current is deflected to the north, forming a counter-clockwise gyre (*c.* 30° S). High-latitude gyres in the southern hemisphere rotate clockwise (Fig. 85). These fundamental patterns of ocean circulation also apply to the Cretaceous. All of the Cretaceous ocean circulation models presented here (Figs 86–88) follow this general pattern and were produced by the HadCM3 global climate model. What made the Cretaceous different from the present day was the changing size and interconnectedness of the ocean basins.

Cretaceous oceanic surface currents. At the beginning of the Cretaceous, the continents were in a Pangaea-like configuration. The combined Panthalassic–Tethys Ocean Basin was huge (spanning >260° of longitude); there were only a few, small, nearly landlocked, intra-Pangaean oceans (e.g.

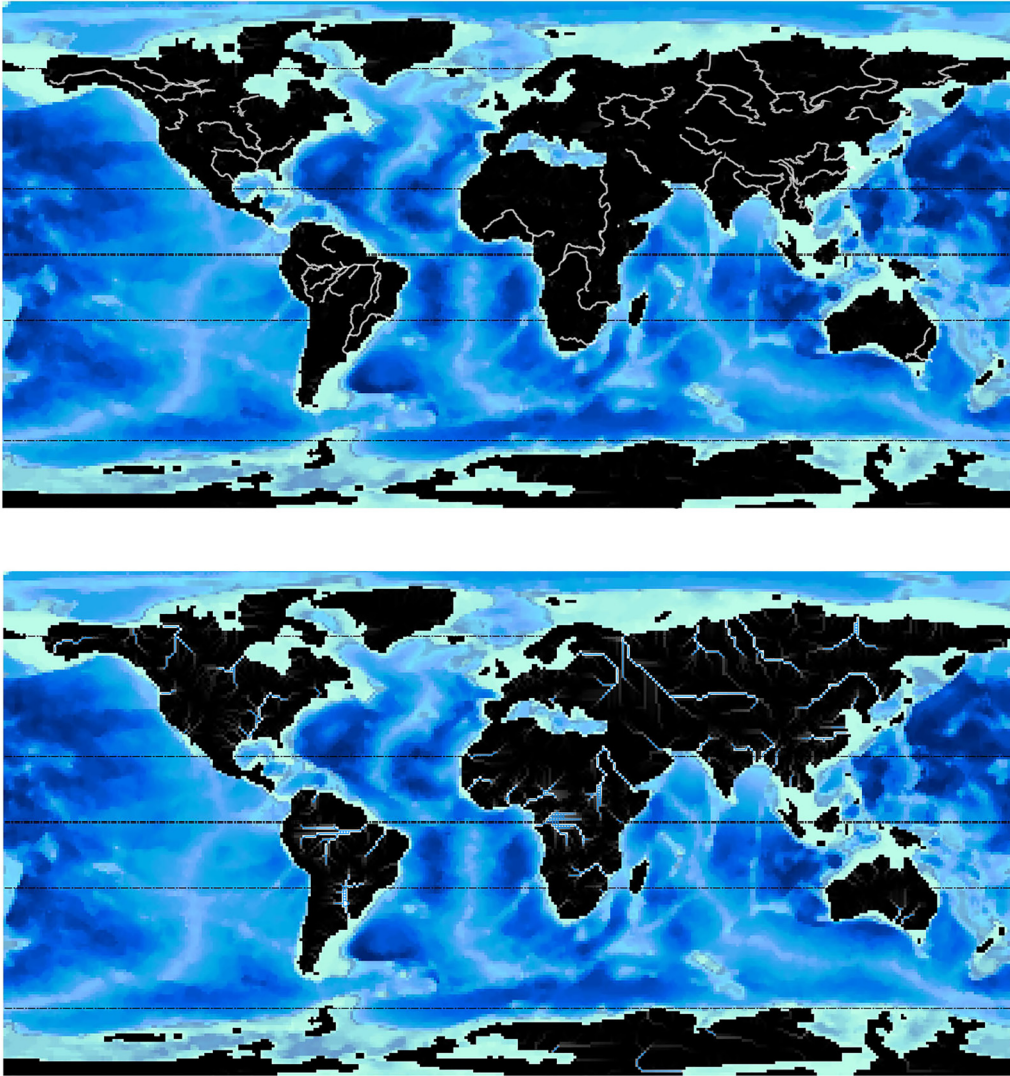


Fig. 83. Major modern river systems, for the legend see Table 11: (top) actual modern rivers (white lines) and (bottom) computer simulation (light blue lines).

Central Atlantic, Somali Basin, Mozambique Basin and Weddell Sea). As Laurasia and Gondwana began to break apart, these ocean basins widened and became interconnected.

During the Early Cretaceous, the westward-flowing Equatorial Current collided with East Africa (Figs 86–88). Approximately half of the water was diverted northwards, where it flowed NW along the coast of Arabia, then along the southern Mediterranean and eventually recycled eastwards after hitting a dead end in the western Mediterranean. This current was active throughout most of the Cretaceous but was closed down in the Late Cretaceous

(Campanian, 75 Ma: Fig. 86) due to the narrowing of the western end of the Tethys Ocean.

It should be noted that there was never a strong, long-lasting connection between the western Tethys and the Central Atlantic. Two factors prohibited a strong, through-going connection: (1) the passage south of Iberia was always narrow and shallow; and (2) during the Cretaceous, the northern coast of Africa was at latitudes of *c.* 30° N and connections between the Equatorial currents on either side of were inhibited by opposing winds. Rather than a single through-going ocean current connecting Tethys and the Atlantic realms, two stable, counter-

Table 11. Cretaceous rivers

| ID | Name | Age (Ma) | | | | | | | | | | | | | | | |
|----|-------------------|----------|-----|-----|-----|-----|-----|-----|-----|-----|----|----|----|----|----|----|----|
| | | 145 | 140 | 135 | 130 | 125 | 120 | 115 | 105 | 100 | 95 | 90 | 85 | 80 | 75 | 70 | 65 |
| 1 | Nile | ✓ | ✓ | ✓ | ✓ | ✓ | ✓ | ✓ | ✓ | r | ✓ | ✓ | ✓ | ✓ | ✓ | ✓ | ✓ |
| 2 | Lena | ✓? | ✓ | ✓? | ✓? | ✓? | ✓ | s? | s? | ✓ | ✓ | ✓ | ✓ | ✓ | ✓ | ✓ | ✓ |
| 3 | McKenzie | ✓ | ✓ | ✓ | ✓ | ✓ | ✓ | ✓ | | ✓ | s | ✓ | ✓ | s | ✓ | ✓ | ✓ |
| 4 | Murray–Darling | N | N | | ✓ | ✓ | | ✓ | | r | ✓ | ✓ | ✓ | ✓ | ✓ | ✓ | ✓ |
| 5 | Amur | N | N | ✓ | | ✓ | r? | ✓ | ✓ | ✓ | ✓ | ✓ | | ✓ | | s | ✓ |
| 6 | Niger | | | | | | | ✓ | ✓ | f | f | f | ✓ | f | ✓ | ✓ | ✓ |
| 7 | Yangtze | | | | | | ✓ | ✓ | ✓ | | ✓ | ✓ | ✓ | | ✓ | ✓ | ✓ |
| 8 | Huang Ho | | | | | | ✓ | ✓ | ✓ | | ✓ | ✓ | ✓ | ✓ | ✓ | ✓ | ✓ |
| 9 | Uruguay | | | | | | s | | s | ✓ | s | ✓ | ✓ | f | ✓ | ✓ | ✓ |
| 10 | Zambezi | ✓ | s | | | | | | ✓ | ✓ | s | ✓ | ✓ | ✓ | ✓ | ✓ | ✓ |
| 11 | Congo | r | r | r | r | S | S | ✓ | r | r | r | r | r | ✓ | | r | r |
| 12 | Amazon | N | r | r | r | r | r | r | r | r | r | r | ✓ | f | ✓ | r | r |
| 13 | Mekong | s | s | ✓ | s | s | | s | s | s | s | s | s | s | | | s |
| 14 | Mississippi | ✓ | ✓ | s | s | s | s | s | s | s | E | f | f | f | ✓ | f | f |
| 15 | Yenisey | s | | | | f | f | | ✓ | ✓ | ✓ | | | ✓ | ✓ | ✓ | ✓ |
| 16 | Ob-Irtysh | s | s | | | s | f | | | ✓? | ✓? | | | | | | |
| 17 | Volga | s | f | f | f | f | f | | | | | | | | s | ✓? | ✓ |
| 18 | Rio Grande | | | | | s | f | f | f | f | f | f | f | f | s | f | f |
| 19 | Syr-Darya | s | | | | | f | f | f | f | f | f | f | f | | | |
| 20 | Yukon | | | | | | | ✓ | | | | | | | | | |
| A | Orinoco | ✓ | ✓ | ✓ | f | f | f | f | ✓ | ✓ | ✓ | ✓ | ✓ | f | ✓ | f | ✓ |
| B | Patagonian | ✓ | ✓ | ✓ | ✓ | | | | | | ✓ | | | | | f | ✓ |
| C | Senegal | ✓ | ✓ | ✓ | | | | ✓ | ✓ | ✓ | ✓ | ✓ | ✓ | ✓ | ✓ | ✓ | ✓ |
| D | Arabian | ✓ | ✓ | ✓ | ✓ | ✓ | ✓ | ✓ | ✓ | ✓ | ✓ | ✓ | ✓ | ✓ | | ✓ | ✓ |
| E | Lamu | ✓ | ✓ | ✓ | ✓ | ✓ | ✓ | ✓ | ✓ | ✓ | ✓ | ✓ | ✓ | ✓ | ✓ | ✓ | ✓ |
| F | Trans-Saharan | | ✓ | ✓ | ✓ | ✓ | ✓ | ✓ | ✓ | ✓ | ✓ | ✓ | ✓ | ✓ | ✓ | ✓ | ✓ |
| G | Australis | | | | | ✓ | ✓ | | | | | | | | | | |
| H | Namib | | | | | | ✓ | ✓ | ✓ | | ✓ | ✓ | ✓ | ✓ | ✓ | | |
| I | Trans-Hudson | N | W | N | E | N | E | N | W | W | W | f | f | f | f | E | E |
| J | Trans-Asian | S | S | S | S | | | | | | | | | | | | |
| K | Trans-Indian | N | | N | N | | | | | | | | | | | | |
| L | Trans-Europe | W | | S | S | | | | | | | | | | S | S | S |
| M | Trans-Siberian | W | W | W | W | W | W | W | W | W | W | W | W | W | W | W | W |
| N | Trans-Antarctic | | W | N | E | E | W | W | W | W | W | E | W | | W | | |
| O | Austral–Antarctic | | | | | | | | N | N | | | | | | | |
| P | Greenland | | | | | S | S | N | N | N | N | E | E | E | N | N | N |

The numbered rivers have modern counterparts. The lettered rivers only existed in the Cretaceous. ✓, Cretaceous river; r, flowing in reverse direction; f, flooded; s, shorter length; N, E, S and W indicate the river flow direction.

The following major modern rivers were not present in the Cretaceous: Amu, Brahmaputra, Colorado, Columbia, Danube, Ganges, Indus, Loire, Paraguay = Uruguay, Parana, Rhine, Rhone, Syr and Tigres–Euphrates.

clockwise gyres occupied the Central Atlantic and western Tethys from the Aptian (115 Ma) until the Campanian (75 Ma).

In the southern hemisphere, a strong current flowed south along the east coast of Africa and then flowed west to east along the Indo-Australian

margin of Gondwana (Figs 86 & 87). This current intensified during the Barremian (125 Ma: Fig. 88) due to the opening of the Somali Basin. A strong, warm, eastward-flowing current remained a dominant feature along the Indo-Australian margin of Gondwana until the Cenomanian–Turonian (95–

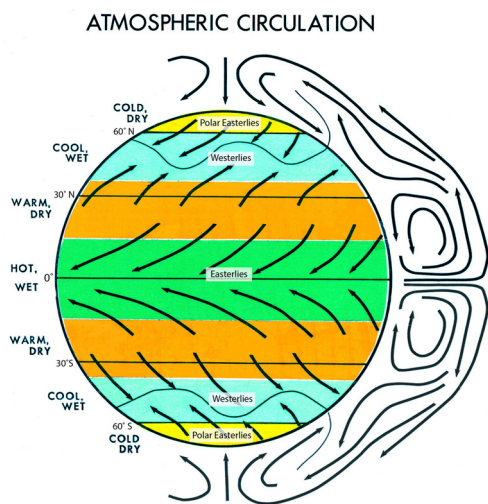


Fig. 84. Modern surface winds.

90 Ma), when cooler waters began to flow into southern Tethys from high southerly latitudes (Weddell Sea) as a result of the growing separation of India and Australia.

There were several other notable ocean currents and circulation changes during the Cretaceous. Throughout most of the Cretaceous (125–75 Ma), there was a well-organized, clockwise rotating gyre in the enclosed Arctic Ocean. During the Coniacian (90–85 Ma), the South Atlantic had grown large enough to sustain a stable, counter-clockwise gyre. The widening proto-Caribbean Sea permitted a

through-going connection between the Central Atlantic and the eastern Pacific Ocean from the late Aptian (115 Ma) through to the latest Cretaceous. And, finally, by the late Maastrichtian, India had moved far enough north to begin to block the westward-flowing Equatorial Current. Oceanic circulation is a very dynamic feature. It is recommended that the reader view the animation of ocean circulation provided in the [Supplementary material](#). The [Supplementary material](#) also contain simulations of oceanic circulation for every stage of the Cretaceous.

Palaeoclimate during the Cretaceous

Introduction

The Cretaceous climate has been a popular research topic over the past 50 years. Some of these studies have focused on changes in global temperature and associated OAEs. Other research has modelled the Cretaceous transition to a more angiosperm-dominated flora and its effect on terrestrial ecosystems. Additional Cretaceous climate research has been the abundance of floral evidence for warm temperatures in polar regions (Spicer *et al.* 1994; Herman and Spicer 1996; Bice *et al.* 2003). In addition, there have been numerous computer simulations of Cretaceous palaeoclimate. Excellent reviews of these topics can be found in Parrish (1998), Huber *et al.* (2000), Skelton (2003), Bice *et al.* (2002) and Summerhayes (2015). In this section we consider the Cretaceous climate in the broader context of Mesozoic climate change, chronologically review climatic events during the

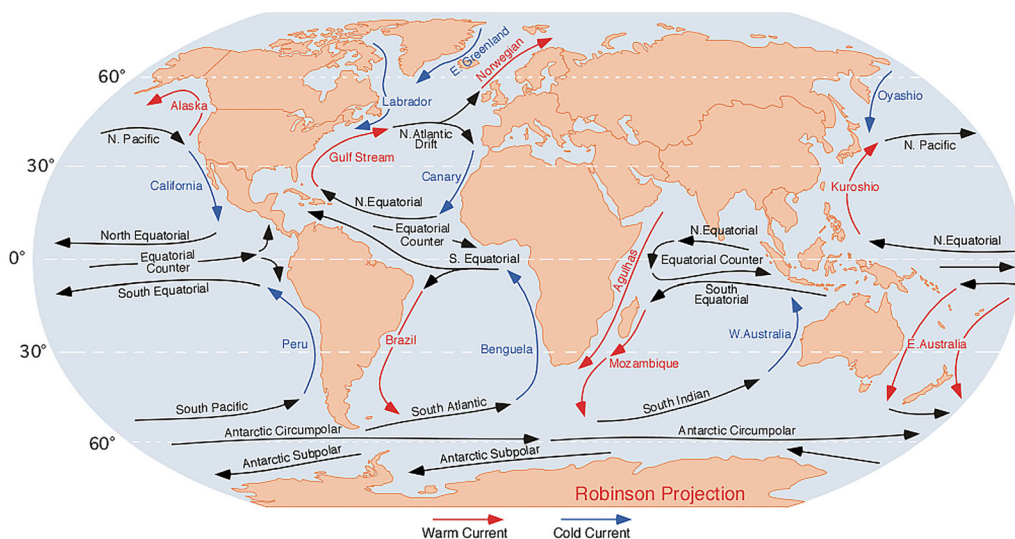


Fig. 85. Modern surface oceanic circulation. Source: https://en.wikipedia.org/wiki/Ocean_current

The Cretaceous world

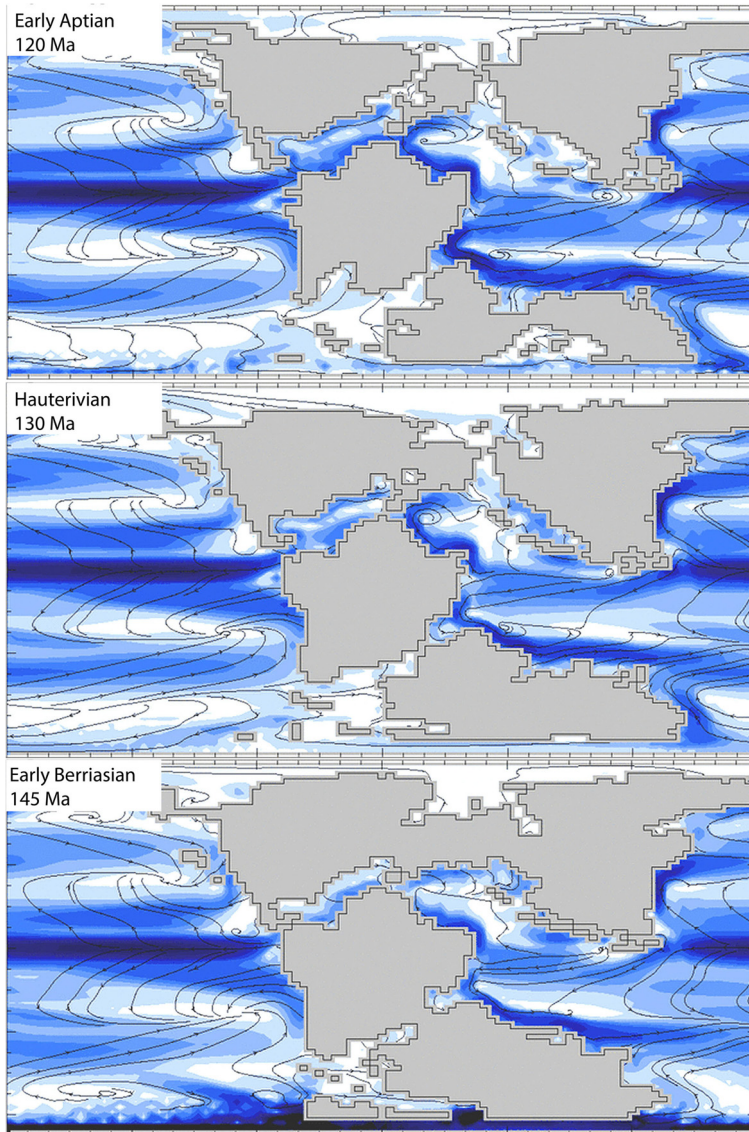


Fig. 86. Oceanic circulation at 145, 130 and 120 Ma; see [Figure 3c](#) for the legend. Source: [Valdes *et al.* \(2021\)](#).

Cretaceous and review the changing patterns of regional precipitation.

For an overview of climate change during the Cretaceous, the reader is referred to the set of Cretaceous palaeo-Köppen maps ([Figs 89–97](#)) from [Burgener *et al.* \(2023\)](#). These maps are the first comprehensive description of the changing extent of the Warm Wet Tropical belt, the Dry Arid belt, the Warm Temperate belt and the Cool Temperate belt during the Cretaceous based entirely on geological, geochemical and palaeontological proxy data. All of the palaeoclimate nomenclature used in this

review is summarized in [Table 12](#). In addition, the reader is referred to the palaeoclimatic reconstructions, digital datasets and animations illustrating the temperature, precipitation and ocean circulation for each stage of the Cretaceous in the [Supplementary material](#).

Cretaceous climate in the context of Mesozoic climate change

Two extreme climatic events bracket the Mesozoic Era. The Permo-Triassic Thermal Maximum

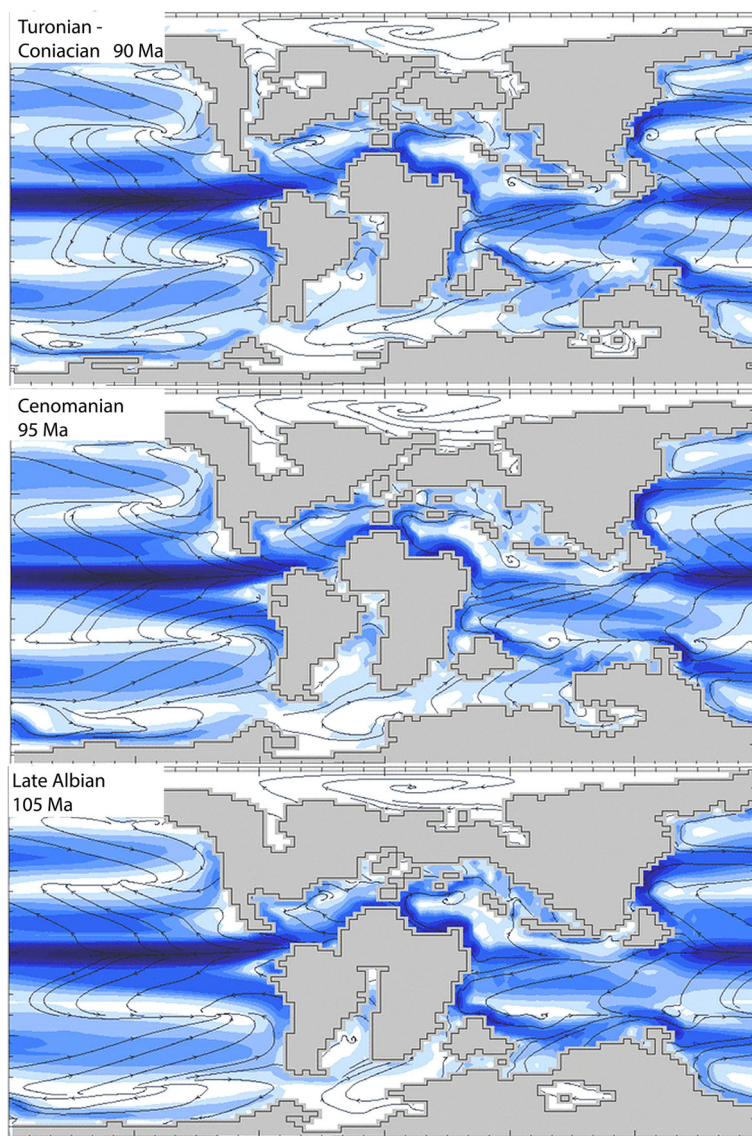


Fig. 87. Oceanic circulation at 105, 95 and 90 Ma, see [Figure 3c](#) for the legend. Source: [Valdes *et al.* \(2021\)](#).

(PTTM: global average temperature (GAT) = *c.* 33°C) and the resulting Permo-Triassic Extinction Event (PTEE: 251 Ma) ([Wignall 2001, 2015](#); [Song and Scotese 2023](#)) define the start of the Mesozoic Era. The End Cretaceous Extinction (ECT, 66.1 Ma: GAT = *c.* 10°C) punctuates the end of the Era. Literally times of ‘Fire and Ice’, these two extreme palaeoclimatic events could not have been more different. The PTTM was caused by massive volcanic eruptions that released an unprecedented amount of CO₂ into the atmosphere, producing torrid, global

temperatures (>40°C in the Tropics), whereas the ECE was the result of a bolide impact (Chicxulub) that plunged the world into a frigid ‘impact winter’ that collapsed the marine and terrestrial ecosystems, killing-off ammonites, large marine reptiles and the dinosaurs; setting the stage for the rise of the mammals. [Table 13](#) lists some of the key sources that describe in detail these eventful times.

[Figure 98](#) illustrates how the GAT changed during the Mesozoic. The Mesozoic lasted for 186 Myr and can be divided into eight pairs of

The Cretaceous world

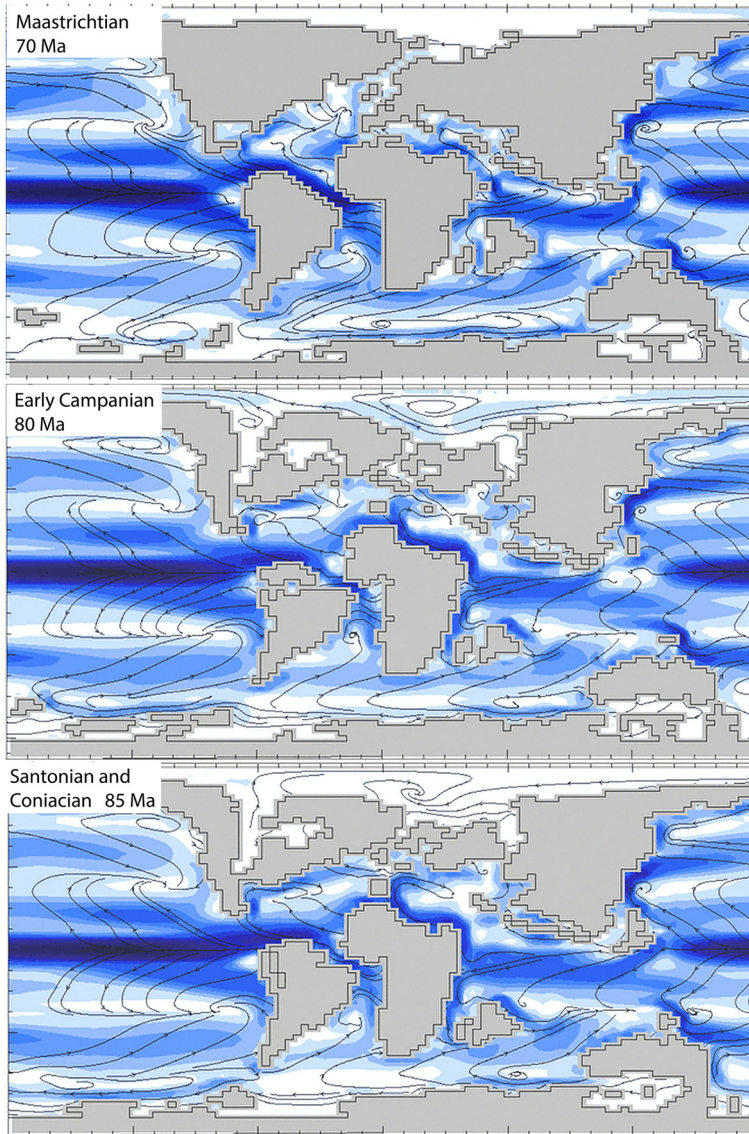


Fig. 88. Oceanic circulation at 85, 80 and 70 Ma, see [Figure 3c](#) for the legend. Source: [Valdes *et al.* \(2021\)](#).

relatively cooler (C) or warmer (W) intervals (chronotemps Mz_{01} – Mz_{08} : [Scotese *et al.* 2021](#)). The early part of the Triassic was the warmest part of the Mesozoic with a GAT of 29°C (chronotemp MzW_{01} : [Table 12](#)). The Jurassic was more equable. It started out relatively cool (GAT = 20°C, chronotemp MzC_{04}), warmed up a bit during the Early Toarcian Thermal Maximum (GAT = 24°C, chronotemp MzW_{05}), and then cooled down at the end of the Jurassic and through the first half of the Early Cretaceous (Late Jurassic – Early Cretaceous

Cool Interval, chronotemp MzC_{06} , 150–125 Ma, GAT = *c.* 20°C).

It should be noted that, with the exception of the end-Cretaceous impact winter, Mesozoic GATs never dipped below 18°C, although this limit was closely approached during the earliest Cretaceous. Permanent polar ice caps can only form if the GAT is less than 18°C. Above that temperature, during the summer months, the average annual temperature of the polar regions (>67° N and S) is warm enough to melt any accumulation of winter snow and ice.

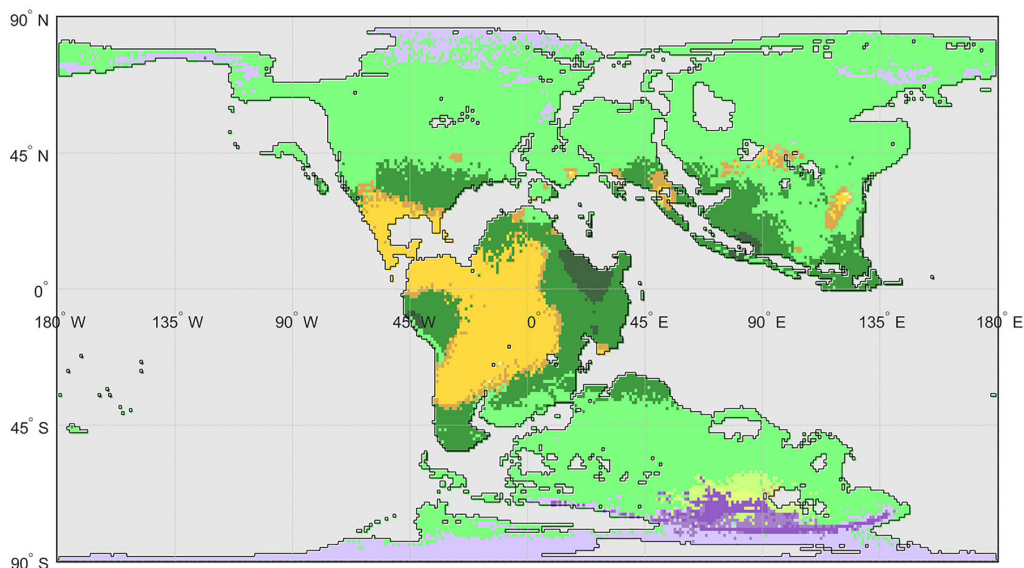


Fig. 89. Palaeo-Köppen map for the earliest Cretaceous (145 Ma), see [Figure 2c](#) for the legend. Source: from [Burgener *et al.* \(2023\)](#).

Only when the average global temperature is below 18°C can snow and ice remain year-round, promoting the growth of large, polar ice caps. A transition zone exists when the GAT ranges between 18°C and 22°C. Snow and ice will be present during the winter months and patches of permanent ice may develop close to the pole or at relatively high

elevations (>500 m). When the GATs are greater than 24°C, even the winter months will be devoid of snow and ice.

[Figure 99](#) (see also [Figure 100](#)) illustrates both the changing global temperature during the last 540 Myr and the associated change in the pole-to-equator temperature gradient. With a quick

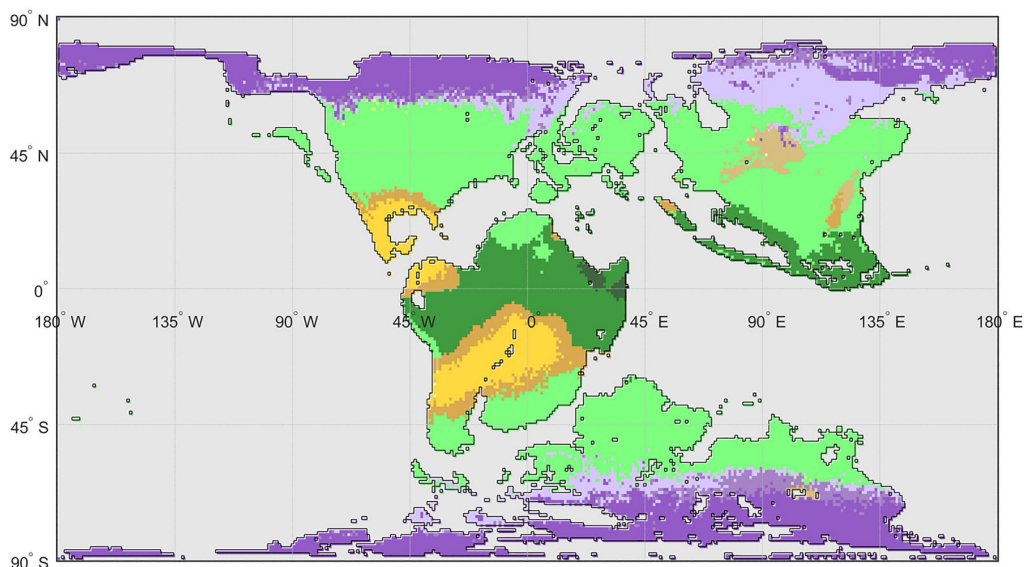


Fig. 90. Palaeo-Köppen map for the Early Cretaceous (Hauterivian, 130 Ma), see [Figure 2c](#) for the legend. Source: from [Burgener *et al.* \(2023\)](#).

The Cretaceous world

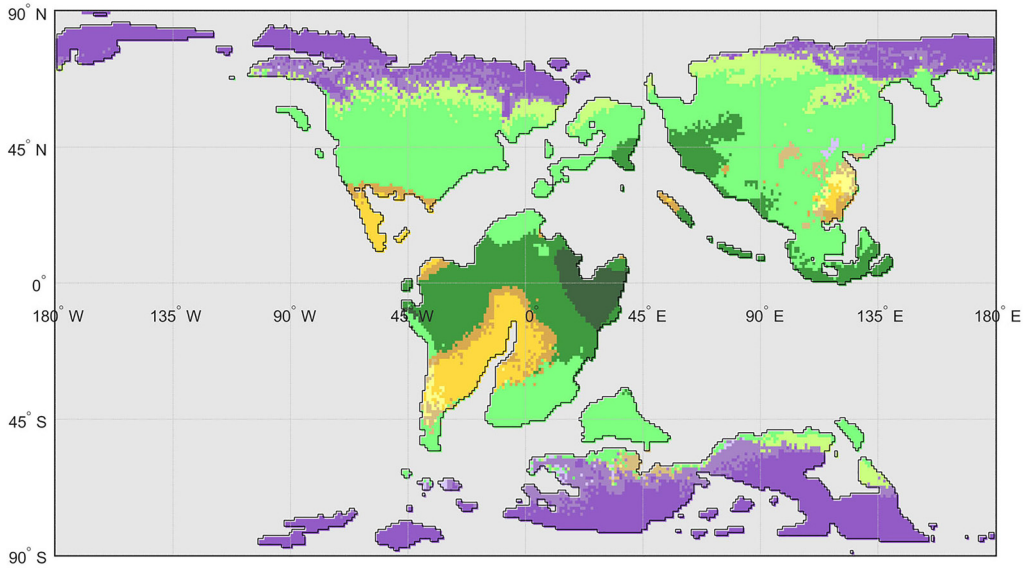


Fig. 91. Palaeo-Köppen map for the Early Cretaceous (Aptian, 120 Ma), see [Figure 2c](#) for the legend. Source: from [Burgener *et al.* \(2023\)](#).

scan of this figure, one can see how global temperature warmed and cooled during the Cretaceous and how temperature varied between the pole and the Equator. The impact winter at the end of the Cretaceous especially stands out.

The pole-to-equator temperature gradient provides an excellent snapshot of the global climate and provides key insights into regional climatic patterns. [Figures 101–109](#) plot pole-to-equator temperature diagrams for nine time intervals during the

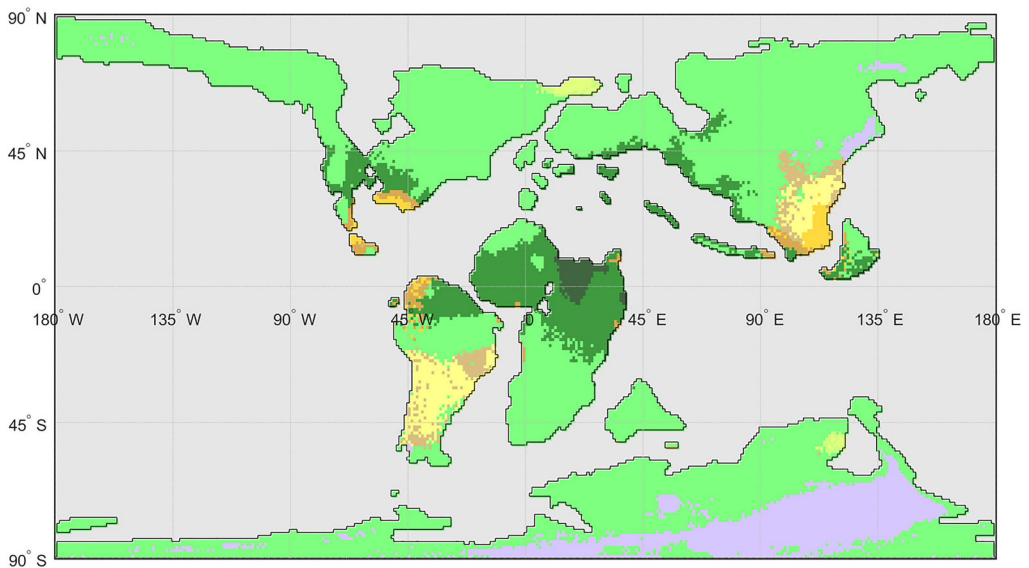


Fig. 92. Palaeo-Köppen map for the Early Cretaceous (Albian, 105 Ma), see [Figure 2c](#) for the legend. Source: from [Burgener *et al.* \(2023\)](#).

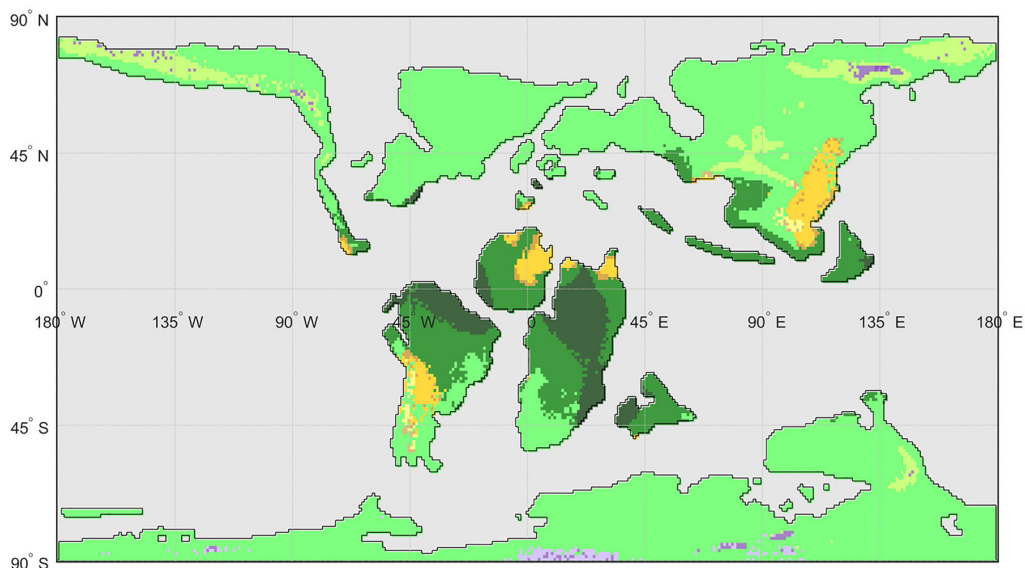


Fig. 93. Palaeo-Köppen map for the mid-Cretaceous (Cenomanian, 95 Ma), see [Figure 2c](#) for the legend. Source: from [Burgener *et al.* \(2023\)](#).

Cretaceous. These time intervals correspond to the Köppen maps in [Figures 89–97](#) ([Burgener *et al.* 2023](#)). Each pole-to-equator diagram is accompanied by a map that illustrates palaeotemperatures ([Figs 101–109](#)) ([Scotese *et al.* 2021](#)). From the pole-to-equator diagrams one can derive the GAT,

the tropical temperature, the polar temperature, the latitudinal temperature gradient, the equatorward limit of permanent ice and the temperature of the deep sea ([Scotese *et al.* 2021](#)). Pole-to-equator diagrams for each stage of the Cretaceous are provided in the [Supplementary material](#).

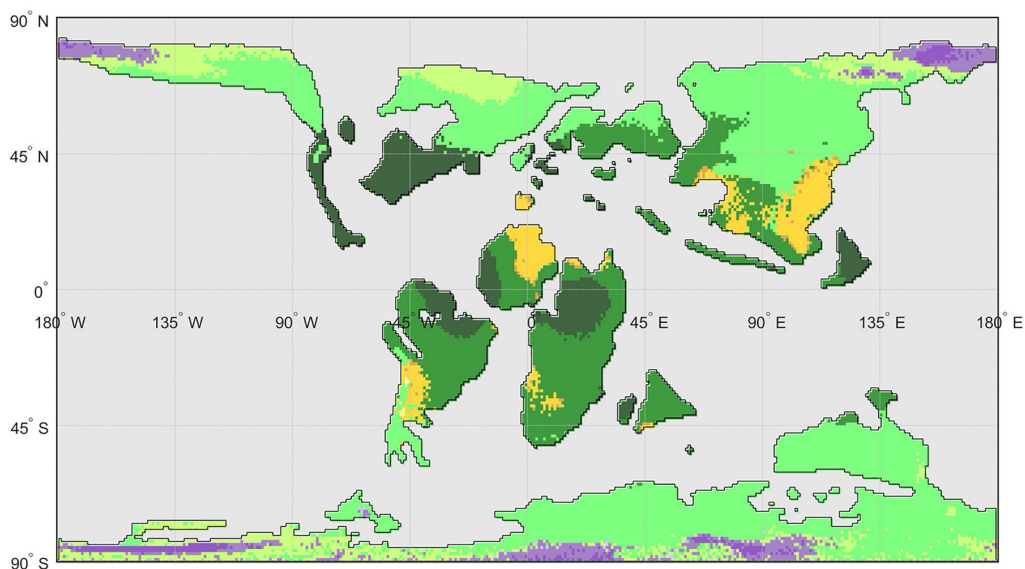


Fig. 94. Palaeo-Köppen map for the mid-Cretaceous (Turonian, 90 Ma); see [Figure 2c](#) for the legend. Source: from [Burgener *et al.* \(2023\)](#).

The Cretaceous world

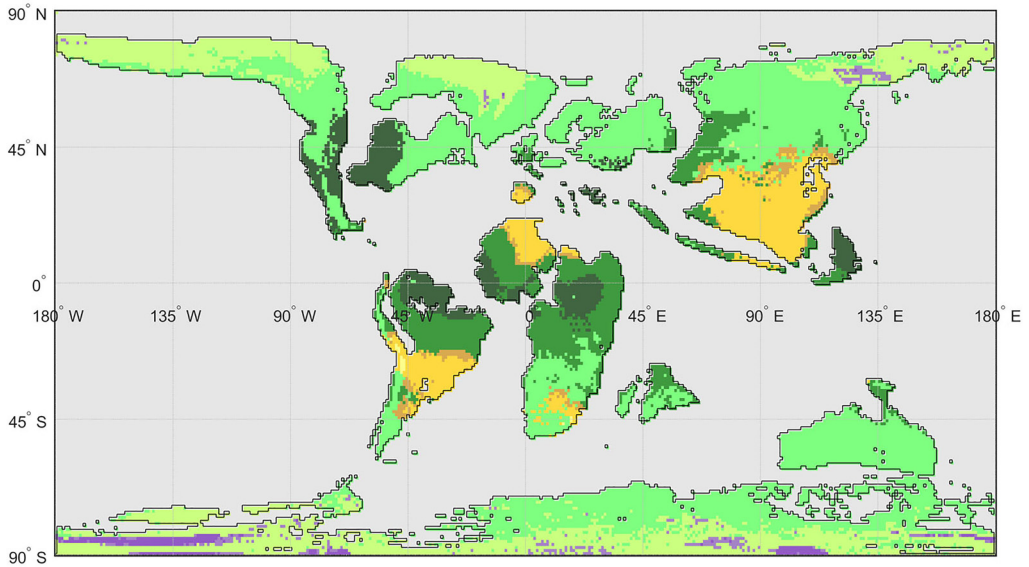


Fig. 95. Palaeo-Köppen map for the Late Cretaceous (Santonian–Coniacian, 85 Ma), see [Figure 2c](#) for the legend. Source: from [Burgener et al. \(2023\)](#).

Chronological review of climate during the Cretaceous

Overview. [Figure 100](#) illustrates the changing tropical temperatures (red line, [Scotese et al. 2021](#); orange dashed line, [Grossman and Joachimski 2022](#)), global average temperatures (GATs: black

line), deep ocean temperatures (blue line) and polar temperatures (light blue line) from the Late Jurassic to the late Eocene ([Scotese et al. 2021](#)). A cool global climate persisted from the Late Jurassic into the Early Cretaceous ([Scotese et al. 2021](#); [Frakes 1999](#)). Both polar regions had cold winters, with snow and ice, and only a small (India-sized)

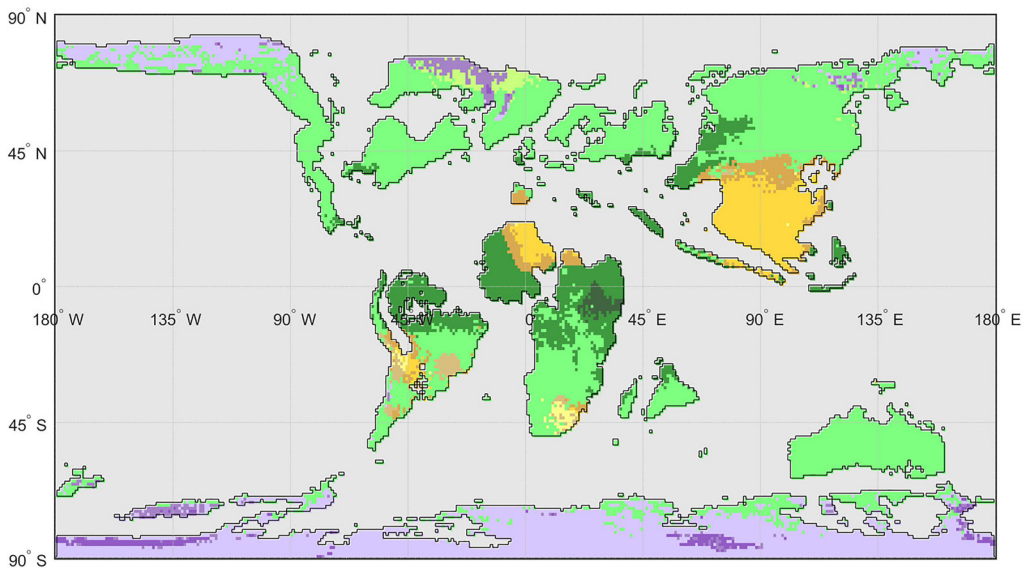


Fig. 96. Palaeo-Köppen map for the Late Cretaceous (Campanian, 80 Ma), see [Figure 2c](#) for the legend. Source: from [Burgener et al. \(2023\)](#).

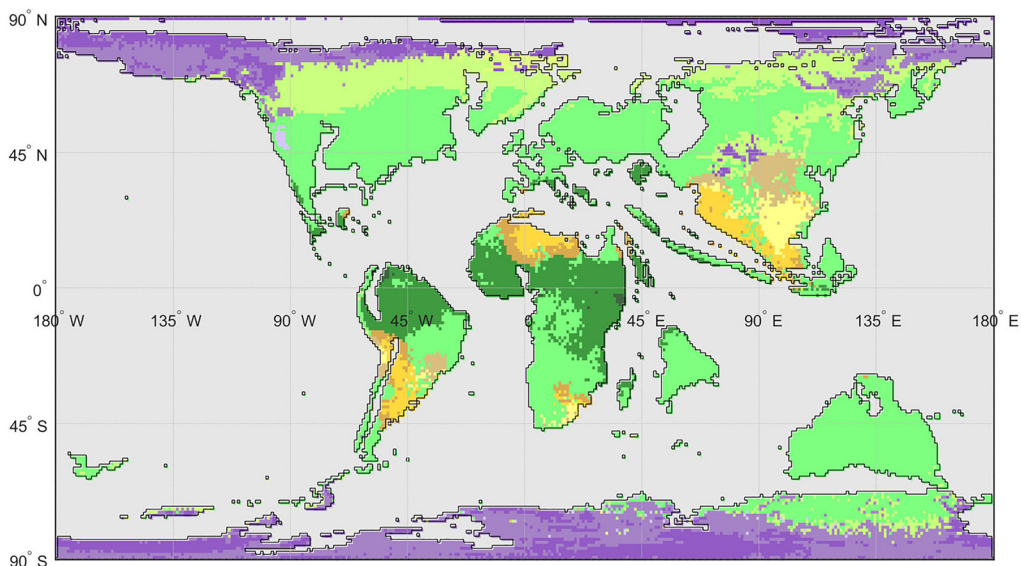


Fig. 97. Palaeo-Köppen map for the Late Cretaceous (Maastrichtian, 70 Ma), see [Figure 2c](#) for the legend. Source: from [Burgener *et al.* \(2023\)](#).

ephemeral ice cap at the South Pole ([Figs 49–52](#)). The climate warmed during the Albian (c. 110 Ma) and reached a high point for the Cretaceous during the Cenomanian–Turonian Thermal Maximum (94 Ma) ([Huber 2012](#)). At that time, the GAT (c. 28°C) was nearly double the modern temperature; tropical temperatures exceeded 40°C along the Equator during the summer months. During the Cenomanian–Turonian, it would have been difficult for large terrestrial animals, like dinosaurs, or shallow-marine fauna to have survived these extremely warm (i.e. lethal >40°C) temperatures. You could have fried an egg on a Cenomanian–Turonian rocky pavement. The global climate cooled significantly during the Late Cretaceous ([Mansour and Wagreich 2021](#)), receiving a ‘coup de grace’ with the arrival of the Chicxulub bolide (66 Ma). The subsequent impact winter caused global temperatures to fall briefly to ice age levels (10–13°C). For more information regarding the climatic events described in the following text, the reader is referred to [Table 12](#).

Early Cretaceous climate. The Kimmeridgian Warm Interval (MzW₀₆, 160–150 Ma) was followed by a long interval characterized by cool, but not frigid, temperatures (Tithonian–early Barremian Cool Interval, MzC₀₆, 150–126 Ma). The Tithonian–early Barremian Cool Interval was punctuated by isolated warm events – the Weissert (136 Ma) and Faraoni (131 Ma) thermal excursions.

The global climate during the earliest Cretaceous (Berriasian–Barremian) can be characterized as

something in between a hothouse and an icehouse ([Frakes *et al.* 1992](#)). The average global temperature was about 17°C. This was 5°C warmer than the Late Cenozoic Icehouse (12°C) but 7–9°C cooler than the mid-Cretaceous–Paleogene Hothouse (MCPH) (MzW₀₈ and CzW₀₁). Evidence for more temperate climatic conditions is based on the occurrence of dropstones, glendonites and a few tillites (pebbly mudstones) ([Boucot *et al.* 2013](#), [Rogov *et al.* 2023](#)) at polar latitudes that co-occur with evidence of temperate forests (coal and plant fossils) and dinosaurs. Dropstones of Early Cretaceous age (Berriasian–Barremian) are widespread in South Australia, Queensland, New South Wales and the Northern Territory of Australia ([Boucot *et al.* 2013](#)). Glendonites occur in South Australia and New South Wales. In the northern hemisphere, there are dropstones in Siberia and Svalbard, as well as glendonites in northern Siberia, Svalbard and the Arctic islands ([Frakes and Francis 1988, 1990](#); [Francis and Frakes 1993](#); [Frakes *et al.* 1995](#); [De Lurio and Frakes 1999](#); [Braswell 2009](#); [Grasby *et al.* 2017](#); [Vickers *et al.* 2019](#)).

The best interpretation for this mixture of cool and warm climatic indicators is that it was cold enough in the winters for lakes and rivers to freeze over. Snow covered the ground and there were glaciers at higher elevations and possibly a small ice cap (<4 × 10⁶ km²; India sized) at the South Pole. In the summer months it was warm enough at high latitudes to support the growth of lush vegetation and an influx of dinosaurs migrating in from warmer regions.

Table 12. Mesozoic palaeotemperature timescale: chronotemps Mz01–Mz08 (Scotese *et al.* 2021; ICS Time Scale v1026/04)

| Climate mode | Chronotemp | Tropical (°C) | Polar (°C) | Global average (°C) | Name | Abbr. | Start Age | End Age | Start Stage | End Stage | Also known as* | Bolide impacts | Large Igneous Provinces | Key references |
|---|-------------|------------------|---------------|---------------------------|---|--------|--------------|------------|-------------------------|-------------------------|--------------------------------------|---------------------|----------------------------|---|
| Mid Cretaceous– Paleogene | CzW01–MzW07 | 28.7 | 7.1 | 22.6 | Mid-Cretaceous– Paleogene Hothouse | MKPH | 128 | 39.4 | Early Barremian | Middle Bartonian | | | | 19, 84, 85, 89, 101 |
| Hothouse | CzW01 | 29.4 | 8.1 | 23.4 | Paleocene–Eocene Hothouse | PEH | 59 | 39.4 | Earliest Thanetian | Middle Bartonian | | | NAIP 62– 54 Ma | 45–49, 60, 65 |
| CzW01–MzW07 39.4–128 Ma $\Delta T = 88.6$ | CzW01.1 | 29.4 | 6.9 | 23.1 | Middle Eocene Thermal Maximum | METM | 41 | 40.5 | Earliest Bartonian | Early Bartonian | MECO | | | 45–49, 60, 65 |
| | CzW01.2 | 29.4 | 6.9 | 23.1 | Late Lutetian Thermal Maximum | LLTM | 41.5 | 41.5 | Latest Lutetian | Latest Lutetian | | | | 65 |
| | CzW01.3 | 27.8 | 4.7 | 21.4 | Middle–Late Eocene Cooling | MLEC | 48.5 | 34 | Late Ypresian | Latest Priabonian | | | | 45–47, 49, 60 |
| | CzW01.4 | 30.8 | 9.6 | 24.8 | <i>Azolla</i> Cool Event | ACE | 48.5 | 48.5 | Late Ypresian | Late Ypresian | | | | 49 |
| | CzW01.5 | 31.1 | 10.1 | 25.2 | Early–Middle Eocene Warm Interval | EMEWI | 56 | 46 | Earliest Ypresian | Early Lutetian | | Montagnais 51 Ma | | 45–47, 49, 60, 65 |
| | CzW01.6 | 31.1 | 10.1 | 25.1 | Early Eocene Thermal Maximum | EETM | 54 | 49 | Middle Ypresian | Late Ypresian | EECO | | | 45–49, 60, 65 |
| | CzW01.7 | 30.9 | 10.3 | 25.0 | Early Eocene Thermal Event 3 | EETE3 | 53 | 53 | Middle Ypresian | Middle Ypresian | ETM3, X-event | | | 45–47, 49, 60, 65 |
| | CzW01.8 | 30.1 | 9.6 | 24.3 | Early Eocene Thermal Event 2 | EETE2 | 54 | 54 | Early Ypresian | Early Ypresian | ETM2, ELMO | | | 45–47, 49, 60, 65 |
| | CzW01.9 | 31.0 | 10.7 | 25.2 | Paleocene–Eocene Thermal Maximum | PETM | 55.6 | 55.6 | Earliest Ypresian | Earliest Ypresian | Paleocene/Eocene_OAE, MDE | | | 45–49, 60, 61–65 |
| | CzW01.10 | 28.0 | 7.9 | 22.3 | Thanetian Thermal Event | TTE | 59 | 59 | Earliest Thanetian | Earliest Thanetian | ELPE, PCIM peak, MPBE | | | 45, 46, 49, 60, 65 |
| | MzC08 | 27.3 | 7.1 | 21.6 | Late Cretaceous - Early Paleocene Cool Interval | LKEPCI | 82 | 59 | Early Campanian | Earliest Thanetian | | Kara 70 Ma | | 19, 20, 30, 32, 36, 44–46, 50, 51, 60 |
| | MzC08.1 | 27.6 | 7.6 | 21.9 | Late Danian Cooling | LDC | 63 | 62 | Late Danian | Latest Danian | LDE, top C27N | Manson 74 Ma | | 45, 46, 65 |
| | MzC08.2 | 29.8 | 9.9 | 24.1 | KT Impact Thermal Excursion | KTITX | 66 | 65 | Latest Maastrichtian | Earliest Danian | DAN-C2 | | | 44–46, 49, 65, 67 |
| | MzC08.3 | 21.4 | 1.4 | 15.7 | KT Impact Winter | KTIW | 66 | 66 | Latest Maastrichtian | Latest Maastrichtian | KT Extinction. K-Pg Extinction | Chicxulub 66 Ma | Deccan 66– 65 Ma | 44, 55–59, 65 |

(Continued)

Table 12. *Continued.*

| Climate mode | Chronotemp | Tropical (°C) | Polar (°C) | Global average (°C) | Name | Abbr. | Start Age | End Age | Start Stage | End Stage | Also known as* | Bolide impacts | Large Igneous Provinces | Key references |
|--------------|------------|------------------|---------------|---------------------------|--|-------|--------------|------------|------------------------|------------------------|------------------|--------------------|----------------------------|--------------------------------------|
| | MzW08 | 30.3 | 8.8 | 24.2 | Mid-Cretaceous Hothouse | MKH | 111 | 82 | Early Albian | Early Campanian | | | | 19, 29, 30, 32, 52–54 |
| | MzW08.1 | 32.6 | 11.9 | 26.7 | Coniacian Thermal Maximum | OAE3 | 87 | 87 | Latest Coniacian | Latest Coniacian | OAE3 | | | 35, 36, 44 |
| | MzW08.2 | 34.2 | 13.0 | 28.2 | Cenomanian–Turonian Thermal Maximum | OAE2 | 94 | 93 | Latest Cenomanian | Earliest Turonian | OAE2 (Bonarelli) | | Madagascar 93–91 Ma | 19, 29, 30, 32 |
| | MzW08.3 | 29.6 | 7.5 | 23.3 | Breistroffer Thermal Maximum | OAE1d | 101 | 100 | Latest Albian | Latest Albian | OAE1d | | Naturaliste 100– 99 Ma | 45 |
| | MzW08.4 | 28.1 | 6.0 | 21.9 | Event 6 Thermal Event | EV6 | 102.5 | 102.5 | Late Albian | Late Albian | | | | 45 |
| | MzW08.5 | 27.5 | 5.4 | 21.3 | Petite Verol Thermal Event | PVTE | 105 | 105 | Late Albian | Late Albian | | | | 45 |
| | MzW08.6 | 27.2 | 5.0 | 20.9 | Amadeus Thermal Maximum | OAE1c | 106 | 106 | Late Albian | Late Albian | OAE1c, Jassines | | | 45 |
| | MzW08.7 | 27.2 | 4.9 | 20.9 | l'Arboudeyesse Thermal Event | ATE | 109 | 109 | Middle Albian | Middle Albian | | | | 45 |
| | MzW08.9 | 27.4 | 5.1 | 21.1 | Leenhardt Thermal Event | LTE | 110 | 110 | Middle Albian | Middle Albian | | | | 45 |
| | MzW08.10 | 27.3 | 4.8 | 20.9 | Paquier/Urbino Thermal Maximum | OAE1b | 111 | 111 | Early middle Albian | Early middle Albian | OAE1b | | | 45 |
| | MzC07 | 27.3 | 3.8 | 20.7 | Aptian–Albian Cold Snap | AACS | 118 | 111 | Late Aptian | Early Albian | | Carswell 115 Ma | | 28, 58, 62–71, 73, 75, 77, 78, 83 |
| | MzC07.1 | 25.9 | 3.0 | 19.5 | Killion Thermal Event | KTE | 113 | 113 | Earliest Albian | Earliest Albian | | | | 45 |
| | MzC07.2 | 25.9 | 2.8 | 19.4 | Jacob Cool Event | JCE | 114 | 114 | Late Aptian | Late Aptian | | | | 45 |
| | MzW07 | 29.5 | 3.1 | 22.2 | Barremian–Aptian Warm Interval | BAWI | 128 | 118 | Early Barremian | Early late Aptian | | | Kerguelen 120– 118 Ma | 6, 19, 23, 27, 29, 33, 48 |
| | MzW07.1 | 30.8 | 4.7 | 23.6 | Fallot Thermal Event | FTE | 119 | 119 | Late middle Aptian | Late middle Aptian | | | Ontong Java 121–119 Ma | 45 |
| | MzW07.2 | 30.7 | 4.0 | 23.4 | Noir Thermal Event | NTE | 122.5 | 122.5 | Middle Aptian | Middle Aptian | | | South Africa 125–118 Ma | 45 |
| | MzW07.3 | 30.2 | 3.5 | 22.8 | NN1 Thermal Event | NN1 | 123 | 123 | Early middle Aptian | Early middle Aptian | | | | 45 |
| | MzW07.4 | 28.8 | 2.2 | 21.5 | Selli/Goguel Thermal Maximum | OAE1a | 124 | 125.5 | Earliest Aptian | Earliest Aptian | OAE1a | | | 45 |
| | MzW07.5 | 26.8 | 0.7 | 19.6 | Hauptblatterton Thermal Event | HTE | 128 | 128 | Early Barremian | Early Barremian | | | | |

(Continued)

Table 12. *Continued.*

| Climate mode | Chronotemp | Tropical (°C) | Polar (°C) | Global average (°C) | Name | Abbr. | Start Age | End Age | Start Stage | End Stage | Also known as* | Bolide impacts | Large Igneous Provinces | Key references |
|---|------------|------------------|---------------|---------------------------|--|-------|--------------|------------|------------------------|-----------------------|---------------------------|---|------------------------------------|--|
| Jurassic–Early Cretaceous Cool Interval | C7-C9 | 27.7 | 3.5 | 21.0 | Late Jurassic–Early Cretaceous Cool Interval | JKCI | 199 | 128 | Latest Hettangian | Early Barremian | | | | |
| MzC04–MzC06 199–128 Ma $\Delta T = 71$ | MzC06 | 26.5 | 1.3 | 19.5 | Tithonian–early Barremian Cool Interval | TEBCI | 150 | 128 | Early Tithonian | Early Barremian | | Tookoonooka 128 Ma | | 6, 7, 10, 19, 25, 27, 28, 66 |
| | MzC06.1 | 29.0 | 3.3 | 21.9 | Faraoni Thermal Excursion | FTX | 131 | 131 | Middle Hauterivian | Middle Hauterivian | | Mjølneri 142 Ma Morokweng 145 Ma | Parana– Entendeka 131–129 Ma | 45 |
| | MzC06.2 | 25.7 | 0.2 | 18.6 | Weissert Thermal Excursion | WTX | 136 | 136 | Middle Valanginian | Middle Valanginian | | | | 45 |
| | MzC06.3 | 26.6 | 2.1 | 19.8 | Early Tithonian Cooling | ETC | 150 | 149 | Early Tithonian | Middle Tithonian | | | | |
| | MzW06 | 27.4 | 3.3 | 20.6 | Kimmeridgian Warm Interval | KWI | 164 | 150 | Earliest Oxfordian | Early Tithonian | Kimmeridgian Anoxic Event | | | 6–8, 10, 11, 19, 22, 27, 28, 34, 37 |
| | MzW06.1 | 27.2 | 3.0 | 20.5 | Early Tithonian Cool Event | ETCE | 152 | 152 | Early Tithonian | Early Tithonian | D-m | | | |
| | MzW06.2 | 28.9 | 5.0 | 22.2 | Latest Oxfordian Thermal Maximum | LOTM | 158 | 157 | Late Oxfordian | Latest Oxfordian | D-l | | | 10, |
| | MzW06.3 | 26.0 | 2.1 | 19.3 | Middle Oxfordian Cooling | MOC | 161 | 158 | Middle Oxfordian | Late Oxfordian | D-k | | | |
| | MzW06.4 | 27.5 | 3.1 | 21 | Late Callovian - early Oxfordian Warming | COW | 164 | 161 | Late Callovian | Early Oxfordian | D-j | | | |
| | MzC05 | 28.9 | 4.2 | 22.0 | Middle Jurassic Cool Interval | MJCI | 174 | 164 | Earliest Aalenian | Earliest Oxfordian | | Puchezh– Katunki 167 Ma | | 6–10, 21, 22, 25– 28, 34, 37, 40– 43 |
| | MzC05.1 | 26.1 | 2.1 | 19.4 | Callovian Cool Event | CCE | 166 | 164 | Early Callovian | Late Callovian | D-i | | | 6, 7, 10 |
| | MzC05.2 | 29.5 | 5.0 | 22.7 | Late Bathonian Warming | LBW | 167 | 166 | Late Bathonian | Latest Bathonian | D-h | | | 10, |
| | MzC05.3 | 29.7 | 5.1 | 22.9 | Late Toarcian - Bajocian Cooling | LTBC | 178 | 168 | Late Toarcian | Late Bajocian | D-e,f,g | | | 6, 7, 10 |
| | MzW05 | 30.0 | 5.2 | 23.1 | Toarcian Warm Interval | TWI | 183 | 174 | Early Toarcian | Latest Toarcian | D-c,d | | Karoo–Ferrar 183–181 Ma | 7, 10, 25, 64 |
| | MzW05.1 | | | | Early Toarcian Thermal Maximum | ETTM | 183 | 180 | Early Toarcian | Late Toarcian | Toarcian_OAE,D-c | | | 6, 10 |
| | MzC04 | 27.5 | 4.9 | 21.2 | Early Jurassic Cool Interval | EJCI | 199 | 183 | Earliest Sinemurian | Late Pliensbachian | D-a,b | | | 6, 7, 10 |

(Continued)

Table 12. *Continued.*

| Climate mode | Chronotemp | Tropical (°C) | Polar (°C) | Global average (°C) | Name | Abbr. | Start Age | End Age | Start Stage | End Stage | Also known as* | Bolide impacts | Large Igneous Provinces | Key references |
|-------------------------------|---------------|------------------|---------------|---------------------------|---|-------|--------------|------------|----------------------|---------------------|--|---------------------|----------------------------|---------------------|
| Triassic Hothouse | MzW01 - MZW04 | 31.1 | 9.0 | 24.9 | Triassic Hothouse | TH | 253 | 199 | Latest Changhsingian | Latest Hettangian | | | | |
| MZW04 | MzW04 | 29.7 | 7.2 | 23.4 | End Triassic Thermal Event | ETTE | 201 | 199 | Latest Rhaetian | Earliest Hettangian | Triassic/Jurassic_OAE, ETE | | CAMP 201–199 Ma | 6, 7, 10 |
| 253–199 Ma $\Delta T = 54$ | MzW04.1 | 30.4 | 8.0 | 24.1 | Central Atlantic Magmatic Province (CAMP) | CAMP | 200 | 200 | Latest Rhaetian | Latest Rhaetian | | | | 6, 7, 10 |
| | MzC03 | 28.4 | 6.1 | 22.1 | Rhaetian Cool Interval | RCI | 209 | 201 | Earliest Rhaetian | Late Rhaetian | | | | 12 |
| | MzW03 | 31.6 | 8.7 | 25.2 | Late Norian Warm Interval | LNWI | 217 | 209 | Middle Norian | Late Norian | R-Tr11 | Manicouagan 214 Ma | | 1, 12 |
| | MzW03.1 | 32.0 | 8.5 | 25.5 | Manicouagan Cool Excursion | MCX | 214 | 214 | Middle Norian | Middle Norian | | | | |
| | MzC02 | 29.7 | 8.2 | 23.6 | Early Norian Cool Interval | ENCI | 227 | 217 | Earliest Norian | Middle Norian | | Saint Martin 220 Ma | | 12, 18 |
| | MzW02 | 30.3 | 8.8 | 24.2 | Mid-Carnian Warm Interval | MCWI | 234 | 227 | Middle Carnian | Latest Carnian | R-Tr10 | | Wrangellia LIP 230 Ma | 1, 12–18 |
| | MzW02.1 | 30.8 | 9.4 | 24.7 | Carnian Pluvial Episode | CPE | 233 | 230 | Middle Carnian | Middle Carnian | NCIE 1–4 | | | 1, 12–18 |
| | MzC01 | 31.0 | 9.3 | 24.8 | Ladinian-Carnian Cooling | LCC | 242 | 234 | Earliest Ladinian | Middle Carnian | R-Tr8–9; Ladinian Humid Interval | | | 12, 14–18 |
| | MzW01 | 34.9 | 12.3 | 28.6 | Early Triassic Extreme Hothouse | ETEH | 253 | 242 | Latest Changhsingian | Latest Anisian | Early Triassic OAE, R-Tr1–7 | | | 1, 4, 5, 12, 13, 18 |
| | MzW01.1 | 34.7 | 12.5 | 28.4 | Latest Olenekian Cooling | LOC | 248 | 247 | Latest Olenekian | Latest Olenekian | Pelsonian Humid Interval | | | 5 |
| | MzW01.2 | 39.0 | 16.7 | 32.7 | Latest Smithian Thermal Maximum | LSTM | 250 | 250 | Late Smithian | Latest Smithian | R-Tr4 | | | 1, 4, 5, 12 |
| | MzW01.3 | 35.8 | 12.5 | 29.2 | Dienerian Cooling | DC | 251 | 250 | Late Griesbachian | Late Smithian | | | | 4, 5, 12 |
| | MzW01.4 | 36.2 | 13.5 | 29.8 | Permo-Triassic Thermal Maximum | PTTM | 253 | 246 | Latest Changhsingian | Early Anisian | R-P8, R-Tr1–3, Permo-Triassic Extinction | | Siberian Traps 252–251 Ma | 1–5 |

Abbreviations: MECO, Middle Eocene Climatic Optimum; ETM, Eocene Thermal Maximum; OAE, Oceanic Anoxic Event; MDE, Middle Danian Event; LDE, Late Danian Event; DAN, Danaina; KT, Cretaceous–Tertiary; K-Pg, Cretaceous–Paleogene; D-a–D-m, Dera *et al.* (2011); ETE, End Triassic Event; R-Tr1–Tr11 = Retallack (2013); NCIE, Norian Carbon Isotope Excursion.

Key References: (1) Retallack (2013); (2) Chen *et al.* (2013); (3) Henderson *et al.* (2012); (4) Retallack *et al.* (2011); (5) Sun *et al.* (2012); (6) Podlaha *et al.* (1998); (7) Jenkyns *et al.* (2002); (8) Malchus and Steuber (2002); (9) Weirzbowski and Joachimski (2007); (10) Dera *et al.* (2011); (11) Vickers *et al.* (2019); (12) Trotter *et al.* (2015); (13) Preto *et al.* (2010); (14) Sun *et al.* (2016); (15) Rigo and Joachimski (2010); (16) Miller *et al.* (2017); (17) Dal Corso *et al.* (2018a, b); (18) Bernardi *et al.* (2018); (19) O'Brien *et al.* (2017); (21) Alsenz *et al.* (2013); (22) Brassell (2009); (23) Erba *et al.* (2015); (24) De Lurio and Frakes (1999); (25) Frakes and Francis (1988); (26) Grasby *et al.* (2017); (27) Vickers *et al.* (2019); (28) Erba *et al.* (2004); (29) Herrle *et al.* (2015); (30) Barral *et al.* (2017); (32) Farnsworth *et al.* (2019); (33) Mutterlose *et al.* (2009); (34) Jenkyns *et al.* (2012); (35) Navarro-Ramirez *et al.* (2017); (36) Ladant and Donnadiu (2016); (37) McArthur *et al.* (2007); (38) Pirrie *et al.* (1995); (39) Pirrie *et al.* (2004); (40) Price (1999); (41) Price and Mutterlose (2004); (42) Price and Nunn (2010); (43) Price and Passey (2013); (44) Puc  at *et al.* (2003); (45) Ogg *et al.* (2016); (46) Vandenberghe *et al.* (2012); (47) Miller *et al.* (2020); (48) Gasson and Kiessling (2020); (49) King (2016); (50) Upchurch *et al.* (1999); (51) Upchurch *et al.* (2015); (52) Kiehl and Shields (2013); (53) Kump and Pollard (2008); (54) Hay *et al.* 2019; (55) Vellekoop *et al.* (2014, 2016); (56) Li and Keller (1998); (57) Wilf *et al.* (2003); (58) Punekar *et al.* (2014); (59) Petersen *et al.* (2016); (60) Zachos *et al.* (2001, 2008); (61) Rea *et al.* (1990); (62) Kennett and Stott (1991); (63) McInerney and Wing (2011); (64) Zeebe *et al.* (2009); (65) Westerhold *et al.* (2020); (66) Alley and Frakes (2003); (67) Wilf *et al.* (2003).

The Cretaceous world

Table 13. Permo-Triassic Extinction and end-Cretaceous Extinction resources

| Events | Year | Author | Title |
|----------|------|---|---|
| PTr | 2023 | Song and Scotese | The end-Paleozoic Great Warming |
| PTr | 2015 | Cui and Kump | Global warming and the end-Permian extinction event: Proxy and modeling perspectives |
| PTr | 2015 | Wignall | The Worst of Times: How Life on Earth Survived Eighty Million Years of Extinctions |
| KPg | 2014 | Wilson, Clemens, Horner, and Hartman (editors) | Through the End of the Cretaceous in the Type Locality of the Hell Creek Formation in Montana and Adjacent Areas |
| KPg, PTr | 2013 | MacLeod | The Great Extinctions: What Causes Them and How They Shape Life |
| KPg | 2012 | Hart, Yancey, Leighton, Miller, Liu, Smart, and Twitchett | The Cretaceous–Paleogene boundary on the Brazos River, Texas: New stratigraphic sections and revised interpretations |
| PTr | 2009 | Sengör and Atayman | The Permian Extinction and Tethys: An Exercise in Global Geology |
| KPg | 2008 | Nichols and Johnson | Plants and the K-T Boundary |
| PTr | 2006 | Erwin | Extinction: How Life on Earth Nearly Ended 250 Million Years Ago |
| KPg, PTr | 2004 | Hallam | Catastrophes and Lesser Calamities |
| PTr | 2004 | Ward | Gorgon: Paleontology, Obsession, and the Greatest Catastrophe in Earth's History |
| PTr | 2003 | Benton | When Life Nearly Died: The Greatest Mass Extinction of All Time |
| Future | 2003 | Ward and Brownlee | The Life and Death of Planet Earth |
| KPg | 2002 | Hartman, Johnson and Nichols (editors) | The Hell Creek Formation and the Cretaceous–Tertiary Boundary in the Northern Great Plains: An Integrated Continental Record of the End of the Cretaceous |
| KPg, PTr | 1999 | Courtillot | Evolutionary Catastrophes: The Science of Mass Extinction |
| KPg | 1998 | Powell | Night Comes to the Cretaceous: Comets, Craters, Controversy, and the Last Days of the Dinosaurs |
| KPg, PTr | 1997 | Hallam and Wignall | Mass Extinctions and their Aftermath |
| KPg, PTr | 1997 | Hart | Biotic Recovery from Mass Extinctions |
| KPg | 1996 | Officer and Page | The Great Dinosaur Extinction |
| KPg | 1996 | Archibald | Dinosaur Extinction and the End of an Era |
| KPg | 1995 | Carlisle | Dinosaurs, Diamonds, and Things from Outer Space: The Great Extinction |
| PTr | 1993 | Erwin | The Great Paleozoic Crisis: Life and Death in the Permian |
| KPg, PTr | 1991 | Raup | Extinction: Bad Genes or Bad Luck? |
| KPg, PTr | 1990 | Kauffman and Walliser (editors) | Extinction Events in Earth History |
| KPg, PTr | 1989 | Donovan (editor) | Mass Extinctions: Processes and Evidence |
| KPg, PTr | 1987 | Stanley | Extinction |
| KPg | 1986 | Raup | The Nemesis Affair: A Story of the Death of Dinosaurs and the Ways of Science |
| KPg | 1986 | Hsü | The Great Dying: Cosmic Catastrophe, Dinosaurs, and the Theory of Evolution |
| KPg, PTr | 1984 | Berggren and Van Couvering (editors) | Catastrophes and Earth History: The New Uniformitariansim |
| KPg, PTr | 1984 | Nitecki (editor) | Extinctions |
| KPg | 1983 | Allaby and Lovelock | The Great Extinction: What killed the dinosaurs and devastated the Earth? |

KPg, Cretaceous-Paleogene Extinction; PTr, Permo-Triassic Extinction.

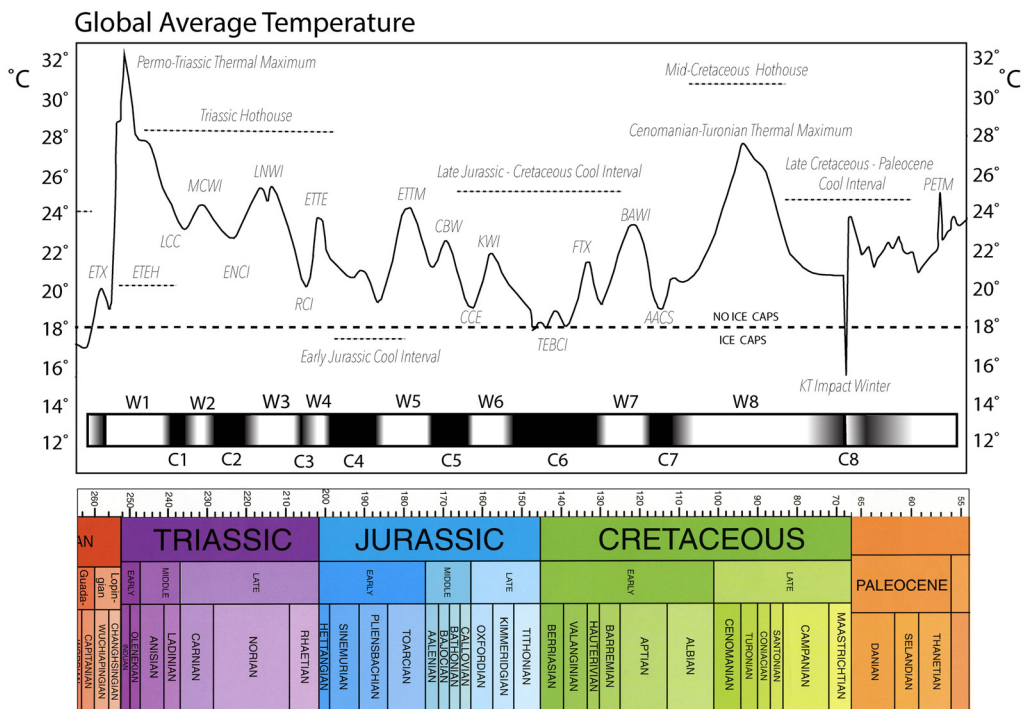


Fig. 98. Global average temperature (GAT) during the Mesozoic: white, warmer intervals (W₁₋₈); black, cooler intervals (C₁₋₈); dashed black line, temperature cutoff for large, permanent polar ice caps. Refer to Table 12 for more information about each chronotemp. Source: Scotese *et al.* (2021); the timescale is from the International Chronostratigraphic Chart v2020/01.

It is interesting to note that the Kimmeridgian Anoxic Event (Jenkyns *et al.* 2012) is the only potential oceanic anoxic event for the time interval spanning the Middle Jurassic (Aalenian, 174 Ma) to the Early Cretaceous (Barremian, 128 Ma). It does not appear to be as widespread as the

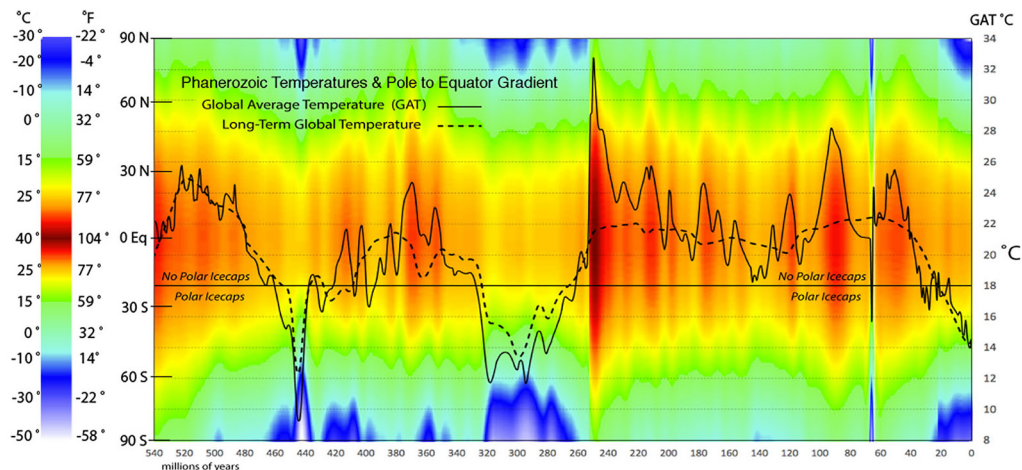


Fig. 99. Phanerozoic heat map. Colours indicate the pole-to-equator temperature gradient; the dotted line is the 40 Myr running average. The blue shading indicates polar ice caps. Source: Scotese *et al.* (2021).

The Cretaceous world

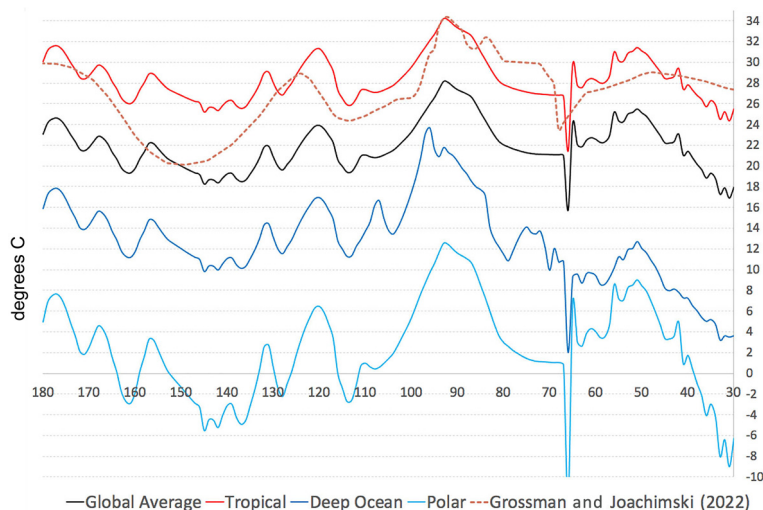


Fig. 100. Tropical, global average, deep ocean and polar temperatures during the Cretaceous. Source: after Scotese *et al.* (2021) and Grossman and Joachimski (2022).

Cretaceous OAEs. The lack of anoxic basins during the earliest Cretaceous seems quite unusual in light of the fact that there were many restricted marine basins that would have been ideal habitats for anoxia to develop. The lack of OAEs may have been due to the fact that the oceanic bottom waters during the Middle and Late Jurassic through to the earliest Cretaceous were relatively well oxygenated. The occurrence of glendonites at high latitudes during much of the Early Cretaceous indicates that cool, oxygen-rich bottom waters were being generated at polar latitudes, preventing the bottom waters in lower latitudes from becoming anoxic.

Mid–Late Cretaceous–Paleogene Hothouse (128–39.4 Ma). If one imagines where the current phase of anthropogenic global warming is heading, one immediately thinks of the hothouse worlds of the Late Cretaceous and Eocene (Huber 1998; Huber *et al.* 2000). During the MCPH, global temperatures were indeed much warmer than the present day (GAT = 28°C during the Late Cretaceous v. GAT = 15°C for the present day). It remains to be seen whether we will succeed in warming the Earth to that degree but at least we now know what a warmer world would look like.

The MCPH is one of the best-documented palaeotemperature intervals. Table 12 lists some of the key references for this time interval and summarizes their primary conclusions regarding regional and global temperatures. The best single source for information about the Cretaceous portion of this hothouse interval is the O'Brien *et al.* (2017) summary of sea surface temperatures (SSTs)

based on oxygen isotope and TEX₈₆ temperature estimates. The TEX₈₆ technique uses the lipid chemistry of the cell membrane of a common group of pelagic protokaryotes (Thaumarchaeota) to estimate temperatures (Schouten *et al.* 2002, 2003, 2007). The palaeotemperatures are derived by measuring the ratio of key lipids (crenarchaeols). It has been noted that TEX₈₆ temperature estimates tend to be c. 50% higher than $\delta^{18}\text{O}$ temperature estimates (O'Brien *et al.* 2017) (Fig. 8). It seems likely that at mid–high latitudes the unusually high temperatures recorded by TEX₈₆ do not represent annual average SSTs but, rather, may be capturing the warmest monthly temperatures (Bijl *et al.* 2009; Burgener *et al.* 2023).

It is notable that approximately 90% of the available TEX₈₆ palaeotemperature estimates for the Cretaceous have been obtained from samples that are Aptian or younger in age. There are very few $\delta^{18}\text{O}$ temperature estimates for times older than the mid-Albian (O'Brien *et al.* 2017). Fortunately, as noted earlier, geological evidence (glendonites, dropstones and rare tillites) from the Early Cretaceous helps to fill in these data gaps.

The MCPH began in the latest Barremian–earliest Aptian (c. 128 Ma) with two thermal events: the Hauptplatterton Thermal Event (Mutterlose *et al.* 2009) and the oldest Cretaceous oceanic anoxic event, OAE1a, the Selli/Goguel Thermal Maximum (W7.4: Erba *et al.* 2015; Herrle *et al.* 2015; O'Brien *et al.* 2017). This warm interval (MzW07; 128–118 Ma) was followed by a cooler period during the late Aptian–early Albian (MzC07, 116–108 Ma, GAT = 19°C), which preceded the rapid

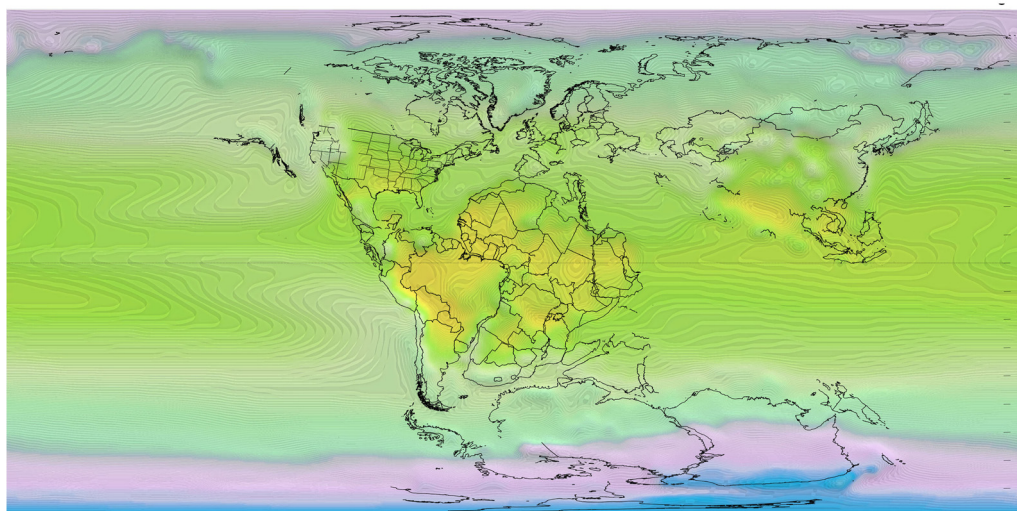
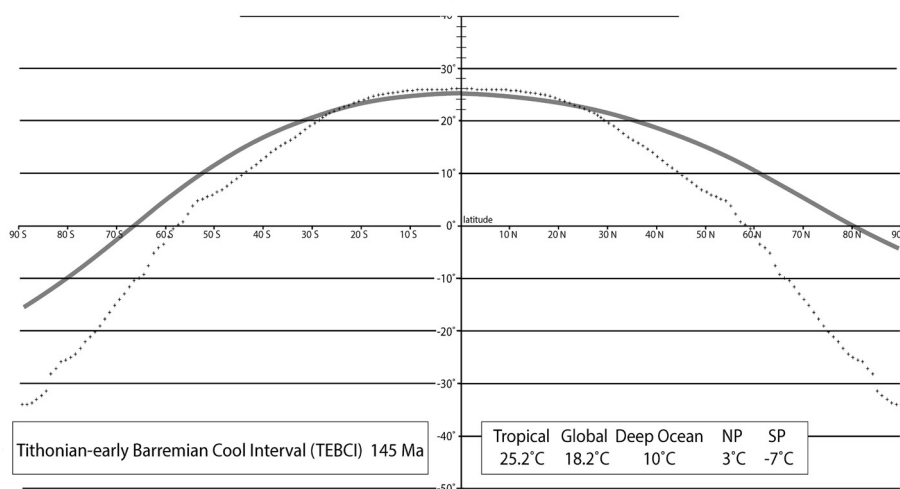


Fig. 101. Cretaceous pole-to-equator temperature gradient and global temperatures (Jurassic–Cretaceous boundary, 145 Ma), see Figure 2a for the legend.

ramping up to a thermal maximum during the latest Cenomanian–earliest Turonian (MzW08, 94–93 Ma, GAT = 28°C). According to O’Brien *et al.* (2017), temperatures cooled gradually during the remainder of the Late Cretaceous, reaching a minimum of *c.* 21°C in the late Maastrichtian, just prior to the Cretaceous–Tertiary (K–T) impact event.

The average global temperature during the MCPH was *c.* 23°C. Surface waters in the Cool Temperate regions (SST = 21–23°C) were only slightly cooler than the superheated tropical seas (29°C: O’Brien *et al.* 2017). Oceanic bottom waters were also much warmer than the present day (9–17°C: Valdes *et al.* 2021; Friedrich *et al.* 2011).

Cretaceous oceanic anoxic events (OAEs). The Selli/Goguel Thermal Maximum (OAE1a) is one of nearly a dozen potential thermal spikes that characterize this time interval (see Table 12). The nature and origin of these OAEs has been much debated (Schlanger and Jenkyns 1976; Arthur and Sageman 1994; Meyer and Kump 2008). Previous notions that OAEs were simply the result of rapid rises in sea level (Arthur and Sageman 1994) or due to the stagnation of the ocean basins caused by thermohaline density stratification (Brass *et al.* 1982) have fallen out of favour. There are two current schools of thought. The first argues that the OAEs were unusual, synchronous, global events. According to this argument, catastrophic tectonic

The Cretaceous world

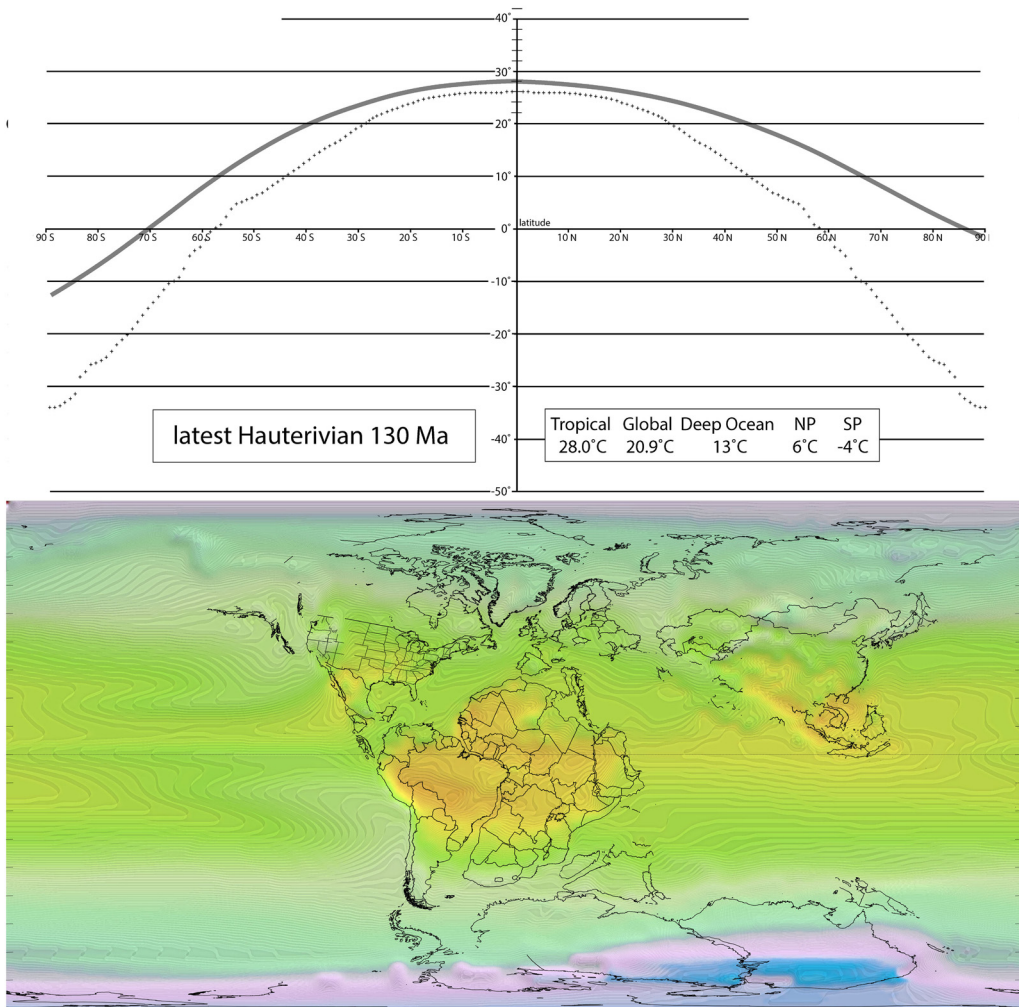


Fig. 102. Cretaceous pole-to-equator temperature gradient and global temperatures (Hauterivian, 130 Ma), see Figure 2a for the legend.

events triggered unusual atmospheric, biological, geochemical and oceanographic conditions that promoted extensive deep-water anoxia which resulted in the formation of carbon-rich black shales (total organic carbon (TOC) often >30%). Proponents of this school of thought argue that the following scenario may explain the widespread occurrence of the carbon-rich black shales associated with the early Aptian Selli/Goguel Thermal Maximum (OAE1a):

- The eruption of the mid-Cretaceous superplume (Larson 1991a, b; Larson and Erba 1999) radically changed atmospheric and oceanic chemistry;
- greenhouse gases from the erupting lavas (i.e. CO₂) warmed the Earth;
- increased warmth accelerated chemical weathering on land; consequently, a greater flux of nutrients was carried to the oceans;
- land-derived nutrients, together with a higher concentration of bio-limiting metals made available by increased hydrothermal activity associated with the extensive submarine eruptions (Duncan and Huard 1997; Jones and Jenkyns 2001), promoted greater marine productivity, resulting in more carbon deposition;
- the increased productivity depleted the available supply of oxygen in the water column, which led to basin-wide anoxic or dysoxic conditions;
- water-column anoxia, in turn, favoured the preservation of carbon by inhibiting bacterial decay and carbon recycling; and

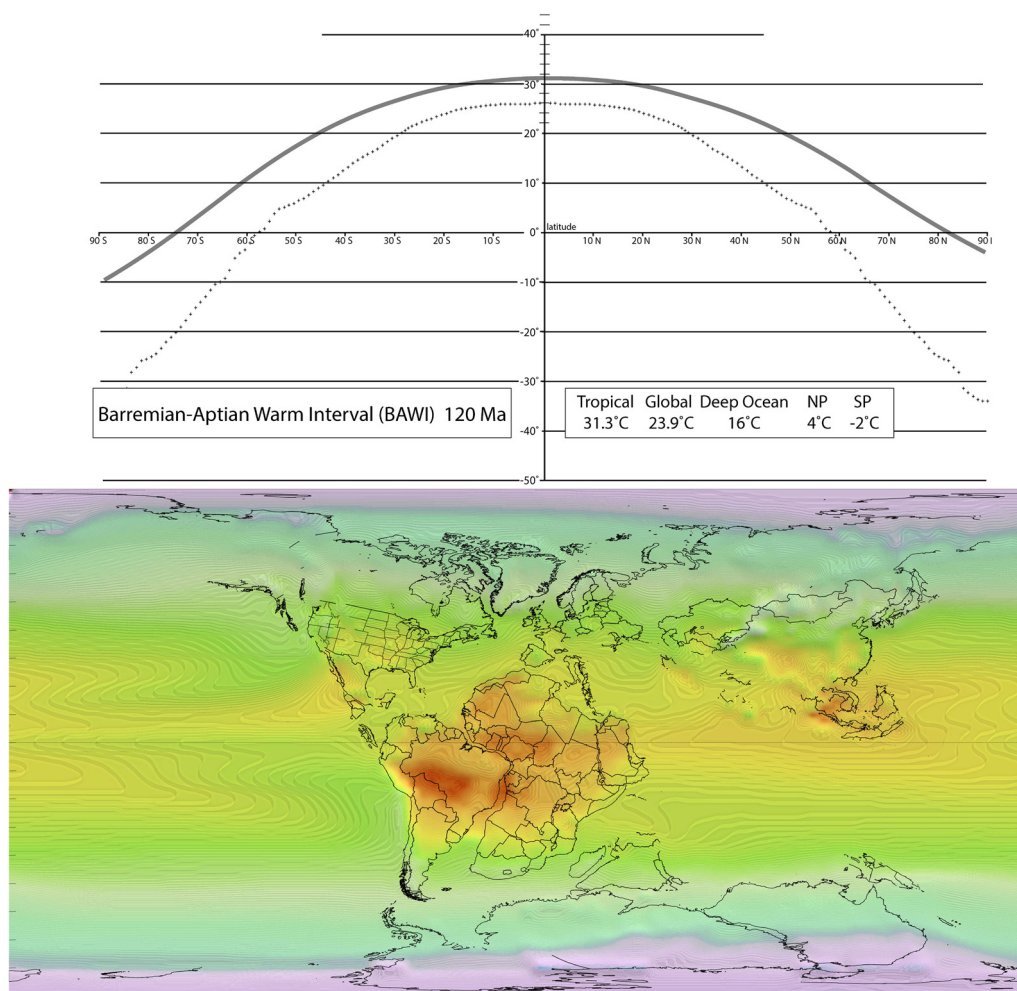


Fig. 103. Cretaceous pole-to-equator temperature gradient and global temperatures (early Aptian, 120 Ma), see Figure 2a for the legend.

- the results were widespread carbon-rich black shales (Demailson and Moore 1980)

A second school of thought argues that the OAEs do not represent unusual or catastrophic global events but, rather, represent business as usual. In other words, a certain constellation of biological, geochemical, tectonic, atmospheric and oceanographic conditions (e.g. Milankovitch cycles) favoured the development of local, basin-wide anoxia. The Cretaceous was unusual only in the sense that this constellation of favourable conditions was more likely to occur than might have been expected. In essence, the palaeogeography of the Aptian–Albian (and Cenomanian–Turonian) was especially favourable for plankton blooms

and high stratified sluggish oceans that resulted in anoxic basins and promoted nutrient trapping (Meyer and Kump 2008).

Each hypothesis may hold part of the answer. Each hypothesis may explain different aspects of the Earth system processes that produce oceanic anoxic events. The catastrophic hypothesis may be the best explanation for the rare, but truly global, mega-OAE events (i.e. Selli/Goguel Thermal Maximum (OAE1a) and Cenomanian–Turonian Thermal Maximum (OAE2)), whereas the uniformitarian hypothesis may be a better explanation for the more frequent, regional and less intense OAEs (OAE1b, OAE1c, OAE1d and OAE3).

The problem of cold polar regions during the Cretaceous. The Aptian–Albian Cold Snap

The Cretaceous world

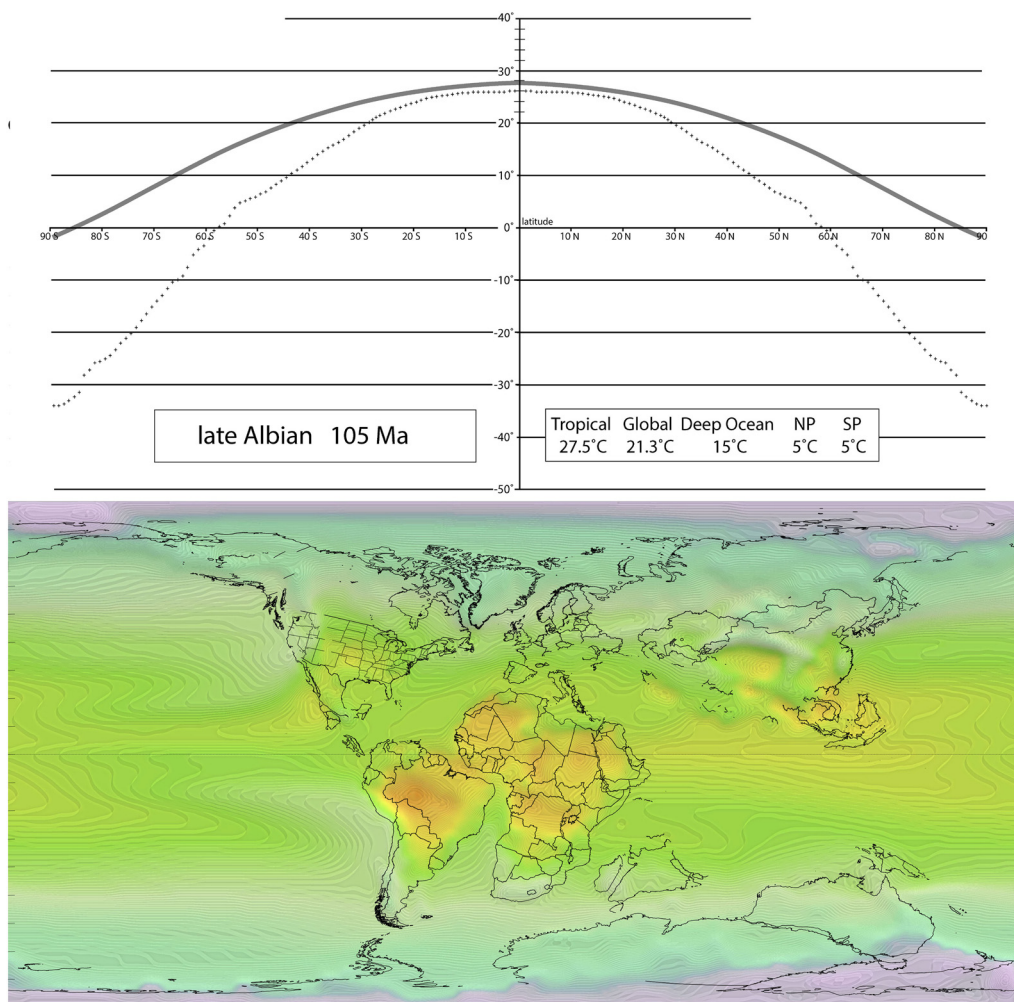


Fig. 104. Cretaceous pole-to-equator temperature gradient and global temperatures (middle Albian, 105 Ma), see Figure 2a for the legend.

(MzC07, 116–109 Ma) separates the Selli/Goguel Thermal Maximum (OAE1a) from the remaining Late Cretaceous OAEs. For a brief interval in the late Aptian and early Albian, the global climate cooled off sufficiently for winter snow and ice to return to the northern and southern polar regions (Puc  at *et al.* 2003; Jenkyns *et al.* 2012; Erba *et al.* 2015; Herrle *et al.* 2015; O’Brien *et al.* 2017). Glendonites are reported from Ellesmere Island, Axel Heiberg Island, Svalbard, northern Greenland and east-central Australia (Eromanga Sea), indicating that cool bottom waters once again had chilled the deep ocean basins (Frakes and Francis 1988; Grasby *et al.* 2017; Vickers *et al.* 2019; Rogov *et al.* 2023).

The warmest Cretaceous temperatures occurred during the Cenomanian–Turonian Thermal

Maximum (MzW08, 94–93 Ma). Second only to the PTTM, the global average temperature reached 28°C and the pole-to-equator temperature gradient was flattened with a temperature differential of only c. 20°C between the polar region (13°C) and the tropics (34°C). No cold bottom water formed during this interval. Instead, warm, salty water from the broad, tropical shelves (Brass *et al.* 1982) warmed the deep oceans and resulted in stratified oceans (Friedrich *et al.* 2011, 2012).

Not even a hint of ice existed at the poles during the Cenomanian–Turonian Thermal Maximum (Ziegler *et al.* 1985). The presence of tropical plants and dinosaurs on Antarctica (Dettmann 1989; Cantrill and Poole 2012) and above the Arctic Circle indicates that temperatures rarely fell below freezing

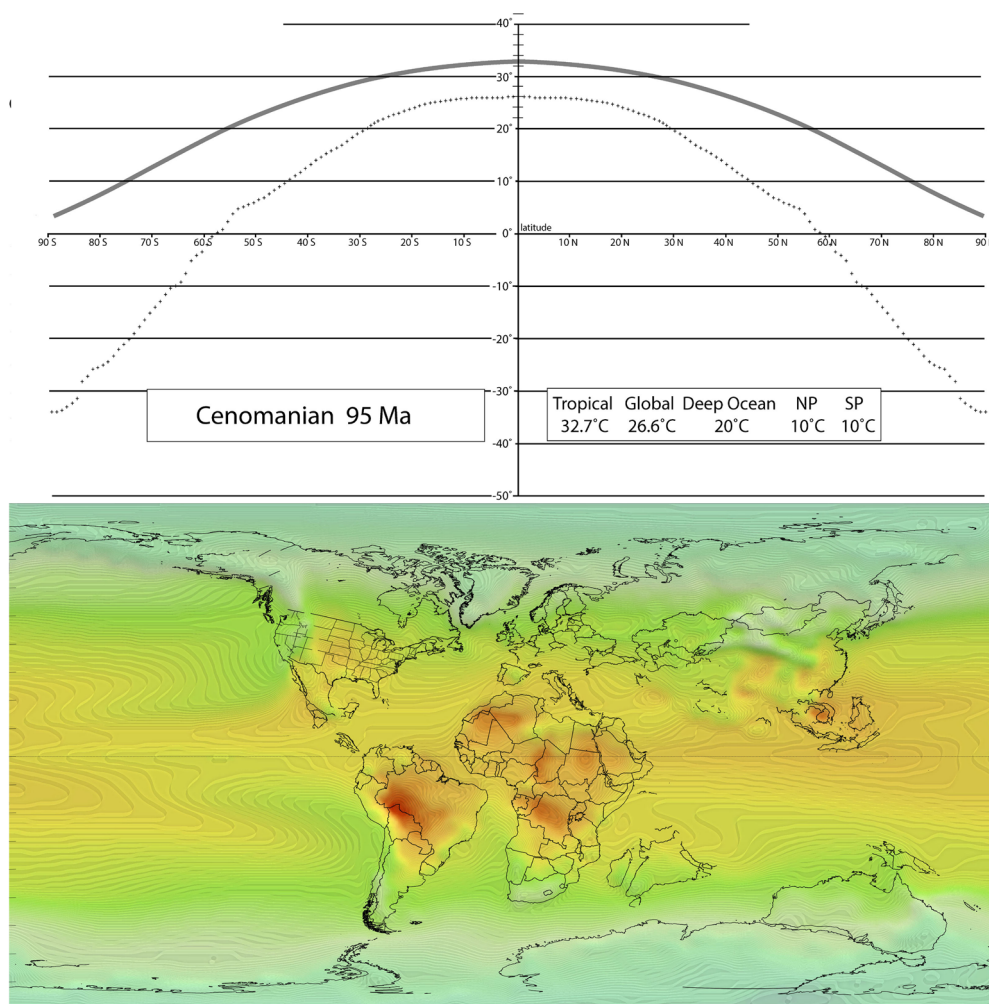


Fig. 105. Cretaceous pole-to-equator temperature gradient and global temperatures (late Cenomanian, 95 Ma); see Figure 2a for the legend.

even during the winter months (Wolfe and Upchurch 1987; Parrish and Spicer 1988; Spicer *et al.* 2008, 2009, 2021; Spicer and Herman 2010). Recent descriptions of angiosperm leaf floras from Antarctica indicate that similar warm and wet conditions existed near the South Pole during the Late Cretaceous (Hayes *et al.* 2006). In general, during times of hothouse conditions, the Equatorial and Subtropical belts expanded slightly polewards; the Polar and Cool Temperate belts were replaced by an expanded Warm Temperate belt that brought tropical conditions to latitudes above 50° N and S (Paratropical belt of Boucot *et al.* 2013; the megathermal rainforests of Morley 2011).

Despite the overwhelming geological and palaeontological evidence for warm polar regions during

the Cenomanian–Turonian Thermal Maximum, early climate simulations of the mid-Cretaceous tended to run cold and had a difficult time modelling these warmer polar temperatures (Barron and Washington 1982a, b, 1985). Various attempts have been made to modify the input parameters to the climate models to produce simulations more consistent with the geological data. Initial attempts to fix this problem used extremely elevated levels of greenhouse gases to warm the poles (15 times modern CO₂; Bice and Norris 2002). There is, however, no geological support for CO₂ concentrations in the Cenomanian–Turonian much above six times the modern value (Fig. 21) (van der Meer *et al.* 2014; Scotese *et al.* 2022). The extreme high levels of CO₂ needed to keep the polar regions ice free

The Cretaceous world

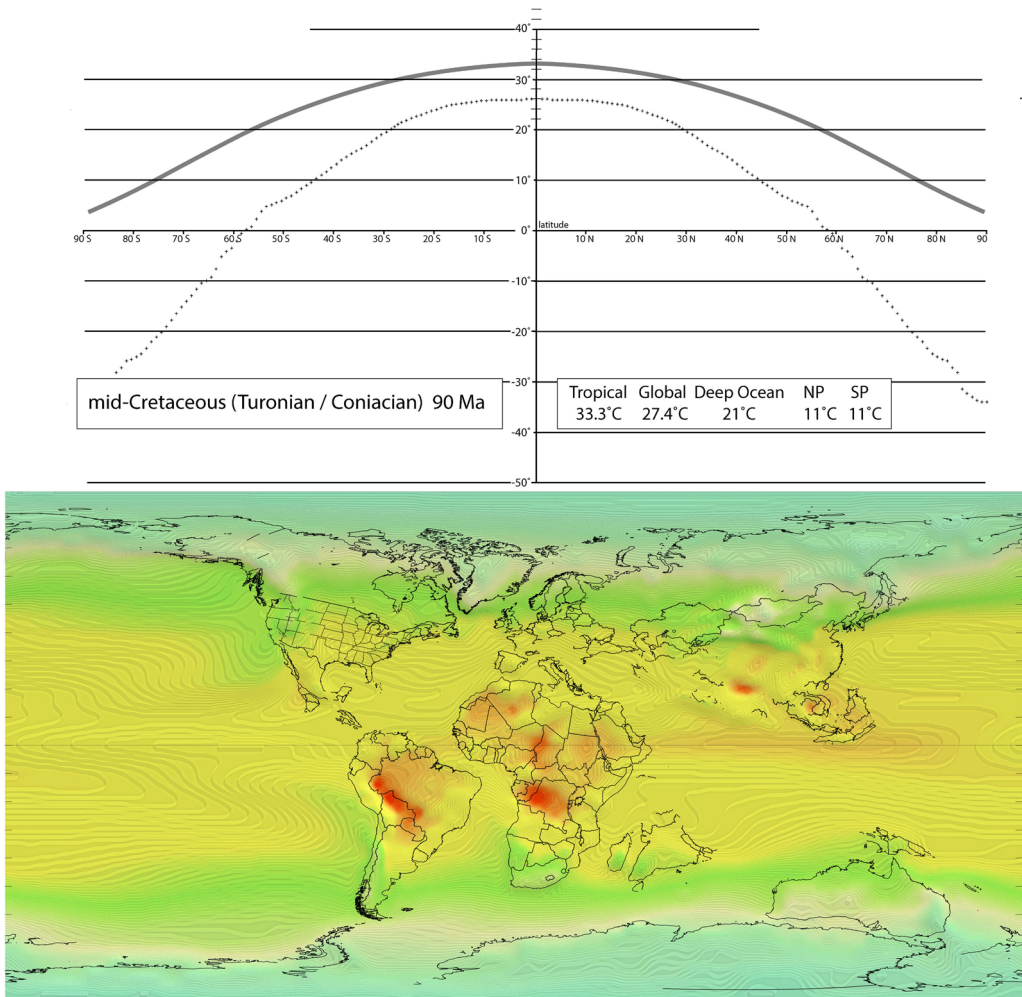


Fig. 106. Cretaceous pole-to-equator temperature gradient and global temperatures (latest Turonian, 90 Ma), see Figure 2a for the legend.

would necessarily make terrestrial and shallow-marine habitats at low latitudes uninhabitable (Jacobs *et al.* 2005).

Another way to make the polar regions warmer is to modestly increase the concentration of greenhouse gases and also to modify the land cover in polar regions to a darker, denser vegetation (Otto-Bliesner and Upchurch 1997; Upchurch *et al.* 1999). The darker vegetation has a lower albedo and, consequently, more solar energy is absorbed at the surface. In this model, positive feedbacks between high-latitude forests, the atmosphere and the ocean all contribute to significantly warmer temperatures at high latitudes during the Late Cretaceous (Upchurch *et al.* 1999).

A third explanation invokes a Late Cretaceous ‘Super-Gulf Stream’ that vigorously carried warmth from the Equator to the poles (Barron *et al.* 1993; Brady *et al.* 1998). Although intuitively appealing, an analysis of the dynamics indicates that it is not possible to carry enough heat polewards using ocean currents alone. The atmosphere must also play an important role. In addition, much like today, the palaeogeography of the Late Cretaceous presents a nearly landlocked polar region that would have been isolated from Gulf Stream-like ocean currents.

One of the more promising approaches has been to change the high-altitude cloud parameterization that is used in climate models like the Community

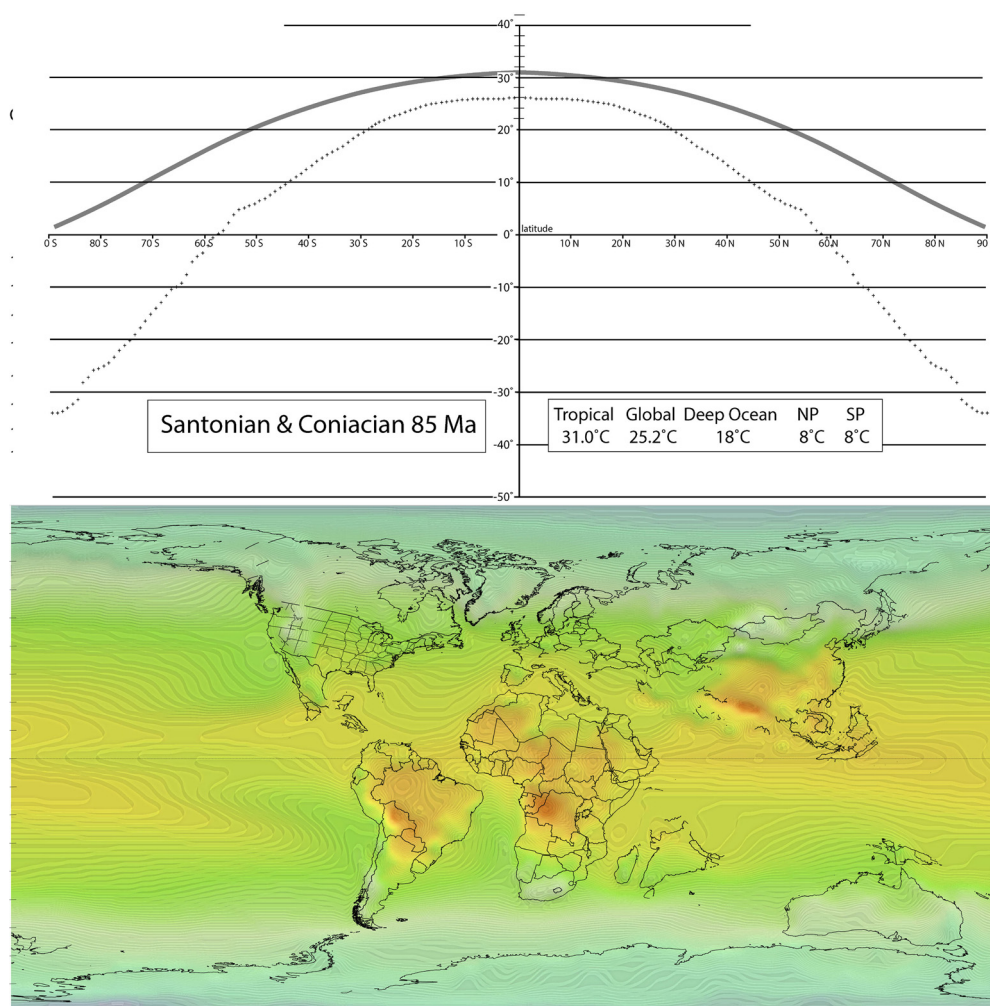


Fig. 107. Cretaceous pole-to-equator temperature gradient and global temperatures (Coniacian–Santonian, 85 Ma), see Figure 2a for the legend.

Climate System Model version 3 (CCSM3: Kiehl and Shields 2013). The high albedo of low-altitude cumulus clouds reflects incoming sunlight back to space, which cools the Earth. Wispy, high-altitude clouds, on the other hand, reflect thermal energy back to the surface of the Earth, resulting in net global warming (Kump and Pollard 2008). Fewer ‘warm clouds’ form in the modern world because anthropogenic atmospheric pollution reduces the amount of warm cloud condensation nuclei. When cloud parameters characteristic of pristine regions are introduced into the climate model, significant additional warming occurs, especially in polar regions (Upchurch *et al.* 2015). Combined with a modest elevation in the concentration of atmospheric CO₂ (two–six times modern levels), the modelled

temperature of polar regions remains above freezing throughout most of the year.

The most radical hypothesis that has been proposed to explain the warm polar climates of the Late Cretaceous involves a fundamental rethinking of the way the atmosphere circulates. One of the basic features of the modern atmosphere is Hadley cell circulation. In the Hadley cell, warm air rises at the Equator, moves polewards, cools and descends over the subtropical desert belt (c. 35° N and S; see Fig. 84). In Hay’s model (Hay 2008, 2016; Hay and Flögel 2012; Hay *et al.* 2019), this simple, well-organized convective flow is replaced by a chaotic system of super-cyclonic eddies, which are like mega-hurricanes. Hundreds of these mega-hurricanes would have annually transferred vast

The Cretaceous world

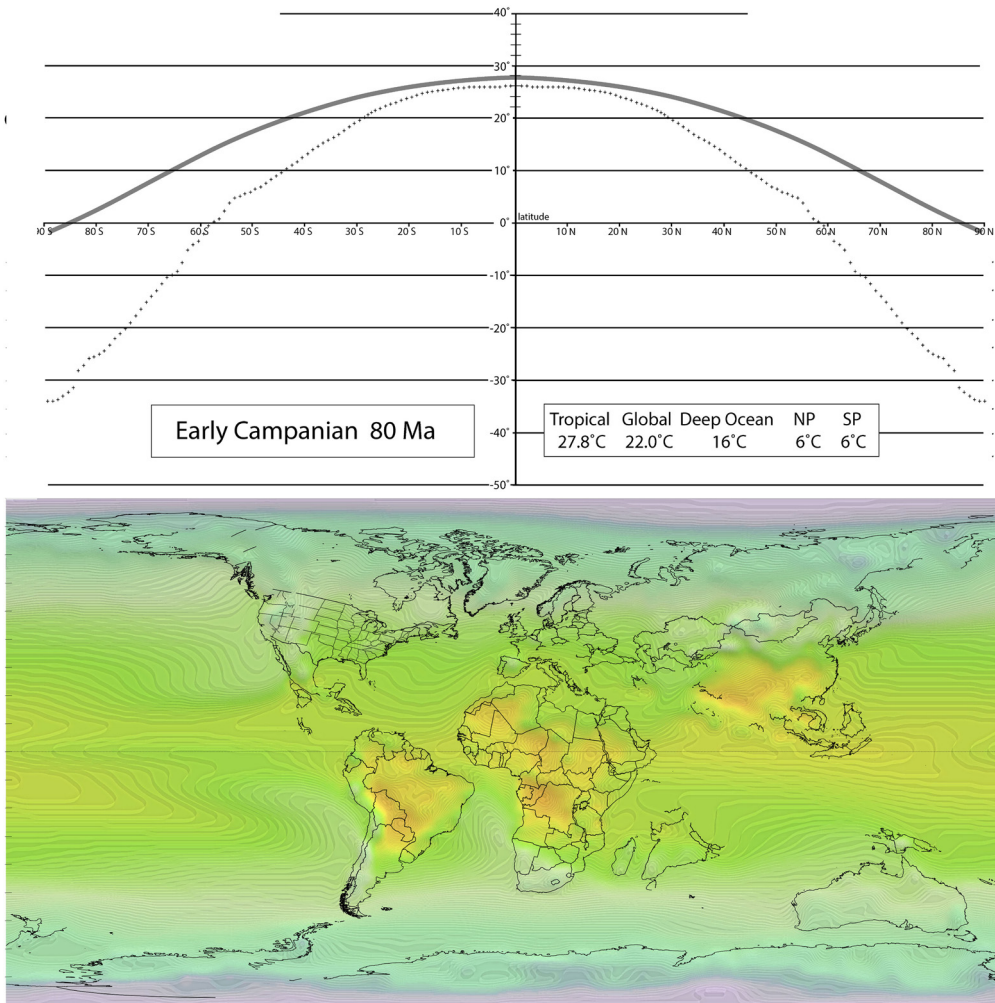


Fig. 108. Cretaceous pole-to-equator temperature gradient and global temperatures (early Campanian, 80 Ma), see Figure 2a for the legend.

amounts of heat from the Equator to the poles during the Late Cretaceous. Although an intriguing and out-of-the-box proposition, no climate model can currently simulate this complex alternative to Hadley cell circulation.

After reaching peak Cretaceous temperatures during the Cenomanian–Turonian Thermal Maximum, temperatures gradually fell during the remainder of the Cretaceous. Maximum SSTs did not drop below 30°C until late in the Santonian (84 Ma) or early in the Campanian (O'Brien *et al.* 2017). This gradual cooling may have been punctuated by several ephemeral cooling events at c. 85, c. 76 and c. 71 Ma (Miller *et al.* 1999, 2004, 2005a, b) as evidenced by $\delta^{18}\text{O}$ temperature estimates from planktonic foraminifera. Also, an enigmatic dropstone

deposit of Campanian–Maastrichtian age (75–70 Ma) has been reported from the region of the Anadyr River in Chukotka (Ahlberg *et al.* 2002).

The end-Cretaceous impact winter. The fall in temperatures during the Late Cretaceous catastrophically culminated in the arrival of the bolide that produced the 150 km-diameter impact crater near the town of Chicxulub (Devil's Tail) in northern Yucatan (Alvarez *et al.* 1980; Hildebrand *et al.* 1991; Schulte *et al.* 2010). The Chicxulub impact is the largest known bolide impact of the Phanerozoic (Spray 2020).

The most likely scenario is that the impact event vaporized 3000 Mt of crustal material and injected this fine particulate matter high into the atmosphere. This material fell back to Earth forming a global

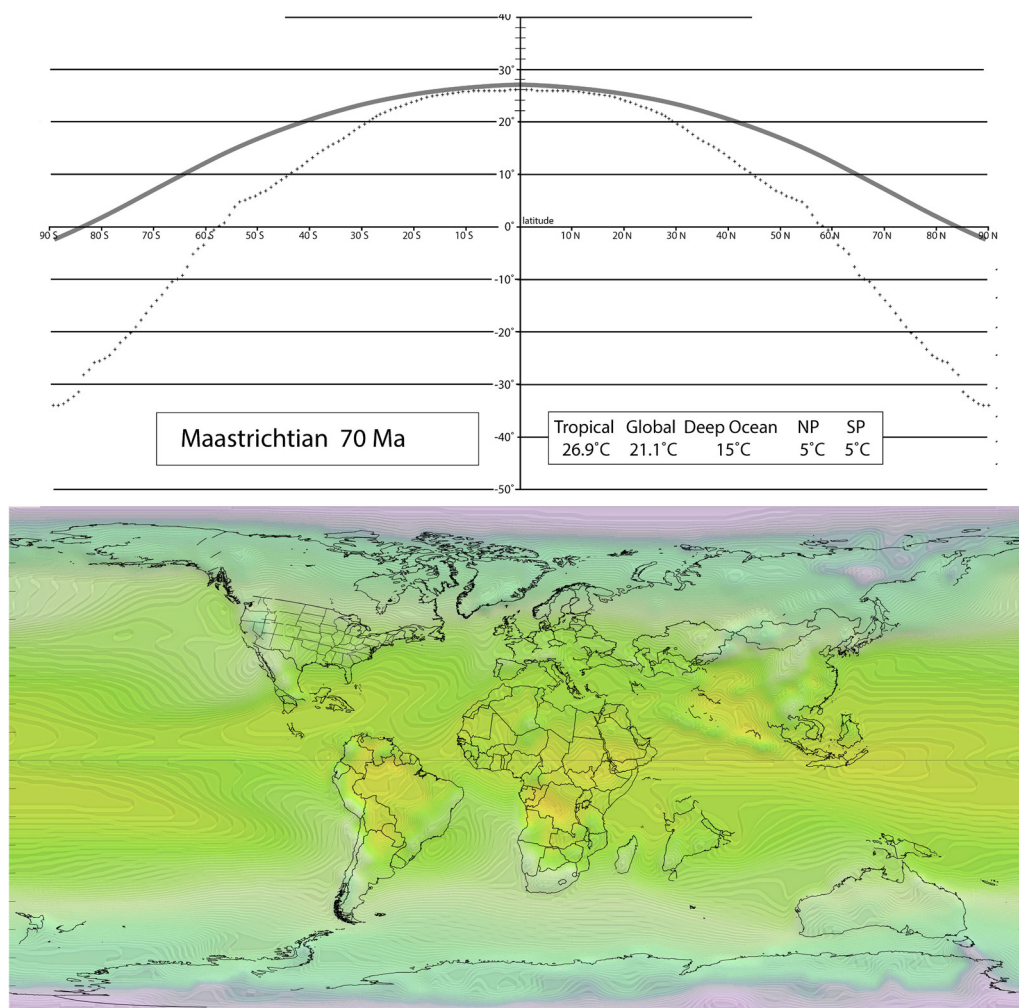


Fig. 109. Cretaceous pole-to-equator temperature gradient and global temperatures (early Maastrichtian, 70 Ma), see Figure 2a for the legend.

‘clay layer’. The Cretaceous–Paleogene boundary clay layer (Hart *et al.* 2012, 2013, 2014; Hart and Koutsoukos 2015) contains several unusual stratigraphic markers: (1) an iridium anomaly (Alvarez *et al.* 1980; Smit 1999; Miller *et al.* 2010); (2) microtektites (Yancey and Guillemette 2008); (3) shocked quartz (Bohor *et al.* 1987; Smit 1999); and (4) soot (from forest fires) that connect it directly to the Chicxulub impact event.

While suspended in the atmosphere, this delicate shroud of material blocked the sun and turned day into night – a wintry night that lasted for months or years. Without sunlight, plants on land and plankton in the oceans died. Small and large herbivores gradually starved. Without herbivores to prey on, predators then starved – all the while, snow

continued to fall (probably for several decades). As a consequence of the collapse of the food chain, approximately 75% of all species were wiped out (Sepkoski 1996). The effect of this extinction event on global ecosystems was second only to the great Permo-Triassic Extinction (McGhee *et al.* 2013).

The ensuing ‘impact winter’ scenario plunged the Earth into a frigid deep-freeze comparable to the coldest glacial stages of any Phanerozoic ice age. The drastic cooling, however, was short lived (Vellekoop *et al.* 2014, 2016) and was followed by an equally short-lived period of global warming, triggered by the final massive eruption of the Deccan LIP (Ernst 2014; Keller *et al.* 2017).

The first eruptions of the Deccan LIP predate the Chicxulub impact by 1–2 Myr (Chenet *et al.* 2008;

Keller 2011, 2014; Schoene *et al.* 2019). It has been proposed that an earlier impact event (Shiva impact) triggered the Deccan eruptions (Chatterjee *et al.* 2006); however, this hypothesis has not received much support. It seems likely, however, that the Chicxulub impact did influence or enhance Deccan volcanism. It has been noted by several authors that the impact site in Yucatan is nearly antipodal to the eruption site of the Deccan LIP in India. Although the antipodal palaeolatitudes are identical (26° N v. 26° S), the antipodal palaeolongitudes are offset by several thousand kilometres. Nevertheless, it seems plausible that shockwaves from the impact passed through the Earth and were reconcentrated beneath the Deccan hotspot, stimulating more voluminous eruptions (Renne *et al.* 2015; Richards *et al.* 2015). In any event, the excess atmospheric CO₂ from the Deccan eruptions caused a 4–8°C spike in global temperatures (Petersen *et al.* 2016; Bond and Grasby 2017) that ushered in the Paleogene warm interval.

Changing patterns of precipitation during the Cretaceous

This section describes: (1) the persistent patterns of regional precipitation during the Cretaceous; (2) important changes in regional precipitation during the Cretaceous; and (3) a comparison of computer simulations of palaeo-rainfall with Köppen climatic belts based on lithological indicators of palaeoclimate and palaeoprecipitation proxies. Palaeoclimatic reconstructions and animations illustrating palaeoprecipitation patterns for each stage of the Cretaceous are provided in the [Supplementary material](#).

Persistent patterns of regional precipitation

As illustrated in Figure 110, the global pattern of modern precipitation is similar in many respects to the pattern of precipitation during the mid-Cretaceous. Both the modern world and the Cretaceous world were dominated by three regional patterns of precipitation: the tropical ever-wet belt; areas of high rainfall along the western margins of continents at mid-latitudes (45°–50° N and S); and the warm, subtropical humid belt along the eastern margins of the continents (30°–40° N and S). Although the regional patterns of precipitation were similar, it is estimated that the annual amount of precipitation was 10 times higher during the Cretaceous (Bao and Hu 2024).

High rainfall occurs along the Equator due to the intense heating, lifting and subsequent cooling of warm, humid tropical air. The Equator is where the Hadley atmospheric circulation cell originates.

Similar to the present-day world, during the Cretaceous the Ever-wet belt (Köppen zone A) was broken up by continental landmasses that straddled the Equator.

The Cool Temperate belt (Köppen zone D) is characterized by a strong westerly airflow that removes moisture from the oceans and delivers it to the western margin of continents at moderately high latitudes (45°–50° N and S). In the modern world this includes rainy locations such as the Pacific NW–British Columbia, Patagonia and New Zealand. During the Cretaceous, the Cool Temperate Rainy belt also impinged upon the Pacific NW–British Columbia, Patagonia, South Africa, southern Madagascar and India, as well as most of Australia.

The Warm Subtropical belt (Köppen zone C) steals much of its moisture from either the Equatorial Rainy belt or the Temperate Rainy belt. The dynamics are strongly seasonal (i.e. monsoonal). During the summer months, warming landmasses pull air masses towards the continents. If these air masses travel over a warm, moist ocean then torrential rains soon follow. The best example of this pattern of airflow is the modern Indian monsoons. Late in the Cretaceous, there was an Indian-like monsoon system; however, in this case the winds were deflected towards the southern hemisphere because India had not yet crossed the Equator.

Changing patterns of regional precipitation

Figures 111–113 illustrate the variable pattern of regional precipitation during the Cretaceous (Valdes *et al.* 2021). Rainfall patterns changed during the Cretaceous due to two palaeogeographical effects: continental motion across climatic belts, and the opening of new ocean basins. Changing sea level, to a lesser extent, also increased atmospheric humidity, producing more frequent and intense rainfall.

Western hemisphere. We begin our tour of the humid Cretaceous world (145 Myr ago) in the region that would become the South Atlantic. All of North Africa from Morocco to Arabia, together with northern South America and most of Brazil, was occupied by a warm, wet tropical rainforest (Fig. 111). Abundant rainfall across the region produced numerous river systems flowing away from the South Atlantic into the Central Atlantic, southern margin of Tethys and the widening Somali Basin (see Fig. 67). North America, in contrast, was much drier during the earliest Cretaceous.

From the Valanginian to the late Aptian (140–115 Ma), the region of high rainfall in northern South America and northwestern Africa persisted, and its southern boundary became more precisely delineated. During the Hauterivian (130 Ma), a sharp, Sahel-like boundary separated the northern

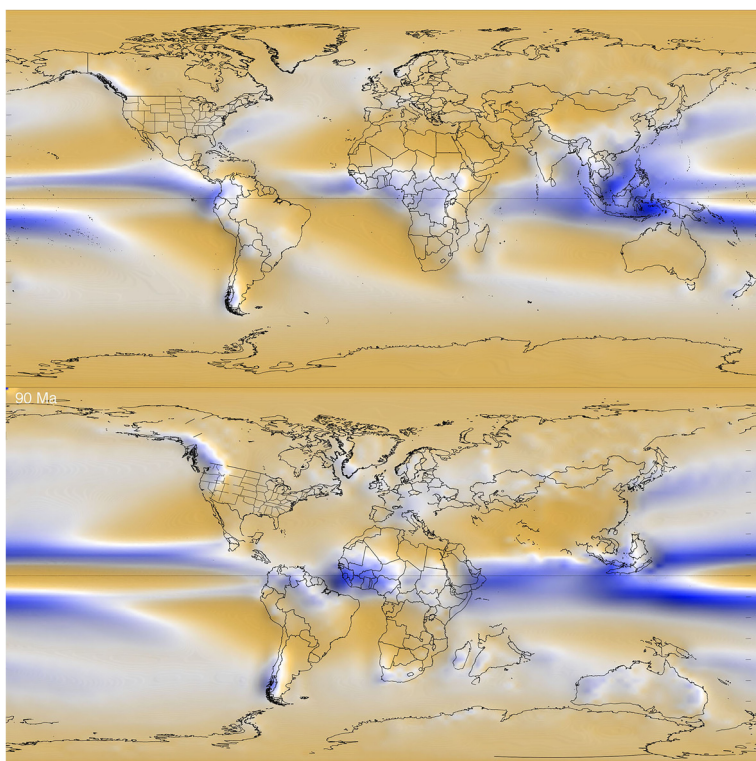


Fig. 110. Comparison of (top) modern and (bottom) mid-Cretaceous patterns of precipitation, see [Figure 3b](#) for the legend.

humid regions from the southern arid regions ([Fig. 111](#)). This Cretaceous Sahel was more than twice as long as its modern counterpart. It trended diagonally across northern Gondwana from southern Colombia, bisecting Brazil, south of Gabon, across the north Congo and into the western Indian Ocean in the vicinity of central Somalia. Thick Aptian salt beds were deposited in the nascent South Atlantic beneath this intense arid belt. At the same time, during the mid-Cretaceous, northern Africa became progressively more arid ([Fig. 111c](#)).

Rainfall patterns began to change dramatically as the South Atlantic opened. During the late Aptian (c. 115 Ma), northern Brazil and the Ivory Coast became noticeably wetter ([Fig. 112](#)). South Africa, which had been arid throughout the Early Cretaceous, started to receive more moisture from the widening South Atlantic during the Albian (110 Ma). West-central Africa and southernmost Africa became increasingly wetter throughout the remainder of the Cretaceous ([Figs 112 & 113](#)).

By the Cenomanian (95 Ma), the continents bordering the northern South Atlantic became much wetter ([Figs 112 & 113](#)). The highstand of sea level during the mid-Cretaceous added enough moisture

to the atmosphere for the Equatorial Wet belt to become a through-going feature stretching from the southeastern tip of Arabia to western Ecuador ([Fig. 113](#)). This Equatorial Ever-wet belt persisted through to the end of the Cretaceous.

One of the most striking changes in precipitation patterns during the Cretaceous occurred along the western margin of the Central Atlantic in eastern North America. During the Early Cretaceous, from 145 to 100 Ma, eastern North America was characterized by an arid climate ([Fig. 111](#)). Rainfall was seasonal and minimal. Starting in the late Albian–earliest Cenomanian (105–100 Ma: [Fig. 112](#)), the eastern seaboard of the USA began to experience higher rates of precipitation. This trend increased steadily through the remainder of the Cretaceous. This transition was due in part to higher sea level and the widening Central Atlantic but primarily to North America’s northward movement out of the dry subtropics and into the more humid Warm Temperate belt (Köppen Zone C).

Throughout the Cretaceous, northern Europe received moderate rainfall (c. 15 cm/month). With an exception of a dry spell in the late Aptian and Albian in Iberia ([Figs 111 & 112](#)), there was a

The Cretaceous world

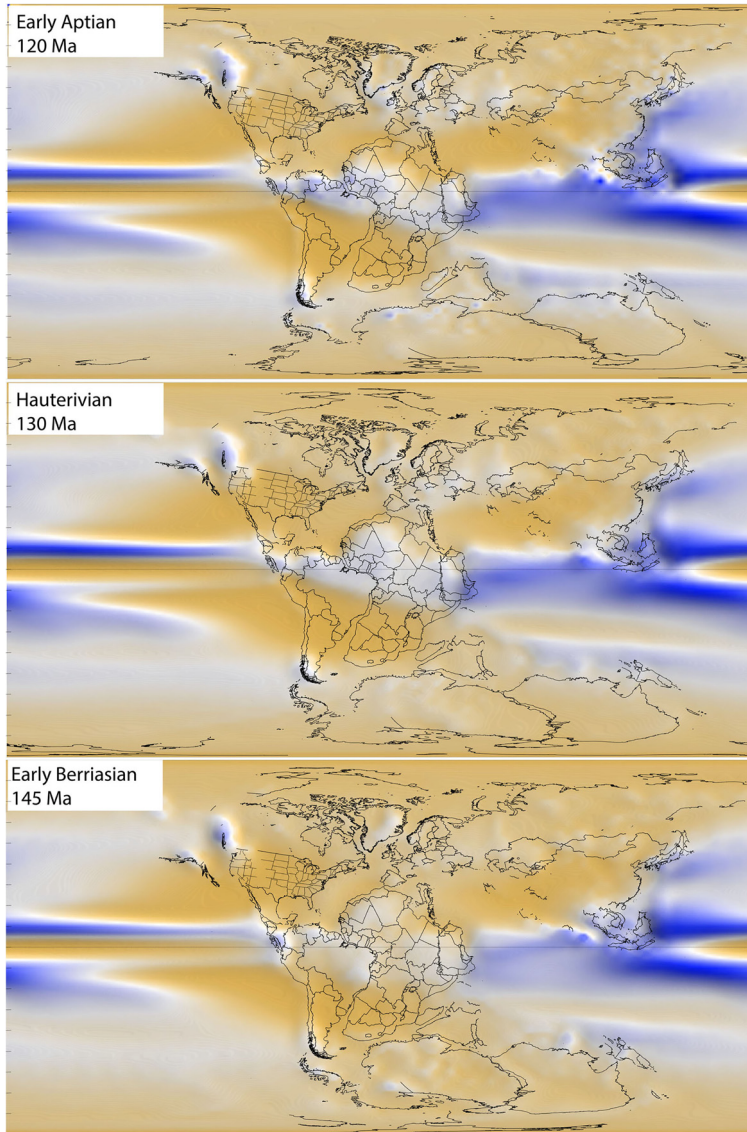


Fig. 111. Cretaceous precipitation during the early Berriasian (145 Ma), Hauterivian (130 Ma) and early Aptian (120 Ma); see [Figure 3b](#) for the legend. Source: [Valdes *et al.* \(2021\)](#).

tendency towards much wetter climates in Europe during the mid and Late Cretaceous.

Eastern hemisphere. We begin our tour of rainfall patterns in the eastern hemisphere with India. The changing precipitation pattern observed in India is primarily due to India's southward, then northward movement through three different climatic belts. At the start of the Cretaceous (145 Ma), India was located between the arid and warm temperate zones of the southern hemisphere (c. 40° S). Its climate was subarid ([Figs 111](#)). During

the Early Cretaceous it moved further south, arriving at 55° S during the early Barremian (125 Ma) and enjoyed more precipitation ([Fig. 111](#)). It remained in the wet Cool Temperate belt for c. 25 Myr, then began to move northwards, returning to the Warm Temperate belt. From 100 to 80 Ma, India's climate was subtropical with heavy seasonal precipitation ([Fig. 112](#)). During the Campanian and early Maastrichtian (75–70 Ma), India moved into the southern Arid belt (20° S) and began to dry out ([Figs 113](#)). At the end of the Cretaceous, India began to accelerate

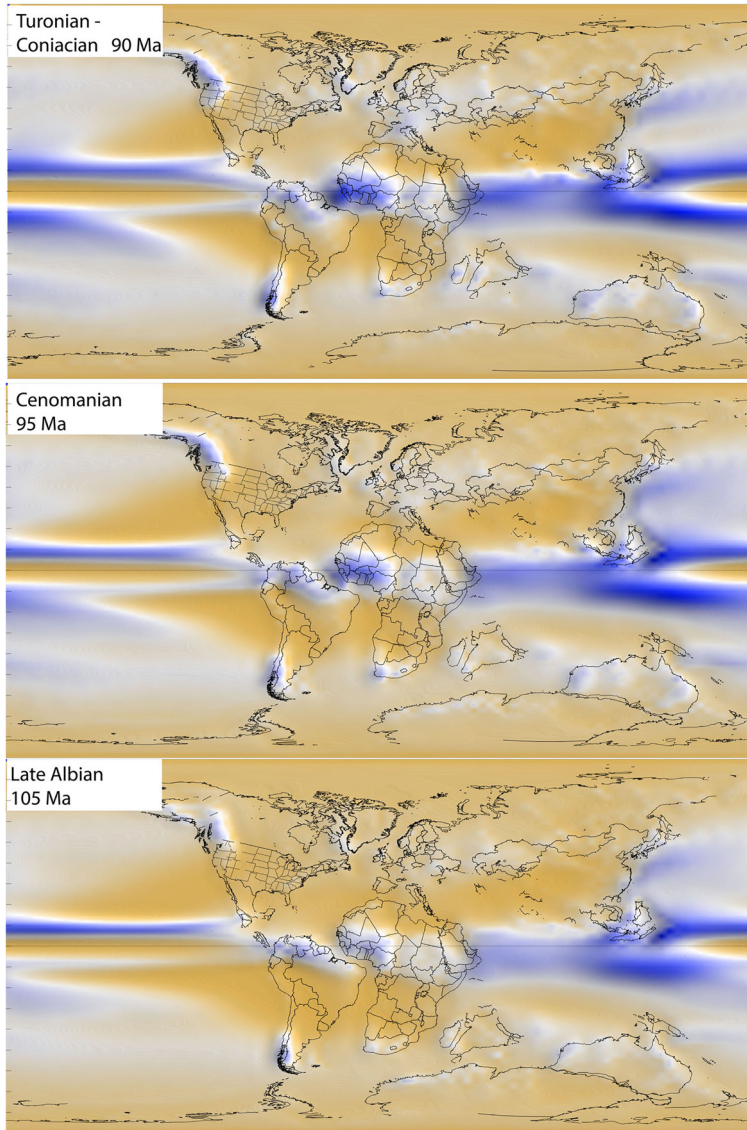


Fig. 112. Cretaceous precipitation during the late Albian (105 Ma), Cenomanian (95 Ma) Turonian–Coniacian (90 Ma); see [Figure 3b](#) for the legend. Source: [Valdes *et al.* \(2021\)](#).

towards Eurasia and a southern hemisphere version of the Indian monsoon kicked in. By the end of the Cretaceous, India was wetter than at any previous time period.

Like India, the record of rainfall on Australia was driven by its movement across different climatic belts. During the Early Cretaceous, an arid Australia occupied high southerly latitudes (75°S) in the eastern rain shadow of Antarctica ([Fig. 111](#)). By the Aptian (120 Ma), the counter-clockwise rotation of Gondwana had carried the northern portion of

Australia into warmer, wetter latitudes (60° S: [Figs 111 & 112](#)). During the next 30 Myr precipitation swept across Australia from north to south, and by the Turonian (90 Ma) Australia was firmly ensconced in the Wet Temperate belt (*c.* 55° S: [Fig. 112c](#)), where it would remain for the rest of the period.

Eurasia, which did not move much during the Cretaceous, was divided into two precipitation regimes. South of Mongolia, in central China and neighbouring countries it was arid, except along

The Cretaceous world

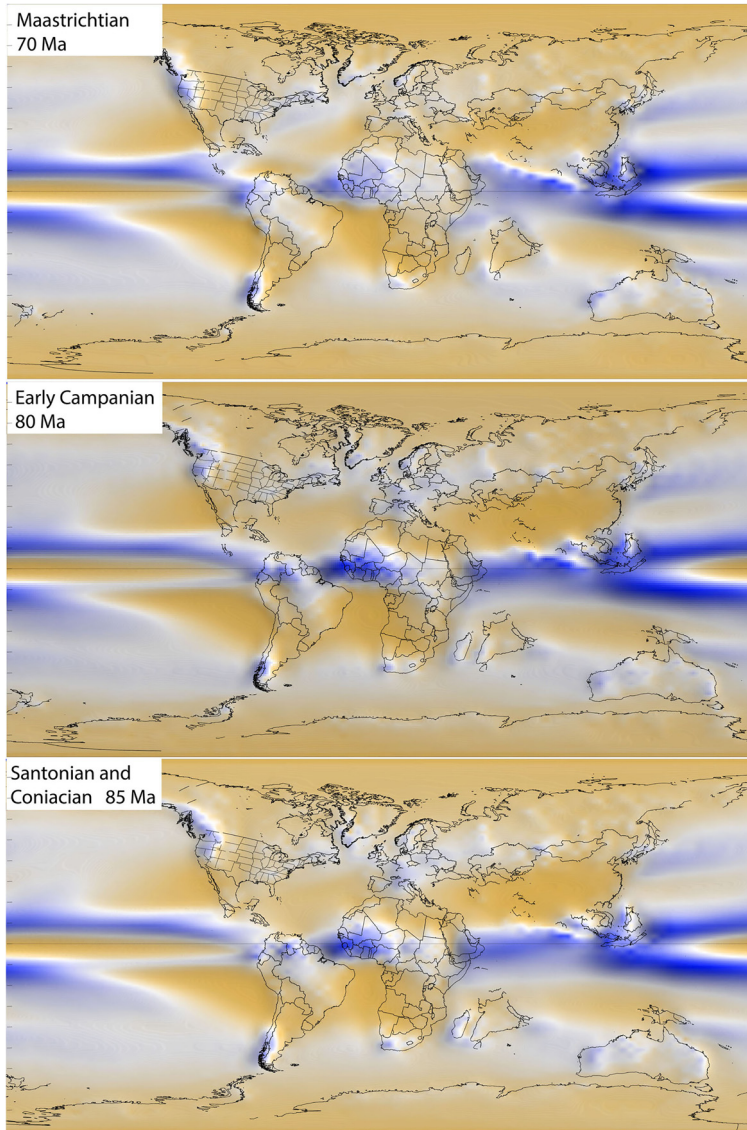


Fig. 113. Cretaceous precipitation during the Santonian and Coniacian (85 Ma), Campanian (80 Ma) and Maastrichtian (70 Ma); see Figure 3b for the legend. Source: [Valdes *et al.* \(2021\)](#).

the eastern coast. North of Mongolia, precipitation was higher, except towards the centre of Siberia, which remained arid.

Comparison of precipitation patterns: computer simulation v. geological evidence. The above description of regional precipitation during the Cretaceous is based on the palaeoclimatic simulations of the HadCM3 model ([Valdes *et al.* \(2021\)](#)). To test the validity of these model predictions, we compared the computer output to the patterns of precipitation revealed by the lithological indicators with

the palaeoprecipitation proxies compiled by [Burgener *et al.* \(2023\)](#). Fourteen key localities were selected worldwide and the relative amount of precipitation at each locality was classified as very wet, wet, subarid or arid. The Hadley simulation results were then compared with the precipitation estimates from the Köppen zone maps of [Burgener *et al.* \(2023\)](#). Figure 114 summarizes the results of this comparison.

A total of 126 localities were compared. For 42 localities (33%) there was an exact match, for 80

localities (64%) there was a fair match (e.g. arid v. semi-arid or wet v. very wet) and for four localities (3%) there was a decided mismatch. All of the mismatched localities were Early Cretaceous in age and, in every case, the computer simulation predicted more arid conditions.

Two of the mismatched localities are in northern Africa during the Aptian and Albian (120–105 Ma). As illustrated in Figure 115, the computer simulation predicts arid to subarid conditions for North Africa, while the Köppen reconstruction indicates much wetter conditions. In the earliest Cretaceous (145 Ma, Berriasian–Valanginian) there are two mismatched localities. The HadCM3 model predicts that much of eastern North America was arid, whereas the Köppen data predict a more humid environment, except along the Gulf Coast and Mexico (Fig. 115). Similarly, the HadCM3 model predicts that all of South Africa was arid during the earliest Cretaceous, whereas the Köppen data predict that although the northern half of South Africa was dry, the southern half was very wet. It is also notable that the precipitation patterns in northern South America are reversed. The Hadley model predicts that the western part of northern South America was dry and the eastern part was wet, whereas the Köppen model indicates that the west was wet and east was dry (Fig. 115).

Summary

Introduction

This paper is organized into six principal sections: (1) plate tectonic data and methods; (2) palaeogeographical data and methods; (3) palaeoclimatic data and methods; (4) plate tectonic events during the Cretaceous; (5) palaeogeographical events during the Cretaceous; and (6) palaeoclimatic events during the Cretaceous. Three additional sections discuss Cretaceous rivers systems, oceanic circulation and precipitation patterns. The following summaries of these sections were written by Claude (v2.1), an AI assistant created by Anthropic, with minor edits by the senior author.

Summary of plate tectonic data and methods

The paper describes the methodology used to construct global plate tectonic models, with a focus on applying these techniques to build Cretaceous reconstructions. The first component of the model is mapping ancient plate boundaries and defining tectonic elements based on the geological and geophysical record. The second component involves modelling the hierarchical motions of these plates and terranes through time.

Integrating diverse lines of evidence helps to constrain the plate tectonic model, including seafloor magnetic anomalies, oceanic fracture zones, hotspot tracks, palaeomagnetic polar wander paths, continental rift and collision histories, subduction zone locations, plate motion geometries, synthetic seafloor isochrons, subducted slab graveyard signatures in the mantle, large igneous provinces (LIPs), palaeobiogeographical patterns, palaeoclimate simulations, and true polar wander.

The goal is to produce a self-consistent model of plate motions and geometries that matches all available constraints during the Cretaceous within estimated uncertainties. As new geological or geophysical evidence emerges, the model can be updated to build an increasingly accurate four-dimensional reconstruction of plate configurations through time.

Adhering to a set of quantitative plate tectonic principles guides the model development, helping to resolve inherent ambiguities in the incomplete geological record. Creating comprehensive reconstructions requires meticulous integration of these global datasets. Continued model refinement will allow construction of accurate plate tectonic models that capture the complex dynamics of Earth system processes through deep time.

Summary of palaeogeographical data and methods

Constructing ancient palaeogeographical maps requires compiling databases of lithological and sedimentary records that indicate different environmental depositional settings across continents over time. For example, mapping extensive limestone distributions helps to delimit past shallow-marine environments. These palaeoenvironmental control points are combined with tectonic constraints from plate reconstructions for areas where the geological record is incomplete.

The palaeogeographical interpretations are converted into digital elevation models (palaeoDEMs) that quantify ancient continental topography and ocean bathymetry. The effects of gradual seafloor subsidence as ocean crust ages away from spreading ridges can be removed to restore ancient ocean depths. Continental elevation models are corrected for tectonic activity such mountain building or erosion, as well as isostatic adjustments.

Changes in sea level over time can be estimated by calculating the percentage of flooded continental area from palaeogeographical maps across different intervals. Matching the amount of marine inundation against continental hypsometry allows estimates of how much sea-level rise would be required to produce the observed flooding. However, the gradients

| Location/Ag | NW Namerica | E N. America | N S.America | S S.America | Europe | North Africa | South Africa | Central Asia | SE Asia | Japan | India | N. Australia | S. Australia | Antarctica | |
|-------------|-------------|--------------|-------------|-------------|--------|--------------|--------------|--------------|---------|-------|-------|--------------|--------------|------------|----------|
| 70 Ma | 2 | 2 | 1 | 2 | 2 | 3 | 3 | 3 | 2 | 2 | 2 | 2 | 2 | 2 | 2 Köppen |
| | 1 | 2 | 2 | 1 | 2 | 3 | 2 | 4 | 1 | 1 | 2 | 2 | 3 | 3 | 3 HADCM3 |
| 80 Ma | 2 | 2 | 1 | 2 | 2 | 3 | 2 | 4 | 1 | 2 | 2 | 2 | 2 | 2 | 2 Köppen |
| | 1 | 2 | 1 | 1 | 2 | 4 | 2 | 4 | 1 | 1 | 3 | 2 | 3 | 3 | 3 HADCM3 |
| 85 Ma | 1 | 1 | 1 | 2 | 2 | 3 | 2 | 4 | 1 | 2 | 1 | 1 | 2 | 2 | 2 Köppen |
| | 1 | 2 | 1 | 1 | 2 | 4 | 2 | 4 | 1 | 1 | 3 | 2 | 3 | 3 | 3 HADCM3 |
| 90 Ma | 1 | 1 | 1 | 2 | 1 | 3 | 2 | 3 | 1 | 2 | 1 | 1 | 2 | 2 | 2 Köppen |
| | 1 | 2 | 1 | 1 | 2 | 4 | 2 | 4 | 1 | 1 | 2 | 2 | 3 | 3 | 3 HADCM3 |
| 95 Ma | 2 | 2 | 1 | 2 | 2 | 3 | 2 | 2 | 1 | 2 | 1 | 2 | 2 | 2 | 2 Köppen |
| | 1 | 3 | 1 | 1 | 2 | 4 | 2 | 3 | 1 | 1 | 2 | 2 | 3 | 3 | 3 HADCM3 |
| 105 Ma | 2 | 3 | 3 | 2 | 2 | 2 | 2 | 2 | 1 | 2 | 2 | 2 | 2 | 2 | 2 Köppen |
| | 1 | 3 | 1 | 1 | 2 | 4 | 2 | 3 | 1 | 1 | 2 | 2 | 3 | 3 | 3 HADCM3 |
| 120 Ma | 2 | 2 | 2 | 2 | 2 | 2 | 2 | 2 | 1 | 2 | 2 | 2 | 2 | 2 | 2 Köppen |
| | 1 | 3 | 1 | 1 | 2 | 4 | 3 | 3 | 1 | 1 | 2 | 2 | 3 | 3 | 3 HADCM3 |
| 130 Ma | 2 | 2 | 3 | 3 | 2 | 2 | 2 | 2 | 1 | 2 | 2 | 2 | 2 | 2 | 2 Köppen |
| | 1 | 3 | 2 | 2 | 2 | 3 | 3 | 3 | 1 | 1 | 2 | 3 | 3 | 3 | 3 HADCM3 |
| 145 Ma | 2 | 1 | 4 | 1 | 2 | 2 | 2 | 2 | 1 | 2 | 2 | 2 | 2 | 2 | 2 Köppen |
| | 1 | 4 | 3 | 2 | 2 | 2 | 4 | 3 | 1 | 1 | 3 | 3 | 3 | 3 | 3 HADCM3 |

Fig. 114. Comparison of rainfall prediction: [Burgener *et al.* \(2023\)](#) (top cell) v. the HadCM3 model (bottom cell). Dark green cells indicate very wet conditions, light green cells indicate wet conditions, light yellow cells indicate semi-arid conditions and dark yellow cells indicate arid conditions. The cells outlined in blue are an exact match ($n = 42$). The cells outlined in red indicate a mismatch between the computer simulation ([Valdes *et al.* 2021](#)) and the Köppen map predictions ($n = 4$); see [Figure 115](#).

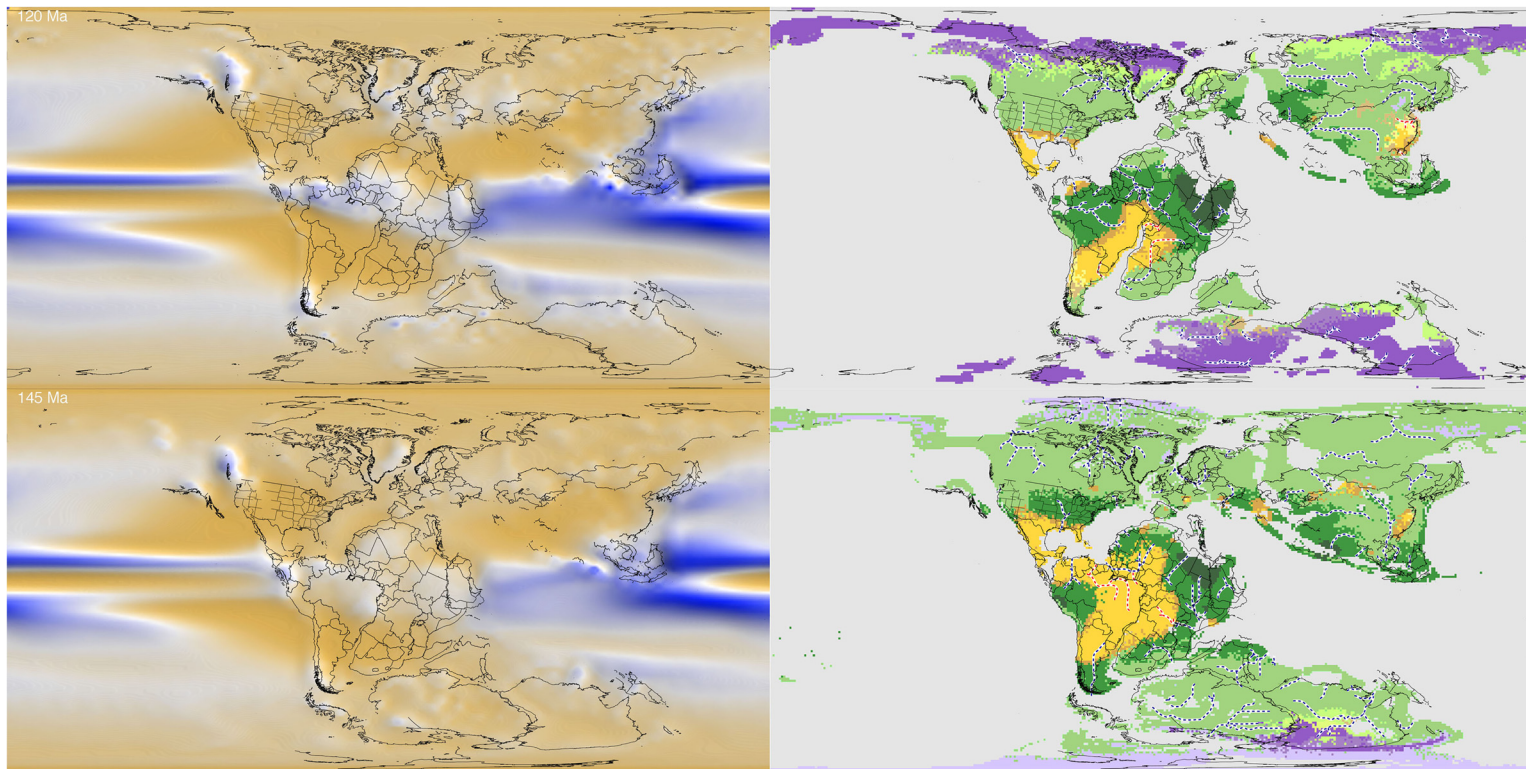


Fig. 115. Precipitation results with the largest mismatch: (top) Aptian–Albian (120 Ma) and (bottom) Berriasian–Valanginian (145 Ma).

The Cretaceous world

of continental slopes have also changed over time, necessitating corrections to this basic flooding approach. Comparisons can be made between the flooding proxy sea-level estimates and the curves derived from sedimentary records.

Integrating constraints from lithological evidence, plate tectonics models and geophysical measurements results in high-fidelity palaeoenvironmental reconstructions encoded in palaeoDEMs that capture the changing surface conditions through deep time, including fluctuations in continental flooding, mountain building and global sea level.

Summary of palaeoclimatic data and methods

Supercomputer simulations can be used to model past climates by specifying palaeogeography, solar insolation levels and atmospheric CO₂ concentrations as critical boundary conditions. Model outputs like temperature and rainfall can be compared against real-world geological climate proxies such as coal deposits and evaporites to evaluate the accuracy of these simulations. Constraining the CO₂ inputs is particularly important for tuning model temperature outputs but proxy CO₂ records contain substantial gaps, so a combination of proxy measurements of CO₂ and independently established Phanerozoic temperature histories can be used to fill in estimates for missing intervals.

In addition to verifying climate model outputs, the distribution of climate-sensitive lithologies can be mapped directly to delineate past Köppen climate belts and latitudinal temperature gradients. Statistical techniques, like Bayesian integration, allow these lithological indicators to be combined with isotope proxy measurements to quantitatively estimate palaeotemperatures and palaeoprecipitation regimes. Comparing proxy-based and simulation-based pole-to-equator temperature curves provides another avenue for model validation.

The increased sophistication of palaeoenvironmental reconstructions also enables an analysis of specific features like ancient river systems. By applying simulated regional rainfall levels to digital palaeotopography models, the likely location and discharge of major palaeorivers can be predicted through time. The length of river drainage basins responds primarily to base-level changes driven by fluctuations in sea level.

Summary of plate tectonics events during the Cretaceous

When the Cretaceous began 145 Myr ago, the supercontinent of Pangaea had begun to rift into several pieces. By the earliest Cretaceous, multiple ocean

basins had begun opening up between the fragments of Pangaea:

- Central Atlantic Ocean: formed 175 Myr ago during the break-up of Pangaea. By the Early Cretaceous, the ocean basin separating NW Africa and North America was 1500 km wide.
- Gulf of Mexico: opened as South America and Africa rifted from North America beginning in the Late Jurassic. It is underlain mostly by extremely stretched continental crust.
- Proto-Caribbean Ocean: formed between North and South America as North America moved NW during the Late Jurassic and Early Cretaceous, opening a seaway between Venezuela and Yucatan. The proto-Caribbean Ocean was bordered on the SW by an active volcanic arc (Greater Antilles island arc).
- South Atlantic Ocean: rifting began in the Late Jurassic, followed by the eruption of the Paraná–Etendeka Large Igneous Province at 135 Ma. Seafloor spreading began in the southern portion, while the central South Atlantic experienced continental rifting. The South Atlantic opened progressively from south to north 110–150 Myr ago.
- Western Indian Ocean: The East Gondwana continent (Madagascar, India, Antarctica and Australia) rifted away from Africa and South America beginning in the Early Jurassic, with strike-slip motion facilitating the opening of the Somali and Mozambique basins during the Cretaceous. Australia was still connected to India and East Antarctica.
- NE Indian Ocean: a continental fragment ‘Argoland’ rifted away from NW Australia in the latest Jurassic (160 Ma) and crossed Tethys during the Cretaceous. The present-day location of Argoland is uncertain.
- Canada Basin: rifting between the North Slope of Alaska and the Canadian Arctic islands began 155 Myr ago.
- Later in the Early Cretaceous, the remnants of Pangaea fragmented into Laurasia (North America, Europe and Asia) in the NW, West Gondwana (Africa and South America) in the centre and East Gondwana (India, Madagascar, Antarctica and Australia) in the SE. Surrounding Pangaea were the Pacific Ocean, Tethys Ocean, Angayucham Ocean and Wrangellian back-arc basin.

From 125 to 105 Myr ago in the Aptian–Albian:

- The Central Atlantic reached 4500 km wide. The proto-Caribbean, bordered by the volcanic Greater Antillean arc, was at its widest 110 Myr ago, before a subduction flip would completely consume this old ocean basin.
- South America fully rifted from Africa by 110 Myr ago, allowing the South Atlantic to link

with the Central Atlantic in an open marine gateway.

- East Gondwana continued rifting as India began separating from Antarctica around 120 Myr ago. By 110 Myr ago, seafloor spreading halted between India, together with Madagascar and Africa.
- In the Angayucham Ocean, North Slope Alaska collided with central Alaska and NE Siberia, closing this ocean. In the Wrangellian back-arc basin, the Wrangellia terrane collided with western North America 105 Myr ago.

During the Cenomanian–Turonian (100–90 Myr ago):

- Iberia rifted away from North America, opening the Bay of Biscay. Extension progressed into the North Atlantic with rifting between Greenland and Europe.
- South America separated fully from Africa, allowing deep circulation between the South Atlantic and Central Atlantic oceans.
- Greater India began its rapid northward drift towards Eurasia about 95 Myr ago.
- The mid-ocean ridge between India and Antarctica jumped northwards, facilitating Australia rifting from Antarctica around 95 Myr ago and opening the Tasman Sea.
- Back-arc basins related to slab rollback opened in the Okhotsk and Bering seas and south of Japan (Philippine back-arc basin).

In the Late Cretaceous (100–66 Myr ago):

- The North Atlantic rift system developed extensively but the Labrador Sea was the only significant area that experienced seafloor spreading.
- India moved rapidly northwards, colliding with the Lut Block of Iran, which was located off the east coast of Arabia (*c.* 70 Myr ago), beginning initial contact between India and continental Asia.
- Rifting progressed between Australia and Antarctica, which were connected until the Late Cretaceous by large volcanic plateaus, including the Naturaliste Plateau and Broken Ridge escarpment, which were generated by the Kerguelen hotspot region.
- The Caribbean Plate became a separate plate by 90 Myr ago and continued overriding proto-Caribbean ocean crust.
- Back-arc extension related to slab rollback opened basins in the Black Sea and Caspian Sea and along the southern margin of Asia prior to the collision of India.

Two important geological events occurred at the end of the period from 70 to 65 Myr ago:

- The Deccan Traps volcanism began with enormous outpourings of basalt lava across western India, lasting several million years. These emissions are linked to global climate changes.
- The Chicxulub bolide impacted the Yucatan Peninsula, inciting chaos throughout the global environment and biosphere, leading to the Cretaceous–Paleogene mass extinction event.

Summary of palaeogeographical events during the Cretaceous

The Cretaceous saw the break-up of Pangaea and the destruction of land bridges between continents due to the opening of new ocean basins. The average sea level was *c.* 70 m higher than today, causing extensive flooding and epeiric seaways across continents.

Mountain building was limited because there were no major continent–continent collisions during the Cretaceous. Existing ranges like the Urals, the Transantarctic ranges, the Caledonides, and the Northern and Southern Appalachians persisted. Most uplift occurred along active Andean margins and newly rifted continental margins.

Sea-level highstands resulted from increased mid-ocean ridge length as a consequence of the break-up of Pangaea. There were no large ice caps. Small, ephemeral ice caps on Antarctica contributed to modest sea-level changes (*c.* 30 m).

In the earliest Cretaceous (145 Ma), Laurasia and Gondwana were still connected via island arcs such as the Greater Antilles. The Turgai Strait separated the land areas of Europe and Asia up until 110 Ma. North America was linked with Asia throughout the Cretaceous via the Beringia land bridge. During the Early Cretaceous, Greater India, Madagascar, Australia and Antarctica all comprised a single land-mass, East Gondwana.

As Pangaea rifted apart, Africa completely separated from South America in the late Albian at 105 Ma. During the Cenomanian (*c.* 95 Ma), Madagascar became a separate island as India rifted away. Antarctica and Zealandia began to rift away from Australia at that time.

The Tasman Gateway fully separated Australia and Antarctica by 85 Ma. The rifting of Zealandia created a submerged continental mass to the east of the Tasman Sea. India rapidly headed north. A high sea level during the mid-Cretaceous flooded all of the continents, dividing North America, Eurasia, South America and Africa into smaller landmasses.

Appalachia, Laramidia and Greater Greenland formed when North America flooded. Low Campanian sea levels at *c.* 75–70 Ma reconnected these landmasses briefly before the end-Cretaceous

regression. Land bridges like Beringia continued to link the northern continents.

Summary of palaeoclimatic events during the Cretaceous

The Early Cretaceous climate represented moderate 'in-between' conditions continuing the Late Jurassic cool phase. Global average temperatures were around 17°C based on a mix of climate indicators:

- Dropstones, glendonites and rare tillites at high latitudes showing cold winter conditions;
- however, also coal deposits and temperate forest biomes at higher latitudes; and
- dinosaurs and other temperate species migrations.

This suggests cold winters with seasonal sea ice but summers warm enough to support forests and mild temperatures. Oxygenated bottom waters prevented widespread ocean anoxia. The lack of black shales is striking compared to later Cretaceous OAEs.

A stepwise warming trend commenced in the late Barremian, culminating in the hot Cenomanian–Turonian interval 95–80 Myr ago. This stable, prolonged thermal maximum constitutes the Mid-Cretaceous–Paleogene Hothouse (MCPH):

The MCPH stages were:

Initial Early Cretaceous warming (128–118 Ma):

- Hauplatterton thermal event;
- Oceanic anoxic event 1a (OAE1a: Selli/Goguel). Aptian–Albian cold snapshot (116–109 Ma):
- Brief return of polar ice and oxic deep oceans.

Mid–Late Cretaceous sustained warmth (109–66 Ma):

- High but fluctuating temperatures, multiple OAEs.

The Aptian–Albian cold snap was marked by glendonites on Axel Heiberg Island and in the Eromanga Sea, signalling the return of cold polar bottom waters and ephemeral ice caps. Lasting for less than 10 Myr, this cool spell preceded sustained Cretaceous warmth.

Peak Cretaceous temperatures occurred during the Cenomanian–Turonian Thermal Maximum (CTTM: 94–93 Ma), which is considered to be the second warmest time in the Phanerozoic after the PTTM (250 Ma). Global average temperatures reached *c.* 28°C compared to *c.* 15°C today. Polar temperatures averaged 13°C and tropical temperatures exceeded 34°C. As a consequence, pole-to-equator thermal gradients were remarkably flat.

The CTTM highlights were:

- tropical ocean temperatures greater than 34°C;
- polar Temperatures of approximately 13°C, ice free;
- low pole-to-equator temperature gradient; and
- a global average temperature (GAT) of *c.* 28°C.

Warm Cretaceous temperatures were at least partially driven by the mid-Cretaceous superplume, which released immense volumes of CO₂ into the atmosphere. Intense weathering would have also delivered more nutrients to spur ocean productivity. Widespread anoxic conditions led to black shale deposition and the preservation of organic carbon (multiple OAE events).

The exact mechanisms behind the low pole-to-equator gradients and warm polar regions remain uncertain but are likely to have involved enhanced atmospheric and oceanic heat transport to high latitudes, while early computer simulations of climate had difficulty simulating such low pole-to-equator thermal gradients. Improvements in cloud and vegetation parameterizations have helped to reduce the discrepancy between simulation results and the geological record.

The Late Cretaceous witnessed a very gradual cooling trend, interrupted by brief warmth spikes. Temperatures remained relatively high, with no permanent polar ice caps. There is some evidence of ephemeral cooling events and even dropstones in the late Campanian and Maastrichtian but predominantly warm conditions continued. Multiple OAEs are associated with high ocean productivity and circulation changes.

This mostly stable, hot climate regime endured for nearly 80 Myr before dramatically terminating with the Chicxulub bolide impact 66 Myr ago. Temperatures plummeted to icehouse levels in the 'impact winter', resulting from sunlight-absorbing dust and aerosols. After a short interval (thousands of years?), warming resumed and continued through the Paleocene and Eocene. About 35 Myr ago the Cenozoic Ice House began, leading to our modern interglacial icehouse world.

In summary, the Cretaceous climate was typified by extreme warmth relative to modern conditions, with the CTTM representing peak Cretaceous heat. While the initiation, duration and ending of such hot climates remains puzzling, the geological record confirms meridional gradients much flatter than anything seen in the Cenozoic. Understanding the mix of continental positions, ocean gateways, atmospheric heat transport, polar vegetation and other variables that permitted low-latitude tropical and high-latitude polar warmth may help climate scientists grapple with anthropogenic global warming. Unlocking deep-time hothouse secrets can offer clues to where our climate system may be heading in the future.

Summary of Cretaceous rivers

The average Cretaceous river length was shortest (*c.* 2500 km) during the mid-Cretaceous sea-level highstand during the Cenomanian–Santonian (95–80 Ma). River length peaked around 5000 km during

the earliest Cretaceous (Berriasian–Valanginian, 145–140 Ma) when sea level was relatively low. Surprisingly, the number of major rivers (>250 km) remained fairly constant throughout the Cretaceous, averaging around 50 rivers during each stage regardless of the land area.

Climate exerts a strong control on river extent, with major river systems existing within the Ever-wet climates and Temperate Rainy belts. Occasionally, the simulated drainage patterns predict rivers in arid regions that should have been dry, like the proto-Congo during the Aptian.

Plate tectonics profoundly impacted Cretaceous river system geometries. Andean-style subduction zones created foredeep basins down which rivers flowed, like the ancient Mackenzie and Amur systems. Continental collisions during the Aptian diverted the Amur River eastwards after the Mongol–Okhotsk Ocean closed. Uplift related to the opening of the South Atlantic created drainage patterns that radiated away from eastern Brazil and west-central Africa.

Nearly half of the Earth's 25 longest modern rivers had Cretaceous precursors, including versions of the Nile, Amazon, Amur and Niger. Exceptions include systems created by later tectonics or areas that were flooded during the Cretaceous sea-level highstand. Intriguing Cretaceous rivers without modern equivalents flowed across now vanished basins and drainage pathways.

The speculative Cretaceous river systems provide a glimpse into the potential arrangements of fluvial regimes transporting sediments across ancient landscapes. Their geometries were dictated primarily by the elevations and climates of those prehistoric Earth surfaces.

Summary of Cretaceous ocean circulation

Ocean surface circulation is primarily wind-driven, with tropical easterlies and temperate westerlies pushing currents that are deflected polewards upon hitting continents due to the Coriolis force. This creates clockwise-rotating gyres in the northern hemisphere and counter-clockwise-gyres in the southern hemisphere.

During the Early Cretaceous, many of the modern continents were still joined together. A strong east-west-flowing Equatorial Current hit the east African coast and split north and south. The northern branch flowed along the southern Tethys for most of the Cretaceous until this sea narrowed in the Campanian.

In the south, a powerful current flowed west to east along the Indo-Australian coast of Gondwana from the Early Cretaceous until the Cenomanian–Turonian (95–90 Ma). After this time, cooling waters flowed northwards from Antarctica through the widening seaway between India and Australia.

There was never a strong connection between Tethys and the Central Atlantic due to narrow seaways and opposing wind patterns. Instead, two stable gyres occupied these oceans starting in the Aptian until the Campanian.

Additional key Cretaceous circulation features include:

- a clockwise Arctic gyre from 125 to 75 Ma;
- a counter-clockwise South Atlantic gyre developing by 90 Ma;
- throughflow between the Atlantic and Pacific from 115 to 65 Ma; and
- India beginning to block the Equatorial Current by 70 Ma.

In summary, Cretaceous circulation patterns followed basic wind-driven models but were heavily influenced by the changing configurations of oceans and continents as Pangaea fragmented. Key surface current pathways opened and closed during the Cretaceous, with stable gyres developing in ocean basins as they widened. The break-up of Gondwana resulted in cooling water exchanges between high southern latitudes and the Tethys by the mid-Cretaceous.

Summary of Cretaceous precipitation patterns

Cretaceous rainfall regimes share similarities with the modern climate system, dominated by a tropical Equatorial Ever-wet belt, strong western continent rainfall from temperate westerlies and eastern continent subtropical humid belts.

The Tropical Ever-wet belt persisted throughout the Cretaceous but at times was segmented by land-masses straddling the Equator. The Temperate Rainy belt impinged on western North and South America, Australia, and southern Africa. Subtropical humidity characterized eastern North America and Asia.

These overall patterns masked important shifts through the Cretaceous driven by continental motions across climate zones and the opening of new oceanic gateways (e.g. connection between the South and Central Atlantic). During the Early Cretaceous, prior to the opening of the South Atlantic, a sharp Sahel-like boundary developed across northern South America and north-central Africa.

As South Atlantic rifting progressed, southwest-ern Africa gained humidity from Atlantic sources during the Albian and Cenomanian. Northern continentality decreased with extensive flooding, enabling a through-going ever-wet tropical belt by the Cenomanian at 95 Ma. During the early and mid-Cretaceous, northeastern North America became wetter as it moved northwards out of the arid subtropics and into more humid warm, temperate latitudes. The increase in rainfall was also, in part, due to the widening of the Central Atlantic and the

increased transport of moisture into the North American continent.

India's initial location was in the southern arid belt. During the Early Cretaceous it moved southwards into the Temperate Rainy belt. India reversed direction in the mid-Cretaceous and by the Late Cretaceous its northward movement brought it into the region of subtropical monsoons. Australia similarly became wetter during its south to north traverse, ending the Cretaceous well within the Temperate Rainy belt.

In general, Cretaceous precipitation patterns recorded in the geological proxies are in good agreement with computer simulations of climate. Some mismatches occurred, however, with models underestimating subtropical rainfall in North Africa and regions of northern South America.

While robust similarities remain with modern rainfall zones, the Cretaceous saw dramatic continental-scale shifts in moisture transport as land-masses travelled across global climate belts in their tectonic voyages.

Discussion

Map projection

The reader may have noticed that most of the maps in this chapter use the same map projection, the equirectangular map projection. The equirectangular map projection is the simplest map projection; latitude and longitude are Cartesian coordinates, where latitude = y and longitude = x . For that reason, palaeolatitudes and palaeolongitudes can be read directly from the map. The main disadvantage of the equirectangular project is that it greatly distorts and exaggerates features at high latitudes. For example, the polar ice caps shown in [Figures 49–52](#) (145–130 Ma) appear relatively larger than they actually are ([Fig. 116](#)).

The most significant advantage of the equirectangular projection is that an equirectangular image can be easily mapped onto the surface of a sphere. This can be done using standard geographical information (GIS) software (e.g. ArcGIS™ or QGIS), or with the mapping software, G.Projector v. 3.2.3, developed by Robert B. Schmunk, NASA Goddard Institute for Space Studies. G.Projector allows users to make maps in over 130 map projections, including Mercator, Mollweide, Orthographic, Robinson and various polar projections. G.Projector was used to produce [Figure 116](#), as well as the maps in the [Supplementary material](#). It can be freely downloaded at <https://www.giss.nasa.gov/tools/gprojector/>

Supplementary materials

The reader, no doubt, has noticed the many references to 'Supplementary material' that are sprinkled

throughout this paper. In many, the text in this paper is simply a brief introduction to the wealth of cartographic and digital data that we are providing in the Supplementary material. One of the important goals of this paper is to provide the original digital data that were used to produce the various plate tectonic, palaeogeographical and palaeoclimatic maps cited here. We also provide ancillary materials such as animations and supplementary reports that may be of interest to the reader. Because of the limitations of the equirectangular projection, we have also provided versions of the principal figures in several complementary map projections (i.e. Mollweide, North and South Polar Orthographic, and Robinson). For easy reference, the Supplementary material that are mentioned throughout this chapter have been compiled into a single, comprehensive table ([Table 14](#)).

Conclusions

Some conclusions about the Cretaceous

We can draw several important conclusions about the Cretaceous from the synthesis presented in this paper. It is clear that the tectonics, geography and climate of the Cretaceous were very different to the modern world and very different to the last 35 Myr of the Cenozoic.

During the Late Cenozoic, the continents were separated by wide ocean basins. In contrast, at the start of the Cretaceous the supercontinent of Pangaea had just begun to break apart and only a few small ocean basins separated Laurasia (Eurasia and North America), West Gondwana (South America, Africa and Arabia) and East Gondwana (Madagascar, India, Antarctica, Australia and Zealandia).

The Late Cenozoic was a time characterized by multiple continent–continent collisions and extensive mountain building. In contrast, there were no significant continent–continent collisions during the Cretaceous and the continents were low lying and easily flooded.

Both the late Cenozoic and the Cretaceous had large ocean basins (Pacific and Panthalassic) covering more than half of the surface area of the globe. The Panthalassic Ocean was significantly larger (c. 20%) than the Pacific Ocean, and contained numerous continental and oceanic island arcs (Wrangellia, North Slope, Okhotsk–Bering Sea, Oman, Ladakh–Gangesi, Philippines and Zealandia). Several of these island arcs collided with adjacent continents during the Cretaceous.

The transition from a Pangaea-like configuration to a more dispersed continental configuration had important effects on the global sea level. During the Early Cretaceous, the length of mid-ocean ridges and subduction zones was approximately equal. As a

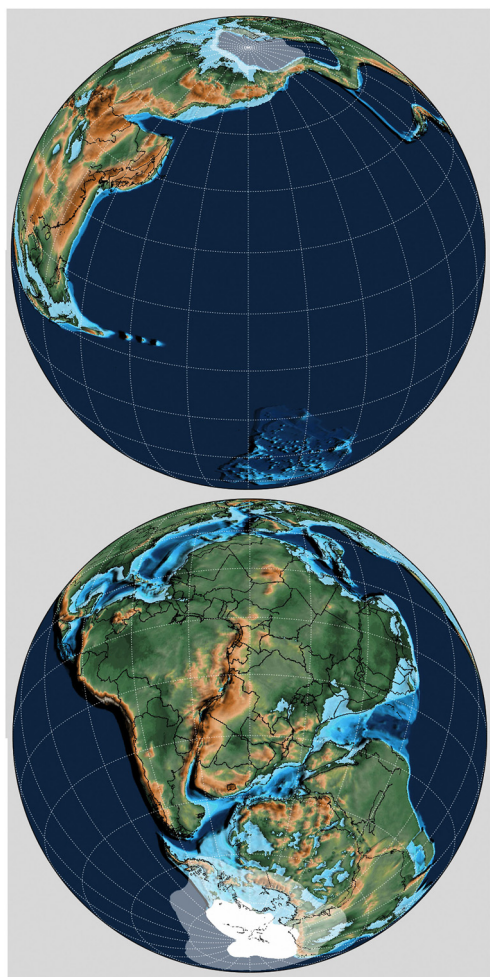


Fig. 116. Earliest Cretaceous (145 Ma) polar orthographic projection illustrating the actual size of the south polar ice cap ($c. 4 \times 10^6 \text{ km}^2$).

consequence, ridges had to spread relatively quickly to keep up with the amount of oceanic lithosphere removed by subduction. Over time, these high rates of spreading produced large areas of young, high-standing ocean floor that displaced water out of the ocean basins and onto the continents. The resulting continental flooding was amplified by the fact that as the continents rifted apart, the new continental rifts were transformed into young ocean basins. The oceanic lithosphere in these young ocean basins was thermally elevated, which further boosted sea level. Sea level was highest during the mid-Cretaceous (90–80 Ma), with a subsidiary peak $c. 120 \text{ Myr}$ ago (early Aptian).

We can now conclude that, overall, the Cretaceous was much warmer than the Late Cenozoic

($>10^\circ\text{C}$ warmer). The Cenomanian–Turonian Thermal Maximum (CTTM: 95–80 Ma) achieved temperatures (28°C) that were only exceeded by the Permo-Triassic Thermal Maximum (PTTM: 32°C). These very warm times caused several episodes of oceanic anoxia (OAEs), and high temperatures in equatorial regions sometimes made terrestrial and shallow-marine ecosystems uninhabitable (temperatures $>40^\circ\text{C}$). This is unlike anything we have seen in the last 35 Myr and may presage the eventual results of man-made global warming.

There were, however, times during the Early Cretaceous when the climate was similar to the late Cenozoic. During parts of the Early Cretaceous there was a small, permanent ice cap on Antarctica. Although half the size of Antarctica ($c. 4 \times 10^6 \text{ km}^2$), the waxing and waning of this ice cap contributed to changes in the global sea level ($c. 30 \text{ m}$). During the Early Cretaceous there were cool conditions in both hemispheres at temperate latitudes ($>55^\circ \text{ N}$ and S), as evidenced by dropstones, glendonites, rare tillites and temperate forest biomes.

How well do we know the Cretaceous?

It depends. If we subdivide our knowledge of the Cretaceous into five categories: time control, life, climate, tectonics and geography, we can give very high marks to the palaeontologists and stratigraphers who, during the last 200 years, have assembled a detailed description of the evolution of life and the correlation of Cretaceous rock units (Gradstein *et al.* 2020). The grades we give to the climatologists, tectonicists and palaeogeographers are more mixed.

Supercomputer models of palaeoclimate are now extremely precise and give excellent results for the modern world and the recent global ice age but the climate simulations still seem to struggle when modelling ancient hothouse worlds. There has been a long-running debate as to whether the Cretaceous was a hothouse world with warm polar regions or, as early climate simulations have suggested, was characterized by cool temperate regions and undetected polar ice caps. This controversy has largely been resolved by incremental improvements to the climate models that have resulted in warmer polar regions. With more lithological indicators of climate, we can now make more nuanced interpretations of the changing Cretaceous climates. The Cretaceous was neither a hothouse nor a mild icehouse but, rather, a combination of both: cool early on (145–130 Ma), warming (125–105 Ma), then very warm (100–85 Ma) and mild towards the end (80–67 Ma), with a chilling punctuation mark at the Cretaceous–Paleogene boundary (66 Ma) as a consequence of the end-Cretaceous impact winter.

Our confidence in the plate tectonic story for the Cretaceous is very mixed. Overall, the

Table 14. Contents of Supplementary Materials

Part 1. Phanerozoic Content (540 Ma–0 Ma) <https://doi.org/10.5281/zenodo.10659112>

1. Text Items

- a. Annotated Bibliography of Paleogeographic Maps.docx
- b. A Brief History of Global Plate Tectonic Models.pdf
- c. The Rules of Plate Tectonics
- d. How to build a 3D palaeogeographic map (tutorials)
- e. A pdf of this paper as well as [Scotese \(2021\)](#) and [Scotese et al. \(2021\)](#)

2. Animations

- a. Plate Tectonic: ‘Plate Tectonics, 1.5 by–Today: Ancient Oceans and Continents’, <https://youtu.be/IlmwyAbczog>
- b. Plate Tectonic: ‘Plate Tectonics, 1.5 by–Today: Ancient Oceans and Continents’, (with continents and oceans labelled) <https://youtu.be/AsCYZ-k0uc>
- c. Palaeogeographic: ‘Plate Tectonics, Paleogeography, and Ice Ages’, <https://youtu.be/UevnAq1MTVA>
- d. Palaeogeographic: ‘Plate Tectonics, Paleogeography, and Ice Ages (dual hemispheres)’, <https://youtu.be/bzvOMee9D1o>
- e. Palaeoclimate: ‘Phanerozoic Global Temperature’, <https://youtu.be/FF3Mz8ZFyh8>
- f. Palaeoclimate: ‘Phanerozoic Rainfall’, <https://youtu.be/88cO9ba0DR8>
- g. Köppen belt evolution during the Phanerozoic ([Scotese et al. 2021](#)), <https://youtu.be/DGf5pZMkjA0>

3. Global Plate Tectonic Model

- a. Rotation model (.rot) and static polygons for plate tectonic reconstructions (v.19o_r1d)
- b. Rotation model (.rot) and static polygons for paleogeographic and paleoclimatic reconstructions (v.m17v2d3_81_v18e)

4. Maps (Equirectangular, Mollweide, Robinson, and North & South Orthographic Polar projections)

- a. Plate Tectonic Maps, 0–1.5 by (see [Figure 2A](#))
- b. Palaeogeographic Maps (with 3D relief, modern coastlines and political boundary overlays, .jpg), 0–750 Ma (see [Figure 2B](#))
- c. Palaeogeographic Maps (no overlays, .bmp), 0–750 Ma
- d. Palaeotemperature Maps, 0–540 Ma ([Valdes et al. 2021](#))
- e. Palaeorainfall Maps, 0–540 Ma ([Valdes et al. 2021](#))
- f. Köppen Maps, 0–540 Ma ([Scotese et al. 2021](#))
- g. Tectonic Map of the World (see [Figure 8](#))
- h. Modern Coastlines & Political Boundaries
- i. Lithologic Indicators for Climate Maps ([Boucot et al. 2009](#))

5. PalaeoDEMs (i.e. palaeo-Digital Elevation Model)

- a. PalaeoDEM (3601×1801) netcdf (nc)
- b. PalaeoDEM (361×181) (csv)b. text format (.csv), 1°×1° resolution
- c. Index to Elevation_wRGB.csv
- d. PBDB test of PaleoDEMs.pdf
- e. Software to convert colour map (bmp) to netcdf (nc)

6. Palaeoclimate Digital Data Files

- a. Mean Annual Temperatures
- b. Mean Annual Precipitation
- c. [Boucot et al. \(2013\)](#) Lithological Indicators of Climate

7. Miscellaneous Diagrams

- a. High resolution figures
- b. Tectonic tree diagram
- c. Pole to equator temperature gradient diagrams
- d. Phanerozoic_Temperature_Poster.jpg
- e. Phanerozoic Pole to Equator Temperature Gradient Summary Diagram.png
- f. Phanerozoic CO₂ estimated from Temperature.png
- g. Comparison of Scotese and Valdes Heat Maps.jpg
- h. CO₂ versus Temperature

8. Tables and Spreadsheets

- a. Phanerozoic Paleotemperature Tables ([Scotese et al. 2021](#))
- b. Phanerozoic Temperatures ([Scotese et al. 2021](#)).xlsx
- c. Phanerozoic_Pole_to_Equator_Temperatures.csv
- d. CO₂_vs_Temperature_v24213.xlsx
- e. Snow and Ice Limits.xlsx

- f. Average_Elevation.xlsx
- g. SeaLevel_from_Continental_Flooding.xlsx
- h. Phanerozoic Eustasy Comparison.xlsx
- i. River_Flow_Stats_All.xlsx
- j. River Flow Stats.xlsx

9. PALEOMAP Paleomagnetic Database

- a. PALEOMAP Paleopole Database, 0–1.5 by (Elling, 2022).csv
- b. APW Paths, 0–1.5 by (Reese, 2022).xlsx. Spreadsheet with list of palaeopoles used to calculate Cretaceous Global Mean Poles (Elling, 2022)
- c. Global Mean Pole Plots (05 Ma_150 Ma)

Part 2. Cretaceous Content (145 Ma–65 Ma) <https://doi.org/10.5281/zenodo.10659104>

1. Text Items

- a. Annotated bibliography of cretaceous paleogeographic sources
- b. The Cretaceous World_(text only)

2. Animations

- a. Plate Tectonics 200 Ma to Today.mp4b.
- b. Palaeoclimate animations (065 Ma KT)
- c. Palaeoclimate animations (090 Ma CT)
- d. Palaeoclimate animations (100 Ma Albian)
- e. Palaeoclimate animations (120 Ma Aptian)
- f. Palaeoclimate animations (140 Ma Berriasian)

3. Maps (Equirectangular, Mollweide, Robinson, and North & South Orthographic Polar projections)

- a. Plate Tectonic Maps (Regional- jpg & svg)
- b. Cretaceous Palaeogeographic Maps (various projections; png)
- c. Palaeogeographic Maps (no overlays; bmp)
- d. Palaeogeographic Maps with Rivers
- e. Palaeo-Köppen Maps with Rivers (ai & jpg)
- f. Palaeorainfall Maps
- g. Palaeoceanic Circulation Maps
- h. Palaeo-Temperature Maps
- i. 3D Basemaps with Coastlines & Political Boundaries

4. PalaeoDEMs (i.e. palaeo-Digital Elevation Model)

- a. PalaeoDEM (3601 × 1801) netcdf (nc)
- b. PalaeoDEM text format (.csv), 1° × 1° resolution
- c. Index to Elevation_wRGB.csv
- d. Software to convert colour map (bmp) to netcdf (nc)

5. Palaeoclimate Digital Data Files

- a. Palaeotemperature (grids & lists)
- b. Palaeo-Rainfall (csv & nc)
- c. Phanerozoic Global Temperature (DRAFT)

6. Miscellaneous Diagrams

- a. Pole_to_Equator_Temperature_Gradient (png)
- b. Midocean_Rift_vs_Subduction_Zone_Length.png
- c. River_Length_&_Numbers.png
- d. Global_Tropical_Deep_Sea_&_Polar_Temperatures.jpg

7. Tables and Spreadsheets

- a. Tables with Cretaceous information
- b. Cretaceous_Temperatures.xlsx
- c. Cretaceous_Rivers.xlsx

8. PALEOMAP Paleomagnetic Database

- a. Cretaceous Global Mean Pole Plots

palaeomagnetic record for the Cretaceous is good and we can place the continents within 5° of their correct latitudes. The plate tectonic development of the intra-Pangaeian ocean basins (Atlantic and Indian) is well documented and precise. The plate tectonic history of the Tethys Ocean, however, is little more than an educated guess. Our understanding

of the plate tectonic development of the vast extra-Pangaeian, Pacific–Panthalassic ocean basin degrades rapidly as we go back through time. We can reimagine subducted ocean floor with some confidence back to the mid-Cretaceous (84 Ma; Chron 34); prior to that time, all plate tectonic reconstructions in the vast Panthalassic Ocean are largely guesswork.

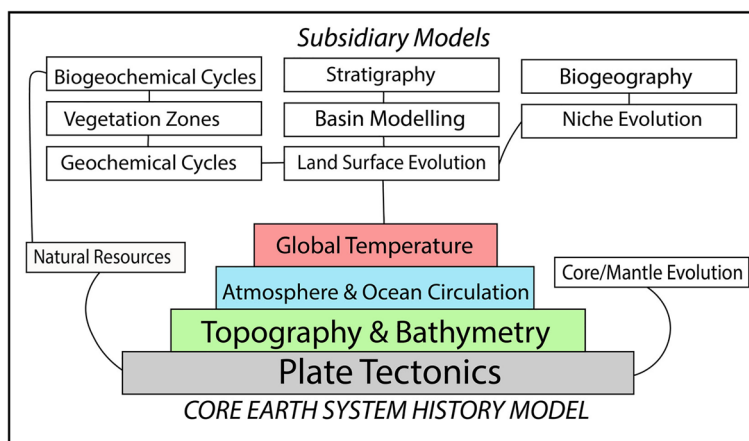


Fig. 118. The Earth system history machine.

exploration databases and built 3D stratigraphic models covering the globe. Immense amounts of high-resolution, digital stratigraphic data are now on hand. So what does the future hold?

The task before us is two-fold. First, a new Earth system history ‘Library of Alexandria’ must be built from this great volume of digital Earth system history data to preserve it for future generations and, more importantly, to create a comprehensive, coherent and authoritative digital data source for the emerging artificial intelligence systems (e.g. GPT5). The Earth sciences – in particular, geochronology, geochemistry, palaeoclimate, tectonics, stratigraphy and palaeontology – should begin to build a large language model (LLM) dedicated to helping Earth scientists unravel the long and complex history of the Earth.

The second task, although daunting, is to use this Earth system history database and LLM to build an ‘Earth system history machine’ (Fig. 118). This Earth System History Machine, with the help of AI, will dynamically simulate the plate tectonic, palaeogeographical, sedimentological, palaeoceanographic, geochemical and palaeoclimatic evolution of the Earth from its beginnings to the present and forward into the future. Numerous researchers, around the globe, are now actively working towards this lofty goal. They include researchers and students at the PALEOMAP Project (Northwestern University), EarthByte (University of Sydney), CEED (Norway), University of Geneva, University of Chicago, Leeds University, Chronosphere Project (Erlangen), University of Bristol, Texas A&M University, NMNH, DDE Project, Purdue University, Chinese Academy of Sciences, Peking University, University of Geosciences (Wuhan), Nanjing University, Paleobiology Database, Macrostrat (University of Wisconsin), Utrecht University, University of

Western Australia, CNRS, ETH, University of Lisbon and many others. This research should be encouraged and supported because understanding how the Earth system has evolved in the past will give us the best opportunity to understand the present-day workings of the Earth system, as well as tackle future challenges. As T.S. Eliot wrote (in *Little Gidding*):

We shall not cease from exploration

And the end of all our exploring

Will be to arrive where we started

And know the place for the first time

Eliot (1943).

Acknowledgements CRS received support to produce the maps in the Paleogeographical Atlas from the PALEOMAP Project industrial consortium (2003–13), and would like to thank innumerable friends, mentors and enthusiastic supporters through the years, in particular A.M. Ziegler, W.S. McKerrow, R. van der Voo, S. Snelson, J. Westrich, P. Untermeier, C.P. Summerhayes, and A.J. Boucot. Alexander Tenesaca helped with the preparation of some of the figures. Malcolm Hart, Michael Wagreich, Irek Walaszczyk and Rachael Kriefman provided valuable critiques and corrections. Special thanks to Phyllis Richmond for correcting grammar, clarifying prose and corralling verbiage. This chapter is dedicated to the life-long work and research in the Cretaceous period of Erle G. Kauffman, Roger L. Larson, Bruce W. Sellwood and Robert A. Spicer.

Competing interests The authors declare that they have no known competing financial interests or personal relationships that could have appeared to influence the work reported in this paper.

Author contributions CRS: conceptualization (lead), writing – original draft (lead), writing – review & editing (lead); CV: writing – original draft (supporting); LB: writing – original draft (supporting); RPE: writing – original draft (supporting); ATK: writing – original draft (supporting).

Funding ATK assembled the online Supplementary material and was supported by the Deutsche Forschungsgemeinschaft (Ko 5382/2-1).

Data availability The datasets generated during and/or analysed during the current study are available in the Zenodo repository, <https://doi.org/10.5281/zenodo.10659112> and <https://doi.org/10.5281/zenodo.10659104>.

References

- Advokaat, E.L. and van Hinsbergen, D.J.J. 2024. Finding Argoland: Reconstructing a microcontinental archipelago from the SE Asian accretionary orogen. *Gondwana Research*, **128**, 161–263, <https://doi.org/10.1016/j.gr.2023.10.005>
- Ahlberg, A., Herman, A.B., Raikevich, M., Rees, A. and Spicer, R. 2002. Enigmatic Late Cretaceous high paleolatitude limestones in Chukotka, northeasternmost Asia. *GFF*, **124**, 197–199, <https://doi.org/10.1080/11035890201244197>
- Algeo, T.J. and Selslavinsky, K.B. 1995. Reconstructing eustasy and epeirogenic trends from Paleozoic continental flooding records. In: Haq, B.U. (ed.) *Sequence Stratigraphy and Depositional Response to Eustatic, Tectonic and Climate Forcing*. Kluwer Academic, Dordrecht, The Netherlands, 209–246.
- Ali, J.R. and Krause, D.W. 2011. Late Cretaceous bioconnections between Indo-Madagascar and Antarctica: refutation of the Gunnerus Ridge causeway hypothesis. *Journal of Biogeography*, **38**, 1855–1872, <https://doi.org/10.1111/j.1365-2699.2011.02546.x>
- Allaby, M. and Lovelock, J. 1983. *The Great Extinction, Paladin*. Granada Publishing, London.
- Alley, N.F. and Frakes, L.A. 2003. First known Cretaceous glaciation: Livingstone Tillite Member of the Cadna-owie Formation. *Australian Journal of Earth Sciences*, **50**, 139–144, <https://doi.org/10.1046/j.1440-0952.2003.00984.x>
- Alroy, J., Aberhan, M. et al. 2008. Phanerozoic trends in the global diversity of marine invertebrates. *Science*, **321**, 97–100, <https://doi.org/10.1126/science.1156963>
- Alsenz, H., Regnery, J. et al. 2013. Sea surface temperature record of a Late Cretaceous tropical southern Tethys upwelling system. *Palaeogeography, Palaeoclimatology, Palaeoecology*, **392**, 350–358, <https://doi.org/10.1016/j.palaeo.2013.09.013>
- Alvarez, L.W., Alvarez, W., Asaro, F. and Michel, H.V. 1980. Extraterrestrial cause for the Cretaceous–Tertiary extinction. *Science*, **208**, 1095–1107, <https://doi.org/10.1126/science.208.4448.1095>
- Antretter, M. 2001. *Moving Hotspots – Evidence from Paleomagnetism and Modeling*. PhD thesis, Ludwig-Maximilians-Universität München, Munich, Germany, https://edoc.ub.uni-muenchen.de/427/1/Antretter_Maria.pdf
- Archibald, J.D. 1996. *Dinosaur Extinction and the End of an Era: What the Fossils Say*. Columbia University Press, New York.
- Artemieva, I. 2006. Global $1^\circ \times 1^\circ$ thermal model TC1 for the continental lithosphere: Implications for lithosphere secular evolution. *Tectonophysics*, **416**, 245–277, <https://doi.org/10.1016/j.tecto.2005.11.022>
- Arthur, M.A. and Sageman, B.B. 1994. Marine black shales: Depositional mechanisms and environments of ancient deposits. *Annual Review of Earth and Planetary Sciences*, **22**, 499–552, <https://doi.org/10.1146/annurev.earth.22.050194.002435>
- Audley-Charles, M.G. 1983. Reconstruction of eastern Gondwanaland. *Nature*, **306**, 48–50, <https://doi.org/10.1038/306048a0>
- Audley-Charles, M.G. 1984. Cold Gondwana, warm Tethys, and Tibetan Lhasa block. *Nature*, **310**, 165, <https://doi.org/10.1038/310165a0>
- Audley-Charles, M.G. 1988. Evolution of the southern margin of Tethys (North Australian region) from early Permian to late Cretaceous. *Geological Society, London, Special Publications*, **37**, 79–100, <https://doi.org/10.1144/GSL.SP.1988.037.01.07>
- Baatsen, M., van Hinsbergen, D.J.J., von der Heydt, A.S., Dijkstra, H.A., Sluijs, A., Abels, H.A. and Bijl, K. 2015. A generalised approach for reconstructing geographical boundary conditions for palaeoclimate modeling. *Climate of the Past Discussions*, **11**, 4917–4942, <https://doi.org/10.5194/cpd-11-4917-2015>
- Bakker, R.T. 1986. *The Dinosaur Heresies: New Theories Unlocking the Mystery of the Dinosaurs and Their Extinction*. Morrow, New York.
- Bakker, R.T. 1995. *Raptor Red*. Bantam Books, New York.
- Bao, X.J. and Hu, Y.Y. 2024. Quantitative estimation of global mean precipitation throughout the Phanerozoic era. *Science China Earth Sciences*, **67**, 1616–1624, <https://doi.org/10.1007/s11430-023-1263-x>
- Barker, P.F. and Hill, I.A. 1981. Back-arc extension in the Scotia Sea. *Philosophical Transactions of the Royal Society of London, Series A: Mathematical, Physical and Engineering Sciences*, **300**, 249–262, <https://doi.org/10.1098/rsta.1981.0063>
- Barral, A., Gomez, B., Legendre, S. and Lécuyer, C. 2017. Evolution of the carbon isotope composition of atmospheric CO₂ throughout the Cretaceous. *Palaeogeography, Palaeoclimatology, Palaeoecology*, **471**, 40–47, <https://doi.org/10.1016/j.palaeo.2017.01.034>
- Barrera, E. and Johnson, C. (eds) 1999. *Evolution of the Cretaceous Ocean–Climate System*. Geological Society of America Special Papers, **332**, <https://doi.org/10.1130/SPE332>
- Barron, E.J. 1983. A warm, equable Cretaceous: The nature of the problem. *Earth-Science Reviews*, **19**, 305–335, [https://doi.org/10.1016/0012-8252\(83\)90001-6](https://doi.org/10.1016/0012-8252(83)90001-6)
- Barron, E.J. 1984. Climatic implications of the variable obliquity explanation of Cretaceous–Paleogene high-latitude floras. *Geology*, **12**, 595–598, [https://doi.org/10.1130/0091-7613\(1984\)12<595:CIOTVO>2.CO;2](https://doi.org/10.1130/0091-7613(1984)12<595:CIOTVO>2.CO;2)

- Barron, E.J. and Washington, W.M. 1982a. Atmospheric circulation during warm geologic periods: Is the equator-to-pole surface-temperature gradient the controlling factor? *Geology*, **10**, 633–636, [https://doi.org/10.1130/0091-7613\(1982\)10<633:ACDWGP>2.0.CO;2](https://doi.org/10.1130/0091-7613(1982)10<633:ACDWGP>2.0.CO;2)
- Barron, E.J. and Washington, W.M. 1982b. Cretaceous climate: A comparison of atmospheric simulations with the geologic record. *Palaeogeography, Palaeoclimatology, Palaeoecology*, **40**, 103–133, [https://doi.org/10.1016/0031-0182\(82\)90086-4](https://doi.org/10.1016/0031-0182(82)90086-4)
- Barron, E.J. and Washington, W.M. 1984. The role of geographic variables in explaining paleoclimates: Results from Cretaceous climate model sensitivity studies. *Journal of Geophysical Research: Atmospheres*, **89**, 1267–1279, <https://doi.org/10.1029/JD089iD01p01267>
- Barron, E.J. and Washington, W.M. 1985. Warm Cretaceous climates: High atmospheric CO₂ as a plausible mechanism. *American Geophysical Union Geophysical Monograph Series*, **32**, 546–553, <https://doi.org/10.1029/GM032p0546>
- Barron, E.J., Thompson, S.L. and Schneider, S.H. 1981. An ice-free Cretaceous? Results from climate model simulations. *Science*, **212**, 501–508, <https://doi.org/10.1126/science.212.4494.501>
- Barron, E.J., Peterson, W.H., Pollard, D. and Thompson, S. 1993. Past climate and the role of ocean heat transport: Model simulations for the Cretaceous. *Paleoceanography*, **8**, 785–798, <https://doi.org/10.1029/93PA02227>
- Barron, E.J., Fawcett, P.J. and Peterson, W.H. 1995. A ‘simulation’ of mid-Cretaceous climate. *Paleoceanography*, **10**, 953–962, <https://doi.org/10.1029/95PA01624>
- Bebout, G.E., Scholl, D.W., Kirby, S.H. and Platt, J.P. (eds) 1996. *Subduction: Top to Bottom*, American Geophysical Union Geophysical Monograph Series, **96**.
- Beccaluva, L., Bianchini, G. and Wilson, M. (eds) 2011. *Volcanism and Evolution of the African Lithosphere*. Geological Society of America Special Papers, **478**, <https://doi.org/10.1130/SPE478>
- Beerling, D.J. and Woodward, F.I. 2001. The Cretaceous. In: *Vegetation and the Terrestrial Carbon Cycle: Modelling the First 400 Million Years*. Cambridge University Press, Cambridge, UK, 183–237.
- Beerling, D.J., Fox, A., Stevenson, D.S. and Valdes, P.J. 2011. Enhanced chemistry-climate feedbacks in past greenhouse worlds. *Proceedings of the National Academy of Sciences of the United States of America*, **108**, 9770–9775, <https://doi.org/10.1073/pnas.1102409108>
- Benton, M.J. 2003. *When Life Nearly Died: The Greatest Mass Extinction of All Time*. Thames and Hudson, London.
- Berggren, W.A. and Van Couvering, J.A. (eds) 1984. *Catastrophes in Earth History: The New Uniformitarianism*. Princeton University Press, Princeton, NJ.
- Bernardi, M., Gianolla, P., Petti, F.M., Mietto, P. and Benton, M.J. 2018. Dinosaur diversification linked with the Carnian Pluvial Episode. *Nature Communications*, **9**, 1499, <https://doi.org/10.1038/s41467-018-03996-1>
- Berner, R.A. 1994. GEOCARB II: A revised model of atmospheric CO₂ over Phanerozoic time. *American Journal of Science*, **294**, 56–91, <https://doi.org/10.2475/ajs.294.1.56>
- Berner, R.A. 2004. *The Phanerozoic Carbon Cycle: CO₂ and O₂*. Oxford University Press, New York.
- Berner, R.A. and Kothavala, Z. 2001. Geocarb III: A revised model of atmospheric CO₂ over Phanerozoic time. *American Journal of Science*, **301**, 182–204, <https://doi.org/10.2475/ajs.301.2.182>
- Berner, R.A., Lasaga, A.C. and Garrels, R.M. 1983. The carbonate silicate geochemical cycle and its effect on atmospheric carbon dioxide over the past 100 million years. *American Journal of Science*, **283**, 641–683, <https://doi.org/10.2475/ajs.283.7.641>
- Bice, K.L. and Norris, R.D. 2002. Possible atmospheric CO₂ extremes of the middle Cretaceous (late Albian to Turonian). *Paleoceanography*, **17**, 22-1–22-17, <https://doi.org/10.1029/2002PA000778>
- Bice, K.L., Bralower, T.J., Duncan, R.A., Huber, B.T., Leckie, R.M. and Sageman, B.B. 2002. Cretaceous climate–ocean dynamics: future directions for IODP. Presented at The Nature Place: a workshop sponsored by JOI/USSSP and NSF, 14–17 July 2002, Florissant, Colorado, USA.
- Bice, K.L., Huber, B.T. and Norris, R.D. 2003. Extreme polar warmth during the Cretaceous greenhouse? Paradox of the late Turonian $\delta^{18}\text{O}$ record at Deep Sea Drilling Project Site 511. *Paleoceanography*, **18**, 1013–1029, <https://doi.org/10.1029/2002PA000848>
- Biddle, K.T. (ed.) 1991. *Active Margin Basins*. AAPG Memoirs, **52**, <https://doi.org/10.1306/M52531>
- Bijl, P.K., Schouten, S., Sluijs, A., Reichert, G.J., Zachos, J.C. and Brinkhuis, H. 2009. Early Palaeogene temperature evolution of the southwest Pacific Ocean. *Nature*, **461**, 776–779, <https://doi.org/10.1038/nature08399>
- Bird, J.M. and Dewey, J.F. 1970. Lithosphere plate–continental margin tectonics and the evolution of the Appalachian orogen. *Geological Society of America Bulletin*, **81**, 1031–1060, [https://doi.org/10.1130/0016-7606\(1970\)81\[1031:LPMTAT\]2.0.CO;2](https://doi.org/10.1130/0016-7606(1970)81[1031:LPMTAT]2.0.CO;2)
- Blakey, R.C. 2002. *Global Paleogeography, Rectilinear Projection*. Colorado Plateau Geosystems, Inc., Flagstaff, AZ.
- Blakey, R.C. 2008. Gondwana paleogeography from assembly to breakup – A 500 m.y. odyssey. *Geological Society of America Special Papers*, **441**, 1–28, [https://doi.org/10.1130/2008.2441\(01\)](https://doi.org/10.1130/2008.2441(01))
- Blakey, R.C. 2011. *Paleogeography of Europe*. Colorado Plateau Geosystems, Inc., Flagstaff, AZ.
- Blakey, R.C. 2013. *Key Time Slices of North American Geologic History*. Colorado Plateau Geosystems, Inc., Flagstaff, AZ.
- Bohor, B.F., Triplehorn, D.M., Nichols, D.J. and Millard, H.T. 1987. Dinosaurs, spherules, and the ‘majic’ layer: A new K–T boundary clay site in Wyoming. *Geology*, **15**, 896–899, [https://doi.org/10.1130/0091-7613\(1987\)15<896:DSATML>2.0.CO;2](https://doi.org/10.1130/0091-7613(1987)15<896:DSATML>2.0.CO;2)
- Bond, D.P.G. and Grasby, S.E. 2017. On the causes of mass extinctions. *Palaeogeography, Palaeoclimatology, Palaeoecology*, **478**, 3–29, <https://doi.org/10.1016/j.palaeo.2016.11.005>
- Bond, D.P.G. and Wignall, P.B. 2014. Large igneous provinces and mass extinction: An update. *Geological Society of America Special Papers*, **505**, 29–55, [https://doi.org/10.1130/2014.2505\(02\)](https://doi.org/10.1130/2014.2505(02))
- Boschman, L.M. 2022. Andean mountain building since the Late Cretaceous: A paleoelevation reconstruction. *Earth-Science Reviews*, **220**, 103640, <https://doi.org/10.1016/j.earscirev.2021.103640>

- Boucot, A.J., Xu, C., Scotese, C.R. and Fan J.X., 2009. *Global Reconstruction of Phanerozoic Climate*. Science Press, Beijing.
- Boucot, A.J., Xu, C. and Scotese, C.R. 2013. *Phanerozoic Paleoclimate: An Atlas of Lithologic Indicators of Climate*. SEPM Concepts in Sedimentology and Paleontology, **11**. Society for Sedimentary Geology, Tulsa, OK.
- Boutelier, D. and Cruden, A. 2013. Slab rollback rate and trench curvature controlled by arc deformation. *Geology*, **41**, 911–914, <https://doi.org/10.1130/G34338.1>
- Bozhko, N.A. and Khain, V.E. 1987. *Gondwana Paleotectonic Maps*. Ministry of Higher and Secondary Special Education of the USSR, and Ministry of Geology, USSR, produced by the Geological Complex of Central Regions of the USSR.
- Bradley, D.C. 2008. Passive margins through Earth history. *Earth-Science Reviews*, **91**, 1–26, <https://doi.org/10.1016/j.earscirev.2008.08.001>
- Bradley, D.C. 2011. Secular trends in the geologic record and the supercontinent cycle. *Earth-Science Reviews*, **1008**, 16–33, <https://doi.org/10.1016/j.earscirev.2011.05.003>
- Brady, E.C., DeConto, R. and Thompson, S.L. 1998. Deep-water formation and poleward ocean heat transport in the warm climate extreme of the Cretaceous (80 Ma). *Geophysical Research Letters*, **25**, 4205–4208, <https://doi.org/10.1029/1998GL900072>
- Brass, G.W., Southam, J.R. and Peterson, W.H. 1982. Warm saline bottom water in the ancient ocean. *Nature*, **296**, 620–623, <https://doi.org/10.1038/296620a0>
- Brassell, S.C. 2009. Steryl ethers in a Valanginian claystone: molecular evidence for cooler waters in the central Pacific during the Early Cretaceous? *Palaeogeography, Palaeoclimatology, Palaeoecology*, **282**, 45–57, <https://doi.org/10.1016/j.palaeo.2009.08.009>
- Briggs, J.C. 1987. *Biogeography and Plate Tectonics*. Developments in Palaeontology and Stratigraphy, **10**. Elsevier, Amsterdam.
- Brown, J.H. and Lomolino, M.V. 1998. *Biogeography*. 2nd edn. Sinauer Associates, Sunderland, MA.
- Brusatte, S. 2018. *The Rise and Fall of the Dinosaurs: New History of Their Lost World*. William Morrow, New York.
- Bryan, S.E., Ewart, A., Stephens, C.J., Parianos, J. and Downes, P.J. 2000. The Whitsunday volcanic province, central Queensland, Australia: lithological and stratigraphic investigations of a silicic-dominated large igneous province. *Journal of Volcanology and Geothermal Research*, **99**, 55078.
- Buffan, L., Jones, L.A., Domeier, Scotese, C.R., Zahirovic, S. and Varela, S. 2023. Mind the uncertainty: Global plate model choice impacts deep-time palaeobiological studies. *Methods in Ecology and Evolution*, **14**, 3007–3019, <https://doi.org/10.1111/2041-210X.14204>
- Buffler, R.T. and Sawyer, D.S. 1983. Distribution of crust and early history, Gulf of Mexico basin. *Gulf Coast Association of Geological Society Transactions*, **35**, 334–344.
- Bullard, E., Everett, J.E. and Smith, A.G. 1965. The fit of the continents around the Atlantic. *Philosophical Transactions of the Royal Society of London, Series A: Mathematical, Physical and Physical Sciences*, **258**, 41–51, <https://doi.org/10.1098/rsta.1965.0020>
- Burchfiel, B.C., Cowan, D.S. and Davis, G.A. 1992a. Tectonic overview of the Cordilleran orogen in the western United States. In: Burchfiel, B.C., Lipman, P.W. and Zoback, M.L. (eds) *The Cordilleran Orogen: Conterminous U.S. Decade of North American Geology*, The Geology of North America, **G-3**. Geological Society of America, Boulder, CO, 407–480.
- Burchfiel, B.C., Lipman, P.W. and Zoback, M.L. (eds) 1992b. *The Cordilleran Orogen: Conterminous U.S. Decade of North American Geology*, The Geology of North America, **G-3**. Geological Society of America, Boulder, CO.
- Burg, J.P. 2011. The Asia–Kohistan–India collision: Review and discussion. In: Brown, D. and Ryan, P.D. (eds) *Arc–Continent Collision*. Frontiers in Earth Sciences. Springer, Berlin, 279–309, https://doi.org/10.1007/978-3-540-88558-0_10
- Burg, J.P. and Ford, M. (eds) 1997. *Orogeny Through Time*. Geological Society, London, Special Publications, **121**, <https://doi.org/10.1144/GSL.SP.1997.121.01.11>
- Burgener, L., Hyland, E., Reich, B.J. and Scotese, C. 2023. Cretaceous climates: Mapping paleo-Löppen climatic zones using a statistical analysis of lithologic, paleontologic, and geochemical proxies. *Palaeogeography, Palaeoclimatology, and Palaeoecology*, **613**, 111373, <https://doi.org/10.1016/j.palaeo.2022.111373>
- Burk, C.A. and Drake, C.L. (eds) 1974. *The Geology of Continental Margins*. Springer, New York.
- Burke, K. and Dewey, J.F. 1975. The Wilson Cycle. In: Geological Society of America, Northeastern Section, 10th Annual Meeting, Syracuse, NY, Abstracts with Programs. Geological Society of America, Boulder, CO, 48.
- Burrett, C. 1974. Plate tectonics and the fusion of Asia. *Earth and Planetary Science Letters*, **21**, 181–189, [https://doi.org/10.1016/0012-821X\(74\)90052-1](https://doi.org/10.1016/0012-821X(74)90052-1)
- Burrett, C., Zaw, K., Meffre, S., Lai, C.K., Somboon, K. and Pol, C. 2014. The configuration of Greater Gondwana – Evidence from LA ICPMS, U–Pb geochronology of detrital zircons from the Palaeozoic and Mesozoic of Southeast Asia and China. *Gondwana Research*, **26**, 31–51, <https://doi.org/10.1016/j.gr.2013.05.020>
- Bush, A.B.G. and Philander, S.G.H. 1997. The late Cretaceous: Simulation with a coupled atmosphere–ocean general circulation model. *Paleoceanography*, **12**, 495–516, <https://doi.org/10.1029/97PA00721>
- Butler, R.F. 1998. *Paleomagnetism: Magnetic Domains to Geologic Terranes*. Blackwell Scientific, Boston, MA, <https://www.geo.arizona.edu/Paleomag/toc-pref.pdf>
- Cande, S.C. and Mutter, J.C. 1982. A revised identification of the oldest sea-floor spreading anomalies between Australia and Antarctica. *Earth and Planetary Science Letters*, **58**, 151–160, [https://doi.org/10.1016/0012-821X\(82\)90190-X](https://doi.org/10.1016/0012-821X(82)90190-X)
- Cande, S.C. and Stegman, D.R. 2011. Indian and African plate motions driven by the push force of the Reunion plume head. *Nature*, **475**, 47–52, <https://doi.org/10.1038/nature10174>
- Cande, S.C., LaBrecque, J.L. and Haxby, W.B. 1988. Plate kinematics of the South Atlantic: Chron 34 to present. *Journal of Geophysical Research: Solid Earth*, **93**,

- 13 479–13 492, <https://doi.org/10.1029/JB093iB11p13479>
- Cande, S.C., LaBrecque, J.L., Larson, R.L., Pitman, W.C., Golovchenko, X. and Haxby, W.F. (compilers) 1989. *Magnetic Lineations of the World's Ocean Basins*. Scale 1:27 400 000 at the Equator. American Association of Petroleum Geologists (AAPG), Tulsa, OK.
- Cantrill, D.J. and Poole, I. 2012. *The Vegetation of Antarctica Through Geological Time*. Cambridge University Press, Cambridge, UK.
- Cao, W., Lee, C.-T.A. and Lackey, J.S. 2017. Episodic nature of continental arc activity since 750 Ma: A global compilation. *Earth and Planetary Science Letters*, **461**, 85–95, <https://doi.org/10.1016/j.epsl.2016.12.044>
- Cao, W., Williams, S., Flament, N., Zahirovic, S., Scotese, C. and Müller, R.D. 2019. Palaeolatitudinal distribution of lithologic indicators of climate in a palaeogeographic framework. *Geological Magazine*, **156**, 331–354, <https://doi.org/10.1017/S0016756818000110>
- Carlisle, D.B. 1995. *Dinosaurs, Diamonds and Things from Outer Space: The Great Extinction*. Stanford University Press, Stanford, CA.
- Casey, R.M. and Rawson, P.F. (eds) 1973. *The Boreal Lower Cretaceous*. Geological Journal, Special Issue, **5**. Seel House Press, Liverpool, UK.
- Catalan, J.R.M., Hatcher, R.D., Jr, Arenas, R. and Garcia, F.D. (eds) 2002. *Variscan–Appalachian Dynamics: The Building of the Late Paleozoic Basement*. Geological Society of America Special Papers, **364**, <https://doi.org/10.1130/SPE364>
- Chamberlin, T.C. 1898. The ulterior basis of time divisions and the classification of geological history. *Journal of Geology*, **6**, 449–462, <https://doi.org/10.1086/608138>
- Chamberlin, T.C. 1906. On a possible reversal of deep-sea circulation and its influence on geologic climates. *Proceedings of the American Philosophical Society*, **45**, 33–43.
- Chamberlin, T.C. 1909. Diastrophism as the ultimate basis for correlation. *Journal of Geology*, **17**, 685–693, <https://doi.org/10.1086/621676>
- Chatterjee, S. 1997. *The Rise of Birds: 225 Million Years of Evolution*. Johns Hopkins University Press, Baltimore, MD.
- Chatterjee, S. and Scotese, C.R. 1999. The breakup of Gondwana and the evolution and biogeography of the Indian plate. *Proceedings of Indian National Science Academy*, **65A**, 397–425.
- Chatterjee, S., Guven, N., Yoshinobu, A. and Donofrio, R. 2006. *Shiva Structure: A Possible KT Boundary Impact Crater on the Western Shelf of India*. Museum of Texas Tech University Special Publications, **50**.
- Chen, B., Joachimski, M.M. *et al.* 2013. Permian ice volume and palaeoclimate history: Oxygen isotope proxies revisited. *Gondwana Research*, **24**, 77–89, <https://doi.org/10.1016/j.gr.2012.07.007>
- Chenet, A.L., Fluteau, F., Courtillot, V., Gerard, M. and Subbarao, K.V. 2008. Determination of rapid Deccan eruptions across the Cretaceous–Tertiary boundary using paleomagnetic secular variation: Results from a 1200-m-thick section in the Mahabaleshwar escarpment. *Journal of Geophysical Research: Solid Earth*, **113**, B04101, <https://doi.org/10.1029/2006JB004635>
- Chiarenza, A.A., Mannion, P.D., Farnsworth, A. and Carrano, M.T. 2022. Climatic constraints on the history of Mesozoic dinosaurs. *Current Biology*, **32**, 570–585, <https://doi.org/10.1016/j.cub.2021.11.061>
- Chumakov, N.M. 1997. The warm biosphere of the Cretaceous Period. In: *Journal of Journals, Review of Global Scientific Achievements, Volume 1*. Nauka, Moscow, 69–74.
- Chumakov, N.M., Zharkov, M.A. *et al.* 1995. Climatic Belts of the Mid-Cretaceous Time. *Stratigraphy and Geological Correlation*, **3**, 241–260.
- Clapham, M.E. and Renne, P.R. 2019. Flood Basalts and Mass Extinctions. *Annual Review of Earth Planetary Sciences*, **47**, 275–303, <https://doi.org/10.1146/annurev-earth-053018-060136>
- Clark, P.U., Shakun, J.D. *et al.* 2016. Consequences of twenty-first-century policy for multi-millennial climate and sea-level change. *Nature Climate Change*, **6**, 360–369, <https://doi.org/10.1038/nclimate2923>
- Clennett, E.J., Holt, A.F., Tetley, M.G., Becker, T.W. and Faccenna, C. 2023. Assessing plate reconstruction models using plate driving force consistency tests. *Scientific Reports*, **13**, 10191, <https://doi.org/10.1038/s41598-023-37117-w>
- Cobbold, P.R. and Rossello, E.A. 2003. Aptian to recent compressional deformation, foothills of the Neuquen Basin, Argentina. *Marine and Petroleum Geology*, **20**, 429–443, [https://doi.org/10.1016/S0264-8172\(03\)00077-1](https://doi.org/10.1016/S0264-8172(03)00077-1)
- Cocks, L.R.M. and Torsvik, T.H. 2021. Ordovician palaeogeography and climate change. *Gondwana Research*, **100**, 53–72, <https://doi.org/10.1016/j.gr.2020.09.008>
- Coffin, M.F. and Eldholm, O. 1991. *Large Igneous Provinces: JOIO/USSAC Workshop Report*. University of Texas at Austin, Institute for Geophysics Technical Report 114.
- Coffin, M.F. and Eldholm, O. 1994. Large igneous provinces: Crustal structure, dimensions, and external consequences. *Reviews of Geophysics*, **32**, 1–36, <https://doi.org/10.1029/93RG02508>
- Coffin, M.F. and Rabinowitz, P.D. 1988. *Evolution of the Conjugate East African–Madagascan Margins and the Western Somali Basin*. Geological Society of America Special Papers, **226**, <https://doi.org/10.1130/SPE226>
- Cohen, K.M., Finney, S.C., Gibbard, P.L. and Fan, J.-X. 2013. The International Chronostratigraphic Chart (version 2023/06). *Episodes*, **36**, 199–204, <https://doi.org/10.18814/epiugs/2013/v36i3/002>
- Colbert, E.H. 1973. Continental drift and the distributions of fossil reptiles. In: Tarling, D.H. and Runcorn, S.K. (eds) *Implications of Continental Drift to the Earth Sciences, Volume 1*. Academic Press, London, 395–412.
- Coleman, R.G. 1977. *Ophiolites: Ancient Oceanic Lithosphere?* Springer, Berlin.
- Collins, A.S., Blades, M.L., Merdith, A.S. and Foden, J.D. 2021. Closure of the Proterozoic Mozambique Ocean was instigated by a late Tonian plate reorganization event. *Communications Earth & Environment*, **2**, 75, <https://doi.org/10.1038/s43247-021-00149-z>
- Condie, K.C. 2001. *Mantle Plumes and Their Record in Earth History*. Cambridge University Press, Cambridge, UK.

- Conrad, C.P. and Lithgow-Bertelloni, C. 2006. Influence of continental roots and asthenosphere on plate–mantle coupling. *Geophysical Research Letters*, **33**, L053312, <https://doi.org/10.1029/2005GL025621>
- Conybeare, W.D. and Phillips, W. 1822. *Outlines of the Geology of England and Wales, with an Introduction Compendium of the General Principles that Science, and Comparative Views of the Structure of Foreign Countries. Part I.* William Phillips, London.
- Cook, P.J. 1990. *Australia: Evolution of a Continent.* Bureau of Mineral Resources Paleogeographic Group, Australian Government Publishing Service, Canberra.
- Cook, T.D. and Bally, A.W. 1975. *Stratigraphic Atlas of North America and Central America.* Princeton University Press, Princeton, NJ.
- Cope, J.C.W., Ingham, J.K. and Rawson, P.F. (eds) 1992. *Atlas of Paleogeography and Lithofacies.* Geological Society, London, Memoirs, **13**, <https://doi.org/10.1144/GSL.MEM.1992.012.01.16>
- Cordani, U.G., Milani, E.J., Thomaz-Filho, A. and Campos, D.A. (eds) 2000. Tectonic evolution of South America: Brazil 2000; 31st International Geological Congress; Rio de Janeiro, Brazil, August 6–17, 2000. Geological Survey of Brazil, Rio de Janeiro, Brazil.
- Corfu, F., Gasser, D. and Chew, D.M. (eds) 2014. *New Perspectives on the Caledonides of Scandinavia and Related Areas.* Geological Society, London, Special Publications, **390**, <https://doi.org/10.1144/SP390.0>
- Courtillot, V. 1999. *Evolutionary Catastrophes: The Science of Mass Extinction.* Cambridge University Press, Cambridge, UK.
- Courtillot, V. and Renne, X. 2003. On the ages of flood basalt events. *Comptes Rendus Geosciences*, **335**, 113–140, [https://doi.org/10.1016/S1631-0713\(03\)00006-3](https://doi.org/10.1016/S1631-0713(03)00006-3)
- Courtillot, V., Feraud, G., Maluski, H., Vandamme, D., Moreau, M.G. and Besse, J. 1988. Deccan flood basalts and the Cretaceous–Tertiary boundary. *Nature*, **333**, 843–846, <https://doi.org/10.1038/333843a0>
- Courtillot, V., Vandamme, D., Besse, J., Jaeger, J.J. and Javoy, M. 1990. Deccan volcanism at the Cretaceous/Tertiary boundary; Data and inferences. *Geological Society of America Special Papers*, **247**, 401–409, <https://doi.org/10.1130/SPE247-p401>
- Coward, M.P., Dietrich, D. and Park, R.G. (eds) 1989. *Alpine Tectonics.* Geological Society, London, Special Publications, **45**, <https://doi.org/10.1144/GSL.SP.1989.045.01.24>
- Cox, A. and Hart, R.B. 1986. *Plate Tectonics: How It Works.* Blackwell Scientific, Palo Alto, CA.
- Creer, K.M. 1954. The measurement of geological intervals of time by paleomagnetic methods. *Journal of Geology*, **62**, 234–238.
- Crough, T.S., Morgan, W.J. and Hardgraves, R.B. 1980. Kimberlites: Their relation to mantle hot spots. *Earth and Planetary Science Letters*, **50**, 260–274, [https://doi.org/10.1016/0012-821X\(80\)90137-5](https://doi.org/10.1016/0012-821X(80)90137-5)
- Crowley, T.J., Short, D.A., Mengel, J.G. and North, G.R. 1986. Role of seasonality in the evolution of climate during the last 100 million years. *Science*, **231**, 579–584, <https://doi.org/10.1126/science.231.4738.579>
- Cui, Y. and Kump, L.R. 2015. Global warming and the end-Permian extinction event: Proxy and modeling perspectives. *Earth-Science Reviews*, **149**, 5–22, <https://doi.org/10.1016/j.earscirev.2014.04.007>
- Cuvier, G. 1831. *A Discourse on the Revolutions of the Surface of the Globe and the Changes thereby produced in the Animal Kingdom, translated from French with illustrations and a glossary.* Carey and Lea, Philadelphia, PA.
- Dal Corso, J., Benton, M.J., Bernardi, M., Franz, M., Gianolla, P., Hohn, S. and Zhang, Y. 2018a. First Workshop on the Carnian Pluvial Episode (Late Triassic): a report. *Albertiana*, **44**, 49–57.
- Dal Corso, J., Gianolla, P. et al. 2018b. Multiple negative carbon-isotope excursions during the Carnian Pluvial Episode (Late Triassic). *Earth-Science Reviews*, **185**, 732–750, <https://doi.org/10.1016/j.earscirev.2018.07.004>
- Davies, A. and Simmons, M.D. 2023. Placing constraints on the nature of short-term eustatic curves. *Basin Research*, **36**, e12832, <https://doi.org/10.1111/bre.12832>
- DeCelles, P.G., Ducea, M.N., Carrapa, B. and Kapp, P.A. (eds) 2015. *Geodynamics of the Cordilleran Orogenic System: The Central Andes of Argentina and Northern Chile.* Geological Society of America Memoirs, **212**, <https://doi.org/10.1130/MEM212>
- DeConto, R.M., Hay, W.W., Thompson, S.L. and Bergengren, J. 1999. Late Cretaceous climate and vegetation interactions: Cold continental interior paradox. *Geological Society of America Special Papers*, **332**, 391–406, <https://doi.org/10.1130/0-8137-2332-9.391>
- de Lurdes Fonseca, M., Scotese, C.R. and Cachao, M. 2019. Late Cretaceous paleobiogeography of *Braarudosphaera bigelowi*. *Marine Micropaleontology*, **152**, 101738, <https://doi.org/10.1016/j.marmicro.2019.03.010>
- De Lurio, J.L. and Frakes, L.A. 1999. Glendonites as a paleoenvironmental tool: Implications for early Cretaceous high latitude climates in Australia. *Geochimica et Cosmochimica Acta*, **63**, 1039–1048, [https://doi.org/10.1016/S0016-7037\(99\)00019-8](https://doi.org/10.1016/S0016-7037(99)00019-8)
- Demaision, G.J. and Moore, G.T. 1980. Anoxic environments and oil source bed genesis. *AAPG Bulletin*, **64**, 1179–1209.
- Dengo, G. and Case, J.E. 1990. *The Caribbean Region.* Decade of North American Geology, The Geology of North America, **H**. Geological Society of America, Boulder, CO.
- Dera, G., Brigaud, B. et al. 2011. Climatic ups and downs in a disturbed Jurassic world. *Geology*, **39**, 215–218, <https://doi.org/10.1130/G31579.1>
- Dercourt, J., Zonenshain, L. et al. 1985. Presentation de 9 cartes paleogeographiques au 1/20 000 000 s'etendant de l'Atlantique au Pamir pour la periode du Lias a l'Actuel. *Bulletin de la Société Géologique de France*, **8**, 637–652, <https://doi.org/10.2113/gssgfbull.L5.637>
- Dercourt, J., Ricou, L.E. and Vrielynck, B. 1993. *Atlas Tethys, Palaeoenvironmental Maps.* Gauthier-Villars, Paris.
- Dercourt, J., Gaetani, M. et al. 2000. *Atlas PeriTethys Palaeogeographic Maps.* Commission de la Carte Géologique du Monde, Paris.
- Dettmann, M.E. 1989. Antarctica: Cretaceous cradle of austral temperate rainforests? *Geological Society, London*,

- Special Publications*, **47**, 89–105, <https://doi.org/10.1144/GSL.SP.1989.047.01.08>
- Dewey, J.F. and Burke, K.C.A. 1973. Tibetan, Variscan, and Precambrian basement reactivation: products of continental collision. *Journal of Geology*, **81**, 683–692, <https://doi.org/10.1086/627920>
- Dewey, J.F. and Burke, K.C.A. 1974. Hot spots and continental break-up: Implications for collisional orogeny. *Geology*, **2**, 57–60, [https://doi.org/10.1130/0091-7613\(1974\)2<57:HSACBI>2.0.CO;2](https://doi.org/10.1130/0091-7613(1974)2<57:HSACBI>2.0.CO;2)
- Dewey, J.F., Pitman, W.C.I.I.I., Ryan, W.B.F. and Bonin, J. 1973. Plate tectonics and the evolution of the Alpine System. *Geological Society of America Bulletin*, **84**, 3137–3180, [https://doi.org/10.1130/0016-7606\(1973\)84<3137:TATEO>2.0.CO;2](https://doi.org/10.1130/0016-7606(1973)84<3137:TATEO>2.0.CO;2)
- Dewey, J.F., Gass, I.G., Curry, G.B., Harris, N.B.W. and Sengor, A.M.C. (eds) 1991. *Allochthonous Terranes*. Cambridge University Press, Cambridge, UK.
- d'Halloy, J.G.J. 1822. Observations sur un essai de cartes géologiques de la France, des Pays-Bas, et des contrées voisines. *Annales de Mines*, **7**, 353–376.
- Dilek, Y. and Furnes, H. 2014. Ophiolites and their origins. *Elements*, **10**, 93–100, <https://doi.org/10.2113/gselements.10.2.93>
- Dilek, Y. and Robinson, P.T. (eds) 2003. *Ophiolites in Earth History*. Geological Society, London, Special Publications, **218**, <https://doi.org/10.1144/GSL.SP.2003.218.01.34>
- Dilek, Y. and Robinson, P.T. (eds) 2009. Mantle dynamics and crust–mantle interactions in collisional orogens. *Lithos*, **113**, 1–346.
- Dilek, Y., Moores, E.M., Elthon, D. and Nicolas, A. (eds) 2000. *Ophiolites and Oceanic Crust: New Insights from Field Studies and the Ocean Drilling Program*. Geological Society of America Special Papers, **349**, <https://doi.org/10.1130/SPE349>
- Dingus, L. and Rowe, T. 1998. *The Mistaken Extinction: Dinosaur Evolution and the Origin of Birds*. W.H. Freeman, New York.
- Direen, N.G., Cohen, B.E., Maas, R., Frey, F.A., Whittaker, J.M., Coffin, M.F., Meffre, S., Halpin, J.A. and Crawford, A.J. 2017. Naturaliste Plateau: constraints on the timing and evolution of the Kerguelen Large Igneous Province and its role in Gondwana breakup. *Australian Journal of Earth Sciences*, **64**, 851–869, <https://doi.org/10.1080/08120099.2017.1367326>
- D'Lemos, R.S., Strachan, R.A. and Topley, C.G. (eds) 1990. *The Cadomian Orogeny*. Geological Society, London, Special Publications, **51**, <https://doi.org/10.1144/GSL.SP.1990.051.01.28>
- Donnadieu, Y., Puceat, E., Moiroud, M., Guillocheau, F. and Deconinck, J.F. 2016. A better-ventilated ocean triggered by Late Cretaceous changes in continental configuration. *Nature Communications*, **7**, 12, <https://doi.org/10.1038/ncomms10316>
- Donovan, S.K. 1989. *Mass Extinctions: Process and Evidence*. Belhaven Press, London.
- D'Orbigny, A. 1840. *Paleontologie française. Terrains crétacés. I. Cephalopodes*. Chez l'auteur, Paris.
- Duncan, R.A. and Huard, J. 1997. Trace metal anomalies and global anoxia: the OJP-Selli hydrothermal plume connection. *EOS Transactions American Geophysical Union*, **78**, F774.
- Duncan, R.A. and Storey, M. 1992. The life cycle of Indian Ocean hotspots. *American Geophysical Union Geophysical Monograph Series*, **70**, 91–103, <https://doi.org/10.1029/GM070p0091>
- Dunhill, A.M., Bestwick, J., Narey, H. and Sciberras, J. 2016. Dinosaur biogeographical structure and Mesozoic continental fragmentation: a network-based approach. *Journal of Biogeography*, **43**, 1691–1704, <https://doi.org/10.1111/jbi.12766>
- Edwards, J.D. and Santogrossi, P.A. (eds) 1989. *Divergent/Passive Margin Basins*. AAPG Memoirs, **48**, <https://doi.org/10.1306/M48508>
- Eglinton, B., Evans, D., Pehrsson, S. and Huston, D. 2017. Reconstructing Phanerozoic and Proterozoic Earth Evolution: building on pre-existing efforts and data. In: Butler, R., Daly, M., Roberts, G., Turner, J. and Watts, T. (convenors) *William Smith Meeting 2017: Plate Tectonics at 50. Abstract Book*. Geological Society, London, 28–29.
- Eliot, T.S. 1943. Little Gidding. In: *Four Quartets*, lines 239–242, Harcourt, Brace & World, New York.
- Elling, R.P. 2022. *Continental Rifting and Precambrian Tectonics: Insights from Gravity Modeling and Apparent Polar Wander Paths*. PhD thesis, Northwestern University, Evanston, Illinois, USA.
- Ellis, R. 2003. *Sea Dragons: Predators of the Prehistoric Oceans*. University Press of Kansas, Lawrence, KS.
- Engelbreton, D.C., Cox, A. and Gordon, R.G. 1985. *Relative Motions between Oceanic and Continental Plates in the Pacific Basin*. Geological Society of America Special Papers, **206**, <https://doi.org/10.1130/SPE206-p1>
- Erba, E., Bartolini, A. and Larson, R.L. 2004. Valanginian Weissert oceanic anoxic event. *Geology*, **32**, 149–152, <https://doi.org/10.1130/G20008.1>
- Erba, E., Duncan, R.A., Bottini, C., Tiraboschi, D., Weisert, H., Jenkyns, H.C. and Malinverno, A. 2015. Environmental consequences of Ontong Java Plateau and Kerguelen Plateau volcanism. *Geological Society of America Special Papers*, **511**, 271–303, [https://doi.org/10.1130/2015.2511\(15\)](https://doi.org/10.1130/2015.2511(15))
- Ernst, R.E. 2014. *Large Igneous Provinces*. Cambridge University Press, Cambridge, UK.
- Ernst, R.E. and Youbi, N. 2017. How Large Igneous Provinces affect global climate, sometimes cause mass extinctions, and represent natural markers in the geological record. *Palaeogeography, Palaeoclimatology, Palaeoecology*, **478**, 30–52, <https://doi.org/10.1016/j.palaeo.2017.03.014>
- Ernst, W.G. (ed.) 1975. *Subduction Zone Metamorphism*. Benchmark Papers in Geology, **19**. Dowden, Hutchinson, and Ross, Stroudsburg, PA.
- Ernst, W.G. (ed.) 2004. *Serpentine and Serpentinities: Mineralogy, Petrology, Geochemistry, Ecology, Geophysics, and Tectonics; A Tribute to Robert G. Coleman*. Geological Society of America International Book Series, **8**. Bellweather Publishing for the Geological Society of America, Columbia, MD.
- Erwin, D.H. 1993. *The Great Paleozoic Crisis: Life and Death in the Permian, Critical Moments in Paleobiology and Earth History Series*. Columbia University Press, New York.
- Erwin, D.H. 2006. *Extinction: How Life on Earth Nearly Ended 250 Million Years Ago*. Princeton University Press, Princeton, NJ.

- Evans, D., Graham, C., Armour, A. and Bathurst, P. 2003. *The Millenium Atlas: Petroleum Geology of the Central and Northern North Sea*. Geological Society, London.
- Evans, D.A.D. 2003. True polar wander and supercontinents. *Tectonophysics*, **362**, 303–320, [https://doi.org/10.1016/S0040-1951\(02\)000642-X](https://doi.org/10.1016/S0040-1951(02)000642-X)
- Evans, D.A.D. and Eglinton, B.M. 2022. Continuous quantitative model of global paleogeography through 2.0 billion years. Abstract GP43A-02 presented at the American Geophysical Union Fall Meeting, 12–16 December 2022, Chicago, Illinois, USA.
- Evans, D.A.D., Pesonen, L.J. *et al.* 2021. An expanding list of reliable paleomagnetic poles for Precambrian tectonic reconstructions. In: Pesonen, L.J., Salminen, J., Elming, S.-A., Evans, D.A.D. and Veikkolainen, T. (eds) *Ancient Supercontinents and the Paleogeography of Earth*. Elsevier, Amsterdam, 605–639, <https://doi.org/10.1016/B978-0-12-818533-9.00007-2>
- Everhart, M.J. 2005. Oceans of Kansas: A natural history of the western Interior Sea. In: Farlow, J.O. (ed.) *Life of the Past*. Indiana University Press, Bloomington, IN.
- Fairhead, J.D. 1988. Mesozoic plate tectonic reconstructions of the South Atlantic Ocean: the role of the West and Central African Rift System. *Tectonophysics*, **155**, 181–191, [https://doi.org/10.1016/0040-1951\(88\)90265-X](https://doi.org/10.1016/0040-1951(88)90265-X)
- Farnsworth, A., Lunt, D.J. *et al.* 2019. Climate sensitivity on geological timescales controlled by non-linear feedbacks and ocean circulation. *Geophysical Research Letters*, **46**, 9880–9889, <https://doi.org/10.1029/2019GL083574>
- Fastovsky, D.E. and Weishampel, D.B. 1996. *The Evolution and Extinction of the Dinosaurs*. Cambridge University Press, Cambridge, UK.
- Fischer, A.G. 1981. Climatic oscillations in the biosphere. In: Nitecki, M.H. (ed.) *Biotic Crises in Ecological and Evolutionary Time*. Academic Press, New York, 103–131.
- Fischer, A.G. 1982. Long-term climatic oscillations recorded in stratigraphy. In: Berger, W.H. and Crowell, J.C. (eds) *Studies in Geophysics: Climate in Earth History*. National Academy Press, Washington, DC, 97–104.
- Fischer, A.G. 1984. The two Phanerozoic supercycles. In: Berggren, W.A. and Van Couvering, J.A. (eds) *Catastrophes and Earth History: The New Uniformitarianism*. Princeton University Press, Princeton, NJ, 129–150.
- Fisher, N.I., Lewis, T. and Embleton, B.J.J. 1987. *Statistical Analysis of Spherical Data*. Cambridge University Press, Cambridge, UK.
- Fisher, R.A. 1953. Dispersion on a sphere. *Proceedings of the Royal Society A: Mathematical, Physical and Engineering Sciences*, **217**, 295–305, <https://doi.org/10.1098/rspa.1953.0064>
- Flögel, S., Wallman, K., Poulsen, C.J., Zhou, J., Oschlies, A., Voigt, S. and Kuhn, W. 2011. Simulating the biogeochemical effects of volcanic CO₂ degassing on the oxygen-state of the deep ocean during the Cenomanian–Turonian Anoxic Event (OAE2). *Earth and Planetary Science Letters*, **305**, 371–384, <https://doi.org/10.1016/j.epsl.2011.03.018>
- Flügel, E. and Kiessling, W. 2002. Patterns of Phanerozoic reef crises. *SEPM Special Publications*, **72**, 691–733, <https://doi.org/10.2110/pec.02.72.0691>
- Forsyth, D. and Uyeda, S. 1975. On the Relative Importance of the Driving Forces of Plate Motion. *Geophysical Journal of the Royal Astronomical Society*, **43**, 163–200, <https://doi.org/10.1111/j.1365-246X.1975.tb00631.x>
- Foster, G.L., Royer, D.L. and Lunt, D.J. 2017. Future climate forcing potentially without precedent in the last 420 million years. *Nature Communications*, **8**, 14845, <https://doi.org/10.1038/ncomms14845>
- Foulger, G.R. and Jurdy, D.M. (eds) 2007. *Plates, Plumes, and Planetary Processes*. Geological Society of America Special Papers, **430**, <https://doi.org/10.1130/SPE430>
- Frakes, L.A. 1999. Estimating the global thermal state from Cretaceous sea surface and continental temperature data. *Geological Society of America Special Papers*, **332**, 49–57, <https://doi.org/10.1130/0-8137-2332-9.49>
- Frakes, L.A. and Francis, J.E. 1988. A guide to Phanerozoic cold polar climates from high latitude ice-rafting in the Cretaceous. *Nature*, **333**, 547–549, <https://doi.org/10.1038/333547a0>
- Frakes, L.A. and Francis, J.E. 1990. Cretaceous palaeoclimates. In: Ginsburg, R.N. and Beaudoin, B. (eds) *Cretaceous Resources, Events, and Rhythms*. Kluwer Academic, Dordrecht, The Netherlands, 373–287.
- Frakes, L.A., Francis, J.E. and Sykes, J.I. 1992. *Climate Modes of the Phanerozoic*. Cambridge University Press, Cambridge, UK.
- Frakes, L.A., Alley, N.F. and Deynoux, M. 1995. Early Cretaceous ice rafting and climate zonation in Australia. *International Geology Review*, **37**, 567–583, <https://doi.org/10.1080/00206819509465419>
- Francis, J.E. and Frakes, L.A. 1993. Cretaceous climates. In: Wright, V.P. (ed.) *Sedimentology Review/1*. Blackwell Scientific, Oxford, UK, 17–30, <https://doi.org/10.1002/9781444304534.ch2>
- Francois, C., Pubellier, M. *et al.* 2021. Temporal and spatial evolution of orogens: a guide for geological mapping. *Episodes*, **45**, 265–283, <https://doi.org/10.18814/epiugs/2021/021025>
- Franke, W., Haal, V., Oncken, O. and Tanner, D. (eds) 2000. *Orogenic Processes: Quantification and Modeling in the Variscan Belt*. Geological Society, London, Special Publications, **179**, <https://doi.org/10.1144/GSL.SP.2000.179.01.27>
- Friedman, R.M. 1983. *Accretionary History of Western North America during the Mesozoic and Cenozoic Eras*. Master's thesis, University of Chicago, Chicago, Illinois, USA.
- Friedrich, O., Norris, R.D. and Erbacher, J. 2011. Evolution of Cretaceous oceans: A 55 million year record of Earth's temperature and carbon cycle. *Grzybowski Foundation Special Publications*, **17**, 85–85.
- Friedrich, O., Norris, R.D. and Erbacher, J. 2012. Evolution of middle to Late Cretaceous oceans – A 55 m.y. record of Earth's temperature and carbon cycle. *Geology*, **40**, 107–110, <https://doi.org/10.1130/G32701.1>
- Furon, R. 1941. *La Paleogeographie, Essai sur l'evolution des continents et des oceans*. Payot, Paris.
- Gabriele, H. and Yorath, C.J. (eds) 1992. *Geology of the Cordilleran Orogen in Canada*. Geology of Canada, **4**/Geological Society of America Geology of North America, **G-2**.

- Gahagan, L., Scotese, C.R. *et al.* 1988. Tectonic fabric map of the ocean basins from satellite altimetry data. *Tectonophysics*, **155**, 1–26.
- Gaina, C., Mueller, R.D., Royer, J.-Y., Stock, J., Hardebeck, J. and Symonds, P.A. 1998a. The tectonics history of the Tasman Sea: a puzzle with 13 pieces. *Journal of Geophysical Research: Solid Earth*, **103**, 12 413–12 433, <https://doi.org/10.1029/98JB00386>
- Gaina, C., Roest, W., Mueller, R.D. and Symonds, P.A. 1998b. The opening of the Tasman Sea: a gravity anomaly grid animation. *Earth Interactions*, **2**, 1–23, [https://doi.org/10.1175/1087-3562\(1998\)002<0001:TOOTTS>2.3.CO;2](https://doi.org/10.1175/1087-3562(1998)002<0001:TOOTTS>2.3.CO;2)
- Gansser, A. 1964. *Geology of the Himalayas*. Interscience, London.
- Gaskell, D.E., Huber, M., O'Brien, C.L., Inglis, G.N., Acosta, R.P., Poulsen, C.J. and Hull, P.M. 2022. The latitudinal temperature gradient and its climate dependence as inferred from foraminiferal $\delta^{18}\text{O}$ over the past 95 million years. *Proceedings of the National Academy of Sciences of the United States of America*, **119**, e2111332119, <https://doi.org/10.1073/pnas.2111332119>
- Gass, I.G., Lippard, S.J. and Shelton, A.W. 1984. *Ophiolites and Oceanic Lithosphere*. Geological Society, London, Special Publications, **13**.
- Gasson, E.G.W. and Kiessling, B.A. 2020. The Antarctic Ice Sheet: A paleoclimate modeling perspective. *Oceanography*, **33**, 90–100, <https://doi.org/10.5670/oceanog.2020.208>
- Gayer, R.A. (ed.) 1989. *The Caledonide Geology of Scandinavia*. Graham and Trotman, London.
- Gee, D.G. and Sturt, B.A. 1985. *The Caledonide Orogen – Scandinavia and Related Areas, Parts 1 and 2*. Wiley-Interscience, Chichester, UK.
- Gibbs, M.T., Rees, P.M., Kutzbach, J.E., Ziegler, A.M., Behling, P.J. and Rowley, D.B. 2002. Simulations of Permian climate and comparisons with climate-sensitive sediments. *Journal of Geology*, **110**, 33–55, <https://doi.org/10.1086/324204>
- Gloaguen, R. and Ratschbacher, L. (eds) 2011. *Growth and Collapse of the Tibetan Plateau*. Geological Society, London, Special Publications, **353**, <https://doi.org/10.1144/SP353.0>
- Goddéris, Y., Donnadié, Y., Lefebvre, V., Le Hir, G. and Nardin, E. 2012. Tectonic control of continental weathering, atmospheric CO_2 , and climate over Phanerozoic times. *Comptes Rendus Geoscience*, **344**, 652–662, <https://doi.org/10.1016/j.crte.2012.08.009>
- Gold, T. 1965. Instability of the Earth's axis of rotation. *Nature*, **175**, 526–529, <https://doi.org/10.1038/175526a0>
- Goldreich, P. and Toomre, A. 1969. Some remarks on polar wandering. *Journal of Geophysical Research*, **74**, 2555–2567, <https://doi.org/10.1029/JB074i010p02555>
- Golonka, J. 2000. *Cambrian–Neogene Plate Tectonic Maps*. Rozprawy Habilitacyjne – Uniwersytet Jagielloński, **350**.
- Golonka, J., Ross, M.I. and Scotese, C.R. 1994. Phanerozoic paleogeographic and paleoclimatic modeling maps. *Canadian Society of Petroleum Geologists Memoirs*, **17**, 1–47.
- Gómez-Tuena, A., Straub, S.M. and Zellmer, G.F. 2014. *Orogenic Andesites and Crustal Growth*. Geological Society, London, Special Publications, **385**, <https://doi.org/10.1144/SP385.0>
- Gordon, C., Cooper, C. *et al.* 2000. The simulation of SST, sea ice extents and ocean heat transports in a version of the Hadley Centre coupled model without flux adjustments. *Climate Dynamics*, **16**, 147–168, <https://doi.org/10.1007/s003820050010>
- Gornitz, V. 2008. Sea level change, post-glacial. In: Gornitz, V. (ed.) *Encyclopedia of Paleoclimatology and Ancient Environments*. Encyclopedia of Earth Sciences Series. Springer, Dordrecht, The Netherlands, 887–893.
- Gough, D.O. 1981. Solar interior structure and luminosity variations. *Solar Physics*, **74**, 21, <https://doi.org/10.1007/BF00151270>
- Grabau, A.W. 1924. *Principles of Stratigraphy, Volumes 1 and 2*. Dover, New York.
- Gradstein, F.M., Ogg, J.G., Schmitz, M. and Ogg, G. (eds) 2020. *Geological Time Scale 2020, Volume 2*. Elsevier, Amsterdam.
- Granot, R. and Dymert, J. 2015. The Cretaceous opening of the South Atlantic. *Earth and Planetary Science Letters*, **414**, 156–163, <https://doi.org/10.1016/j.epsl.2015.01.015>
- Grasby, S.E., McCune, G.E., Beauchamp, B. and Gallo-way, J.M. 2017. Lower Cretaceous cold snaps led to widespread glendonite occurrences in the Sverdrup Basin, Canadian High Arctic. *Geological Society of America Bulletin*, **129**, 771–787, <https://doi.org/10.1130/B31600.1>
- Green, A.R., Kaplan, A.A. and Vierbuchen, R.G. 1986. Circum-Arctic petroleum potential. *AAPG Memoirs*, **40**, 101–130, <https://doi.org/10.1306/M40454C4>
- Grossman, E.L. 2012a. Applying oxygen isotope paleothermometry in deep time. *The Paleontological Society Papers*, **18**, 39–67, <https://doi.org/10.1017/S1089332600002540>
- Grossman, E.L. 2012b. Oxygen isotope stratigraphy. In: Gradstein, F.M., Ogg, J.G., Schmitz, M.D. and Ogg, G.M. (eds) *The Geologic Time Scale 2012, Volume 1*. Elsevier, Amsterdam, 181–206.
- Grossman, E.L. and Joachimski, M.M. 2020. Oxygen isotope stratigraphy. In: *Geologic Time Scale 2020, Volume 1*. Elsevier, Amsterdam, 279–307, <https://doi.org/10.1016/B978-0-12-824360-2.00010-3>
- Grossman, E.L. and Joachimski, M.M. 2022. Ocean temperatures through the Phanerozoic reassessed. *Scientific Reports*, **12**, 8938, <https://doi.org/10.1038/s41598-022-11493-1>
- Habicht, J.K.A. 1979. *Paleoclimate, Paleomagnetism, and Continental Drift*. AAPG Studies in Geology, **9**.
- Haggart, J.W., Enkin, R.J. and Monger, J.W.H. (eds) 2006. *Paleogeography of the North American Cordillera: Evidence for and Against Large-Scale Displacements*. Geological Association of Canada Special Papers, **46**.
- Hallam, A. 1973. *Atlas of Palaeobiogeography*. Elsevier, Amsterdam.
- Hallam, A. 1984a. Continental humid and arid zones during the Jurassic and Cretaceous. *Palaeogeography, Palaeoclimatology and Palaeoecology*, **47**, 195–223, [https://doi.org/10.1016/0031-0182\(84\)90094-4](https://doi.org/10.1016/0031-0182(84)90094-4)
- Hallam, A. 1984b. Pre-Quaternary sea-level changes. *Annual Review of Earth and Planetary Sciences*, **12**,

- 205–243, <https://doi.org/10.1146/annurev.ea.12.050184.001225>
- Hallam, A. 2004. *Catastrophes and Lesser Calamities: The Causes of Mass Extinctions*. Oxford University Press, Oxford, UK.
- Hallam, A. and Wignall, P.B. 1997. *Mass Extinctions and Their Aftermath*. Oxford University Press, Oxford, UK.
- Hambrey, M.J. and Harland, W.B. 1981. *Earth's Pre-Pleistocene Glacial Record*. Cambridge University Press, Cambridge, UK.
- Hamilton, W. 1970. The Uralides and the motion of the Russian and Siberian Platforms. *Geological Society of America Bulletin*, **81**, 2553–2576, [https://doi.org/10.1130/0016-7606\(1970\)81\[2553:TUATMOJ2.0.CO;2](https://doi.org/10.1130/0016-7606(1970)81[2553:TUATMOJ2.0.CO;2)
- Haq, B.U. 2014. Cretaceous eustasy revisited. *Global and Planetary Change*, **113**, 44–58, <https://doi.org/10.1016/j.gloplacha.2013.12.007>
- Haq, B.U. and Schutter, S.R. 2009. A chronology of Paleozoic sea-level changes. *Science*, **322**, 64–68, <https://doi.org/10.1126/science.1161648>
- Haq, B.U., Hardenbol, J. and Vail, P.R. 1987. Chronology of fluctuating sea levels since the Triassic. *Science*, **235**, 1156–1167, <https://doi.org/10.1126/science.235.4793.1156>
- Haq, B.U., Hardenbol, J. and Vail, P.R. 1988. Mesozoic and Cenozoic chronostratigraphy and cycles of sea-level change. *SEPM Special Publications*, **42**, 71–108, <https://doi.org/10.2110/pec.88.01.0071>
- Harper, D.A.T. and Servais, T. (eds) 2013. *Early Paleozoic Biogeography and Palaeogeography*. Geological Society, London, Memoirs, **38**, <https://doi.org/10.1144/M38.0>
- Harper, D.A.T., Rasmussen, C.M.Ø. et al. 2013. Biodiversity, biogeography and phylogeography of Ordovician rhynchonelliform brachiopods. *Geological Society, London, Memoirs*, **38**, 127–144, <https://doi.org/10.1144/ME38.11>
- Harper, D.A.T., Lefebvre, B., Percival, I.G. and Servais, T. (eds) 2023. *A Global Synthesis of the Ordovician System: Part I*. Geological Society, London, Special Publications, **535**, <https://doi.org/10.1144/SP535-2022-168>
- Harris, A.L. and Fettes, D.J. (eds) 1988. The Caledonian–Appalachian orogen. *Geological Society, London, Special Publications*, **38**.
- Harris, A.L., Holland, C.H. and Leake, B.E. (eds) 1979. *The Caledonides of the British Isles – Reviewed*. Scottish Academic Press, Edinburgh.
- Hart, M.B. (ed.) 1997. *Biotic Recovery from Mass Extinction Events*. Geological Society, London, Special Publications, **102**, <https://doi.org/10.1144/GSL.SP.1996.102.01.28>
- Hart, M.B. 2000. Climatic modelling in the Cretaceous using the distribution of planktonic Foraminifera. In: Hart, M.B. (ed.) *Climates: Past and Present*. Geological Society, London, Special Publications, **181**, 33–41, <https://doi.org/10.1144/GSL.SP.2000.181.01.04>
- Hart, M.B. and Koutsoukos, E.A.M. 2015. Paleocology of Cretaceous Foraminifera: Examples from the Atlantic Ocean and Gulf of Mexico Region. *Transactions of the Gulf Coast Association of Geological Societies*, **65**, 175–199.
- Hart, M.B., Yancey, T.E., Leighton, A.D., Miller, B., Liu, C., Smart, C.W. and Twitchett, R.J. 2012. The Cretaceous–Paleogene boundary on the Brazos River, Texas: New stratigraphic sections and revised interpretations. *Journal of the Gulf Coast Association of Geological Societies*, **1**, 69–80.
- Hart, M.B., Harries, P.J. and Cardenas, A.L. 2013. The Cretaceous/Paleogene boundary events in the Gulf Coast: comparisons between Alabama and Texas. *Transactions of the Gulf Coast Association of Geological Societies*, **63**, 235–255.
- Hart, M.B., Leighton, A. et al. 2014. Cretaceous–Paleogene boundary events in Texas: New sections, revised micropalaeontological interpretations, and clarification of the stratigraphy. In: Rocha, R., Pais, J., Kullberg, J. and Finney, S. (eds) *STRATI 2013*. Springer Geology. Springer, Cham, Switzerland, 37–41, https://doi.org/10.1007/978-3-319-04364-7_8
- Hartman, J.H., Johnson, K.R. and Nichols, D.J. (eds) 2002. *The Hell Creek Formation and the Cretaceous–Tertiary Boundary in the Northern Great Plains*. Geological Society of America Special Papers, **361**, <https://doi.org/10.1130/SPE361>
- Hasegawa, H., Tada, R. et al. 2012. Drastic shrinking of the Hadley circulation during the mid-Cretaceous Super-greenhouse. *Climate of the Past*, **8**, 1323–1337, <https://doi.org/10.5194/cp-8-1323-2012>
- Hatcher, R.D., Jr, Williams, H. and Zietz, I. (eds) 1983. *Contributions to the Tectonics and Geophysics of Mountain Chains*. Geological Society of America Memoirs, **158**, <https://doi.org/10.1130/MEM158>
- Hatcher, R.D., Jr, Carlson, M.P. and McBride, J.H. (eds) 2007. *4-D Framework of Continental Crust*. Geological Society of America Memoirs, **200**, <https://doi.org/10.1130/MEM200>
- Hawkesworth, C.J., Cawood, P.A., Dhuime, B. and Kemp, T.I.S. 2017. Earth's continental lithosphere through time. *Annual Reviews of Earth and Planetary Sciences*, **45**, 169–198, <https://doi.org/10.1146/annurev-earth-063016-020525>
- Hay, W.W. 2008. Evolving ideas about the Cretaceous climate and ocean circulation. *Cretaceous Research*, **29**, 725–753, <https://doi.org/10.1016/j.cretres.2008.05.025>
- Hay, W.W. 2016. *Experimenting on a Small Planet: A History of Scientific Discoveries, a Future of Climate Change and Global Warming*. Springer, Cham, Switzerland.
- Hay, W.W. and Flügel, S. 2012. New thoughts about the Cretaceous climate and oceans. *Earth-Science Reviews*, **115**, 262–272, <https://doi.org/10.1016/j.earscirev.2012.09.008>
- Hay, W.W., DeConto, R.M., de Boer, P., Flügel, S., Song, Y. and Stepashko, A. 2019. Possible solutions to several enigmas of Cretaceous climate. *International Journal of Earth Sciences*, **108**, 587–620, <https://doi.org/10.1007/s00531-018-1670-2>
- Hayes, P.A., Francis, J.E., Cantrill, D.J. and Crame, J.A. 2006. Palaeoclimate analysis of Late Cretaceous angiosperm leaf floras, James Ross Island, Antarctica. *Geological Society, London, Special Publications*, **258**, 49–62, <https://doi.org/10.1144/GSL.SP.2006.258.01.04>
- Haywood, A.M., Valdes, P.J. et al. 2019. What can Palaeoclimate Modelling do for you? *Earth Systems and Environment*, **3**, 1–18, <https://doi.org/10.1007/s41748-019-00093-1>

- Henderson, C.M., Davydov, V.I. and Wardlaw, B.R. 2012. The Permian Period. In: Gradstein, F.M., Ogg, J.G., Schmitz, M.D. and Ogg, G.M. (eds) *The Geologic Time Scale 2012, Volume 2*. Elsevier, Amsterdam, 653–679.
- Henderson, L.J. 1985. *Motion of the Pacific Plate Relative to the Hot Spots Since the Jurassic and Model of Oceanic Plateaus of the Farallon Plate*. PhD thesis, Northwestern University, Evanston, Illinois, USA.
- Hendrix, M.S. and Davis, G.A. (eds) 2001. *Paleozoic and Mesozoic Tectonic Evolution of Central Asia: From Continental Assembly to Intracontinental Deformation*. Geological Society of America Memoirs, **194**, <https://doi.org/10.1130/MEM194>
- Henkes, G.A., Passey, B.H., Grossman, E.L., Shenton, B.J., Yancey, T.E. and Pérez-Huerta, A. 2018. Temperature evolution and oxygen isotope composition of Phanerozoic oceans from carbonate clumped isotope thermometry. *Earth and Planetary Science Letters*, **490**, 40–50, <https://doi.org/10.1016/j.epsl.2018.02.001>
- Herman, A.B. and Spicer, R.A. 1996. Paleobotanical evidence for a warm Cretaceous Arctic Ocean. *Nature*, **380**, 330–333, <https://doi.org/10.1038/380330a0>
- Herman, A.B. and Spicer, R.A. 1997. New quantitative paleoclimate data for the Late Cretaceous Arctic: Evidence for a warm polar ocean. *Palaeogeography, Palaeoclimatology, and Palaeoecology*, **128**, 227–251, [https://doi.org/10.1016/S0031-0182\(96\)00080-6](https://doi.org/10.1016/S0031-0182(96)00080-6)
- Herrle, J.O., Schröder-Adams, C.J., Davis, W., Pugh, A.T., Galloway, J.M. and Fath, J. 2015. Mid-Cretaceous High Arctic stratigraphy, climate, and Oceanic Anoxic Events. *Geology*, **43**, 403–406, <https://doi.org/10.1130/G36439.1>
- Hibbard, J.P., Pollock, J.C., Murphy, J.B., van Staal, C.R. and Greenough, J.D. 2015. *Reeltime Geological Syntheses: Remembering Harold 'Hank' Williams*. Geoscience Canada Reprint Series, **10**. Geological Association of Canada, Ottawa.
- Hildebrand, A.R., Penfield, G.T., Kring, D.A., Pilkington, M., Camargo, Z.A., Jacobsen, S.B. and Boynton, W.V. 1991. Chicxulub crater: A possible Cretaceous–Tertiary boundary impact crater on the Yucatan Peninsula, Mexico. *Geology*, **19**, 867–871, [https://doi.org/10.1130/0091-7613\(1991\)019<0867:CCAPCT>2.3.CO;2](https://doi.org/10.1130/0091-7613(1991)019<0867:CCAPCT>2.3.CO;2)
- Hillhouse, J.W. (ed.) 1989. *Deep Structure and the Past Kinematics of Accreted Terranes*. American Geophysical Union Geophysical Monograph Series, **50**, <https://doi.org/10.1029/GM050>
- Hoffman, P.F. 1988. United Plates of America, birth of a craton: Early Proterozoic assembly and growth of Laurentia. *Annual Reviews of Earth and Planetary Sciences*, **16**, 543–603, <https://doi.org/10.1146/annurev.ea.16.050188.002551>
- Hönisch, B., Royer, D. *et al.* 2023. Toward a Cenozoic history of atmospheric CO₂. *Science*, **382**, eadi5177, <https://doi.org/10.1126/science.adi5177>
- Horrell, M.A. 1991. Phytogeography and palaeoclimatic interpretation of the Maastrichtian. *Palaeogeography, Palaeoclimatology, Palaeoecology*, **86**, 87–138, [https://doi.org/10.1016/0031-0182\(91\)90007-E](https://doi.org/10.1016/0031-0182(91)90007-E)
- Howell, D.G. 1989. *Tectonics of Suspect Terranes: Mountain Building and Continental Growth*. Chapman and Hall, London.
- Hsü, K.J. (ed.) 1982. *Mountain Building Processes*. Academic Press, London.
- Hsü, K.J. 1986. *The Great Dying*. Harcourt Brace Jovanovich, San Diego, CA.
- Huber, B.T. 1998. Tropical paradise at the Cretaceous poles? *Science*, **282**, 2199–2200, <https://doi.org/10.1126/science.282.5397.2199>
- Huber, B.T., MacLeod, K.G. and Wing, S.L. 2000. *Warm Climates in Earth History*. Cambridge University Press, Cambridge, UK.
- Huber, M. 2012. Progress in greenhouse climate modeling. *The Paleontological Society Papers*, **18**, 213–262, <https://doi.org/10.1017/S108933260000262X>
- Hughes, N.F. 1973. *Organisms and Continents through Time*. Special Papers in Palaeontology, **12**.
- Hulver, M. 1985. *Cretaceous Marine Paleogeography of Africa*. Master's thesis, University of Chicago, Chicago, IL.
- Hunter, S.J., Valdes, P.J. *et al.* 2008. Modelling Maastrichtian climate: investigating the role of geography, atmospheric CO₂, and vegetation. *Climates of the Past Discussion*, **4**, 981–1019.
- Hutchison, C.S. 1989. *Geological Evolution of South-east Asia*. Oxford Monographs on Geology and Geophysics, **13**.
- IPCC 2007. Summary for Policymakers. In: Solomon, S., Qin, D. *et al.* (eds) *Climate Change 2007: The Physical Science Basis. Contribution of Working Group I to the Fourth Assessment Report of the Intergovernmental Panel on Climate Change*. Cambridge University Press, Cambridge, UK.
- IPCC 2018. Summary for Policymakers. In: Masson-Delmotte, V., Zhai, P. *et al.* (eds) *Global Warming of 1.5°C. An IPCC Special Report on the Impacts of Global Warming of 1.5°C above Pre-Industrial Levels and Related Greenhouse Gas Emission Pathways, in the context of Strengthening the Global Response to the Threat of Climate Change, Sustainable Development, and Efforts to Eradicate Poverty*. Cambridge University Press, Cambridge, UK.
- IPCC 2019. Summary for Policymakers. In: Portner, H.-O., Roberts, D.C. *et al.* (eds) *IPCC Special Report on the Ocean and Cryosphere in a Changing Climate*. Cambridge University Press, Cambridge, UK.
- Isozaki, Y. 2014. Memories of pre-Jurassic lost oceans: How to retrieve them from extant lands. *Geoscience Canada: Journal of the Geological Association of Canada*, **41**, 283–311.
- Isozaki, Y., Maruyama, S. and Furuoka, F. 1990. Accreted oceanic materials in Japan. *Tectonophysics*, **131**, 179–205, [https://doi.org/10.1016/0040-1951\(90\)90016-2](https://doi.org/10.1016/0040-1951(90)90016-2)
- Isozaki, Y., Aoki, K., Nakam, T. and Yanai, S. 2010. New insight into a subduction-related orogen: a reappraisal of the geotectonic framework and evolution of the Japanese Islands. *Gondwana Research*, **18**, 82–105, <https://doi.org/10.1016/j.gr.2010.02.015>
- Jabri, N., Scotese, C.R. and Main, D.J. 2010. Dinosaur biogeography: Migration pathways and refugia. *Geological Society of America Abstracts with Programs*, **42**, 249.
- Jacobs, L.L., Polcyn, M.J., Taylor, L.H. and Ferguson, K. 2005. Sea-surface temperatures and paleoenvironments of dolichosaurs and early mosasaurs. *Netherlands*

- Journal of Geosciences*, **84**–3, 269–281, <https://doi.org/10.1017/S0016774600021053>
- Jenkyns, H.C., Jones, C.J., Grocke, D.R., Hesselbo, S.P. and Parkinson, D.N. 2002. Chemostratigraphy of the Jurassic System: applications, limitations and implications for palaeoceanography. *Journal of the Geological Society, London*, **159**, 351–378, <https://doi.org/10.1144/0016-764901-130>
- Jenkyns, H.C., Schouten-Huibers, L., Schouten, S. and Sinninghe Damste, J.S. 2012. Warm Middle Jurassic–Early Cretaceous high-latitude sea-surface temperatures from the Southern Ocean. *Climate of the Past*, **8**, 215–226, <https://doi.org/10.5194/cp-8-215-2012>
- Johnson, H., Dore, T., Gatliff, R.W., Holdsworth, R.W., Lundin, E.R. and Ritchie, J.D. (eds) 2008. *The Nature and Origin of Compression in Passive Margins*. Geological Society, London, Special Publications, **306**, <https://doi.org/10.1144/SP306.0>
- Johnston, S.T. and Thorkelson, D.J. 2000. Continental flood basalts: Episodic magmatism above long-lived hotspots. *Earth and Planetary Science Letters*, **175**, 247–256, [https://doi.org/10.1016/S0012-821X\(99\)00293-9](https://doi.org/10.1016/S0012-821X(99)00293-9)
- Jones, C.E. and Jenkyns, H.C. 2001. Seawater strontium isotopes, oceanic anoxic events, and seafloor hydrothermal activity in the Jurassic and Cretaceous. *American Journal of Science*, **301**, 112–149, <https://doi.org/10.2475/ajs.301.2.112>
- Judd, E.J., Tierney, J.E. et al. 2022. The PhanSST global database of Phanerozoic sea surface temperature proxy data. *Scientific Data*, **9**, 753, <https://doi.org/10.1038/s41597-022-01826-0>
- Kauffman, E.G. and Walliser, O.H. (eds) 1990. *Extinction Events in Earth History*. Springer, Berlin.
- Kay, S.M. and Ramos, V.A. (eds) 2006. *Evolution of an Andean Margin: A Tectonic and Magmatic View from the Andes to the Neuquén Basin (35°–39° S lat)*. Geological Society of America Special Papers, **407**, <https://doi.org/10.1130/SPE407>
- Kazmin, V.G. and Natapov, L.M. 1998. *The Paleogeographic Atlas of Northern Eurasia: Paleogeographic Maps on the Palinspastic Reconstruction, Orthographic Projection*. Institute of Lithospheric Plates, Russian Academy of Natural Sciences, Moscow.
- Keller, G. 2011. Defining the Cretaceous–Tertiary boundary: a practical guide and return to first principles. *SEPM Special Publications*, **100**, 23–42.
- Keller, G. 2014. Deccan volcanism, the Chicxulub impact, and the end-Cretaceous mass extinction: Coincidence? Cause and effect? *Geological Society of America Special Papers*, **505**, 57–89, [https://doi.org/10.1130/2014.2505\(03\)](https://doi.org/10.1130/2014.2505(03))
- Keller, G., Adatte, T., Gardin, S., Bartolini, A. and Bajpai, S. 2008. Main Deccan volcanism phase ends near the K–T boundary: Evidence from Krishna–Godavari Basin, SE India. *Earth and Planetary Science Letters*, **268**, 293–311, <https://doi.org/10.1016/j.epsl.2008.01.015>
- Keller, G., Mateo, P. et al. 2017. Environmental changes during the Cretaceous–Paleogene Mass Extinction and Paleocene–Eocene Thermal Maximum: Implications for the Anthropocene. *Gondwana Research*, **56**, 69–89, <https://doi.org/10.1016/j.gr.2017.12.002>
- Kennett, J.P. and Stott, L.D. 1991. Abrupt deep-water warming, palaeoceanographic changes and benthic extinctions at the end of the Paleocene. *Nature*, **353**, 225–229, <https://doi.org/10.1038/353225a0>
- Kennett, L.N. and Engdahl, E.R. 1991. Traveltimes for global earthquake location and phase identification. *Geophysical Journal International*, **105**, 429–465.
- Kent, W., Saunders, A.D., Kempton, P.D. and Ghose, N.C. 1997. Rajmahal Basalts, Eastern India: Mantle sources and melt distribution at a volcanic rifted margin. *American Geophysical Union Geophysical Monograph Series*, **100**, 145–182, <https://doi.org/10.1029/GM100p0145>
- Kerr, A.C., Tarney, J., Marriner, G.F., Nivia, A. and Saunders, A.D. 1997. The Caribbean–Colombian Cretaceous Igneous Province: The internal anatomy of an oceanic plateau. *Geophysical Union Geophysical Monograph Series*, **100**, 123–144, <https://doi.org/10.1029/GM100p0123>
- Khain, V.Y., Ronov, A.B. and Balukhovskiy, A.N. 1976. Cretaceous lithologic associations of the world. *International Geology Review*, **18**, 1269–1295, <https://doi.org/10.1080/00206817609471344>
- Kidder, D.L. and Worsley, T.R. 2010. Phanerozoic Large Igneous Provinces (LIPs), HEATT (Haline Euxinic Acidic Thermal Transgression) episodes, and mass extinctions. *Palaeogeography, Palaeoclimatology, Palaeoecology*, **295**, 162–191, <https://doi.org/10.1016/j.palaeo.2010.05.036>
- Kidder, D.L. and Worsley, T.T. 2012. A human-induced hothouse climate? *GSA Today*, **22**, 4–11, <https://doi.org/10.1130/G131A.1>
- Kiehl, J.T. and Shields, C.A. 2013. Sensitivity of the Paleocene–Eocene Thermal Maximum climate to cloud properties. *Philosophical Transactions of the Royal Society of London, Series A: Mathematical, Physical and Engineering Sciences*, **371**, 20130093, <https://doi.org/10.1098/rsta.2013.0093>
- Kiessling, W. 2001. Paleoclimatic significance of Phanerozoic Reefs. *Geology*, **29**, 751–754, [https://doi.org/10.1130/0091-7613\(2001\)029<0751:PSOPR>2.0.CO;2](https://doi.org/10.1130/0091-7613(2001)029<0751:PSOPR>2.0.CO;2)
- Kiessling, W. and Flügel, E. 2002. Paleoreefs: A database on Phanerozoic reefs. *SEPM Special Publications*, **72**, 77–92, <https://doi.org/10.2110/pec.02.72.0077>
- Kiessling, W., Flügel, E. and Golonka, J. (eds) 2002. *Phanerozoic Reef Patterns*. SEPM Special Publications, **72**, <https://doi.org/10.2110/pec.02.72>
- King, C.A. 2016. *A Revised Correlation of Tertiary Rocks in the British Isles and adjacent areas of NW Europe*. Geological Society, London, Special Report, **27**.
- Kirschvink, J.L., Ripperdan, R.L. and Evans, D.A. 1997. Evidence for a large-scale reorganization of Early Cambrian Continental masses by inertial interchange true polar wander. *Science*, **277**, 541–545, <https://doi.org/10.1126/science.277.5325.541>
- Kocsis, A.T. and Scotese, C.R. 2020. Mapping paleocoastlines and continental flooding during the Phanerozoic. *Earth-Science Reviews*, **213**, 103463, <https://doi.org/10.1016/j.earscirev.2020.103463>
- Köppen, W. 1918. Klassifikation der Klimate nach Temperatur, Niederschlag und Jahreslauf. *Petermanns Geographische Mitteilungen*, **64**, 193–248.
- Köppen, W. 1936. Das geographische System der Klimate. In: Köppen, W. and Gieger, G. (eds) *Handbuch der Klimatologie, Band 1*. Gebrüder Borntraeger, Berlin, 1–44.

- Koppers, A.A.P., Becker, T.W. *et al.* 2021. Mantle plumes and their role in Earth processes. *Nature Reviews*, **2**, 382–401, <https://doi.org/10.1038/s43017-021-00168-6>
- Kraus, D.W., Sertich, J.J.W., O'Connor, P.M., Rodgers, K.C. and Rogers, R.R. 2019. The Mesozoic biogeographic history of Gondwanan terrestrial vertebrates: Insights from Madagascar's fossil record. *Annual Reviews of Earth and Planetary Sciences*, **47**, 519–553, <https://doi.org/10.1146/annurev-earth-053018-060051>
- Kriest, J. 1991. Plate-Tectonic Atlas. *Exploration Bulletin*, **258**(1995/5). Shell Exploration Company, The Hague, The Netherlands.
- Kumar, P., Yuan, X.H., Kumar, M.R., Kind, R., Li, X.Q. and Chadha, R.K. 2007. The rapid drift of the Indian tectonic plate. *Nature Letters*, **449**, 894–897, <https://doi.org/10.1038/nature06214>
- Kump, L.R. and Pollard, D. 2008. Amplification of Cretaceous warmth by biological cloud feedbacks. *Science*, **320**, 195, <https://doi.org/10.1126/science.1153883>
- Kusky, T., Windley, B., Safonova, I., Wakita, K., Wakabayashi, J., Polat, A. and Santosh, M. 2013. Recognition of ocean plate stratigraphy in accretionary orogens through Earth history: A record of 3.8 billion years of sea floor spreading, subduction, and accretion. *Gondwana Research*, **24**, 501–547, <https://doi.org/10.1016/j.gr.2013.01.004>
- Ladant, J.B. and Donnadiou, Y. 2016. Palaeogeographic regulation of glacial events during the Cretaceous supergreenhouse. *Nature Communications*, **7**, 12771, <https://doi.org/10.1038/ncomms12771>
- Ladant, J.B., Poulsen, C.J. *et al.* 2020. Paleogeographic controls on the evolution of Late Cretaceous ocean circulation. *Climate of the Past*, **16**, 973–1006, <https://doi.org/10.5194/cp-16-973-2020>
- Lamb, S. 2004. *Devil in the Mountain: A Search for the Origin of the Andes*. Princeton University Press, Princeton, NJ.
- Landwehrs, J., Feulner, G., Petri, S., Sames, B. and Wagreich, M. 2021. Investigating Mesozoic climate trends and sensitivities with a large ensemble of climate simulations. *Paleoceanography and Paleoclimatology*, **36**, e2020PA004134, <https://doi.org/10.1029/2020PA004134>
- Larson, R.L. 1975. Late Jurassic seafloor spreading in the eastern Indian Ocean. *Geology*, **3**, 69–71, [https://doi.org/10.1130/0091-7613\(1975\)3<69:LJSSIT>](https://doi.org/10.1130/0091-7613(1975)3<69:LJSSIT>)
- Larson, R.L. 1991a. Geological consequences of superplumes. *Geology*, **19**, 963–966, [https://doi.org/10.1130/0091-7613\(1991\)019<0963:GCOS>2.3.CO;2](https://doi.org/10.1130/0091-7613(1991)019<0963:GCOS>2.3.CO;2)
- Larson, R.L. 1991b. Latest pulse of Earth: Evidence for a mid-Cretaceous superplume. *Geology*, **19**, 547–550, [https://doi.org/10.1130/0091-7613\(1991\)019<0547:LPOEEF>2.3.CO;2](https://doi.org/10.1130/0091-7613(1991)019<0547:LPOEEF>2.3.CO;2)
- Larson, R.L. and Erba, E. 1999. Onset of the mid-Cretaceous greenhouse in the Barremian–Aptian: Igneous events and biological sedimentary, and geochemical responses. *Paleoceanography*, **14**, 663–678, <https://doi.org/10.1029/1999PA900040>
- Larson, R.L., Mutter, J.C., Diebold, J.B., Carpenter, G.B. and Symonds, P. 1979. Cuvier basin: A product of ocean crust formation by Early Cretaceous rifting off western Australia. *Earth and Planetary Science Letters*, **45**, 104–114, [https://doi.org/10.1016/0012-821X\(79\)90112-2](https://doi.org/10.1016/0012-821X(79)90112-2)
- Larson, R.L., Pitman, W.C., III, Golovchenko, X., Cande, S.C., Dewey, J.F., Haxby, W.F. and LaBrecque, J.L. 1985. *The Bedrock Geology of the World* (scale 1:23 230 300 at the Equator). W.H. Freeman, New York.
- Lawver, L.A. and Müller, R.D.M. 1994. The Iceland Hot-spot Track. *Geology*, **22**, 311–314, [https://doi.org/10.1130/0091-7613\(1994\)022<0311:IHT>2.3.CO;2](https://doi.org/10.1130/0091-7613(1994)022<0311:IHT>2.3.CO;2)
- Lawver, L.A. and Scotese, C.R. 1987. A revised reconstruction of Gondwanaland. *American Geophysical Union Geophysical Monograph Series*, **40**, 17–24, <https://doi.org/10.1029/GM040p0017>
- Lawver, L.A. and Scotese, C.R. 1990. A review of tectonic models for the evolution of the Canada Basin. In: Grantz, A., Johnson, L. and Sweeney, J.F. (eds) *The Arctic Ocean Region. Decade of North American Geology, The Geology of North America, L*. Geological Society of America, Boulder, CO, 593–618.
- Legates, D.R. and Willmott, C.J. 1990. Mean seasonal and spatial variability in global surface air temperature. *Theoretical and Applied Climatology*, **41**, 11–21, <https://doi.org/10.1007/BF00866198>
- Leggett, J.K. 1982. *Trench–Forearc Geology: Sedimentation and Tectonics on Modern and Ancient Active Plate Margins*. Blackwell Scientific, Oxford, UK.
- Le Pichon, X., Sengor, A.M.C., Jellinek, M., Lenardic, A. and Imren, C. 2023. Breakup of Pangea and the Cretaceous revolution. *Tectonics*, **42**, E2022TC007489, <https://doi.org/10.1029/2022TC007489>
- Li, X., Hu, Y. *et al.* 2022. A high-resolution climate simulation dataset for the past 540 million years. *Scientific Data*, **9**, 371, <https://doi.org/10.1038/s41597-022-01490-4>
- Li, L. and Keller, G. 1998. Abrupt deep-sea warming at the end of the Cretaceous. *Geology*, **26**, 995–998.
- Li, Z.-X., Liu, Y. and Ernst, R. 2023. A dynamic 2000–540 Ma earth history: from cratonic amalgamation to the age of supercontinent cycle. *Earth-Science Reviews*, **238**, 104336, <https://doi.org/10.1016/j.earscirev.2023.104336>
- Lieberman, B.S. 2000. *Paleobiogeography: Using Fossils to Study Global Change, Plate Tectonics, and Evolution*. Topics in Geobiology, **16**. Kluwer Academic/Plenum Publishers, New York.
- Lieberman, B.S. 2003. Paleobiogeography: The relevance of fossils to biogeography. *Annual Reviews of Ecology, Evolution, and Systematics*, **34**, 51–69, <https://doi.org/10.1146/annrev.ecolsys.34.121101.153549>
- Linnemann, U., Nance, R.D., Kraft, P. and Zulauf, G. (eds) 2007. *The Evolution of the Rheic Ocean: From Avalonian–Cadomian Active Margin to Alleghenian–Variscan Collision*. Geological Society of America Special Papers, **423**, <https://doi.org/10.1130/SPE423>
- Lonsdale, P. 2005. Creation of the Cocos and Nazca plates by fission of the Farallon plate. *Tectonophysics*, **404**, 237–264, <https://doi.org/10.1016/j.tecto.2005.05.011>
- Lowrie, W. 2007. *Fundamentals of Geophysics*. 2nd edn. Cambridge University Press, Cambridge, UK.
- Lunt, D.J., Farnsworth, A. *et al.* 2016. Palaeogeographic controls on climate and proxy interpretation. *Climate of the Past*, **12**, 1181–1198, <https://doi.org/10.5194/cp-12-1181-2016>

- Lunt, D.J., Valdes, P. and Scotese, C. 2023. Changes in climate sensitivity and polar amplification over the last 500 million years. Abstract EGU23-9574 presented at the EGU General Assembly 2023, 24–28 April 2023, Vienna, Austria, <https://doi.org/10.5194/egusphere-egu23-9574>
- Luyendyk, B. 1995. Hypothesis for Cretaceous rifting of East Gondwana caused by subducted slab capture. *Geology*, **23**, 373–376, [https://doi.org/10.1130/0091-7613\(1995\)023%3C0373:HFCROE%3E2.3.CO;2](https://doi.org/10.1130/0091-7613(1995)023%3C0373:HFCROE%3E2.3.CO;2)
- Lyell, C. 1830. *Principles of Geology, Being an Attempt to Explain the Former Changes of the Earth's Surface, by Reference to Causes Now in Operation, Volume 1*. 1st edn. John Murray, London.
- Lyell, C. 1832. *Principles of Geology, Being an Attempt to Explain the Former Changes of the Earth's Surface, by Reference to Causes Now in Operation, Volume 2*. 1st edn. John Murray, London.
- Lyell, C. 1833. *Principles of Geology, Being an Attempt to Explain the Former Changes of the Earth's Surface, by Reference to Causes Now in Operation, Volume 3*. 1st edn. John Murray, London.
- Macfarlane, A., Sorkhabi, R.B. and Quade, J. (eds) 1999. *Himalaya and Tibet: Mountain Roots to Mountain Tops*. Geological Society of America Special Papers, **328**, <https://doi.org/10.1130/SPE328>
- MacLeod, N. 2013. *The Great Extinctions: What Causes them and How they Shape Life*. Firefly Books, Buffalo, NY.
- Mahoney, J.J. and Coffin, M.F. (eds) 1997. *Large Igneous Provinces: Continental Oceanic, and Planetary Flood Volcanism*. American Geophysical Union Geophysical Monograph Series, **100**, <https://doi.org/10.1029/GM100>
- Malchus, N. and Steuber, T. 2002. Stable isotope records (O, C) of Jurassic aragonitic shells from England and NW Poland: palaeoecologic and environmental implications. *Geobios*, **35**, 29–39, [https://doi.org/10.1016/S0016-6995\(02\)00007-4](https://doi.org/10.1016/S0016-6995(02)00007-4)
- Mallory, W.W. (ed.) 1972. *Geological Atlas of the Rocky Mountain Region*. Rocky Mountain Association of Geologists, Denver, CO.
- Mann, P. (ed.) 1995. *Geologic and Tectonic Development of the Caribbean Plate Boundary in Southern Central America*. Geological Society of America Special Papers, **295**, <https://doi.org/10.1130/SPE295>
- Mansour, A. and Wagreich, M. 2021. Earth system changes during the cooling greenhouse phase of the Late Cretaceous: Coniacian–Santonian OAE3 subevents and fundamental variations in organic carbon deposition. *Earth-Science Reviews*, **229**, 104022, <https://doi.org/10.1016/j.earscirev.2022.104022>
- Markwick, P.J. 2004. Palaeo-digital elevation models for use as boundary conditions in coupled ocean-atmosphere GCM experiments: a Maastrichtian (late Cretaceous) example. *Palaeogeography, Palaeoclimatology, Palaeoecology*, **213**, 37–63, [https://doi.org/10.1016/S0031-0182\(04\)00330-X](https://doi.org/10.1016/S0031-0182(04)00330-X)
- Markwick, P.J. 2007. The palaeogeographic and palaeoclimatic significance of climate proxies for data-model comparisons. In: Williams, M., Haywood, A.M., Gregory, F.J. and Schmidt, D.N. (eds) *Deep-Time Perspectives on Climate Change: Marrying the Signal from Computer Models and Biological Proxies*. Micropalaeontological Society Special Publications. Geological Society, London, 251–312.
- Markwick, P.J. 2019. Palaeogeography in exploration. *Geological Magazine*, **156**, 366–407, <https://doi.org/10.1017/S0016756818000468>
- Matthews, K.J., Williams, S.E., Whittaker, J.M., Müller, R.D., Seton, M. and Clarke, G.L. 2015. Geologic and kinematic constraints on the Late Cretaceous to mid-Eocene plate boundaries in the southwest Pacific. *Earth-Science Reviews*, **140**, 72–107, <https://doi.org/10.1016/j.earscirev.2014.10.008>
- McArthur, J.M., Janssen, N.M.M., Reboulet, S., Leng, M.J., Thirwall, M.F. and van de Schootbrugge, B. 2007. Palaeotemperatures, polar ice-volume, and isotope stratigraphy (Mg/Ca, $\delta^{18}\text{O}$, $\delta^{13}\text{C}$, $^{87}\text{Sr}/^{86}\text{Sr}$): The Early Cretaceous (Berriasian, Valanginian, Hauterivian). *Palaeogeography, Palaeoclimatology, Palaeoecology*, **248**, 391–430, <https://doi.org/10.1016/j.palaeo.2006.12.015>
- McCall, G.J.H. (ed.). 1983. *Ophiolitic and Related Melanges*. Benchmark Papers in Geology, **66**. Hutchinson Ross, Stroudsburg, PA.
- McClay, K.R. and Price, N.J. (eds) 1981. *Thrust and Nappe Tectonics*. Geological Society, London, Special Publications, **9**.
- McCrossan, R.G., Glaister, R.P., Austin, G.H. and Nelson, S.J. 1964. *Geological History of Western Canada*. Alberta Society of Petroleum Geologists, Calgary, AB, Canada.
- McElhinny, M.W. 1973. *Palaeomagnetism and Plate Tectonics*. Cambridge Earth Science Series. Cambridge University Press, Cambridge, UK.
- McElhinny, W.W. and McFadden, P.L. 2000. *Paleomagnetism: Continents and Oceans*. International Geophysics Series, **73**. Academic Press, San Diego, CA.
- McGhee, G.R., Clapham, M.E., Sheehan, P.M., Bottjer, D.J. and Droser, M.L. 2013. A new ecological-severity ranking of major Phanerozoic biodiversity crises. *Palaeogeography, Palaeoclimatology, Palaeoecology*, **370**, 260–270, <https://doi.org/10.1016/j.palaeo.2012.12.019>
- McInerney, F.A. and Wing, S.L. 2011. The Paleocene–Eocene Thermal Maximum: a perturbation of carbon cycle, climate, and biosphere with implications for the future. *Annual Review of Earth Planetary Sciences*, **39**, 489–516, <https://doi.org/10.1146/annurev-earth-040610-133431>
- McKenna, M.C. 1973. Sweepstakes, Filters, Corridors, Noah's Arks, and Beach Viking Funeral Ships in Palaeogeography. In: Tarling, D.H. and Runcorn, S.K. (eds) *Implications of Continental Drift to the Earth Sciences, Volume 1*. Academic Press, London, 295–308.
- McKenzie, N.R. and Jiang, H. 2019. Earth's outgassing and climatic transitions: The slow burn towards environmental 'catastrophes'? *Elements*, **15**, 325–330, <https://doi.org/10.2138/gselements.15.5.325>
- McKenzie, N.R., Horton, B.K., Loomis, S.E., Stockli, D.F., Planavsky, N.J. and Lee, C.-T.A. 2016. Continental arc volcanism as the principal driver of icehouse-greenhouse variability. *Science*, **352**, 444–447, <https://doi.org/10.1126/science.aad5787>
- McKerrow, W.S. and Scotese, C.R. (eds) 1990. *Paleozoic Paleogeography and Biogeography*. Geological Society, London, Memoirs, **12**, <https://doi.org/10.1144/GSL.MEM.1990.012.01.41>

- Meissner, R., Wever, T. and Sadowiak, P. 1991. Continental collisions and seismic signature. *Geophysical Journal International*, **105**, 15–23, <https://doi.org/10.1111/j.1365-246X.1991.tb03440.x>
- Menzies, M.A., Klemperer, S.L., Ebinger, C.J. and Baker, J. (eds) 2002. *Volcanic Rifted Margins*. Geological Society of America Special Papers, **362**, <https://doi.org/10.1130/SPE362>
- Merdith, A.S., Williams, S.E., Brune, S., Collins, A.S. and Müller, R.D. 2019. Rift and plate boundary evolution across two supercontinent cycles. *Global and Planetary Change*, **173**, 1–14, <https://doi.org/10.1016/j.gloplacha.2018.11.006>
- Merdith, A.S., Williams, S.E. *et al.* 2021. Extending full-plate tectonic models into deep time: Linking the Neoproterozoic and the Phanerozoic. *Earth-Science Reviews*, **214**, 103477, <https://doi.org/10.1016/j.earscirev.2020.103477>
- Metcalfe, I. 1984. Stratigraphy, palaeontology and palaeogeography of the Carboniferous of Southeast Asia. *Memoires Societe Geologiques France (New Series)*, **174**, 107–118.
- Metcalfe, I. 1993. Southeast Asian terranes: Gondwanaland origins and evolution. In: Findlay, R.H., Uhrug, R., Banks, M.R. and Veevers, J.J. (eds) *Gondwana Eight: Assembly, Evolution And Dispersal*. Balkema, Rotterdam, The Netherlands, 181–200.
- Metcalfe, I. 1999. Gondwana dispersion and Asian accretion: An overview. In: Metcalfe, I., Jishun, R., Charvet, J. and Hada, S. (eds) *Gondwana Dispersion and Asia Accretion*. A.A. Balkema, Rotterdam, The Netherlands, 9–28.
- Metcalfe, I. 2011. Tectonic framework and Phanerozoic evolution of Sundaland. *Gondwana Research*, **19**, 3–21, <https://doi.org/10.1016/j.gr.2010.02.016>
- Metzler, M. 2006. *The Formation and Obduction of Ophiolites since the Late Precambrian*. Master's thesis, University of Texas at Arlington, Arlington, Texas, USA.
- Meyer, K.M. and Kump, L.R. 2008. Oceanic euxinia in Earth history: Causes and consequences. *Annual Review of Earth and Planetary Sciences*, **36**, 251–288, <https://doi.org/10.1146/annurev.earth.36.031207.124256>
- Middlemiss, F.A., Rawson, P.F. and Newall, G. 1971. *Faunal Provinces in Space and Time*. Geological Journal, Special Issue, **4**. Seel House Press, Liverpool, UK.
- Mihalynuk, M.G., Nelson, J. and Diakow, L.J. 1994. Cache Creek terrane entrapment: Oroclinal paradox with the Canadian Cordillera. *Tectonics*, **13**, 575–595, <https://doi.org/10.1029/93TC03492>
- Miller, C.S., Petersen, F., da Silva, A.-C., Baranyi, V., Reichart, G.J. and Kürschner, W.M. 2017. Astronomical age constraints and extinction mechanisms of the Late Triassic Carnian crisis. *Scientific Reports*, **7**, 2557, <https://doi.org/10.1038/s41598-017-02817-7>
- Miller, K.G., Barrera, E., Olsson, R.K., Sugarman, P.J. and Savin, S.M. 1999. Does ice drive early Maastrichtian eustasy? *Geology*, **27**, 783–786, [https://doi.org/10.1130/0091-7613\(1999\)027<0783:DIDEME>2.3.CO;2](https://doi.org/10.1130/0091-7613(1999)027<0783:DIDEME>2.3.CO;2)
- Miller, K.G., Sugarman, P.J., Browning, J.V., Kominz, M.A., Olsson, R.K., Feigenson, M.D. and Hernández, J.C. 2004. Upper Cretaceous sequences and sea-level history, New Jersey coastal plain. *Geological Society of America Bulletin*, **116**, 368–393, <https://doi.org/10.1130/B25279.1>
- Miller, K.G., Kominz, M.A. *et al.* 2005a. The Phanerozoic record of global sea-level change. *Science*, **310**, 1293–1298, <https://doi.org/10.1126/science.1116412>
- Miller, K.G., Wright, J.D. and Browning, J.V. 2005b. Visions of ice sheets in a greenhouse world. *Marine Geology*, **217**, 215–231, <https://doi.org/10.1016/j.margeo.2005.02.007>
- Miller, K.G., Sherrell, R.M. *et al.* 2010. Relationship between mass extinction and iridium across the Cretaceous–Paleogene boundary in New Jersey. *Geology*, **38**, 867–870, <https://doi.org/10.1130/G31135.1>
- Miller, K.G., Browning, J.V., Smetz, W.J., Kopp, R.E., Mountain, G.S. and Wright, J.D. 2020. Cenozoic sea-level and cryosphere evolution from deep-sea geochemical and continental margin records. *Science Advances*, **6**, eaaz1346, <https://doi.org/10.1126/sciadv.aaz1346>
- Mills, B.J.W., Krause, A.J., Scotese, C.R., Hill, D.J., Shields, G.A. and Lenton, T.M. 2019. Modelling the long-term carbon cycle, atmospheric CO₂, and Earth surface temperature from late Neoproterozoic to present-day. *Gondwana Research*, **67**, 172–186, <https://doi.org/10.1016/j.gr.2018.12.001>
- Molnar, P. and Tapponnier, P. 1975. Cenozoic tectonics of Asia: Effects of a continental collision. *Science*, **189**, 419–426, <https://doi.org/10.1126/science.189.4201.419>
- Monger, J.W.H. 2008. *The Evolution of Canada's Western Mountains*. Geological Survey of Canada Open File Report, **504**.
- Monger, J.W.H. and Nokleberg, W.J. 1996. Evolution of the northern North American Cordillera: generation, fragmentation, displacement and accretion of successive North American plate margin arcs. In: Coyner, A.R. and Fahey, P.L. (eds) *Geology and Ore Deposits of the American Cordillera*. Geological Society of Nevada, Reno, NV, 1133–1152.
- Moore, T.L. and Scotese, C.R. 2012. *Ancient Earth: Breakup of Pangea, Vers. 1.0*. iOS Mobile Application. Apple App Store, <https://apps.apple.com/us/app/ancient-earth/id509943912>
- Moores, E.M. 2002. Pre-1 Ga (pre-Rodinia) ophiolites: Their tectonic and environmental implications. *Geological Society of America Bulletin*, **114**, 80–95, [https://doi.org/10.1130/0016-7606\(2002\)114<0080:PGPROT>2.0.CO;2](https://doi.org/10.1130/0016-7606(2002)114<0080:PGPROT>2.0.CO;2)
- Moreno, T., Wallis, S., Kojima, T. and Gibbons, W. 2016. *The Geology of Japan*. Geological Society, London.
- Morgan, J.P., Reston, T.J. and Ranero, C.R. 2004. Contemporaneous mass extinctions, continental flood basalts, and 'impact signals': are mantle plume-induced lithospheric gas explosions the causal link? *Earth and Planetary Science Letters*, **217**, 263–284, [https://doi.org/10.1016/S0012-821X\(03\)00602-2](https://doi.org/10.1016/S0012-821X(03)00602-2)
- Morgan, P. and Baker, B.H. (eds) 1983. *Processes of Continental Rifting: Selected Papers from the Lunar and Planetary Institute Topical Conference on the Processes of Planetary Rifting*. Developments in Geotectonics, **19**. Elsevier, Amsterdam.
- Morley, R.J. 2000. *Origin and Evolution of Tropical Rain Forests*. John Wiley and Sons, Chichester, UK.
- Morley, R.J. 2011. Cretaceous and Tertiary climate change and the past distribution of megathermal rainforests. In:

- Bush, M.B., Flenley, J.R. and Gosling, W.D. (eds) *Tropical Rainforest Responses to Climatic Change*. Springer, Berlin, 1–31, https://doi.org/10.1007/978-3-540-48842-2_1
- Mossop, G. and Shetson, I. 1994. *Geological Atlas of Western Canada Sedimentary Basins*. Canadian Society of Petroleum Geologists, Calgary, AB, Canada.
- Müller, R.D., Royer, J.Y. and Lawver, L.A. 1993a. Revised plate motions relative to hotspots combined Atlantic and Indian Ocean hotspot tracks. *Geology*, **21**, 275–278, [https://doi.org/10.1130/0091-7613\(1993\)021<0275:RPMRTT>2.3.CO;2](https://doi.org/10.1130/0091-7613(1993)021<0275:RPMRTT>2.3.CO;2)
- Müller, R.D., Roest, W.R., Royer, J.Y., Gahagan, L.M. and Sclater, J.G. 1993b. *A Digital Age Map of the Ocean Floor*. Scripps Institution of Oceanography (SIO) Reference Series, **93-30**. Scripps Institution of Oceanography, San Diego, CA.
- Müller, R.D., Roest, W.R., Royer, J., Gahagan, L.M. and Sclater, J.G. 1997. Digital isochrons of the world's ocean floor. *Journal of Geophysical Research: Solid Earth*, **102**, 3211–3214, <https://doi.org/10.1029/96JB01781>
- Müller, R.D., Sdrolias, M., Gaina, C. and Roest, W.R. 2008a. Age, spreading rates, and spreading asymmetry of the world's ocean crust. *Geochemistry Geophysics Geosystems*, **9**, Q04006, <https://doi.org/10.1029/2007GC001743>
- Müller, R.D., Sdrolias, M., Gaina, C., Steinberger, B. and Heine, C. 2008b. Long-term sea-level fluctuations driven by ocean basin dynamics. *Science*, **319**, 1357–1362, <https://doi.org/10.1126/science.1151540>
- Müller, R.D., Cannon, J. et al. 2018. GPlates: Building a virtual Earth through deep time. *Geochemistry, Geophysics, Geosystems*, **19**, 2243–2261, <https://doi.org/10.1029/2018GC007584>
- Mutterlose, J., Pauly, S. and Steuber, T. 2009. Temperature controlled deposition of early Cretaceous (Barremian–early Aptian) black shales in an epicontinental sea. *Palaeogeography, Palaeoclimatology, Palaeoecology*, **273**, 330–345, <https://doi.org/10.1016/j.palaeo.2008.04.026>
- Muttoni, G. and Kent, D.V. 2019. Jurassic monster polar shift confirmed by sequential paleopoles from Adira, promontory of Africa. *Journal of Geophysical Research: Solid Earth*, **124**, 3288–3306, <https://doi.org/10.1029/2018JB017199>
- Muttoni, G., Dallanave, E. and Channell, J.E.T. 2013. The drift history of Adira and Africa from 280 Ma to present, Jurassic true polar wander, and zonal climate control on Tethyan sedimentary facies. *Palaeogeography, Palaeoclimatology, and Palaeoecology*, **386**, 415–435, <https://doi.org/10.1016/j.palaeo.2013.06.011>
- Nakanishi, M., Sager, W.W. and Korenaga, J. 2015. Reorganization of the Pacific–Izanagi–Farallon triple junction in the Late Jurassic: Tectonic events before the formation of the Shatsky Rise. *Geological Society of America Special Papers*, **511**, 85–101, [https://doi.org/10.1130/2015.2511\(05\)](https://doi.org/10.1130/2015.2511(05))
- Nance, R.D. and Murphy, J.B. 2013. Origins of the supercontinent cycle. *Geoscience Frontiers*, **4**, 439–448, <https://doi.org/10.1016/j.gsf.2012.12.007>
- Nance, R.D. and Thompson, M.D. (eds) 1996. *Avalonian and Related Peri-Gondwanan Terranes of the Circum-North Atlantic*. Geological Society of America Special Papers, **304**, <https://doi.org/10.1130/SPE304>
- Nance, R.D., Worsley, T.R. and Moody, J.B. 1988. The supercontinent cycle. *Scientific American*, **259**, 72–79, <https://doi.org/10.1038/scientificamerican0788-72>
- Nance, R.D., Murphy, J.B. and Santosh, M. 2014. The supercontinent cycle: A retrospective essay. *Gondwana Research*, **25**, 4–29, <https://doi.org/10.1016/j.jgr.2012.12.026>
- Navarro-Ramirez, J.P., Bodin, S., Consorti, L. and Immenhauser, A. 2017. Response of western South American epeiric–neritic ecosystem to middle Cretaceous Oceanic Anoxic Events. *Cretaceous Research*, **75**, 61–80, <https://doi.org/10.1016/j.cretres.2017.03.009>
- Neal, C.R., Mahoney, J.J., Kroenk, L.W., Duncan, R.A. and Petterson, M.G. 1997. The Ontong Java Plateau. *American Geophysical Union Geophysical Monograph Series*, **100**, 183–216, <https://doi.org/10.1029/GM100p0183>
- Neal, C.R., Sager, W.W., Sano, T. and Erba, E. (eds) 2015. *The Origin, Evolution, and Environmental Impact of Oceanic Large Igneous Provinces*. Geological Society of America Special Papers, **511**, <https://doi.org/10.1130/SPE511>
- Nichols, D.J. and Johnson, K.R. 2008. *Plants and the K–T Boundary*. Cambridge University Press, Cambridge, UK.
- Nitecki, M.H. (ed.) 1984. *Extinctions*. University of Chicago Press, Chicago, IL.
- Nokleberg, W.J., Parfenov, L.M. et al. 2001. *Phanerozoic Tectonic Evolution of the Circum-North Pacific*. United States Geological Society Professional Papers, **1626**.
- O'Brien, C.L., Robinson, S.A. et al. 2017. Cretaceous sea-surface temperature evolution: Constraints for TEX 86 and planktonic foraminiferal Oxygen isotopes. *Earth-Science Reviews*, **172**, 224–247, <https://doi.org/10.1016/j.earscirev.2017.07.012>
- Officer, C.B. and Drake, C.L. 1985. Terminal Cretaceous environmental events. *Science*, **227**, 1161–1167, <https://doi.org/10.1126/science.227.4691.1161>
- Officer, C.B. and Page, J. 1996. *The Great Dinosaur Extinction Controversy*. Helix Books, Reading, MA.
- Ogg, J.G., Ogg, G.M. and Gradstein, F.M. 2016. *A Concise Geological Time Scale 2016*. Elsevier, Amsterdam.
- Olsson, R.K., Miller, K.G., Browning, J.V., Wright, J.D. and Cramer, B.S. 2002. Sequence stratigraphy and sea-level change across the Cretaceous–Tertiary boundary on the New Jersey passive margin. *Geological Society of America Special Papers*, **356**, 97–108, <https://doi.org/10.1130/0-8137-2356-6.97>
- Oncken, O., Chong, G. et al. (eds) 2006. *The Andes: Active Subduction Orogeny*. Springer, Berlin.
- Ostrom, J.H. and Orville, P.M. (eds) 1975. *Tectonics and Mountain Ranges, A Special Volume of the American Journal of Science Dedicated to John Rodgers*. American Journal of Science, **275-A**.
- Otto-Bliesner, B.L. and Upchurch, G.R. 1997. Vegetation-induced warming of high latitude regions during the Late Cretaceous period. *Nature*, **385**, 804–807, <https://doi.org/10.1038/385804a0>
- Oxburgh, E.E. 1968. *The Geology of the Eastern Alps*. The Geologists' Association, London.

- Panayiotou, A. (ed.) 1980. Ophiolites: Proceedings of the International Ophiolite Symposium, Cyprus, 1979. Ministry of Agriculture and Natural Resources, Geological Survey Department, Nicosia.
- Pankhurst, R.J. and Rapela, C.W. (eds) 1998. *The Proterozoic Margin of Gondwana*. Geological Society, London, Special Publications, **142**, <https://doi.org/10.1144/GSL.SP.1998.142.01.18>
- Parfenov, L.M., Berzin, N.A. *et al.* 2010. Tectonic and metallogenic model for northeast Asia. *United States Geological Survey Professional Papers*, **1765**, 9-1-9-55, https://pubs.usgs.gov/pp/1765/chapter_9
- Parfenov, L.M., Nokleberg, W.J. *et al.* (eds) 2011. *Tectonic and Metallogenic Model for Northeast Asia*. United States Geological Survey Open-File Report, **2011-1026**.
- Parrish, J.T. 1998. *Interpreting Pre-Quaternary Climate from the Geologic Record*. Columbia University Press, New York.
- Parrish, J.T. and Spicer, R.A. 1988. Late Cretaceous terrestrial vegetation: A near polar temperature curve. *Geology*, **16**, 22-25, [https://doi.org/10.1130/0091-7613\(1988\)016<0022:LCTVAN>2.3.CO;2](https://doi.org/10.1130/0091-7613(1988)016<0022:LCTVAN>2.3.CO;2)
- Parrish, J.T., Ziegler, A.M. and Scotese, C.R. 1982. Rainfall patterns and the distribution of coals and evaporites in the Mesozoic and Cenozoic. *Palaeogeography, Palaeoclimatology, Palaeoecology*, **40**, 67-101, [https://doi.org/10.1016/0031-0182\(82\)90085-2](https://doi.org/10.1016/0031-0182(82)90085-2)
- Parsons, B. and Sclater, J.G. 1977. An analysis of the variation of ocean floor bathymetry and heat flow with age. *Journal of Geophysical Research*, **82**, 803-827, <https://doi.org/10.1029/JB082i005p00803>
- Patriat, P. and Segoufin, J. 1988. Reconstruction of the Central Indian Ocean. *Tectonophysics*, **155**, 211-234, [https://doi.org/10.1016/0040-1951\(88\)90267-3](https://doi.org/10.1016/0040-1951(88)90267-3)
- Paul, G.S. 2016. *The Princeton Field Guide to Dinosaurs*. 2nd edn. Princeton University Press, Princeton, NJ.
- Paul, G.S. 2022a. *The Princeton Field Guide to Mesozoic Sea Reptiles*. Princeton University Press, Princeton, NJ.
- Paul, G.S. 2022b. *The Princeton Field Guide to Pterosaurs*. Princeton University Press, Princeton, NJ.
- Peate, D.W. 1997. The Parana-Entendeka Province. *American Geophysical Union Geophysical Monograph Series*, **100**, 217-245, <https://doi.org/10.1029/GM100p0217> <https://doi.org/10.1144/SP544-2023-88>
- Peltier, W.R. 2004. Global glacial isostasy and the surface of the Ice-Age Earth: The ICE-5G (VM2) model and GRACE. *Annual Review of Earth and Planetary Sciences*, **32**, 111-149, <https://doi.org/10.1146/annurev.earth.32.082503.144359>
- Percival, L.M.E., Matsumoto, H., Callegaro, S., Erba, E., Kerr, A.C., Mutterlose, J. and Suzuki, K. 2024. Cretaceous large igneous provinces: from volcanic formation to environmental catastrophes and biological crises. *Geological Society, London, Special Publications*, **544**, <https://doi.org/10.1144/SP544-2023-88>
- Petersen, S.V., Dutton, A. and Lohmann, K.C. 2016. End-Cretaceous extinction in Antarctica linked to both Deccan volcanism and meteorite impact via climate change. *Nature Communications*, **7**, 12079, <https://doi.org/10.1038/ncomms12079>
- Pfiffner, O.A. 2014. *Geology of the Alps. Revised and updated Translation of Geologie der Alpen*. 2nd edn. Wiley-Blackwell, Chichester, UK.
- Pindell, J. and Barrett, S.F. 1990. Geological evolution of the Caribbean region: a plate tectonic perspective. In: Dengo, G. and Case, J.E. (eds) *The Caribbean Region. Decade of North American Geology*, The Geology of North America, **H**. Geological Society of America, Boulder, CO, 405-432.
- Pindell, J. and Kennan, L. 2009. Tectonic evolution of the Gulf of Mexico, Caribbean, and northern South America in the mantle reference frame: an update. *Geological Society, London, Special Publications*, **328**, 1-55, <https://doi.org/10.1144/SP328.1>
- Pindell, J., Cande, S.C., Pitman, W.C., III, Rowley, D.B., Dewey, J.F., LaBrecque, J. and Haxby, W. 1988. A plate-kinematic framework for models of Caribbean evolution. *Tectonophysics*, **155**, 121-138, [https://doi.org/10.1016/0040-1951\(88\)90262-4](https://doi.org/10.1016/0040-1951(88)90262-4)
- Pindell, J., Kennan, L., Maresch, W.V., Stanel, K.-P., Draper, G. and Higgs, R. 2005. Plate-kinematics and crustal dynamics of circum-Caribbean arc-continent interactions: Tectonic controls on basin development in Proto-Caribbean margins. *Geological Society of America Special Papers*, **394**, 7-52, <https://doi.org/10.1130/0-8137-2394-9.7>
- Pirrie, D., Doyle, P., Marshall, J. and Ellis, G. 1995. Cool Cretaceous climates: new data from the Albian of Western Australia. *Journal of the Geological Society, London*, **152**, 739-742, <https://doi.org/10.1144/gsjgs.152.5.0739>
- Pirrie, D., Marshall, J., Doyle, P. and Riccardi, A. 2004. Cool early Albian climates; new data from Argentina. *Cretaceous Research*, **25**, 27-33, <https://doi.org/10.1016/j.cretres.2003.10.002>
- Pisarevsky, S.A. 2005. New edition of the Global Paleomagnetic Database (GPMDB4.6b). *Eos, Transactions of the American Geophysical Union*, **86**, 170, <https://doi.org/10.1029/2005EO170004>
- Pisarevsky, S.A., Li, Z.X., Tetley, M.G., Liu, Y. and Beardmore, J.P. 2022. An updated internet-based Global Paleomagnetic Database. *Earth-Science Reviews*, **235**, 104258, <https://doi.org/10.1016/j.earscirev.2022.104258>
- Pitman, W.C., III 1978. Relationship between eustasy and stratigraphic sequences of passive margins. *Geological Society of America Bulletin*, **89**, 389-1403.
- Poblete, F., Dupont-Nivet, G. *et al.* 2014. Towards interactive global paleogeographic maps, new reconstructions at 60, 40 and 20 Ma. *Earth-Science Reviews*, **235**, 103508, <https://doi.org/10.1016/j.earscirev.2021.103508>
- Podlaha, O.G., Mutterlose, J. and Veizer, J. 1998. Preservation of delta ¹⁸O and delta ¹³C in belemnite rostra from Jurassic/early Cretaceous successions. *American Journal of Science*, **298**, 324-347, <https://doi.org/10.2475/ajs.298.4.324>
- Pope, V.D., Gallani, M.L., Rowntree, P.R. and Stratton, R.A. 2000. The impact of new physical parametrizations in the Hadley Centre climate model: HadAM3. *Climate Dynamics*, **16**, 123-146, <https://doi.org/10.1007/s003820050009>
- Poulsen, C.J., Barron, E.J., Peterson, W.H. and Wilson, P.A. 1999. A reinterpretation of mid-Cretaceous shallow marine temperatures through model-data comparison. *Palaeogeography*, **14**, 679-697, <https://doi.org/10.1029/1999PA900034>
- Poulsen, C.J., Barron, E.J., Arthur, M.A. and Peterson, W.H. 2001. Response of the mid-Cretaceous global

- oceanic circulation to tectonic and CO₂ forcings. *Paleoceanography*, **16**, 576–592, <https://doi.org/10.1029/2000PA000579>
- Poulsen, C.J., Pollard, D. and White, T.S. 2007. General circulation model simulation of the $\delta^{18}\text{O}$ content of continental precipitation in the middle Cretaceous: A model-proxy comparison. *Geology*, **35**, 199–202, <https://doi.org/10.1130/G23343A.1>
- Powell, C.McA., Roots, S.R. and Veevers, J.J. 1988. Pre-breakup continental extension in East Gondwanaland and the early opening of the eastern Indian Ocean. *Tectonophysics*, **155**, 261–283, [https://doi.org/10.1016/0040-1951\(88\)90269-7](https://doi.org/10.1016/0040-1951(88)90269-7)
- Powell, J.L. 1998. *Night Comes to the Cretaceous: Comets, Craters, Controversy, and the Last Days of the Dinosaurs*. Harcourt Brace and Company, San Diego, CA.
- Preto, N., Kustatscher, E. and Wignall, P.B. 2010. Triassic climates – state of the art and perspectives. *Palaeogeography, Palaeoclimatology, Palaeoecology*, **290**, 1–10, <https://doi.org/10.1016/j.palaeo.2010.03.015>
- Price, G.D. 1999. The evidence and implications of polar ice during the Mesozoic. *Earth-Science Reviews*, **48**, 183–210, [https://doi.org/10.1016/S0012-8252\(99\)00048-3](https://doi.org/10.1016/S0012-8252(99)00048-3)
- Price, G.D. and Mutterlose, J. 2004. Isotopic signals from late Jurassic–early Cretaceous (Volgian–Valanginian) sub-Arctic belemnites, Yatria River, Western Siberia. *Journal of the Geological Society, London*, **161**, 959–968, <https://doi.org/10.1144/0016-764903-169>
- Price, G.D. and Nunn, E.V. 2010. Valanginian isotope variation in glendonites and belemnites from Arctic Svalbard: Transient glacial temperatures during the Cretaceous greenhouse. *Geology*, **38**, 251–254, <https://doi.org/10.1130/G30593.1>
- Price, G.D. and Passey, B.H. 2013. Dynamic polar climates in a greenhouse world: evidence from clumped isotope thermometry of Early Cretaceous belemnites. *Geology*, **41**, 923–926, <https://doi.org/10.1130/G34484.1>
- Price, G.D., Valdes, P.J. and Sellwood, B.W. 1998. A comparison of GCM simulated Cretaceous ‘greenhouse’ and ‘icehouse’ climates: implications for the sedimentary record. *Palaeogeography, Palaeoclimatology, Palaeoecology*, **142**, 123–138, [https://doi.org/10.1016/S0031-0182\(98\)00061-3](https://doi.org/10.1016/S0031-0182(98)00061-3)
- Price, R.A. and Monger, J.W.H. 2000. A transect of the southern Canadian Cordillera from Calgary to Vancouver. In: Annual Meeting of the Cordilleran Section of the Geological Society of America, Vancouver, April 2000. Geological Association of Canada –Cordilleran Section, Vancouver, BC, Canada.
- Prokoph, A., Shields, G.A. and Veizer, J. 2008. Compilation and time-series analysis of a marine carbonate $\delta^{18}\text{O}$, $\delta^{13}\text{C}$, $^{87}\text{Sr}/^{86}\text{Sr}$ and $\delta^{34}\text{S}$ database through Earth history. *Earth-Science Reviews*, **87**, 113–133, <https://doi.org/10.1016/j.earscirev.2007.12.003>
- Pucéat, E., Lécuyer, C., Sheppard, S.M., Dromart, G., Reboulet, S. and Grandjean, P. 2003. Thermal evolution of Cretaceous Tethyan marine waters inferred from oxygen isotope composition of fish tooth enamels. *Paleoceanography*, **18**, 1029, <https://doi.org/10.1029/2002PA000823>
- Punekar, J., Mateo, P. and Keller, G. 2014. Effects of Deccan volcanism on paleoenvironment and planktic foraminifera: A global survey. *Geological Society of America Special Papers*, **505**, 91–116, [https://doi.org/10.1130/2014.2505\(04\)](https://doi.org/10.1130/2014.2505(04))
- Rae, J.W.B., Zhang, Y.G., Liu, X., Foster, G.L., Stoll, H.M. and Whiteford, R.D.M. 2021. Atmospheric CO₂ over the past 66 million years from marine archives. *Annual Review of Earth and Planetary Sciences*, **49**, 609–641, <https://doi.org/10.1146/annurev-earth-082420-063026>
- Rampino, M.R. and Self, S. 2015. Large igneous provinces and biotic extinctions. In: Sigurdsson, H., Houghton, B., Rymer, H., Stix, J. and McNutt, S. (eds) *The Encyclopedia of Volcanoes*. 2nd edn. Elsevier, Amsterdam, 1049–1158.
- Rampino, M.R. and Stothers, R.B. 1988. Flood basalt volcanism during the past 250 million years. *Science*, **241**, 663–668, <https://doi.org/10.1126/science.241.4866.663>
- Raup, D.M. 1986. *The Nemesis Affair: A Story of the Death of the Dinosaurs and the Ways of Science*. W.W. Norton and Company, New York.
- Raup, D.M. 1991. *Extinction: Bad Luck or Bad Gene?* W.W. Norton, New York.
- Ravizza, G. and Peucker-Ehrenbrink, B. 2003. Chemostratigraphic evidence of Deccan volcanism from the marine Osmium isotope record. *Science*, **302**, 1392–1395.
- Rea, D.K., Zachos, J.C., Owen, R.M. and Gingerich, P.D. 1990. Global change at the Paleocene–Eocene boundary: climatic and evolutionary consequences of tectonic events. *Palaeogeography, Palaeoclimatology, Palaeoecology*, **79**, 117–128, [https://doi.org/10.1016/0031-0182\(90\)90108-J](https://doi.org/10.1016/0031-0182(90)90108-J)
- Rees, P.M., Gibbs, M.T., Ziegler, A.M., Kutzbach, J.E., Behling, P.J. and Rowley, D.B. 2002. Permian phytogeographic patterns and climate data/model comparisons. *Journal of Geology*, **27**, 891–894, [https://doi.org/10.1130/0091-7613\(1999\)027<0891:PCEMPU>2.3.CO;2](https://doi.org/10.1130/0091-7613(1999)027<0891:PCEMPU>2.3.CO;2)
- Renault, R.W. and Ashley, G.M. (eds) 2002. *Sedimentation in Continental Rifts*. SEPM Special Publications, **73**.
- Renne, P.R., Sprain, C.J., Richards, M.A., Self, S., Vanderkluysen, L. and Pande, K. 2015. State shift in Deccan volcanism at the Cretaceous–Paleogene boundary, possibly induced by impact. *Science*, **350**, 76–78, <https://doi.org/10.1126/science.aac7549>
- Retallack, G.J. 2013. Permian and Triassic greenhouse crises. *Gondwana Research*, **24**, 90–103, <https://doi.org/10.1016/j.gr.2012.03.003>
- Retallack, G.J., Sheldon, N.D. et al. 2011. Multiple Early Triassic greenhouse crises impeded recovery from Late Permian mass extinction. *Palaeogeography, Palaeoclimatology, Palaeoecology*, **308**, 233–251, <https://doi.org/10.1016/j.palaeo.2010.09.022>
- Richards, M.A., Duncan, R. and Courtillot, V. 1989. Flood basalts and hot-spot tracks. *Science*, **246**, 103–107, <https://doi.org/10.1126/science.246.4926.103>
- Richards, M.A., Alvarez, W., Self, S., Karlstrom, L., Renne, P.R., Manga, M., Sprain, C.J., Smit, J., Vanderkluysen, L. and Gibson, S.A. 2015. Triggering of the largest Deccan eruptions by the Chicxulub impact. *Geological Society of America Bulletin*, **127**, 1507–1520, <https://doi.org/10.1130/B31167.1>
- Rigo, M. and Joachimski, M.M. 2010. Palaeoecology of Late Triassic conodonts: constraints from oxygen isotopes in biogenic apatite. *Acta Palaeontologica*

- Polonica, **55**, 471–478, <https://doi.org/10.4202/app.2009.0100>
- Roberts, D.G. and Bally, A.W. (eds) 2012a. *Regional Geology and Tectonics: Phanerozoic Rift systems and Sedimentary Basins, Volume 1B*. Elsevier, Amsterdam.
- Roberts, D.G. and Bally, A.W. (eds) 2012b. *Regional Geology and Tectonics: Phanerozoic Passive Margins, Cratonic Basins, and Global Tectonic Maps, Volume 1C*. Elsevier, Amsterdam.
- Roche, V. and Ringebach, J.C. 2022. The Davie Fracture Zone: A recorder of continents drifts and kinematic changes. *Tectonophysics*, **823**, 229188, <https://doi.org/10.1016/j.tecto.2021.229188>
- Rodgers, J. 1970. *The Tectonics of the Appalachians*. Wiley-Interscience, New York.
- Rogov, M., Ershova, V., Gaina, C., Vershchagin, O., Vasileva, K., Mikhailova, K. and Krylov, A. 2023. Glendonites throughout the Phanerozoic. *Earth-Science Reviews*, **241**, 104430, <https://doi.org/10.1016/j.earscirev.2023.104430>
- Ronov, A.B., Khain, V.Y. and Balukhovskiy, A. 1989. *Atlas of Lithological–Paleogeographical Maps of the World, Mesozoic and Cenozoic of the Continents*. USSR Academy of Sciences, Leningrad, USSR.
- Ross, C.A. and Ross, J.R. 1985. Late Paleozoic depositional sequences are synchronous and worldwide. *Geology*, **13**, 194–197, [https://doi.org/10.1130/0091-7613\(1985\)13<194:LPDSAS>2.0.CO;2](https://doi.org/10.1130/0091-7613(1985)13<194:LPDSAS>2.0.CO;2)
- Ross, M.I. and Scotese, C.R. 1988. A hierarchical tectonic model of the Gulf of Mexico and Caribbean region. *Tectonophysics*, **155**, 139–168, [https://doi.org/10.1016/0040-1951\(88\)90263-6](https://doi.org/10.1016/0040-1951(88)90263-6)
- Rowley, D.B. 2018. Oceanic axial depth and age–depth distribution of oceanic lithosphere: Comparison of magnetic anomaly picks versus age–grid models. *Lithosphere*, **11**, 21–43, <https://doi.org/10.1130/L1027.1>
- Rowley, D.B. and Currie, B.S. 2006. Paleo-altimetry of the late Eocene to Miocene Lunpola basin, central Tibet. *Nature*, **439**, 677–681, <https://doi.org/10.1038/nature04506>
- Rowley, D.B. and Garzione, C.N. 2007. Stable isotope-based paleoaltimetry. *Annual Review of Earth and Planetary Science*, **35**, 463–508, <https://doi.org/10.1146/annurev.earth.35.031306.140155>
- Rowley, D.B. and Lottes, A.L. 1988. Plate-kinematic reconstructions of the North Atlantic and Arctic: Late Jurassic to Present. *Tectonophysics*, **155**, 73–120, [https://doi.org/10.1016/0040-1951\(88\)90261-2](https://doi.org/10.1016/0040-1951(88)90261-2)
- Rowley, D.B., Pierrehumbert, R.T. and Currie, B.S. 2001. A new approach to stable isotope-based paleoaltimetry: Implications for paleoaltimetry and paleohypsometry of the High Himalaya since the Late Miocene. *Earth and Planetary Science Letters*, **188**, 253–226, [https://doi.org/10.1016/S0012-821X\(01\)00324-7](https://doi.org/10.1016/S0012-821X(01)00324-7)
- Royden, L.H. and Husson, L. 2006. Trench motion, slab geometry, and viscous stresses in subduction systems. *Geophysical Journal International*, **167**, 881–906, <https://doi.org/10.1111/j.1365-246X.2006.03079.x>
- Royer, D.L., Berner, R.A., Montañez, I.P., Tabor, N.J. and Beerling, D.J. 2004. CO₂ as a primary driver of Phanerozoic climate. *GSA Today*, **14**, 4, [https://doi.org/10.1130/1052-5173\(2004\)014<4:CAAPDO>2.0.CO;2](https://doi.org/10.1130/1052-5173(2004)014<4:CAAPDO>2.0.CO;2)
- Royer, J.-Y. and Sandwell, D.T. 1989. Evolution of the eastern Indian Ocean since the Late Cretaceous: Constraints from Geosat altimetry. *Journal of Geophysical Research: Solid Earth*, **94**, 775–782, <https://doi.org/10.1029/JB094iB01p00775>
- Royer, J.-Y., Patriat, P., Bergh, H.W. and Scotese, C.R. 1988. Evolution of the Southwest Indian Ridge from the late Cretaceous (Anomaly 34) to the Middle Eocene (anomaly 20). *Tectonophysics*, **155**, 235–260, [https://doi.org/10.1016/0040-1951\(88\)90268-5](https://doi.org/10.1016/0040-1951(88)90268-5)
- Royer, J.-Y., Müller, R.D., Gahagan, L.M., Lawver, L.A., Mayes, C.L., Nürnberg, D. and Sclater, J.G. 1992a. *A Global Isochron Chart*. University of Texas Institute for Geophysics Technical Report 117.
- Royer, J.-Y., Sclater, J.G. *et al.* 1992b. Indian Ocean plate reconstructions since the Late Jurassic. *American Geophysical Union Geophysical Monograph Series*, **70**, 471–475, <https://doi.org/10.1029/GM070p0471>
- Safonova, I.Y., Simonov, V., Buslov, M., Ota, T. and Maruyama, S. 2008. Neoproterozoic basalts of the Paleo-Asian Ocean (Kurai accretionary zone, Gorny Altai, Russia): geochemistry, petrogenesis, and geodynamics. *Russian Geology and Geophysics*, **49**, 254–271, <https://doi.org/10.1016/j.rgg.2007.09.011>
- Sager, W.W. 2007. Divergence between paleomagnetic and hotspot-model-predicted polar wander for the Pacific plate with implications for hotspot fixity. *Geological Society of America Special Papers*, **430**, 335–357, [https://doi.org/10.1130/2007.2430\(17\)](https://doi.org/10.1130/2007.2430(17))
- Salles, T., Husson, L. *et al.* 2023. Hundred million years of landscape dynamics from catchment to global scale. *Science*, **379**, 918–923, <https://doi.org/10.1126/science.add2541>
- Salvador, A. 1991. *The Gulf of Mexico*. Decade of North American Geology, The Geology of North America, **J**. Geological Society of America, Boulder, CO, <https://doi.org/10.1130/DNAG-GNA-J>
- Sandwell, D., Garcia, E., Soofi, K., Wessel, P., Chandler, M. and Smith, W.H.F. 2013. Towards 1 mGal global marine gravity from CryoSat-2, Envisat, and Jason-1. *The Leading Edge*, **32**, 892–899, <https://doi.org/10.1190/tle32080892.1>
- Schaer, J.-P. and Rodgers, J. 1987. *The Anatomy of Mountain Ranges*. Princeton University Press, Princeton, NJ.
- Schandelmeier, H. and Reynolds, P.O. 1997. *Paleogeographic–Palaeotectonic Atlas of North-Eastern Africa, Arabia, and Adjacent Areas: Late Proterozoic to Holocene*. A.A. Balkema, Rotterdam, The Netherlands.
- Schettino, A. and Scotese, C.R. 2005. Apparent polar wander paths for the major continents (200 Ma to the present day): a palaeomagnetic reference frame for global plate tectonic reconstructions. *Geophysical Journal International*, **163**, 727–759, <https://doi.org/10.1111/j.1365-246X.2005.02638.x>
- Schettino, A. and Turco, E. 2011. Tectonic history of the western Tethys since the late Triassic. *Geological Society of America Bulletin*, **123**, 89–105, <https://doi.org/10.1130/B30064.1>
- Schlanger, S.O. and Jenkyns, H.C. 1976. Cretaceous oceanic anoxic events: causes and consequences. *Geologie en Mijnbouw*, **55**, 179–184.
- Schneider, S.H., Thompson, S.L. and Barron, E.J. 1985. Mid-Cretaceous continental surface temperatures: Are

- high CO₂ concentrations needed to simulate above-freezing winter conditions? *American Geophysical Union Geophysical Monograph Series*, **32**, 554–559, <https://doi.org/10.1029/GM032p0554>
- Schobben, M., van de Schootbrugge, B. and Wignall, P.B. 2019. Interpreting the carbon isotope record of mass extinctions. *Elements*, **15**, 331–337, <https://doi.org/10.2138/gselements.15.5.331>
- Schoene, B., Eddy, M.P., Samperton, K.M., Keller, C.B., Keller, G., Adatte, T. and Khadri, S.F.R. 2019. U–Pb constraints on pulsed eruption of the Deccan Traps across the end-Cretaceous mass extinction. *Science*, **363**, 862–866, <https://doi.org/10.1126/science.aau2422>
- Schouten, S., Hopmans, E.C., Schefuß, E. and Sinninghe Damsté, J.S. 2002. Distributional variations in marine crenarchaeotal membrane lipids: a new tool for reconstructing ancient sea water temperatures? *Earth and Planetary Science Letters*, **204**, 265–274, [https://doi.org/10.1016/S0012-821X\(02\)00979-2](https://doi.org/10.1016/S0012-821X(02)00979-2)
- Schouten, S., Hopmans, E.C., Forster, A., van Bruegel, Y., Kuypers, M.M. and Sinninghe, D. 2003. Extremely high sea-surface temperatures at low latitudes during the middle Cretaceous as revealed by archaeal membrane lipids. *Geology*, **31**, 1069–1072, <https://doi.org/10.1130/G19876.1>
- Schouten, S., Forster, A., Panoto, F.E. and Damsté, J.S.S. 2007. Towards calibration of the TEX₈₆ palaeothermometer for tropical sea surface temperatures in ancient greenhouse worlds. *Organic Geochemistry*, **38**, 1537–1546, <https://doi.org/10.1016/j.orggeochem.2007.05.014>
- Schuchert, C. 1955. *Atlas of Paleogeographic Maps of North America*. John Wiley & Sons, New York (published posthumously).
- Schulte, P., Alegret, L. *et al.* 2010. The Chicxulub asteroid impact and mass extinction at the Cretaceous–Paleogene boundary. *Science*, **327**, 1214–1218, <https://doi.org/10.1126/science.1177265>
- Slater, J.G., Jaupart, C. and Galson, D. 1980. The heat flow through oceanic and continental crust and the heat loss of the Earth. *Reviews of Geophysics and Space Physics*, **18**, 269–311, <https://doi.org/10.1029/RG018i001p00269>
- Scotese, C.R. 1976. A continental drift ‘flip book’. *Computers & Geosciences*, **2**, 113–116, [https://doi.org/10.1016/0098-3004\(76\)90096-0](https://doi.org/10.1016/0098-3004(76)90096-0)
- Scotese, C.R. 1983. *Plate Tectonic Reconstruction Software, PALEOMAP Fortran program (Subroutines MAIN.FTN, RECON8.FTN, ADDER.FTN, ROTATE.FTN, MOLL.FTN)*. Department of Geophysical Science, University of Chicago, Chicago, IL.
- Scotese, C.R. 1990. *Atlas of Phanerozoic Plate Tectonic Reconstructions*. PALEOMAP Progress 01-1090a. University of Texas at Arlington, Arlington, TX.
- Scotese, C.R. 1991. Jurassic and Cretaceous plate tectonic reconstructions. *Palaeogeography, Palaeoecology, and Palaeoclimatology*, **87**, 493–501, [https://doi.org/10.1016/0031-0182\(91\)90145-H](https://doi.org/10.1016/0031-0182(91)90145-H)
- Scotese, C.R. 1998. *Digital Paleogeographic Map Archive on CD-ROM*. PALEOMAP Project, Arlington, TX.
- Scotese, C.R. 2001a. Animation of plate motions and global plate boundary evolution since the Late Precambrian. *Geological Society of America Abstracts with Programs*, **33**, 85.
- Scotese, C.R. 2001b. *Atlas of Earth History, Volume 1, Paleogeography*. PALEOMAP Project, Arlington, TX.
- Scotese, C.R. 2004. Cenozoic and Mesozoic paleogeography: Changing terrestrial biogeographic pathways. In: Lomolino, M.V. and Heaney, L.R. (eds) *Frontiers of Biogeography: New Directions in the Geography of Nature*. Sinauer Associates, Inc., Sunderland, MA, 1–26.
- Scotese, C.R. 2008. *Circum-Arctic Regional Study, Part 1. A Plate Tectonic Model of the Arctic Ocean and Its Borderlands: ‘Windshield Wiper’ and ‘Rollback’ Tectonics*. PALEOMAP Project, Arlington, TX.
- Scotese, C.R. 2014a. *Atlas of Early Cretaceous Paleogeographic Maps, PALEOMAP Atlas for ArcGIS, Volume 2, The Cretaceous, Maps 23–31, Mollweide Projection*. PALEOMAP Project, Evanston, IL.
- Scotese, C.R. 2014b. *Atlas of Late Cretaceous Paleogeographic Maps, PALEOMAP Atlas for ArcGIS, Volume 2, The Cretaceous, Maps 16–22, Mollweide Projection*. PALEOMAP Project, Evanston, IL.
- Scotese, C.R. 2014c. *Atlas of Plate Tectonic Reconstructions (Mollweide Projection), Volumes 1–6, PALEOMAP Project PaleoAtlas for ArcGIS*. PALEOMAP Project, Evanston, IL.
- Scotese, C.R. 2016a. A new global temperature curve for the Phanerozoic. Abstract presented at the Geological Society of America Annual Meeting, 25 September 2016, Denver, Colorado, USA.
- Scotese, C.R. 2016b. *Tutorial: PALEOMAP Paleoatlas for GPlates and the PaleoData Plotter Program*, <https://www.earthbyte.org/paleomap-paleoatlas-for-gplates/>
- Scotese, C.R. 2018. *Plate tectonic evolution during the last 1.5 billion years: The movie*. Paper No. 93-1 presented at the Geological Society of America Annual Meeting, 5 November 2018, Indianapolis, Indiana, USA, <https://doi.org/10.1130/abs/2018AM-320136>
- Scotese, C.R. 2021. An atlas of Phanerozoic paleogeographic maps: The seas come in and the seas go out. *Annual Review of Earth and Planetary Sciences*, **49**, 679–728, <https://doi.org/10.1146/annurev-earth-081320-064052>
- Scotese, C.R. and Baker, D.W. 1975. Continental drift reconstructions and animation. *Journal of Geological Education*, **23**, 167–171, <https://doi.org/10.5408/0022-1368-23.5.167>
- Scotese, C.R. and Dammrose, R. 2008. Plate boundary evolution and mantle plume eruptions during the last billion years. *Geological Society of America Abstracts with Programs*, **40**, 328.
- Scotese, C.R. and Denham, C.R. 1988. *User’s Manual for Terra Mobilis™: Plate Tectonics for the Macintosh®*. Earth in Motion Technologies, Houston, TX.
- Scotese, C.R. and Elling, R.P. 2017. Plate tectonic evolution during the last 1.3 billion years: The movie In: Butler, R., Daly, M., Roberts, G., Turner, J. and Watts, T. (convenors) *William Smith Meeting 2017: Plate Tectonics at 50. Abstract Book*. Geological Society, London, 28–29, 16–17, <https://www.youtube.com/watch?v=CnVGFv-1Wqc>
- Scotese, C.R. and Golonka, J. 1992. *Paleogeographic Atlas*. PALEOMAP Progress Report 20-0692. Department of Geology, University of Texas, Arlington, TX.
- Scotese, C.R. and McKerrow, W.S. 1990. Revised world maps and introduction. *Geological Society, London*

- Memoirs*, **12**, 1–21, <https://doi.org/10.1144/GSL.MEM.1990.012.0101>
- Scotese, C.R. and Sager, W. (eds) 1988. *Mesozoic and Cenozoic Plate Tectonic Reconstructions*. *Tectonophysics*, **155**, 1–399.
- Scotese, C.R., and Rowley, D.B. 1985. The orthogonality of subduction: An empirical rule? *Tectonophysics*, **116**, 173–187.
- Scotese, C.R. and Schettino, A. 2017. Late Permian–Early Jurassic paleogeography of western Tethys and the world. In: Soto, J.I., Flinch, J. and Tari, G. (eds) *Permo-Triassic Salt Provinces of Europe, North Africa and the Atlantic Margins*. Elsevier, Amsterdam, 57–95.
- Scotese, C.R. and Van der Voo, R. 2017. *A Paleomagnetic Database for GPlates: Paleopoles, Declination Arrows, and Paleolatitudes*, <https://www.earthbyte.org/a-paleomagnetic-database-for-gplates-paleopoles-declination-arrows-and-paleolatitudes/>, <https://doi.org/10.13140/RG.2.2.35883.75043>.
- Scotese, C.R. and Winn, K. 1987. *Phanerozoic Paleogeographic Maps*. Paleogeographic Mapping Project, Paleogeographic Mapping Project (POMP) Progress Report 33-1287/UTIG Technical Report 84.
- Scotese, C.R. and Wright, N. 2018. *PALEOMAP Paleodigital Elevation Models (PaleoDEMS) for the Phanerozoic*, <https://www.earthbyte.org/paleodem-resource-scotese-and-wright-2018>
- Scotese, C.R., Snelson, S.S. and Ross, W.C. 1980. A computer animation of continental drift. *Journal of Geomagnetism and Geoelectricity*, **32**(Suppl. III), 61–70, https://doi.org/10.5636/jgg.32.Supplement3_SIII61
- Scotese, C.R., Totterdell, J.M., Holliday, S. and Langford, R.P. 1985. *Paleogeographic Mapping Software for the Intergraph Work Station*. BMR-AMIRA Paleogeographic Project Special Report. Bureau of Mineral Resources, Canberra.
- Scotese, C.R., Gahagan, L.M. and Larson, R.L. 1988. Plate tectonic reconstructions of the Cretaceous and Cenozoic ocean basins. *Tectonophysics*, **155**, 27–48, [https://doi.org/10.1016/0040-1951\(88\)90259-4](https://doi.org/10.1016/0040-1951(88)90259-4)
- Scotese, C.R., Nökleberg, W.J. *et al.* 2005. Tectonic and metallogenic evolution of northeast Asia: Key to regional understanding. In: *Mineral Deposit Research: Meeting the Global Challenge*. Springer, Berlin, 1183–1184, https://doi.org/10.1007/3-540-27946-6_302
- Scotese, C.R., Illich, H., Zumberge, J., Brown, S. and Moore, T. 2007. *The GANDOLPH Project: Year One Report: Paleogeographic and Paleoclimatic Controls on Hydrocarbon Source Rock Deposition, A Report on the Methods Employed, the Results of the Paleoclimate Simulations (FOAM), and Oils/Source Rock Compilation, Conclusions at the End of Year One: Cenomanian/Turonian (93.5 Ma), Kimmeridgian/Tithonian (151 Ma), Sakmarian/Artinskian (284 Ma), Frasnian/Famennian (375 Ma), February, 2007*. GeoMark Research Ltd, Houston, TX.
- Scotese, C.R., Illich, H., Zumberge, J., Brown, S. and Moore, T. 2008. *The GANDOLPH Project: Year Two Report: Paleogeographic and Paleoclimatic Controls on Hydrocarbon Source Rock Deposition, A Report on the Methods Employed, the Results of the Paleoclimate Simulations (FOAM), and Oils/Source Rock Compilation, Conclusions at the End of Year Two: Miocene (10 Ma), Aptian/Albian (120 Ma), Berriasian/Barremian (140 Ma), Late Triassic (220 Ma), and Early Silurian (430 Ma), July, 2008*. GeoMark Research Ltd, Houston, TX.
- Scotese, C.R., Song, H., Mills, B.J.W. and van der Meer, D.G. 2021. Phanerozoic paleotemperatures: The earth's changing climate during the last 540 million years. *Earth-Science Reviews*, **215**, 103503, <https://doi.org/10.1016/j.earscirev.2021.103503>
- Scotese, C.R., Royer, D., Summerhayes, C.P. and Mills, B. 2022. Atmospheric CO₂ during the last 540 million years. Abstract PPI2D-0657 presented at the American Geophysical Union Annual Meeting, 12 December 2022, Chicago, Illinois, USA.
- Sears, J.W., Harms, T.A. and Evenchick, C.A. (eds) 2007. *Whence the Mountains? Inquiries into the Evolution of Orogenic Systems: A Volume in Honor of Raymond A. Price*. Geological Society of America Special Papers, **433**, <https://doi.org/10.1130/SPE433>
- Segoufin, J. and Patriat, P. 1981. Reconstitutions de l'Océan Indien occidental pour les époques des anomalies M21, M2 et 34, paleoposition de Madagascar. *Bulletin de la Société Géologique de France*, **23**, 605–607.
- Sellwood, B.W. and Price, G.D. 1994. Sedimentary facies as indicators of Mesozoic palaeoclimate. In: Allen, J.R.L., Hoskins, B.J., Sellwood, B.W., Spicer, R.A. and Valdes, P.J. (eds) *Palaeoclimates and their Modelling, with Special Reference to the Mesozoic Era*. Chapman and Hall, London, 17–25.
- Sellwood, B.W. and Valdes, P.J. 2006. Mesozoic climates: General circulation models and the rock record. *Sedimentary Geology*, **190**, 269–287, <https://doi.org/10.1016/j.sedgeo.2006.05.013>
- Sellwood, B.W., Price, G.D. and Valdes, P.J. 1994. Cooler estimates of Cretaceous temperatures. *Nature*, **370**, 453–492, <https://doi.org/10.1038/370453a0>
- Şengör, A.M.C. and Atayman, S. 2009. *The Permian Extinction and Tethys: An Exercise in Global Geology*. Geological Society of America Special Papers, **448**, <https://doi.org/10.1130/SPE448>
- Şengör, A.M.C. and Natalin, B.A. 1996. Paleotectonics of Asia: fragments of a synthesis. In: Yin, A. and Harrison, M. (eds) *The Tectonic Evolution of Asia*. Cambridge University Press, Cambridge, UK, 486–640.
- Şengör, A.M.C. and Natal'in, B.A. 2001. Rifts of the world. *Geological Society of America Special Papers*, **352**, 389–482, <https://doi.org/10.1130/0-8137-2352-3.389>
- Şengör, A.M.C., Altiner, D., Cin, A., Ustaomer, T. and Hsu, K. 1988. Origin and assembly of the Tethyside orogenic collage at the expense of Gondwana Land. *Geological Society, London, Special Publications*, **37**, 119–181, <https://doi.org/10.1144/GSL.SP.1988.037.0109>
- Şengör, A.M.C., Cin, A., Rowley, D.B. and Nie, S.Y. 1993. Space–time patterns of magmatism along the Tethysides: A preliminary study. *Journal of Geology*, **101**, 51–84, <https://doi.org/10.1086/648196>
- Şengör, A.M.C., Natal'in, B.A., Sunal, G. and van der Voo, R. 2014a. A new look at the Altai: A super-orogenic complex in northern and central Asia as a factory of continental crust, Part I: Geological data compilation (exclusive of paleomagnetic

- observations). *Austrian Journal of Earth Sciences*, **107**(1), 169–232.
- Şengör, A.M.C., Natal'in, B.A., van der Voo, R. and Sunal, G. 2014b. A new look at the Altaids: A super-orogenic complex in northern and central Asia as a factory of continental crust, Part II: Palaeomagnetic data, reconstructions, crustal growth, and global sea-level. *Austrian Journal of Earth Sciences*, **107**(2), 131–181.
- Şengör, A.M.C., Altiner, D., Zabcı, C., Sunal, G., Lom, N., Aylan, E. and Öner, T. 2023. On the nature of the Cimmerian continent. *Earth-Science Reviews*, **247**, 104520, <https://doi.org/10.1016/j.earscirev.2023.104520>
- Sepkoski, J.J., Jr 1996. Patterns of Phanerozoic extinction: a perspective from global data bases. In: Walliser, O.H. (ed.) *Global Events and Event Stratigraphy in the Phanerozoic*. Springer, Berlin, 35–51.
- Servais, T., Harper, D.A.T., Kröger, B., Scotese, C.R., Stigall, A.L. and Xhen, Y.Y. 2023. Changing palaeobiogeography during the Ordovician. *Geological Society, London, Special Publications*, **535**, 111–136, <https://doi.org/10.1144/SP532-2022-168>
- Seton, M., Muller, R.D. *et al.* 2012. Global continental and ocean basin reconstructions since 200 Ma. *Earth-Science Reviews*, **113**, 212–270, <https://doi.org/10.1016/j.earscirev.2012.03.002>
- Seton, M., Müller, R.D. *et al.* 2020. A global data set of present-day oceanic crustal age and seafloor spreading parameters. *Geochemistry, Geophysics, and Geosystems*, **21**, e2020GC009214, <https://doi.org/10.1029/2020GC009214>
- Seton, M., Williams, S.E., Domeier, M., Collins, A. and Sigloch, K. 2023. Deconstructing plate tectonic reconstructions. *Nature Reviews, Earth & Environment*, **4**, 185–204, <https://doi.org/10.1038/s43017-022-00384-8>
- Sewall, J.O., van de Wal, R.S.W., van der Zwan, K., van Oosterhout, C., Dijkstra, H.A. and Scotese, C.R. 2007. Climate model boundary conditions for four Cretaceous time slices. *Climate of the Past*, **3**, 647–657, <https://doi.org/10.5194/cp-3-647-2007>
- Sharman, G.F. and Risch, D.L. 1988. Northwest Pacific tectonic evolution in the Middle Mesozoic. *Tectonophysics*, **155**, 331–344, [https://doi.org/10.1016/0040-1951\(88\)90273-9](https://doi.org/10.1016/0040-1951(88)90273-9)
- Siegesmund, S., Fügenschuh, B. and Froitzheim, N. (eds) 2008. *Tectonic Aspects of the Alpine–Dinaride–Carpathian System*. Geological Society, London, Special Publications, **298**, <https://doi.org/10.1144/SP298.0>
- Simmons, M.D. 2012. Sequence stratigraphy and sea-level change. In: Gradstein, F.M., Ogg, J.G., Schmitz, M.D. and Ogg, G.M. (eds) *The Geologic Time Scale 2012*. Elsevier, Amsterdam, 239–267.
- Simmons, M.D., Miller, K.G., Ray, D.C., Davies, A., van Buchem, F.S.P. and Gréselle, B. 2020. Phanerozoic eustasy. In: Gradstein, F.M., Ogg, J.G., Schmitz, M.D. and Ogg, G.M. (eds) *Geological Time Scale 2020*, Volume 1, Elsevier, Amsterdam.
- Skelton, P. 2003. *The Cretaceous World*. Cambridge University Press, Cambridge, UK.
- Skogseid, J., Planke, S., Faleide, J.I., Pedersen, T., Eldholm, O. and Neverdal, F. 2000. NE Atlantic continental rifting and volcanic margin formation. *Geological Society, London, Special Publications*, **167**, 295–326, <https://doi.org/10.1144/GSL.SP.2000.167.01.12>
- Sloan, L.C. and Pollard, D. 1998. Polar stratospheric clouds: A high latitude warming mechanism in an ancient greenhouse world. *Geophysical Research Letters*, **25**, 3517–3520, <https://doi.org/10.1029/98GL02492>
- Sloss, L.L. 1963. Sequences in the cratonic interior of North America. *Geological Society of America Memoirs*, **39**, 91–124, <https://doi.org/10.1130/MEM39-p91>
- Smit, J. 1999. The global stratigraphy of the Cretaceous–Tertiary boundary impact ejecta. *Annual Review of Earth and Planetary Sciences*, **27**, 75–91, <https://doi.org/10.1146/annurev.earth.27.1.75>
- Smith, A.G. and Hallam, A. 1970. The fit of the southern continents. *Nature*, **225**, 139–144, <https://doi.org/10.1038/225139a0>
- Smith, A.G., Smith, D.G. and Funnell, B.M. 1994. *Atlas of Mesozoic and Cenozoic Coastlines*. Cambridge University Press, Cambridge, UK.
- Smith, W. 1815. *A Delineation of the Strata of England and Wales and Part of Scotland*. Geological Society, London.
- Smith, W.H.F. and Sandwell, D.T. 1997. Global sea floor topography from satellite altimetry and ship depth soundings. *Science*, **277**, 1956–1962, <https://doi.org/10.1126/science.277.5334.1956>
- Snedden, J.W. and Liu, C. 2010. A compilation of Phanerozoic sea-level change, coastal onlaps and recommended sequence designations. AAPG Search Discovery Article #40594, https://www.searchanddiscovery.com/documents/2010/40594snedden/ndx_snedden.pdf
- Snedden, J.W. and Liu, C. 2011. Recommendations for a uniform chronostratigraphic designation system for Phanerozoic depositional sequences. *AAPG Bulletin*, **95**, 1095–1122, <https://doi.org/10.1306/010311.10138>
- Song, H. and Scotese, C.R. 2023. The end-Paleozoic great warming. *Science Bulletin*, **68**, 2523–2526, <https://doi.org/10.1016/j.scib.2023.09.009>
- Song, H., Wignall, P.B., Song, H., Dai, X. and Chu, D. 2019. Seawater temperature and dissolved oxygen over the past 500 million years. *Journal of Earth Science*, **30**, 236–243, <https://doi.org/10.1007/s12583-018-1002-2>
- Spakman, W. and Nolet, G. 1988. Imaging algorithms, accuracy and resolution in delay time tomography. In: Vlaar, N.J., Nolet, G., Wortel, M.J.R. and Cloetingh, S.A.P.L. (eds) *Mathematical Geophysics. Modern Approaches in Geophysics*, **3**. Springer, Dordrecht, The Netherlands, 155–187, https://doi.org/10.1007/978-94-009-2857-2_8
- Spencer, A.M. (ed.) 1974. *Mesozoic–Cenozoic Orogenic Belts: Data for Orogenic Studies*. Geological Society, London, Special Publications, **4**.
- Spicer, R.A. and Herman, A.B. 2010. The Late Cretaceous environment of the Arctic: A quantitative reassessment based on plant fossils. *Palaeogeography, Palaeoclimatology, Palaeoecology*, **295**, 423–442, <https://doi.org/10.1016/j.palaeo.2010.02.025>
- Spicer, R.A., Rees, P.M. and Chapman, J.L. 1994. Cretaceous phytogeography and climate signals. In: Allen, J.R.L., Hoskins, B.J., Sellwood, B.W., Spicer, R.A.

- and Valdes, P.J. (eds) *Palaeoclimates and their Modelling*. Springer, Dordrecht, The Netherlands, 69–78, https://doi.org/10.1007/978-94-011-1254-3_9
- Spicer, R.A., Ahlberg, A., Herman, A.B., Hofmann, C.C., Raikevich, M., Valdes, P.J. and Markwick, P.J. 2008. The Late Cretaceous continental interior of Siberia: A challenge for climate models. *Earth and Planetary Science Letters*, **267**, 228–235, <https://doi.org/10.1016/j.epsl.2007.11.049>
- Spicer, R.A., Valdes, P.J., Spicer, T.E.V., Craggs, H.J., Srivastava, G., Mehrotra, R.C. and Yang, J. 2009. New developments in CLAMP: Calibration using global gridded meteorological data. *Palaeogeography, Palaeoclimatology, Palaeoecology*, **283**, 91–98, <https://doi.org/10.1016/j.palaeo.2009.09.009>
- Spicer, R.A., Yang, J., Spicer, T.E.V. and Farnsworth, A. 2021. Woody dicot leaf traits as a palaeoclimate proxy: 100 years of development and application. *Palaeogeography, Palaeoclimatology, Palaeoecology*, **562**, 110138, <https://doi.org/10.1016/j.palaeo.2020.110138>
- Spray, J. 2020. *Earth Impact Database (EID)*, https://passc.net/EarthImpactDatabase/New%20website_05-2018/Index.html
- Srivastava, R.K., Ernst, R.E., Buchan, K.L. and de Kock, M. (eds) 2022. *Large Igneous Provinces and their Plumbing System*. Geological Society, London, Special Publications, **518**, <https://doi.org/10.1144/SP518>
- Srivastava, S.P. 1985. Evolution of the Eurasian Basin and its implications to the motion of Greenland along the Nares Strait. *Tectonophysics*, **114**, 29–53, [https://doi.org/10.1016/0040-1951\(85\)90006-X](https://doi.org/10.1016/0040-1951(85)90006-X)
- Srivastava, S.P. and Roest, W.R. 1989. Sea-floor spreading in the Labrador Sea; a new reconstruction. *Geology*, **17**, 1000–1003.
- Srivastava, S.P. and Tapscott, C. 1986. Plate kinematics of the North Atlantic. In: Vogt, P.R. and Tucholke, B.E. (eds) *The Western North Atlantic Region*. Decade of North American Geology, The Geology of North America, **M**. Geological Society of America, Boulder, CO, 379–404.
- Stampfli, G.M. and Kozur, H.W. 2006. Europe from the Variscan to the Alpine cycles. *Geological Society, London, Memoirs*, **32**, 57–82, <https://doi.org/10.1144/GSL.MEM.2006.032.01>
- Stampfli, G.M., Mosar, J., Favre, P., Pillevuit, A. and Vanney, J.C. 2001. Permo-Mesozoic evolution of the western Tethys realm: the Neo-Tethys East Mediterranean Basin connection. In: Ziegler, A., Cavazza, W., Robertson, A.H.F. and Crasquin-Soleau, S. (eds) *Peri-Tethys Memoir 6; Peri-Tethyan Rift/Wrench Basins and Passive Margins*. Mémoires du Muséum national d'histoire naturelle, **186**, 51–108.
- Stampfli, G.M., Borel, G.D. *et al.* 2004. The TRANSMED transects in space and time: Constraints on the paleotectonic evolution of the Mediterranean domain. In: Cavazza, W. (ed.) *The TRANSMED Atlas: The Mediterranean Region from Crust to Mantle*. Springer, Berlin, 53–80.
- Stanley, S.M. 1987. *Extinction*. Scientific American Library, New York.
- Stein, C.A. and Stein, S. 1992. A model for the global variation in oceanic depth and heat flow with lithospheric age. *Nature*, **359**, 123–129, <https://doi.org/10.1038/359123a0>
- Steinberger, B. and O'Connell, R.J. 1998. Advection of plumes in mantle flow: Implications for hot spot motion, mantle viscosity, and plume distribution. *Geophysical Journal International*, **132**, 412–434, <https://doi.org/10.1046/j.1365-246x.1998.00447.x>
- Steinberger, B. and Torsvik, T.H. 2010. Toward and explanation for the present and past locations of the poles. *Geochemistry, Geophysics, Geosystems*, **11**, Q06W06, <https://doi.org/10.1029/2009GC002889>
- Stern, R.J. 2002. Subduction zones. *Reviews of Geophysics*, **40**, 1–38, <https://doi.org/10.1029/2001RG000108>
- Storey, M., Mahoney, J.J. and Saunders, A.D. 1997. Cretaceous basalts in Madagascar and the transition between plume and continental lithosphere mantle sources. *American Geophysical Union Geophysical Monograph Series*, **100**, 95–122, <https://doi.org/10.1029/GM100p0095>
- Strand, T. and Kulling, O. 1972. *Scandinavian Caledonides*. Wiley-Interscience, London.
- Suarez, C.A., Edmonds, M. and Jones, A.P. 2019. Earth catastrophes and their impact on the carbon cycle. *Elements*, **15**, 301–306, <https://doi.org/10.2138/gselements.15.5.301>
- Suess, E. 1908. *The Face of the Earth (Das Antlitz der Erde)*, Vol. 3. Clarendon Press, Oxford, viii.
- Summerhayes, C.P. 2015. *Earth's Climate Evolution*. Wiley-Blackwell, Chichester, UK.
- Sun, Y., Joachimski, M.M. *et al.* 2012. Lethally hot temperatures during the Early Triassic Greenhouse. *Science*, **338**, 366–370, <https://doi.org/10.1126/science.1224126>
- Sun, Y.D., Wignall, P.B. *et al.* 2016. Climate warming, euxinia and carbon isotope perturbations during the Carnian (Triassic) Crisis in South China. *Earth and Planetary Science Letters*, **444**, 88–100, <https://doi.org/10.1016/j.epsl.2016.03.037>
- Talwani, M. and Pitman, W.C., III 1977. *Island Arcs, Deep Sea Trenches, and Back-Arc Basins*. American Geophysical Union Maurice Ewing Series, **1**.
- Tarduno, J.A., Sliter, W.V. *et al.* 1991. Rapid formation of the Ontong Java plateau by Aptian mantle volcanism. *Science*, **254**, 399–403, <https://doi.org/10.1126/science.254.5030.399>
- Tauxe, L. 2002. *Paleomagnetic Principles and Practice*. Modern Approaches in Geophysics, **18**. Kluwer Academic, London.
- Taylor, B. 2006. The single largest oceanic plateau: Ontong Java–Manihiki–Hikurangi. *Earth and Planetary Science Letters*, **241**, 372–380, <https://doi.org/10.1016/j.epsl.2005.11.049>
- Tetley, M.G. 2018. *Constraining Earth's Plate Tectonic Evolution through Data Mining and Knowledge Discovery*. PhD thesis, University of Sydney, Sydney, Australia.
- Tetley, M.G., Williams, S.E., Gurnis, M., Flament, N. and Müller, R.D.M. 2019. Constraining absolute plate motions since the Triassic. *Journal of Geophysical Research: Solid Earth*, **124**, 7231–7258, <https://doi.org/10.1029/2019JB017442>
- Tierney, J.E. and Tingley, M.P. 2014. A Bayesian, spatially-varying calibration model for the TEX86

- proxy. *Geochimica et Cosmochimica Acta*, **127**, 83–106, <https://doi.org/10.1016/j.gca.2013.11.026>
- Tierney, J.E. and Tingley, M.P. 2015. A TEX₈₆ surface sediment database and extended Bayesian calibration. *Scientific Data*, **2**, 150029, <https://doi.org/10.1038/sdata.2015.29>
- Torsvik, T.H. and Cocks, L.R.M. 2017. *Earth History and Palaeogeography*. Cambridge University Press, Cambridge, UK.
- Torsvik, T.H., Muller, R., Van der Voo, R. and Steinberger, B. 2008. Global plate motion frames: Toward a unified model. *Reviews of Geophysics*, **46**, RG3004, <https://doi.org/10.1029/2007RG000227>
- Torsvik, T.H., Van der Voo, R. et al. 2012. Phanerozoic polar wander, palaeogeography and dynamics. *Earth-Science Reviews*, **114**, 325–368, <https://doi.org/10.1016/j.earscirev.2012.06.007>
- Torsvik, T.H., Svensen, H.H., Steinberger, B., Royer, D.L., Jerram, D.A., Jones, M.T. and Domeier, M. 2021. Connecting the deep Earth and the atmosphere. *American Geophysical Union Geophysical Monograph Series*, **263**, 413–453, <https://doi.org/10.1002/9781119528609.ch16>
- Trotter, A.J., Williams, S.I., Nicora, A., Mazza, M. and Rigo, M. 2015. Long-term cycles of Triassic climate change: A new $\delta^{18}\text{O}$ record from conodont apatite. *Earth and Planetary Science Letters*, **415**, 165–174, <https://doi.org/10.1016/j.epsl.2015.01.038>
- Uliana, M.A. and Leggarreta, L. 1993. Hydrocarbon habitat in a Triassic-to-Cretaceous Sub-Andean setting: Neuquen Basin, Argentina. *Journal of Petroleum Geology*, **16**, 397–420, <https://doi.org/10.1111/j.1747-5457.1993.tb00350.x>
- Ulmishek, G.F. and Klemme, H.D. 1990. *Depositional Controls, Distribution, and Effectiveness of the World's Petroleum Source Rocks*. United States Geological Survey Bulletin, **1931**, <https://doi.org/10.3133/b1931>
- Untermehr, P., Curie, D., Olivet, J.L., Goslin, J. and Beuzart, P. 1988. South Atlantic fits and intraplate boundaries in Africa and South America. *Tectonophysics*, **155**, 169–180, [https://doi.org/10.1016/0040-1951\(88\)90264-8](https://doi.org/10.1016/0040-1951(88)90264-8)
- Upchurch, G.R., Otto-Bliesner, B.L. and Scotese, C.R. 1999. Terrestrial vegetation and its effects on climate during the latest Cretaceous. *Geological Society of America Special Papers*, **332**, 407–426, <https://doi.org/10.1130/0-8137-2332-9.407>
- Upchurch, P., Hunn, C.A. and Norman, D.B. 2002. An analysis of dinosaurian biogeography: evidence for existence of vicariance and dispersal patterns caused by geological events. *Proceedings of the Royal Society B: Biological Sciences*, **269**, 613–621, <https://doi.org/10.1098/rspb.2001.1921>
- Upchurch, G.R., Kiehl, J., Shields, C., Scherer, J. and Scotese, C.R. 2015. Latitudinal temperature gradients and high latitude temperatures during the latest Cretaceous: Congruence of geologic data and climate models. *Geology*, **43**, 683–686, <https://doi.org/10.1130/G36802.1>
- Uyeda, S. and Kanamori, H. 1979. Back-arc opening and the mode of subduction. *Journal of Geophysical Research: Solid Earth*, **84**, 1049–1061, <https://doi.org/10.1029/JB084iB03p01049>
- Vaes, B. 2023. *On Pole Position: New Approaches to Quantifying Polar Wander and Relative Paleomagnetic Displacements*. PhD thesis, Utrecht University, Utrecht, The Netherlands, <https://doi.org/10.33540/1794>
- Vaes, B., van Hinsbergen, D.J.J. and Boschman, L.M. 2019. Reconstruction of subduction and back-arc spreading in the NW Pacific and Aleutian Basin: Clues to the causes of Cretaceous and Eocene plate reorganizations. *Tectonics*, **38**, 1367–1413, <https://doi.org/10.1029/2018TC005164>
- Vaes, B., van Hinsbergen, D.J.J. et al. 2023. A global apparent polar wander path for the last 320 Ma calculated from site-level paleomagnetic data. *Earth-Science Reviews*, **245**, 104547, <https://doi.org/10.1016/j.earscirev.2023.104547>
- Vail, P.R., Mitchum, R.M. and Thompson, S., III 1977a. Seismic stratigraphy and global changes of sea level: Part 4: Global cycles of relative changes of sea level. *AAPG Memoirs*, **26**, 83–97, <https://doi.org/10.1306/M26490C6>
- Vail, P.R., Mitchum, R.M. et al. 1977b. Seismic stratigraphy and global changes in sea level. *AAPG Memoirs*, **26**, 49–212.
- Valdes, P.J., Sellwood, B.W. and Price, G.D. 1996. Evaluating concepts of Cretaceous equability. *Paleoclimates*, **2**, 139–158.
- Valdes, P.J., Armstrong, E. et al. 2017. The BRIDGE HadCM3 family of climate models: HadCM3@Bristol v1.0. *Geoscientific Model Development*, **10**, 3715–3743, <https://doi.org/10.5194/gmd-10-3715-2017>
- Valdes, P.J., Scotese, C.R. and Lunt, D.J. 2021. Deep ocean temperatures through time. *Climate of the Past*, **17**, 1483–1506, <https://doi.org/10.5194/cp-17-1483-2021>
- Vallier, T.L., Dean, W.E., Rea, D.K. and Thede, J. 1983. Geologic evolution of Hess Rise, central North Pacific Ocean. *Geological Society of America Bulletin*, **94**, 1289–1307.
- van de Lagemaat, S.H.A., Kamp, P.J.J., Boschman, L.M. and Van Hinsbergen, D.J.J. 2023. Reconciling the Cretaceous breakup and demise of the Phoenix Plate with East Gondwana orogenesis in New Zealand. *Earth-Science Reviews*, **236**, 104276, <https://doi.org/10.1016/j.earscirev.2022.104276>
- Vandenbergh, N., Hilgen, F.J. and Speijer, R.P. 2012. The Paleogene Period. In: Gradstein, F.M., Ogg, J.G., Schmitz, M.D. and Ogg, G.M. (eds) *The Geologic Time Scale 2012, Volume 2*. Elsevier, Amsterdam, 855–922.
- Vanderkluyse, L. and Gibson, S.A. 2015. Triggering of the largest Deccan eruptions by the Chicxulub impact. *Geological Society of America Bulletin*, **127**, 1507–1520, <https://doi.org/10.1130/B31167.1>
- van der Linden, T.J.M., Dupont-Nivet, G. and van Hinsbergen, D.J.J. 2020. Towards a quantitative paleogeography calculator. Paper EGU2020-2402 (Powerpoint) presented at the online EGU General Assembly 2020, 8 May 2020.
- van der Meer, D.G., Zeebe, R.E., van Hinsbergen, J.J., Sluijs, A., Spakman, W. and Torsvik, T. 2014. Plate tectonic controls on atmospheric CO₂ levels since the Triassic. *Proceedings of the National Academy of Sciences of the United States of America*, **111**, 4380–4385, <https://doi.org/10.1073/pnas.1315657111>
- van der Meer, D.G., van den Berg van Saparoea, A.P.H., van Hinsbergen, D.J.J., van de Weg, R.M.B., Godderis,

- Y., Le Hir, G. and Donnadieu, Y. 2017. Reconstructing first-order changes in sea level during the Phanerozoic and Neoproterozoic using strontium isotopes. *Gondwana Research*, **44**, 22–34, <https://doi.org/10.1016/j.gr.2016.11.002>
- van der Meer, D.G., van Hinsbergen, D.J.J. and Spakman, W. 2018. Atlas of the underworld: Slab remnants in the mantle, their sinking history, and a new outlook on lower mantle viscosity. *Tectonophysics*, **723**, 309–448, <https://doi.org/10.1016/j.tecto.2017.10.004>
- van der Meer, D.G., Scotese, C.R., Mills, B.L.W., Sluijs, A., van den Berg van Saparoea, A.-P. and van de Weg, R.M.B. 2022. Long-term Phanerozoic global mean sea level: Insights from strontium isotope variations and estimates of continental glaciation. *Gondwana Research*, **111**, 103–121, <https://doi.org/10.1016/j.gr.2022.07.014>
- van der Voo, R. 1993. *Paleomagnetism of the Atlantic, Tethys, and Iapetus Oceans*. Cambridge University Press, Cambridge, UK.
- van Hinsbergen, D.J.J., Edwards, M.A. and Govers, R. (eds) 2009. *Collision and Collapse at the Africa–Arabia–Eurasia Subduction Zone*. Geological Society, London, Special Publications, **311**, <https://doi.org/10.1144/SP311.0>
- van Hinsbergen, D.J.J., de Groot, L. *et al.* 2015. A paleolatitude calculator for paleoclimate studies. *PLoS ONE*, **10**, e0126946, <https://doi.org/10.1371/journal.pone.0126946>
- van Hinsbergen, D.J.J., Torsvik, T.H. *et al.* 2020. Orogenic architecture of the Mediterranean region and kinematic reconstruction of its tectonic evolution since the Triassic. *Gondwana Research*, **81**, 79–229, <https://doi.org/10.1016/j.gr.2019.07.009>
- Vaughan, A.P.M., Leat, P.T. and Pankhurst, R.J. (eds) 2005. *Terrane Processes at the Margins of Gondwana*. Geological Society, London, Special Publications, **246**, <https://doi.org/10.1144/GSL.SP.2005.246.01.18>
- Veevers, J.J. 1984. *Phanerozoic Earth History of Australia*. Oxford Monographs on Geology and Geophysics, **2**. Oxford University Press, New York.
- Veevers, J.J. 2000. *Billion-Year History of Australia and Neighbours in Gondwanaland*. GEMOC Press, Sydney, Australia.
- Veikkolainen, T., Biggin, A., Pesonen, L., Evans, D. and Jarboe, N. 2017. Advancing Precambrian palaeomagnetism with the PALEOMAGIA and PINT_(QPI) databases. *Scientific Data*, **4**, 170068, <https://doi.org/10.1038/sdata.2017.68>
- Veizer, J. 1995. Reply to the Comment by L.S. Land on ‘Oxygen and carbon isotopic composition of Ordovician brachiopods: Implications for coeval seawater’. *Geochimica et Cosmochimica Acta*, **59**, 2845–2846, [https://doi.org/10.1016/0016-7037\(95\)00177-2](https://doi.org/10.1016/0016-7037(95)00177-2)
- Veizer, J. and Hoefs, J. 1976. The nature of $^{18}\text{O}/^{16}\text{O}$ and $^{13}\text{C}/^{12}\text{C}$ secular trends in sedimentary carbonate rocks. *Geochimica et Cosmochimica Acta*, **40**, 1387–1395, [https://doi.org/10.1016/0016-7037\(76\)90129-0](https://doi.org/10.1016/0016-7037(76)90129-0)
- Veizer, J. and Prokoph, A. 2015. Temperatures and oxygen isotopic composition of Phanerozoic oceans. *Earth-Science Reviews*, **146**, 92–104, <https://doi.org/10.1016/j.earscirev.2015.03.008>
- Veizer, J., Ala, D. *et al.* 1999. $^{87}\text{Sr}/^{86}\text{Sr}$, $\delta^{13}\text{C}$ and $\delta^{18}\text{O}$ evolution of Phanerozoic seawater. *Chemical Geology*, **161**, 59–88, [https://doi.org/10.1016/S0009-2541\(99\)00081-9](https://doi.org/10.1016/S0009-2541(99)00081-9)
- Vellekoop, J., Sluijs, A., Smit, J., Schouten, S., Weijers, J.W.H., Damsté, S. and Brinkhuis, H. 2014. Rapid short-term cooling following the Chicxulub impact at the Cretaceous–Paleogene boundary. *Proceedings of the National Academy of Science of the United States of America*, **111**, 7537–7541, <https://doi.org/10.1073/pnas.1319253111>
- Vellekoop, J., Esmerayenlet, S. *et al.* 2016. Evidence for Cretaceous–Paleogene boundary bolide ‘impact winter’ conditions from New Jersey, USA. *Geology*, **44**, 619–622, <https://doi.org/10.1130/G37961.1>
- Vérard, C. 2019. Panalexis: towards global synthetic palaeogeographies using integration and coupling manifold models. *Geological Magazine*, **156**, 320–330, <https://doi.org/10.1017/S0016756817001042>
- Vérard, C., Hochard, C., Baumgartner, O. and Stampfli, G.M. 2015. 3D palaeogeographic reconstructions of the Phanerozoic v. sea-level and Sr-ratio variations. *Journal of Palaeogeography*, **4**, 64–84, <https://doi.org/10.3724/SP.J.1261.2015.00068>
- Vérard, C., Stampfli, G.M., Borel, G. and Hochard, C. 2017. The Indian Promontory: A bridge between plate tectonics and life evolution models. *Universal Journal of Geoscience*, **5**, 25–32, <https://doi.org/10.13189/ujg.2017.050202>
- Vickers, M.L., Bajnai, D., Price, G.D., Linckens, J. and Fiebig, J. 2019. Southern high-latitude warmth during the Jurassic–Cretaceous: New evidence from clumped isotope thermometry. *Geology*, **47**, 724–728, <https://doi.org/10.1130/G46263.1>
- Vine, F.J. and Smith, A.G. (eds) 1981. *Extensional Tectonics Associated with Convergent Boundaries*. The Royal Society, London.
- Vinogradov, A.P., Vereshchagin, V.N., Nalivkin, V.D., Ronov, A.B., Khabakov, A.V. and Khain, V.E. 1968. *Atlas of Lithological–Palaeogeographical Maps of the U.S.S.R., 1:7 500 000, Tome III, Triassic, Jurassic, and Cretaceous, Tome III*. Ministry of Geology, Academy of Sciences of the USSR, Moscow.
- Vrielynck, B. and Bouyessé, P. 2001. *Le Visage Changeant de la Terre, L’éclatement de la Pangée et la mobilité des continents au cours des derniers 250 million d’années en 10 cartes*. Commission de la Carte Géologique du Monde, Paris.
- Wagreich, M., Lein, R. and Sames, B. 2014. Eustasy, its controlling factors, and the lino-eustatic hypothesis – concepts inspired by Eduard Suess. *Austrian Journal of Earth Sciences*, **107**, 115–131.
- Wakabayashi, J. and Dilek, Y. (eds) 2021. *Plate Tectonics, Ophiolites, and Societal Significance of Geology: A Celebration of the Career of Eldridge Moores*. Geological Society of America Special Papers, **552**, <https://doi.org/10.1130/SPE552>
- Walsh, D.B. 1996. *Late Jurassic through Holocene Paleogeographic Evolution of the South Atlantic Borderlands*. Master’s thesis, University of Texas at Arlington, Arlington, Texas, USA.
- Walsh, D.B. and Scotese, C.R. 1993. PALEOMAP PC: plate tectonic reconstructions on IBM compatible computers. *Geological Society of America Abstracts with Programs*, **25**, 44–45.

- Wang, H.Z. 1985. *Atlas of the Paleogeography of China*. Chinese Academy of Sciences Cartographic Publishing House, Beijing.
- Ward, P.D. 2004. *Gorgon: Paleontology, Obsession, and the Greatest Catastrophe in Earth's History*. Viking Press, New York.
- Ward, P.D. and Brownlee, D. 2003. *The Life and Death of Planet Earth: How the New Science of Astrobiology Charts the Ultimate Fate of Our World*. Times Books, Henry Holt and Company, New York.
- Watkins, J.S., Feng, Z.Q. and McMillen, K.J. (eds) 1992. *Geology and Geophysics of Continental Margins*. AAPG Memoirs, **53**, <https://doi.org/10.1306/M53552>
- Weirzbowski, H. and Joachimski, M. 2007. Reconstruction of late Bajocian–Bathonian marine palaeoenvironments using carbon and oxygen isotope ratios of calcareous fossils from the Polish Jura Chain (central Poland). *Palaeogeography, Palaeoclimatology, Palaeoecology*, **254**, 523–540, <https://doi.org/10.1016/j.palaeo.2007.07.010>
- Weishampel, D.B., Dodson, P. and Osmolska, H. (eds) 1990. *The Dinosauria*. University of California Press, Berkeley, CA.
- Wellnhofer, P. 1991. *The Illustrated Encyclopedia of Pterosaurs*. Crescent Books, New York.
- Westerhold, T., Marwan, N. et al. 2020. An astronomically dated record of Earth's climate and its predictability over the last 66 million years. *Science*, **369**, 1383–1387, <https://doi.org/10.1126/science.aba6853>
- Wignall, P.B. 2001. Large igneous provinces and mass extinctions. *Earth-Science Reviews*, **53**, 1–33, [https://doi.org/10.1016/S0012-8252\(00\)00037-4](https://doi.org/10.1016/S0012-8252(00)00037-4)
- Wignall, P.B. 2015. *The Worst of Times, How life on Earth Survived Eighty Million Years of Extinctions*. Princeton University Press, Princeton, NJ.
- Wilf, P., Johnson, K. and Huber, B.T. 2003. Correlated terrestrial and marine evidence for global climate changes before mass extinction at the Cretaceous–Paleogene boundary. *Proceedings of the National Academy of Sciences of the United States of America*, **100**, 599–604, <https://doi.org/10.1073/pnas.0234701100>
- Wilford, G.E. 1979. Phanerozoic paleogeography. In: Carter, E.K. (ed.) *BMR Earth Science Atlas of Australia*. Bureau of Mineral Resources, Geology & Geophysics, Canberra, 4.
- Willeit, M., Ganopolski, A., Robinson, A. and Edwards, N.R. 2022. The Earth system model CLIMBER-X v1.0 – Part 1: Climate model description and validation. *Geoscientific Model Development*, **15**, 5905–5948, <https://doi.org/10.5194/gmd-15-5905-2022>
- Williams, H. (ed.) 1995. *Geology of the Appalachian–Caledonian Orogen in Canada and Greenland*. Geology of Canada, **6**/Geology of North America, **F-1**. Geological Survey of Canada, Ottawa.
- Willis, K.J. and McElwain, J.C. 2002. *The Evolution of Plants*. Oxford University Press, Oxford, UK.
- Wilson, G.P., Clemens, W.A., Horner, J.R. and Horton, J.H. 2014. *Through the End of the Cretaceous in the Type Locality of the Hell Creek Formation in Montana and Adjacent Areas*. Geological Society of America, Special Papers, **503**, <https://doi.org/10.1130/SPE503>
- Wilson, J.T. 1966. Did the Atlantic close and then re-open? *Nature*, **211**, 676–681. <https://doi.org/10.1038/211676a0>
- Wilson, J.T. 1968. Static or mobile Earth: The current scientific revolution. *Proceedings of the American Philosophical Society*, **112**, 309–320.
- Wilson, R.C.L., Whitmarsh, R.B., Taylor, B. and Froitzheim, N. (eds) 2001. *Non-Volcanic Rifting of Continental Margins: A Comparison of Evidence from Land and Sea*. Geological Society, London, Special Publications, **187**, <https://doi.org/10.1144/GSL.SP.2001.232.01.28>
- Wilson, R.W., Houseman, G.A., McCaffrey, K.J., Dore, A.G. and Buiter, S.J.H. 2019. Fifty years of the Wilson Cycle concept in plate tectonics. *Geological Society, London, Special Publications*, **470**, 1–17, <https://doi.org/10.1144/SP470-2019-58>
- Winchester, J.A., Pharaoh, T.C. and Verniers, J. (eds) 2002. *Palaeozoic Amalgamation of Central Europe*. Geological Society, London, Special Publications, **201**, <https://doi.org/10.1144/GSL.SP.2002.201.01.17>
- Windley, B.F., Alexeev, D., Xiao, W.J., Kroner, A. and Badarch, G. 2007. Tectonic models for the accretion of the Central Asian Orogenic Belt. *Journal of the Geological Society, London*, **164**, 31–47, <https://doi.org/10.1144/0016-76492006-022>
- Witton, M.P. 2013. *Pterosaurs: Natural History, Evolution, Anatomy*. Princeton University Press, Princeton, NJ.
- Wolfe, J.A. and Upchurch, G.R. 1987. North American nonmarine climates and vegetation during the Late Cretaceous. *Palaeogeography, Palaeoclimatology, Palaeoecology*, **61**, 33–77, [https://doi.org/10.1016/0031-0182\(87\)90040-X](https://doi.org/10.1016/0031-0182(87)90040-X)
- Wortel, R. and Cloetingh, S. 1981. On the origin of the Cocos-Nazca spreading center. *Geology*, **9**, 425–430, [https://doi.org/10.1130/0091-7613\(1981\)9<425:OTOOTC>2.0.CO;2](https://doi.org/10.1130/0091-7613(1981)9<425:OTOOTC>2.0.CO;2)
- Wright, J.E. and Shervais, J.W. (eds) 2008. *Ophiolites, Arcs, Batholiths: A Tribute to Cliff Hopson*. Geological Society of America Special Papers, **438**, <https://doi.org/10.1130/SPE438>
- Wright, N.M., Seton, M., Williams, S.E. and Müller, R.D. 2016. The late Cretaceous to recent history of the Pacific Ocean basin. *Earth-Science Reviews*, **154**, 138–173, <https://doi.org/10.1016/j.earscirev.2015.11.015>
- Wright, N.M., Seton, M., Williams, S.E., Whittaker, J.M. and Müller, R.D. 2020. Sea-level fluctuations driven by changes in global ocean basin volume following supercontinent break-up. *Earth Science Reviews*, **208**, 103293, <https://doi.org/10.1016/j.earscirev.2020.103293>
- Yancey, T.E. and Guillemette, R.N. 2008. Carbonate accretionary lapilli in distal deposits of the Chicxulub impact event. *Geological Society of America Bulletin*, **120**, 1105–1118, <https://doi.org/10.1130/B26146.1>
- Yilmaz, O., Norton, I.O., Leary, D. and Chuchla, R.J. 1996. Tectonic evolution and paleogeography of Europe. In: Ziegler, A. and Horvath, F. (eds) *Peri-Tethys Memoir 2: Structure and Prospects of Alpine Basins and Forelands*. Mémoires du Muséum national d'histoire naturelle, **170**, 47–60.
- Yin, A. and Harrison, T.M. (eds). 1996. *The Tectonic Evolution of Asia*. Cambridge University Press, New York.
- Zachos, J., Pagani, M., Sloan, L., Thomas, E. and Billups, K. 2001. Trends, rhythms and aberrations in global climate 65 Ma to present. *Science*, **292**, 686–693, <https://doi.org/10.1126/science.1059412>

- Zachos, J.C., Dickens, G.R. and Zeebe, R.E. 2008. An early Cenozoic perspective on greenhouse warming and carbon-cycle dynamics. *Nature*, **451**, 279–283, <https://doi.org/10.1038/nature06588>
- Zahirovic, S., Seton, M. and Müller, R.D. 2014. The Cretaceous and Cenozoic tectonic evolution of Southeast Asia. *Solid Earth*, **5**, 227–273, <https://doi.org/10.5194/se-5-227-2014>
- Zeebe, R.E., Zachos, J.C. and Dickens, G.R. 2009. Carbon dioxide forcing alone insufficient to explain Palaeocene–Eocene Thermal Maximum warming. *Nature Geoscience*, **2**, 576–580, <https://doi.org/10.1038/ngeo578>
- Zhang, L., Wang, C. *et al.* 2016. A new paleoclimate classification for deep time. *Palaeogeography, Palaeoclimatology, Palaeoecology*, **443**, 98–106, <https://doi.org/10.1016/j.palaeo.2015.11.041>
- Zhou, J., Poulsen, C.J., Pollard, D. and White, T.S. 2008. Simulation of modern and middle Cretaceous marine $\delta^{18}\text{O}$ with an ocean–atmosphere general circulation model. *Paleoceanography*, **23**, PA3223, <https://doi.org/10.1029/2008PA001596>
- Ziegler, A.M., Scotese, C.R., McKerrow, W.S., Johnson, M.E. and Bambach, R.K. 1979. Paleozoic paleogeography. *Annual Review of Earth and Planet Sciences*, **7**, 473–302, <https://doi.org/10.1146/annurev.ea.07.050179.002353>
- Ziegler, A.M., Bambach, , *et al.* 1981. Paleozoic biogeography and climatology. In: Niklas, K.J. (ed.) *Paleobotany, Paleocology, and Evolution, Volume 2*. Praeger, New York, 231–266.
- Ziegler, A.M., Scotese, C.R. and Barrett, S.F. 1983. Mesozoic and Cenozoic paleogeographic maps. In: Broche, P. and Sunder Mann, J. (eds) *Tidal Friction and the Earth's Rotation II*. Springer, Berlin, 241–252.
- Ziegler, A.M., Rowley, D.B., Lottes, A.L., Sahagian, D.L., Hulver, M.L. and Gierlowski, T.C. 1985. Paleogeographic interpretation: With an example from the Mid-Cretaceous. *Annual Review of Earth and Planetary Sciences*, **13**, 385–425, <https://doi.org/10.1146/annurev.ea.13.050185.002125>
- Ziegler, A.M., Raymond, A.L., Gierlowski, T.C., Horrell, M.A., Rowley, D.B. and Lottes, A.L. 1987. Coal, climate and terrestrial productivity: the present and early Cretaceous compared. *Geological Society, London, Special Publications*, **32**, 25–49, <https://doi.org/10.1144/GSL.SP.1987.032.01.04>
- Ziegler, A.M., Rees, P.M., Rowley, D.B., Bekker, A., Li, Q. and Hulver, M.L. 1996. Mesozoic Assembly of Asia: Constraints from fossil floras, tectonics, and paleomagnetism. In: Yin, A. and Harrison, M. (eds) *The Tectonic Evolution of Asia*. Cambridge University Press, Cambridge, UK, 371–400.
- Ziegler, A.M., Eshel, G., Rees, P.M., Rothfus, T., Rowley, D. and Sunderlin, D. 2003. Tracing the tropics across land and sea: Permian to present. *Lethaia*, **36**, 227–254, <https://doi.org/10.1080/00241160310004657>
- Ziegler, P.A. 1982. *Geological Atlas of Western and Central Europe*. Shell Internationale Petroleum, The Hague, The Netherlands.
- Ziegler, P.A. (ed.) 1988. *Evolution of the Arctic–North Atlantic and the Western Tethys*. AAPG Memoirs, **43**, <https://doi.org/10.1306/M43478>
- Ziegler, P.A. 1990. *Geological Atlas of Western and Central Europe*. 2nd edn. Geological Society, London.
- Ziegler, P.A. (ed.) 1992. *Geodynamics of Rifting, Volume 1. Case History Studies of Rifts: Europe and Asia. Tectonophysics*, **108**, 1–363.
- Ziegler, P.A. and Horvath, F. 1996. Structure and prospects of Alpine basins and forelands. In: Ziegler, A. and Horvath, F. (eds) *Peri-Tethys Memoir 2; Structure and Prospects of Alpine Basins and Forelands*. Mémoires du Muséum national d'histoire naturelle, **170**, 15–45.
- Ziegler, P.A., Cavazza, W., Robertson, A.H.F. and Crasquin-Soleau, S. (eds) 2001. *Peri-Tethys Memoir 6; Peri-Tethyan Rift/Wrench Basins and Passive Margins*. Mémoires du Muséum national d'histoire naturelle, **186**.
- Zonenshain, L.P., Kuzmin, M.I. and Natapov, L.M. (eds) 1990. *Geology of the USSR: A Plate Tectonic Synthesis*. American Geophysical Union Geodynamics Series, **21**.